

Systematic Development of a Limited Authority Flight Control  
System for Helicopters

Thesis submitted for the degree of  
Doctor of Philosophy  
at the University of Leicester

by

Arun Nair  
Department of Engineering  
University of Leicester

April, 2010

For their unconditional love and support, I dedicate  
this thesis to my parents.

# Abstract

Over the last three decades, there has been increased interest in full authority (FA) control systems for helicopters. Despite their great potential, it will be some time before all operational helicopters are able to benefit from such flight control systems. Therefore, interim methods to deliver similar levels of performance are required, and it is natural to explore ways of improving current limited authority (LA) systems to achieve this. The study described herein investigates this topic and contributes a new LA design method.

The first part of the thesis describes the construction of the baseline FA controller for the AgustaWestland EH101 helicopter. The FA controller was designed using the 2DOF  $\mathcal{H}_\infty$  loop shaping methodology. Details of the controller design are presented, together with an analysis of linear and nonlinear simulation results. These reveal the controller's abilities to provide good levels of performance, across the portion of the flight envelope tested, without the aid of gain scheduling.

The second half describes the derivation of state-space formulae that enables the transformation of the above (FA) controller into LA form such that the latter controller replicates the small-signal FA responses. Extensive analysis and simulations are carried out for this architecture, both at the design point and at other conditions throughout the flight envelope. Also, the results are contrasted against a simpler LA architecture and the effectiveness of the proposed LA controller over this is shown. Both FA and LA results are complemented by an evaluation of handling qualities information against the design standard ADS-33.

It is believed that the results presented in the thesis show the strengths of the proposed LA architecture and suggest that current helicopter hardware should be able to provide much of the functionality of FA systems without requiring a complete overhaul.

# Acknowledgements

First and foremost, I would like to express my deepest gratitude to my supervisor Dr. Matthew Turner for his unconditional support and guidance. His expertise have contributed to the development of this project and also ensured my growth as an individual. I thank you for being an invaluable source of inspiration. I also thank Prof. Ian Postlethwaite as his constant guidance and encouragement were key to the completion of this thesis.

I warmly thank Dr. Prathyush Menon, for his invaluable advice and friendly help. His extensive discussions around my work have been very helpful for this study. Also, I would like to thank Prof. Chris Edwards for the constructive inputs during each assessment stage of this study.

My parents, Sasidharan and Geetha Nair, deserve a special mention for having faith in me and for encouraging my ambitions. It was under their watchful eye that I gained so much drive and ability to tackle challenges head on. I thank my brother Arvind Nair, for being supportive and caring, as well as humouring me when I was at the end of my tether.

I would like to express my appreciation for my partner, Anu Bhogal, who despite going through her own PhD journey, provided me with much needed encouragement and understanding even when I retreated to long days with my computer.

Last but not least, I would like to thank the many friends, near and far, who have saved me from insanity during this challenging period. I greatly value your friendship and I appreciate your belief in me that has helped me to stay focused to achieve my goals.

# Contents

<b>1</b>	<b>Introduction</b>	<b>1</b>
1.1	Helicopter flight control systems: an overview . . . . .	2
1.1.1	Full authority control system architecture . . . . .	3
1.1.2	Limited authority control system architecture . . . . .	7
1.2	Motivation for limited authority architecture . . . . .	9
1.3	Objectives . . . . .	10
1.4	Research activities . . . . .	11
1.5	Main contributions of this study . . . . .	13
1.6	Thesis organisation . . . . .	13
<b>2</b>	<b>Background to <math>\mathcal{H}_\infty</math> controller design</b>	<b>16</b>
2.1	Signals . . . . .	16
2.2	Systems . . . . .	18
2.3	$\mathcal{H}_\infty$ optimal control . . . . .	21
2.3.1	Uncertainty modelling . . . . .	22
2.3.2	Small Gain Theorem . . . . .	26
2.3.3	$\mathcal{H}_\infty$ control problem . . . . .	27
2.4	Conclusion . . . . .	38

<b>3</b>	<b>Helicopter control problem</b>	<b>39</b>
3.1	Overview . . . . .	39
3.2	Helicopter flight . . . . .	40
3.3	Helicopter FCS architectures . . . . .	42
3.4	Helicopter model . . . . .	44
3.5	Control response types . . . . .	46
3.6	Handling qualities . . . . .	47
3.7	Conclusion . . . . .	51
<b>4</b>	<b>Full authority controller design</b>	<b>52</b>
4.1	Introduction . . . . .	52
4.2	EH101 design model . . . . .	53
4.2.1	Open loop characteristics . . . . .	55
4.3	Controller design . . . . .	65
4.3.1	Selection of reference model . . . . .	65
4.3.2	Loop shaping and controller synthesis . . . . .	67
4.4	Linear simulation results . . . . .	75
4.4.1	Longitudinal response . . . . .	76
4.4.2	Lateral response . . . . .	77
4.4.3	Directional response . . . . .	77
4.4.4	Comparison to Design 2 . . . . .	78
4.4.5	Controller order reduction . . . . .	79
4.5	Conclusion . . . . .	80
<b>5</b>	<b>Transformation to limited authority controllers</b>	<b>93</b>
5.1	Limited authority control systems . . . . .	93

5.1.1	EH101 interlinks model . . . . .	96
5.2	Proposed limited authority architecture . . . . .	99
5.3	Developing the state-space formulae . . . . .	100
5.3.1	Small signal analysis . . . . .	101
5.3.2	Translation to limited authority . . . . .	102
5.4	Alternative reference demand injection . . . . .	111
5.5	Conclusion . . . . .	116
<b>6</b>	<b>Linear limited authority simulation</b>	<b>118</b>
6.1	Modifications to the full authority controller . . . . .	118
6.2	Linear simulation . . . . .	127
6.2.1	Series actuation only . . . . .	128
6.2.2	Limited authority controller with series and parallel actuation . . . . .	135
6.2.3	Other choices for parallel actuator controller . . . . .	142
6.2.4	Robustness . . . . .	145
6.3	Conclusion . . . . .	147
<b>7</b>	<b>Nonlinear simulation and quantitative ADS-33 analysis</b>	<b>154</b>
7.1	Full authority simulation results . . . . .	154
7.1.1	Longitudinal response (pitch-down) . . . . .	156
7.1.2	Lateral response (roll-right) . . . . .	156
7.1.3	Directional response (right pedal forward) . . . . .	157
7.1.4	Robustness . . . . .	157
7.1.5	Note on symmetry . . . . .	159
7.1.6	Summary . . . . .	161
7.2	Limited authority simulation results . . . . .	180

7.2.1	Longitudinal response (pitch-down) . . . . .	180
7.2.2	Lateral responses (roll-right) . . . . .	182
7.2.3	Directional response (right pedal forward) . . . . .	185
7.2.4	Robustness . . . . .	189
7.2.5	Note on symmetry . . . . .	191
7.2.6	Summary . . . . .	193
7.3	Handling qualities rating assessment . . . . .	196
7.3.1	Small amplitude input criteria . . . . .	196
7.3.2	Moderate amplitude input criteria . . . . .	198
7.3.3	Large amplitude input criteria . . . . .	202
7.3.4	Inter-axis coupling criteria . . . . .	206
7.3.5	Summary . . . . .	206
7.4	Conclusion . . . . .	207
<b>8</b>	<b>Conclusions and recommendations</b>	<b>210</b>
8.1	Conclusion . . . . .	210
8.1.1	Design of a robust FA controller . . . . .	210
8.1.2	Derivation of the transformation formulae . . . . .	211
8.1.3	Case study results . . . . .	213
8.2	Recommendations for future work . . . . .	213

# List of Figures

1.1	AgustaWestland EH101 Helicopter [57] . . . . .	1
1.2	FA schematic . . . . .	4
1.3	LA schematic [85] . . . . .	7
2.1	Common uncertainty representation [72] . . . . .	23
2.2	Coprime factor uncertainty configuration [72] . . . . .	24
2.3	Small Gain Theorem [43] . . . . .	27
2.4	$M - \Delta$ structure [72] . . . . .	28
2.5	Standard feedback configuration [72] . . . . .	28
2.6	S/T/KS mixed sensitivity problem [72] . . . . .	32
2.7	Design specification for singular values of $GK$ [72] . . . . .	33
2.8	1DOF loop shaping problem [72] . . . . .	34
2.9	2DOF loop shaping problem [72] . . . . .	37
3.1	Collective control [5] . . . . .	41
3.2	Cyclic control [5] . . . . .	42
3.3	Helicopter flight control system architectures [84] . . . . .	42
3.4	Series Actuator [14] . . . . .	43
3.5	Parallel Actuator [14] . . . . .	44
4.1	MIMO open-loop singular value comparison . . . . .	58

4.2	MIMO open-loop singular value comparison . . . . .	58
4.3	MIMO open-loop singular value comparison . . . . .	59
4.4	MIMO open-loop singular value comparison . . . . .	60
4.5	MIMO open-loop singular value comparison . . . . .	60
4.6	Comparison between 8-state (dashed) and 25-state (solid) model . . . . .	61
4.7	Eigen value variation as a function of speed (0 - 120kts) for 14200kg . . . . .	62
4.8	Eigen value variation as a function of speed (0 - 120kts) for 11000kg . . . . .	63
4.9	Bode magnitude plots . . . . .	64
4.10	Desired responses from each channel . . . . .	67
4.11	Open loop singular values - Nominal . . . . .	68
4.12	Shaped open loop singular values - Design 1 . . . . .	69
4.13	Stabilised open loop singular values - Design 1 . . . . .	70
4.14	Closed loop frequency response - Design 1 . . . . .	70
4.15	Shaped open loop singular values - Design 2 . . . . .	71
4.16	Stabilised open loop singular values - Design 2 . . . . .	72
4.17	Closed loop frequency response - Design 2 . . . . .	73
4.18	Shaped open loop singular values - Design 3 . . . . .	74
4.19	Stabilised open loop singular values - Design 3 . . . . .	74
4.20	Closed loop frequency response - Design 3 . . . . .	74
4.21	25-state SIMULINK model for time domain analysis . . . . .	75
4.22	16 <sup>th</sup> order controller . . . . .	80
4.23	12 <sup>th</sup> order controller . . . . .	80
4.24	8 <sup>th</sup> order controller . . . . .	81
4.25	4 <sup>th</sup> order controller . . . . .	81
4.26	Pitch attitude time response - Design 3 . . . . .	84

4.27	Variation in longitudinal response with flight condition (14200kg)	85
4.28	Variation in longitudinal response with flight condition (11000kg)	85
4.29	Roll attitude time response - Design 3	86
4.30	Variation in lateral response with flight condition (14200kg)	87
4.31	Variation in lateral response with flight condition (11000kg)	87
4.32	Yaw rate time response - Design 3	88
4.33	Variation in directional response with flight condition (14200kg)	89
4.34	Variation in directional response with flight condition (11000kg)	89
4.35	Pitch attitude time response - Design 2	90
4.36	Roll attitude time response - Design 2	91
4.37	Yaw rate time response - Design 2	92
5.1	LA schematic [85]	95
5.2	EH101 interlinks	97
5.3	Proposed LA control architecture	99
5.4	Unconstrained LA architecture	101
5.5	FA architecture	102
5.6	FA controller	103
5.7	LA controller	103
5.8	Block diagram realisation	107
5.9	Alternate LA architecture	112
5.10	Block diagram realisation - alternative scheme	114
6.1	FA response - 40kts/0ft/14200kg (Design point)	121
6.2	FA response - 40kts/0ft/11000kg	122
6.3	FA response - Hover/14200kg	123

6.4	FA response - Hover/11000kg . . . . .	124
6.5	FA response - 80kts/2500ft/14200kg . . . . .	125
6.6	FA response - 80kts/4500ft/11000kg . . . . .	126
6.7	LA architecture - series actuators only . . . . .	128
6.8	Longitudinal Response (5%) . . . . .	129
6.9	Longitudinal Response (9.25%) . . . . .	129
6.10	Series Actuator Response - Pitch channel . . . . .	130
6.11	Lateral Response (8%) . . . . .	130
6.12	Lateral Response (12%) . . . . .	131
6.13	Lateral Response (18%) . . . . .	131
6.14	Series Actuator Response - Roll channel . . . . .	132
6.15	Directional Response (5%) . . . . .	133
6.16	Directional Response (9%) . . . . .	134
6.17	Series Actuator Response - Yaw channel . . . . .	134
6.18	Longitudinal Response (8%) . . . . .	135
6.19	Longitudinal Response (16%) . . . . .	136
6.20	Series Actuator Response . . . . .	136
6.21	Parallel Actuator Response . . . . .	137
6.22	Lateral Response (12%) . . . . .	137
6.23	Lateral Response (20%) . . . . .	138
6.24	Series Actuator Response . . . . .	138
6.25	Parallel Actuator Response . . . . .	139
6.26	Directional Response (10%) . . . . .	139
6.27	Directional Response (20%) . . . . .	140
6.28	Series Actuator Response . . . . .	140

6.29	Parallel Actuator Response . . . . .	141
6.30	Longitudinal Response (10%) ( $\alpha = 0.05$ ) . . . . .	143
6.31	Longitudinal Response (10%) ( $\alpha = 0.5$ ) . . . . .	144
6.32	Longitudinal Response (10%) ( $\alpha = 0.005$ ) . . . . .	145
6.33	LA response - 40kts/0ft/11000kg . . . . .	149
6.34	LA response - Hover/14200kg . . . . .	150
6.35	LA response - Hover/11000kg . . . . .	151
6.36	LA response - 80kts/2500ft/14200kg . . . . .	152
6.37	LA response - 80kts/4500ft/11000kg . . . . .	153
7.1	Linear and Nonlinear FA architecture comparison . . . . .	154
7.2	Nonlinear pitch attitude response - 40kts/0ft . . . . .	162
7.3	Nonlinear roll attitude response - 40kts/0ft . . . . .	163
7.4	Nonlinear yaw rate response - 40kts/0ft . . . . .	164
7.5	Nonlinear pitch attitude response - 0kts/0ft . . . . .	165
7.6	Nonlinear roll attitude response - 0kts/0ft . . . . .	166
7.7	Nonlinear yaw rate response - 0kts/0ft . . . . .	167
7.8	Nonlinear pitch attitude response - 80kts/2500ft . . . . .	168
7.9	Nonlinear roll attitude response - 80kts/2500ft . . . . .	169
7.10	Nonlinear yaw rate response - 80kts/2500ft . . . . .	170
7.11	Nonlinear pitch attitude symmetry - 40kts/0ft . . . . .	171
7.12	Nonlinear pitch attitude symmetry - 00kts/0ft . . . . .	172
7.13	Nonlinear pitch attitude symmetry - 80kts/2500ft . . . . .	173
7.14	Nonlinear roll attitude symmetry - 40kts/0ft . . . . .	174
7.15	Nonlinear roll attitude symmetry - 00kts/0ft . . . . .	175
7.16	Nonlinear roll attitude symmetry - 80kts/2500ft . . . . .	176

7.17	Nonlinear yaw rate symmetry - 40kts/0ft . . . . .	177
7.18	Nonlinear yaw rate symmetry - 00kts/0ft . . . . .	178
7.19	Nonlinear yaw rate symmetry - 80kts/2500ft . . . . .	179
7.20	Nonlinear LA pitch attitude response - 40kts/0ft . . . . .	180
7.21	Nonlinear LA pitch attitude response - 40kts/0ft . . . . .	181
7.22	Series actuator response . . . . .	182
7.23	Parallel actuator response . . . . .	182
7.24	Nonlinear LA roll attitude response - 40kts/0ft . . . . .	183
7.25	Nonlinear LA roll attitude response - 40kts/0ft . . . . .	183
7.26	Series actuator response . . . . .	184
7.27	Parallel actuator response . . . . .	184
7.28	Nonlinear LA yaw rate response - 40kts/0ft . . . . .	185
7.29	Nonlinear LA yaw rate response - 40kts/0ft . . . . .	185
7.30	Series actuator response . . . . .	186
7.31	Parallel actuator response . . . . .	187
7.32	Nonlinear LA responses - 0kts/0ft . . . . .	188
7.33	Nonlinear LA response - 80kts/2500ft . . . . .	190
7.34	Nonlinear LA pitch attitude symmetry - 40kts/0ft . . . . .	192
7.35	Nonlinear LA roll attitude symmetry - 40kts/0ft . . . . .	193
7.36	Nonlinear LA yaw rate symmetry - 40kts/0ft . . . . .	194
7.37	Nonlinear LA yaw rate symmetry - 40kts/0ft . . . . .	194
7.38	ADS plot for pitch and roll performance . . . . .	199
7.39	ADS plot for yaw performance . . . . .	200
7.40	Pitch attitude quickness . . . . .	201
7.41	Roll attitude quickness . . . . .	203

# List of Tables

3.1	Helicopter structure overview . . . . .	45
3.2	Helicopter model variables . . . . .	46
3.3	Cooper-Harper rating scale [13] . . . . .	48
4.1	EH101 plant states . . . . .	54
4.2	EH101 plant inputs . . . . .	55
4.3	EH101 plant outputs . . . . .	55
4.4	EH101 8-state plant states . . . . .	56
4.5	EH101 8-state plant inputs and outputs . . . . .	56
4.6	EH101 trim points . . . . .	57
4.7	Open loop condition number (0.1 rads/s) . . . . .	57
4.8	Open loop poles - 8-state plant (11000kg) . . . . .	61
4.9	Open loop poles - 8-state plant (14200kg) . . . . .	62
4.10	Open loop zeros - 8-state plant . . . . .	63
4.11	Reference model description . . . . .	66
4.12	Controller order $\nu - gap$ variation . . . . .	80
4.13	Pitch attitude time response features . . . . .	83
4.14	Roll attitude time response features . . . . .	83
4.15	Yaw rate time response features . . . . .	83

6.1	Limits for the nonlinear elements . . . . .	127
6.2	Maximum pilot input for identical FA response . . . . .	142
6.3	Maximum pilot input for stable LA response . . . . .	142
6.4	Maximum pilot input for a identical response with variation to value of $\alpha$ .	145
6.5	Series actuation robustness and summary . . . . .	147
6.6	Series and parallel actuation robustness summary . . . . .	147
7.1	Trim points and variables values . . . . .	156
7.2	Summary of nonlinear results . . . . .	187
7.3	Summary of max input for identical response . . . . .	195
7.4	Summary of max input for stable response . . . . .	195
7.5	Small amplitude short term handling quality ratings . . . . .	198
7.6	FA pitch attitude quickness . . . . .	201
7.7	LA pitch attitude quickness . . . . .	202
7.8	FA roll attitude quickness . . . . .	203
7.9	LA roll attitude quickness . . . . .	204
7.10	Large amplitude handling quality rating requirement . . . . .	204
7.11	FA large amplitude handling quality rating . . . . .	205
7.12	LA large amplitude handling quality rating . . . . .	206
7.13	Nonlinear inter-axis coupling . . . . .	207

# List of Symbols

$\epsilon$	=	Uncertainty margin with respect to normalised coprime factor perturbations
$\epsilon_{max}$	=	Optimal (maximum) uncertainty margin
$\exists$	=	Existential qualification, $\exists X \geq 0$ means there exists a positive definite $X$
$\gamma$	=	$\mathcal{H}_\infty$ norm bound
$\gamma_{min}$	=	Optimal (minimum) $\mathcal{H}_\infty$ norm bound
$\psi$	=	Helicopter heading
$\phi$	=	Helicopter roll attitude
$\Phi$	=	Phase lag at $2\omega_{180}$
$\rho$	=	2 DOF loop shaping trade-off parameter
$\rho(X)$	=	Spectral radius of square matrix $X$
$\bar{\sigma}$	=	Maximum singular value
$\underline{\sigma}$	=	Minimum singular value
$\tau_r$	=	Attitude quickness parameter
$\theta$	=	Helicopter pitch attitude
$\xi$	=	Damping ratio
$\nu - gap$	=	Error measuring tool
$\mathcal{H}$	=	Hardy space
$\mathcal{L}$	=	Lebesgue space
$p$	=	Helicopter roll rate
$q$	=	Helicopter pitch rate
$r$	=	Helicopter yaw rate / Pilot demand vector
$u$	=	Helicopter longitudinal velocity / Control input vector to the generalised plant, $P$
$u_p$	=	Parallel actuator signal
$u_s$	=	Series actuator signal
$u_t$	=	Total control signal
$v$	=	Helicopter lateral velocity / Input Signal vector to nominal controller, $K$
$w$	=	Helicopter vertical velocity / Exogenous inputs
$y$	=	System output
$z$	=	Exogenous outputs

$\omega_n$	=	Natural frequency
$\omega_{180}$	=	Phase crossover frequency
$\omega_B$	=	Bandwidth frequency
$\Delta$	=	Norm bounded stable uncertainty model
$F_l$	=	Symbol for linear fractional transformation
$G$	=	Nominal flight mechanics model
$G_s$	=	Shaped nominal plant, $W_2GW_1$
$K$	=	Nominal controller
$K_\infty$	=	2 DOF $\mathcal{H}_\infty$ controller, $K_\infty = [K_1 \quad K_2]$
$K$	=	Controller for the nominal plant ( $G$ ), $W_1 \begin{bmatrix} K_1 & K_2W_2 \end{bmatrix}$
$K_s$	=	Series component of the LA controller, $\begin{bmatrix} K_{s1} & K_{s2} \end{bmatrix}$
$K_p$	=	Parallel component of the LA controller
$L$	=	Mechanical interlinks gain between series actuator to swash plate
$M$	=	Mechanical interlinks gain between stick datum to swash plate
$S$	=	Sensitivity function, $(I + GK)^{-1}$
$T$	=	Complimentary sensitivity function, $(I + GK)^{-1} GK$
$T_{ref}$	=	Reference model
$P$	=	Generalised plant model (nominal plant plus weighting functions)
$W_S$	=	Weighting function associated with $S$
$W_T$	=	Weighting function associated with $T$
$W_{KS}$	=	Weighting function associated with $KS$
$W_1$	=	Pre-compensator
$W_2$	=	Post-compensator

## List of Acronyms

ACAH	=	Attitude Command Attitude Hold
ADS	=	Aeronautical Design Standard
AFCS	=	Automatic Flight Control System
AFDD	=	AeroFlightDynamics Directorate
AHS	=	American Helicopter Society

DERA	=	Defence Evaluation and Research Agency
DOF	=	Degree Of Freedom
FA	=	Full Authority
FBW	=	Fly-By-Wire
FCS	=	Flight Control System
HQR	=	Handling Qualities Rating
ICD	=	Individual Channel Design
LA	=	Limited Authority
LFT	=	Linear Fractional Transformation
LMI	=	Linear Matrix Inequality
LTI	=	Linear Time Invariant
LQG	=	Linear Quadratic Gaussian
MIMO	=	Multi Input Multi Output
NAOMI	=	New Aircraft Overall Modelling Initiative
NRC	=	National Research Council
PAFCA	=	Partial Authority Flight Control Augmentation
PFCS	=	Primary Flight Control System
PID	=	Proportional Integral Derivative
RCAH	=	Rate Command Attitude Hold
RHP	=	Right Half Plane
SISO	=	Single Input Single Output
TRC	=	Translational Rate Command

## List of Abbreviations

<i>dB</i>	=	Decibel
<i>deg</i>	=	Degrees
<i>deg/s</i>	=	Degrees per second
<i>ft</i>	=	Feet
<i>kts</i>	=	Knots, nautical mile per hour
<i>kg</i>	=	Kilograms
<i>m</i>	=	Metres
<i>m/s</i>	=	Metres per second
<i>m/s<sup>2</sup></i>	=	Metres per square second
<i>Nm</i>	=	Newton metre
<i>rad</i>	=	Radians
<i>rad/s</i>	=	Radians per second
<i>sec</i>	=	Seconds

# Chapter 1

## Introduction



Figure 1.1: AgustaWestland EH101 Helicopter [57]

## 1.1 Helicopter flight control systems: an overview

Helicopters are the most common form of rotorcraft, easily identifiable by their most salient feature - a rotating aerofoil. This rotor is responsible for both vertical and rotational motion of the helicopter and provides the helicopter with the unique ability to hover over a stationary point for extended periods of time. For this reason, helicopters play a vital role in the military and civil aviation industries. However, this particular feature is also the reason why helicopters are characterised as a highly nonlinear, multivariable and cross coupled dynamic system [82], inevitably making the helicopter flight control system (FCS) design challenging [70]. In addition, helicopters are also open-loop unstable and most mathematical models are unable to predict cross-coupling satisfactorily, thus, further complicating the FCS design process. There is, however, a definite requirement for an automatic control augmentation for assisting the pilot because, when executing certain manoeuvres or in the presence of degraded visual or operating conditions, the pilot is prone to fatigue as an effect of intense and prolonged levels of concentration. Moreover, helicopters are also expected to satisfy the handling qualities requirements listed in the Aeronautical Design Standard (ADS)-33 document [3], which outlines the control system specifications in order to achieve adequate decoupling, stability and manoeuvrability for a given task.

Traditionally, practitioners have solved the helicopter flight control problem by using an architecture that is commonly known as *limited authority* (LA). Within LA architectures, the pilot has complete influence over the actuators through mechanical interlinks, and basic handling qualities augmentation is then achieved through an electronic controller that only has partial authority over the actuators. This constraint over the electronic controller activity has a significant, yet in some cases negative, impact on helicopter performance. However, during instances where the controller encounters saturation, the LA architecture has the *advantage* of allowing the pilot to override the electronic controller and this makes it highly popular in helicopter industries. It was also observed, that increasing the authority level of this electronic controller had a positive impact upon helicopter performance. Within the rotorcraft community, it is strongly believed that optimum handling qualities is best achieved through what is called a *full authority* (FA) architecture. Specific to this architecture, the pilot demands are communicated to the electronic controller, which now has complete in-

fluence over the entire actuator range. Compared to the LA system this architecture is less complex; where in the absence of signal constraints, this approach offers a more straightforward solution for helicopter FCS design. There are ample studies that reflect the success of this architecture ([6, 8, 32, 46, 87]), prompting the anticipated implementation of FA control system in many next generation helicopters. Unfortunately the upgrading of current operational helicopters which use LA architecture is likely to be very costly and it would therefore be useful to seek the functionality of FA architectures within the constrained structure of existing LA architectures.

The study presented in this thesis details the design of a LA architecture for the AgustaWestland EH101 (Figure 1.1) helicopter and this architecture is essentially capable of replicating the behaviour of a highly augmented FA controller for certain levels of pilot command. For the purpose of comparative analysis of both architectures, a comprehensive design of the FA controller is also presented. It should be noted, that as a FA study of the EH101 helicopter has not previously been conducted, the incorporation of the FA controller design helps to emphasise benefits of this type of architecture. However, before proceeding into the design process, it is important to appreciate the main differences between the two architectures in more detail and also explore the past studies that have been presented in these two FCS architectures.

### **1.1.1 Full authority control system architecture**

In a FA architecture, as shown in Figure 1.2, the pilot's demands are directly supplied to an automatic controller which calculates the appropriate blade angle demand that is consistent with the pilot demand. FA control systems are similar to the standard control configuration that feature in all control textbooks [28, 72]. FA architectures also have the advantage that they are straightforward to understand. Also, while executing aggressive manoeuvres the helicopter is less likely to revert to unstable behaviour with a FA control system as no restrictions are imposed either on the magnitude or the rate of control signals. There is a potential drawback however with the helicopter behaviour being dominated by the automatic controller, the FA control system must be constructed to extremely strict levels of safety and reliability standards. It should be noted at this point in time, that not many helicopters fea-

ture FA control systems and most, if not all, of the FA studies have come from the research community.

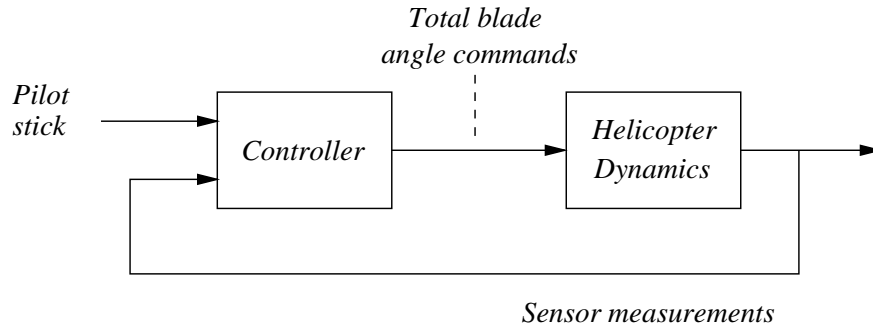


Figure 1.2: FA schematic

Early helicopter FA control systems designs have largely utilised classical methods due to their transparency and ease of implementation. In spite of their simplicity they have been able to provide significant improvements in handling qualities. However, with the quantitative specifications such as the ADS-33 becoming an essential part of controller validation process, it was observed by controller designers that classical control methods were not able to effectively meet the strict standards [68], such as low inter axis coupling, fast response, high robustness properties. Thus, over the last two and a half decades, many modern strategies that handle multivariable systems in a methodical manner have been proposed for the design of FA controllers. The earliest and the one that proved inspirational to other researchers was the study conducted by [32] that demonstrated the usefulness of a Linear Quadratic Gaussian (LQG) based controller in generating low-order and robust controllers. The controller was designed for the CH-47 Chinook helicopter model and desktop simulations results were successfully substantiated with flight test data. Next, a two-loop feedback structure that featured an eigen-structure assignment as an inner loop and an outer loop that was designed using  $\mathcal{H}_\infty$  synthesis was proposed by [6] and showed acceptable levels of performance, robustness and decoupling in the rotorcraft responses. Another prominent study that was backed with flight test results was conducted by [8], who described the design and implementation of a Translational Rate Command (TRC) type system using the Bell 205 Airborne Simulator. Also, a computer based flight simulation of a decoupled controller based on fuzzy logic and genetic algorithms was conducted for the UH-1 “Huey” helicopter by [40]. This method was further advocated by a study conducted by [87] that presented successful

flight test results using an adaptive fuzzy logic controller and also showed that the learning ability allowed this controller to be easily applicable to other helicopters as well. Around the same time, an Individual Channel Design (ICD) that simplified the  $4 \times 4$  multivariable control problem into two simpler  $2 \times 2$  multivariable problems - one for the longitudinal dynamics and the other for the lateral dynamics was proposed by [47]. A quantitative ADS-33 evaluation showed that this controller was capable of bestowing good handling qualities on the aircraft and, also its effectiveness against cross-coupling was also found to be acceptable. Another strategy that started to take effect during this period was the method of adaptive neural networks where a nominal controller was designed using a standard methodology and performance augmentation was then provided by the neural network. A significant study in this area was conducted by [46] which showed, that good tracking was achievable despite the presence of uncertainties due to modelling errors. More recently, studies were conducted that looked at the application of a sliding mode control method to design a rate [54] and an attitude [55] command FCS for the PUMA helicopter. The controller was designed using a linearised model of the helicopter in hover and the controller was found to satisfy the optimum handling qualities requirements set out by ADS-33. All of the above approaches have been continuously explored by researchers, such as [2, 17, 19, 56, 79, 92], and most have been able to demonstrate useful performance improvement in simulation. However, only some of the above strategies have been supported by extensive piloted simulation and flight tests and some (e.g. neural network based) have little chance of obtaining the necessary certification by the relevant authorities.

In addition to the aforementioned methodology, another technique which has been explored in the context of helicopter control is that of  $\mathcal{H}_\infty$  optimal control. There are several desirable features of this particular technique which are thought to make it appropriate for the control of helicopters. Firstly, the technique is an *inherently* multivariable technique, that is, it is suitable for controlling systems where there are multiple inputs and multiple outputs. Although fixed wing aircraft often exhibit some quite obvious decoupling between the lateral and longitudinal dynamics, this is not the case for helicopters: while the structure is roughly diagonal, there is strong coupling between the pitch and roll dynamics and vice versa, and strong interaction between the yaw rate and heave velocity. Another appealing feature of the  $\mathcal{H}_\infty$  technique is that it allows the *uncertainty* always present in mathematical models of

the helicopter, to be directly accounted for in the design stage. For multivariable controller design of the helicopter this is considered particularly important as, for example rotor characteristics are often imprecisely known and sometimes omitted from models; similarly some of the lateral-longitudinal coupling is often poorly captured by mathematical models and hence care must be taken when designing decoupling controllers. Thus in many ways  $\mathcal{H}_\infty$ , on paper at least, is an ideal technique to use for helicopter flight control system design.

For the above reasons, over the last two decades researchers have made several attempts at applying  $\mathcal{H}_\infty$  to helicopter control problems and, over this period, the work has progressed from purely desktop simulation studies to extensive, piloted flight tests. This interest began in the UK during the late 1980s with collaboration between the Defence Evaluation and Research Agency (DERA) and the University of Oxford, with the research mainly focussing of  $\mathcal{H}_\infty$  control of the Lynx helicopter with [94] formulating the problem as a mixed sensitivity  $\mathcal{H}_\infty$  optimisation and [89] applying the  $\mathcal{H}_\infty$  loop shaping method. Since then, further studies involving collaboration between QinetiQ, University of Leicester, Westland Helicopters and the National Research Council (NRC), Canada on FA  $\mathcal{H}_\infty$  design for the QinetiQ model of the Bell 205 helicopter [78, 91] have proved fruitful. Initial work reported in [75] describes the first flight test results obtained using a  $\mathcal{H}_\infty$  controller on the Bell 205 and later studies reported in [77], [66], [67] and [85] showed how these results could be improved. Flight test results for the Bell 205 reported in [65] showed successful implementation of one controller designed using the  $\mathcal{H}_\infty$  loop shaping method as it yielded Level 1 handling qualities in all tested manoeuvres. These later results showed a high degree of consistency between desktop simulations and flight test results and it was found that it was relatively easy to design controllers which achieved borderline Level 1 handling qualities ratings, with only minor tuning (based on flight tests) required to achieve optimum rating. On this basis, the  $\mathcal{H}_\infty$  method is a very strong contender for FCS design and will thus be used as the FA controller design tool.

In spite of the number of successes shown by the application of FA control systems, most, if not all, currently operational helicopter FCS has been dominated by the LA architecture. It appears that in the short term, this will continue to be the case.

### 1.1.2 Limited authority control system architecture

In LA architectures (Figure 1.3), the pilot's stick input directly influences blade angle deflection through mechanical interlinks known as the Primary Flight Control System (PFCS), but the stick datum is also used to drive an Automatic Flight Control System (AFCS) which influences blade angle through an electronic system that is strictly limited by the *series* actuators [35]. In certain LA architectures, slower rate-limited *parallel* actuators are also used in order to off-load the series actuators and prevent their long term saturation. The idea behind LA control is to provide the pilots with small signal augmentation in helicopter handling qualities whilst also allowing them to override the controller for sufficiently large stick demands that results in unstable behaviour. In such circumstances, global stability guarantees provided by the electronic control system are more difficult to enforce within a LA architecture due to the constrained control signal and the complexity of the architecture makes it harder to assess. However, LA systems are popular amongst practitioners as they also do not require to be manufactured to the same strict levels of safety like the FA systems.

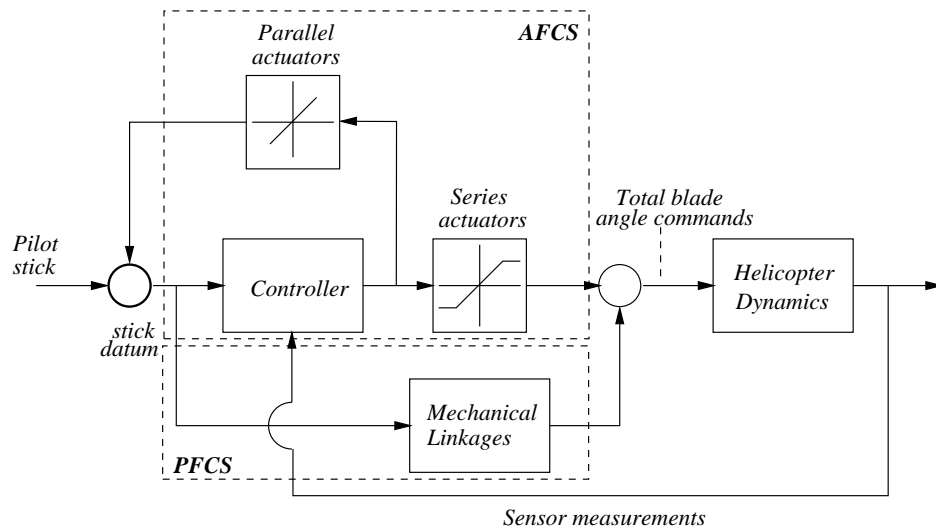


Figure 1.3: LA schematic [85]

The study of LA control systems has mainly been addressed by the practitioners from the rotorcraft community and input from the control research community has been notably lacking. A key study in the LA control area is reported in [7], where a series of flight test results using the NRC Bell 205 Airborne Simulator are described, that showed the benefits of FA controller within the LA architecture. One of the important observations was that series actuator

saturation did not always result in degraded handling qualities and could provide assistance during aggressive manoeuvring. Not long after, a series of ground based piloted simulation studies of Partial Authority Flight Control Augmentation (PAFCA) were conducted jointly by Defence Evaluation and Research Agency (DERA) and the US Army Aeroflightdynamics Directorate (AFDD). A study that investigated further the impact of AFCS saturation on handling qualities in ADS-33 hover/low-speed flight test manoeuvres was that conducted by [35] and the results reinforced the findings of [7]. A subsequent simulation study, conducted by the same research team, considered the impact of series actuator saturation on handling qualities in moderate aggression hover/low speed manoeuvres in a degraded visual environment [93]. They concluded that increasing the series actuator authority increased the handling quality rating by one. It should be noted at this stage that parallel actuation was not implemented in any of the studies above as they were mainly concentrated at the effects of series actuator saturation. Another study that showed the application of limited rate parallel actuation with the aim of maintaining the series actuators close to the centre of their limited authority was conducted jointly by DERA and NRC [33]. Also, research conducted by University of Leicester and Westland Helicopters discussed and presented results from the ground based piloted simulation of an  $\mathcal{H}_\infty$  LA control system [85]. The study presented the application of  $\mathcal{H}_\infty$  mixed-sensitivity methodology in designing a FCS for the Westland Lynx helicopter in order to attain the required performance and robustness properties, with unchanged series actuator limits. Piloted simulations and desktop testing results suggested that this type of system could offer an attractive solution to the LA problem, however, parallel actuators were seen as an external parameter. An important paper [31] was presented to the American Helicopter Society (AHS) which dealt with evaluation of various LA attitude command architectures for rotorcraft. According to his study the best architecture was the one which had implemented an attitude-blend out to minimise the effect of saturation. Also, a study was conducted by [58], that was presented at the European Control Conference, describing a transfer function based method for the transformation of a FA single-input-single-output (SISO) PID controller for the Bell 205 helicopter. This method ensured a successful implementation of a FA controller within the proposed LA architecture which was similar to Figure 1.3 and provided small-signal (before actuator saturation) performance matching. Any large signal instabilities due to actuator saturation were mitigated with the use of simple

anti-windup (AW) compensator.

## 1.2 Motivation for limited authority architecture

Most current generation helicopters utilise some form of LA control architecture and it would be a fair assessment to say that its design is surrounded by a great of deal of engineering intuition. Apart from the well documented PAFCA system [33, 35] and LA control system studied by [84], there has been little in the way of systematic and rigorous theory to assist the engineers with the construction of LA control systems. Even the advanced state of the art LA control architectures [31] suffer from a “cobbled-up” appearance with controller elements included in a fairly *ad hoc* manner based on prior experiences rather than any clear design rules. This presents a definite need for *deriving a systematic method that would enable the construction of LA control systems*. Furthermore, there is a lot of evidence to suggest that the application of robust control methods within the FA architecture has the potential to deliver optimum handling qualities and it would definitely be of interest to *observe how well this could be replicated within LA architectures that contain various structural constraints*.

It is evident from the past research that FA control systems offer better handling qualities than LA control systems and from an architectural point of view the former is less constrained. In spite of these shortcomings LA control systems are still the chosen FCS in EH101,

1. as the existing EH101 FCS utilises a LA architecture, it is *easier and more economical* to try and achieve the functionality of a FA controller within the existing structure than completely overhauling the FCS [35];
2. the reliability standards with a LA control system are *more relaxed* compared to the FA control system because if there is a malfunction with the stabilisation strategy in a LA architecture, the pilot is still able to control the helicopter via the manual control [84]; and
3. in certain parts of the flight envelope the EH101, like other helicopters, suffers with *chaotic vortex ring state* [38] where it exhibits excessive nonlinear type behaviour, and a LA controller is preferred over a FA control system here as the situation requires a greater control power from the pilot.

LA controllers, however, do suffer from the distinct disadvantage that their control signal magnitudes are limited to only a certain, often small, percentage of the actuators' full scale deflection. This restricts the magnitude of pilot demand that would produce a stable response and at large pilot demands the system can become unstable [85] and add to the already heavy pilot workload.

### 1.3 Objectives

The *primary* objective of this study was to produce a systematic methodology that would enable an engineer to design a LA controller which has the performance and robustness of an arbitrary FA controller. The process included developing a *systematic transformation methodology* that could then be applied to the FA controller in order to obtain the series actuator controller component that is fully functional within the LA architecture. There are some general design specifications that both the baseline FA controller, and the LA controller are required to satisfy in order to be flight test worthy.

1. **Meeting high performance levels and achieving acceptable levels of stability:** Performance and stability of a particular controller are usually judged by the handling qualities ratings returned by the pilot after a series of flight tests. However, in cases where flight tests are not possible then the performance could be analysed using desktop simulations - frequency and time domain responses. Quantitative analysis tools for small, medium and large amplitude pilot demands are provided in the ADS-33 document that are also used to rate the simulation results. Also, controllers that satisfy these desktop simulation criteria have shown in previous studies to equate to good handling quality ratings during flight.
2. **Decoupling the control inputs and achieving accurate tracking of pilot demands:** It is known that helicopters exhibit high levels of inter-axis coupling (pitch to roll, roll to pitch, roll to yaw and so on) and this results in high pilot workload. One of the motivations for requiring an automatic controller is to decouple these control signals and provide accurate responses to the pilot demands. In loop shaping terms, this is

achieved by acquiring the desired shape for the sensitivity frequency response function [53].

3. **Good disturbance rejection capability:** Helicopters are always subject to external disturbances as they are required to operate in highly demanding environments. Therefore, the controller should have the required disturbance rejection capability. This requirement is satisfied by acquiring the desired shape for the cosensitivity frequency response function [53].
4. **Coverage of the full flight envelope:** The helicopter behaviour is known to vary significantly from one flight condition to another and most controllers require gain scheduling in order to attain robust performance. It is therefore highly challenging to obtain a controller that could guarantee robust stability and performance without the need of gain scheduling.

## 1.4 Research activities

The research presented here builds upon the earlier studies in the areas of robust control design and LA architecture development with particular attention focused on designing robust controllers that function correctly in LA environment. This study also carries out a FA FCS design for the EH101 which generates the baseline set of responses to be reproduced by the LA FCS. The design therefore also illustrates the advantages of using FA architecture within helicopters. The research was mainly divided into three areas,

1. **Robust FA controller design:** The initial phase of this study includes the design of a baseline FA control system for the EH101. The methodology chosen for developing this controller is the well documented 2 degree-of-freedom (DOF)  $\mathcal{H}_\infty$  loop-shaping. [65] has shown its application to the Bell 205 helicopter that produced optimum handling qualities and a similar  $\mathcal{H}_\infty$  based FA control system for the Lynx helicopter was used in trials in the Advanced Engineering Simulator at AgustaWestland [85]. This methodology thus provides a good starting point for FA controller design. The controller is designed for an 8-state representation of the EH101 model at the 40kts/0ft

flight condition. An overview of this methodology is presented in Chapter 2 and the details of the design process are presented in Chapter 4.

2. **Deriving a transformation method:** The second phase of this study is to derive a systematic procedure for designing a LA controller that matches the performance of a given FA controller. The developed formulae is capable of taking an arbitrary 2DOF FA controller and “transforming” it to acquire an equivalent LA series actuator controller component. Such an approach guarantees that, at least for small amplitude pilot demands and disturbances, the LA system would behave identically to the FA system. This means that any theoretical properties of the FA controller are preserved, at least locally, by the LA controller. Another important feature of such an approach is that conventional linear controller design tools could be used to obtain the baseline FA behaviour. The formulae presented here accounts for the presence of the parallel actuators and are more involved than the simplified approach used in [35] and [85]. The transformation formulae along with its derivation are presented in Chapter 5.
3. **Linear and nonlinear simulation:** Finally, in order to verify the effectiveness of both the FA and LA controller designs, extensive linear and nonlinear simulations are carried out. The linear simulations are conducted for the 25-state linear representation derived from the flight mechanics model provided by AgustaWestland and these are presented in Chapters 4 (FA) and 6 (LA). The LA simulation presented in Chapter 6 is tagged linear because of the linear flight mechanics model, although nonlinear elements such as magnitude and rate limits are present in the architecture. The nonlinear simulations are carried out using the models provided by AgustaWestland and these are detailed in Chapter 7. This allowed for the appropriate large signal analysis to be conducted and also provide useful indications for further controller tuning. Also, this work provided AgustaWestland with the ability to compare the designed controller with their existing designs.

## 1.5 Main contributions of this study

1. **Application of 2DOF  $\mathcal{H}_\infty$  loop shaping methodology to design a FA controller for the EH101 helicopter:** The aim here was to design baseline FA controller to obtain a performance and response criteria that the LA control system attempts to reproduce, and to show the benefits of such a control system within the EH101 helicopter. The EH101 helicopter appears to demonstrate more cross-coupling and dynamic variation across the flight envelope than the Bell 205 and Lynx helicopters considered in previous studies. It was thus more of a challenge to design a satisfactory  $\mathcal{H}_\infty$  controller.
2. **Derivation of a formula that enables the implementation of an arbitrary FA controller to a LA environment:** Previous studies failed to present a systematic method for constructing a LA control system. This contribution now enables the engineer to design an arbitrary FA controller and then apply this conversion methodology to obtain a LA controller that guarantees identical small amplitude response.
3. **Inclusion of the parallel actuator compensator during the design process of the LA controller:** Parallel actuators are extremely critical in LA control systems and this study thoroughly examines the parallel actuator behaviour during both small amplitude and large amplitude pilot demands. Unlike the previous studies where parallel actuators were excluded during the main design stage, here they are made integral to the main design process.
4. **Extensive nonlinear simulation of the FA and LA controller:** This study contributes to the rapidly growing understanding of helicopter behaviour by analysing the nonlinear performance obtained due to the application of  $\mathcal{H}_\infty$  optimal controller. The analysis is conducted in both FA and LA architectures and gives an accurate and useful indication to some of the properties of the two very different controller architectures.

## 1.6 Thesis organisation

The work presented in this thesis attempts to explore the benefits of using modern control methodology for FA controller design and also attempts to develop an approach by which an

arbitrary FA controller can be systematically implemented in a LA environment. The thesis consists of eight chapters, the contents of which are outlined below:

- **Chapter 2:** This is the first of the two introductory chapters and it presents the main notions and concepts behind  $\mathcal{H}_\infty$  optimal control. The chapter places the main focus on  $\mathcal{H}_\infty$  loop shaping procedure as it is the chosen methodology for the design of a baseline FA controller.
- **Chapter 3:** This is the second introductory chapter and it provides a description of the helicopter flight control system including a brief overview into the complexities faced while flying and controlling one. It also presents the main elements of handling qualities rating specifications that are used to objectively quantify the controller performance.
- **Chapter 4:** This chapter describes the design of a baseline FA  $\mathcal{H}_\infty$  controller and presents linear desktop simulation results for the AgustaWestland EH101 helicopter. Details of the controller design are presented, together with an analysis of the frequency response functions.
- **Chapter 5:** This chapter presents the problems that arise while designing a LA controller and more specifically discusses the problem of using parallel actuators in this system. It compares the LA architectures obtained using two reference signal generation schemes. Also, a state-space based formula is developed that would transform an arbitrary 2DOF FA controller into a LA controller that would guarantee small signal performance matching.
- **Chapter 6:** This chapter describes the desktop linear simulation results obtained due to the proposed LA controller for the EH101 helicopter. It demonstrates the application of the transformation formula derived in Chapter 5 and shows the successful realisation of a given FA controller in a LA architecture. Also, it presents results that emphasise the importance of parallel actuators in a LA architecture.
- **Chapter 7:** This chapter presents the results obtained using the nonlinear EH101 simulation model which should enable a more accurate appraisal of both FA and LA controller's performance. These are further complemented by a quantitative evaluation of

handling qualities ratings information against the design standard ADS-33. The analysis presented in Chapters 4 to 7 expand upon the results that were highlighted in [59] and [60].

- **Chapter 8:** The main conclusions and findings are discussed, with directions for future research indicated.

# Chapter 2

## Background to $\mathcal{H}_\infty$ controller design

This chapter introduces the primary notions and concepts behind the  $\mathcal{H}_\infty$  optimal control strategy. This strategy appears to be ideal for helicopter applications and some previously conducted studies [76, 83, 84, 88, 89, 95] have supported this idea. For these reasons this study uses solely  $\mathcal{H}_\infty$  algorithms in the design of both the full and the equivalent LA controller. This chapter will describe the concepts underpinning  $\mathcal{H}_\infty$  control and will briefly present the two most commonly used  $\mathcal{H}_\infty$  design methodologies: mixed sensitivity and loop shaping. It is important to note that a significant amount of literature has already been presented by [15, 27, 72] and many others on the topics of signals and systems, and feedback control theory. Therefore, this chapter will simply highlight some of the important results related to  $\mathcal{H}_\infty$  optimal control.

### 2.1 Signals

One of the ways by which the performance of a given control system is described is in terms of the *size* of certain signals of interest. For instance, minimising the size of error signal in a feedback system is essential to solve the problem of reference tracking and tracking performance is judged by the size of the error signal. Signals are defined as a mapping of the time variable,  $t \in [0, \infty)$ , to a vector space  $\mathbb{R}^n$  [27] and this mapping represents at each time instant, a *vector*

$$x(t) = \begin{bmatrix} x_1(t) & x_2(t) & \cdots & x_n(t) \end{bmatrix}^T \quad (2.1)$$

For the above vector signal  $x$ , its length, or distance from the origin, is given by

$$\|x(t)\| = \sqrt{x_1(t)^2 + x_2(t)^2 + \cdots + x_n(t)^2} \quad (2.2)$$

This length is also known as the *Euclidean distance* and the associated norm is known as the *Euclidean norm* and is represented by the square root of the inner product of the vector and itself,

$$\|x(t)\| = \sqrt{x(t)^T x(t)} \quad (2.3)$$

where  $x(t)^T$  denotes the transpose of  $x(t)$ . Notice that the Euclidean norm only measures the size of signal point-wise in time and to get some idea of the size of the signal across all time, there is a need to introduce other concepts. The norms of interest within the scope of this study is the class of  $\mathcal{L}_p$  norms which, for a Lebesgue measurable signal  $x(t)$  and integers  $p \in [1, \infty)$ , are defined by

$$\|x(t)\|_p = \left( \int_0^\infty |x(t)|^p dt \right)^{1/p} \quad (2.4)$$

The vector signals for which the above norm is finite is said to belong to the linear signal space  $\mathcal{L}_p$  that is defined as [20]

$$\mathcal{L}_p = \left\{ x \in \mathbb{R}^n \mid \|x\|_p < \infty \right\} \quad (2.5)$$

The  $\mathcal{L}_2$  norm is a special case of the  $\mathcal{L}_p$  norm and is the specific signal norm used in  $\mathcal{H}_\infty$  control theory. The  $\mathcal{L}_2$  signal space consists of the signals that have a finite  $\mathcal{L}_2$  norm and is defined as

$$\mathcal{L}_2 = \left\{ x \in \mathbb{R}^n \mid \|x\|_2 < \infty \right\} \quad (2.6)$$

Noting Equation (2.4) the  $\mathcal{L}_2$  norm of a signal is given by

$$\|x(t)\|_2 = \left( \int_0^\infty \|x(t)\|^2 dt \right)^{1/2} = \left( \int_0^\infty \sum_{i=1}^n x_i(t)^2 dt \right)^{1/2} \quad (2.7)$$

A useful interpretation of  $\mathcal{L}_2$  norm is that  $\|x(t)\|_2^2$  represents the total “energy” associated with the signal  $x(t)$ . A special property of the  $\mathcal{L}_2$  norm is given by Parseval’s theorem which states, that the  $\mathcal{L}_2$  norm of the signal in time domain is equal to the  $\mathcal{L}_2$  norm in frequency domain, i.e.

$$\|x(t)\|_2 = \|\hat{x}(jw)\|_2 = \left( \frac{1}{2\pi} \int_{-\infty}^\infty \|\hat{x}(jw)\|^2 dw \right)^{1/2} = \left( \frac{1}{2\pi} \int_{-\infty}^\infty \hat{x}(jw)^* \hat{x}(jw) dw \right)^{1/2} \quad (2.8)$$

where  $\hat{x}(jw)$  is the Fourier transform of the signal  $x(t)$  and  $\hat{x}(jw)^*$  is the complex conjugate transpose of  $\hat{x}(jw)$ .

## 2.2 Systems

A system  $\mathcal{G}$  is defined as a mapping of one signal space,  $\mathcal{U}$ , to another signal space,  $\mathcal{Y}$  [27].

$$\mathcal{G} : \mathcal{U} \mapsto \mathcal{Y} \quad (2.9)$$

Thus, for a given input  $u(t) \in \mathcal{U}$ , the output  $y(t) \in \mathcal{Y}$  is written as  $y(t) = \mathcal{G}u(t)$ . This system is called *time-invariant* if a time shift in the input signal also produces a time shift in the output signal.

$$y(t - \tau) = \mathcal{G}u(t - \tau) \quad (2.10)$$

System  $\mathcal{G}$  is defined *causal* if its current output  $y(t)$  is a function of the present,  $u(t)$ , and the past inputs,  $u(\tau)$  (where  $\tau < t$ ).

$$y(t) = 0, \quad \tau > t \quad (2.11)$$

$\mathcal{G}$  is defined *linear* if, for all  $u_1(t), u_2(t) \in \mathcal{U}$  and a positive real scalar  $\alpha$ , it satisfies both the superposition (Equation (2.12)) and homogeneity (Equation (2.13)) properties.

$$\mathcal{G}(u_1(t) + u_2(t)) = \mathcal{G}u_1(t) + \mathcal{G}u_2(t) \quad (2.12)$$

$$\mathcal{G}(\alpha u_1(t)) = \alpha \mathcal{G}(u_1(t)) \quad (2.13)$$

The above linear time-invariant (LTI) system could also be represented as a convolution integral

$$y(t) = \int_0^t g(t - \tau)u(\tau)d\tau \quad (2.14)$$

where  $g(t - \tau)$  is time shifted impulse response of the system  $\mathcal{G}$ . Linear systems could be expressed as a function in the Laplace variable ' $s$ ' known as the *transfer function*. This transfer function is obtained by taking Laplace transforms of the integral in equation 2.14.

$$y(s) = \mathcal{G}(s)u(s) \quad (2.15)$$

Systems that are described by linear differential equation are often represented in state space form as

$$\begin{aligned} \dot{x}(t) &= A(t)x(t) + B(t)u(t) \\ y(t) &= C(t)x(t) + D(t)u(t) \end{aligned} \quad (2.16)$$

Also, as  $\mathcal{G}$  is assumed to be linear time-invariant then the above matrices are constant and the transfer function matrix of the system is obtained by evaluating

$$\mathcal{G}(s) = D + C(sI - A)^{-1}B \quad (2.17)$$

However, real control applications can rarely be represented as linear systems as most of them, if not all, are *nonlinear*. A given system is said to be nonlinear if the mapping  $\mathcal{G} : \mathcal{U} \mapsto \mathcal{Y}$  does not satisfy either the superposition or the homogeneity properties, i.e.

$$\mathcal{G}(\alpha u_1(t) + \beta u_2(t)) \neq \alpha \mathcal{G}u_1(t) + \beta \mathcal{G}u_2(t) \quad (2.18)$$

for all scalars  $\alpha, \beta$  and for all  $u_1(t), u_2(t) \in \mathcal{U}$  [27]. The input-output behaviour of a nonlinear system can usually be represented as a set of differential equations

$$\begin{aligned} \dot{x}(t) &= f(x, u, t) \\ y(t) &= g(x, u, t) \end{aligned} \quad (2.19)$$

Linearity of a system could also be assessed by checking whether the above set of differential equations could be realised to the form shown in Equation (2.16).

Now, the size of a given linear system defined by  $\mathcal{G} : \mathcal{U} \mapsto \mathcal{Y}$  is rather difficult to define, especially if it is a multivariable system (i.e. either  $\mathcal{U}$  or  $\mathcal{Y}$  has a greater dimension than unity). In  $\mathcal{H}_\infty$  methodology, the size is defined by the norms that are dependent on the class of inputs  $\mathcal{U}$  and the norms for the signals  $u(t) \in \mathcal{U}$ . A different class of inputs or different norms on the input signals result in different operator norms of  $\mathcal{G}$ . This type of norm is called the *induced norm* and it has the interpretation of the maximal “energy gain” of the mapping  $\mathcal{G} : \mathcal{U} \mapsto \mathcal{Y}$ . If it is assumed that  $\mathcal{G}$  is a stable LTI system in the sense that bounded inputs produce bounded outputs, then by the following condition

$$\mathcal{G} : \mathcal{L}_p \mapsto \mathcal{L}_p \quad (2.20)$$

where  $p \in [1, \infty)$ , the  $\mathcal{L}_p$  induced norm for  $\mathcal{G}$  is defined by [15]

$$\|\mathcal{G}\|_{(i,p)} := \sup_{u \in \mathcal{L}_p} \frac{\|\mathcal{G}(u)\|_p}{\|u\|_p} \quad (2.21)$$

An important special case that is derived under the following condition

$$\mathcal{G} : \mathcal{L}_2 \mapsto \mathcal{L}_2 \quad (2.22)$$

is the induced  $\mathcal{L}_2$  norm, which is defined by [15]

$$\|\mathcal{G}\|_{(i,2)} := \sup_{u \in \mathcal{L}_2} \frac{\|\mathcal{G}(u)\|_2}{\|u\|_2} \quad (2.23)$$

Induced  $\mathcal{L}_2$  norm (also known as the  $\mathcal{H}_\infty$  norm) can also be defined as [20]

$$\|\mathcal{G}\|_{(i,2)} := \|\mathcal{G}\|_\infty := \sup_{w \in [0, \infty]} \bar{\sigma} [\mathcal{G}(jw)] \quad (2.24)$$

where  $\bar{\sigma} [\mathcal{G}(jw)]$  represents the maximum singular value of  $\mathcal{G}(jw)$ , where  $\mathcal{G}(jw)$  represents the frequency response function of  $\mathcal{G}$ . Also, if the induced  $\mathcal{L}_2$  norm is well defined, i.e.  $u \in \mathcal{L}_2$  then  $y \in \mathcal{L}_2$ , the system is then said to be *finite gain  $\mathcal{L}_2$  stable*. The  $\mathcal{H}_\infty$  norm of a stable LTI system can be read directly from its singular value plot, and in the SISO case it is simply equal to the peak value of the Bode magnitude plot (Equation (2.25)). Also, minimisation of the  $\mathcal{H}_\infty$  norm of a system corresponds to minimising the energy of the worst case output signal vector. In other words, the output energy is minimised over all non-zero finite energy input signals.

$$\|\mathcal{G}\|_\infty := \sup_{w \in [0, \infty]} |\mathcal{G}(jw)| \quad (2.25)$$

### 2.3 $\mathcal{H}_\infty$ optimal control

The above discussion naturally leads to the topic of robust optimisation as signal and system norms are highly involved in both design and analysis of robust optimal controllers. Most, if not all, engineering systems are always subjected to external disturbances. Also, dynamical differences between the actual system and the model lead to the presence of uncertainty in even the most sophisticated of mathematical representation. Researchers have always been interested in designing a controller for a system that is not only able to stabilise the system but also is able to deliver certain robustness and performance guarantees in the presence of these disturbances and uncertainties [28]. Historically, robustness had been judged by ensuring good gain and phase margins, however, these concepts were mainly applicable for decoupled SISO systems and did not always provide useful information about coupled multi-input-multi-output (MIMO) systems. Initial MIMO design techniques included methods

such as LQG that had placed more emphasis on the system performance than robustness. While this approach still remains widely used today, in the early 1980s the control system literature started to change as both theory and practice noticed the limitations of the LQ approach [83]. This spurred the researchers to develop theories that could deal with the issue of uncertainty directly during the feedback design stage and this led to the development of the theory known as  $\mathcal{H}_\infty$  optimal control. The breakthrough in the study of  $\mathcal{H}_\infty$  optimal control was made by [96] and [97] who tackled a SISO disturbance rejection problem by minimising the  $\infty$ -norm of the sensitivity function. Despite the emergence of this methodology, it was not until the studies conducted by [16] and [25] that an efficient state space formulation was in place to solve this problem. The results in these studies showed that a  $\mathcal{H}_\infty$  optimal controller would exist if there existed a unique positive definite solution to two algebraic Riccati equations and the two solutions must also satisfy the spectral radius condition [84].

An overview of this particular methodology is presented in this section, however, prior to discussing the details it is important to discuss the two core concepts that form the backbone of  $\mathcal{H}_\infty$  optimal control - *Uncertainty Modelling* and *Small Gain Theorem*.

### 2.3.1 Uncertainty modelling

As mentioned previously, uncertainties are unavoidable in real control applications and these can normally be classified into two categories: *disturbance signals* and *dynamic perturbations* [11]. Disturbance signals are mainly caused by external factors and do not affect the system stability, whereas the dynamic perturbations represent discrepancies with the mathematical model and can dramatically affect the stability if not treated carefully. Robustness implies that a system can tolerate a level of uncertainty being present, without becoming unstable. There are several ways of describing uncertainty, and robustness to one type does not always guarantee robustness to another. The most commonly used models of system uncertainty are shown below, and in all of these cases  $G_0(s)$  represents the transfer function matrix corresponding to the nominal plant, i.e. a best estimate of the true plant behaviour and  $G_P(s)$  represents the transfer function matrix corresponding to the true plant.

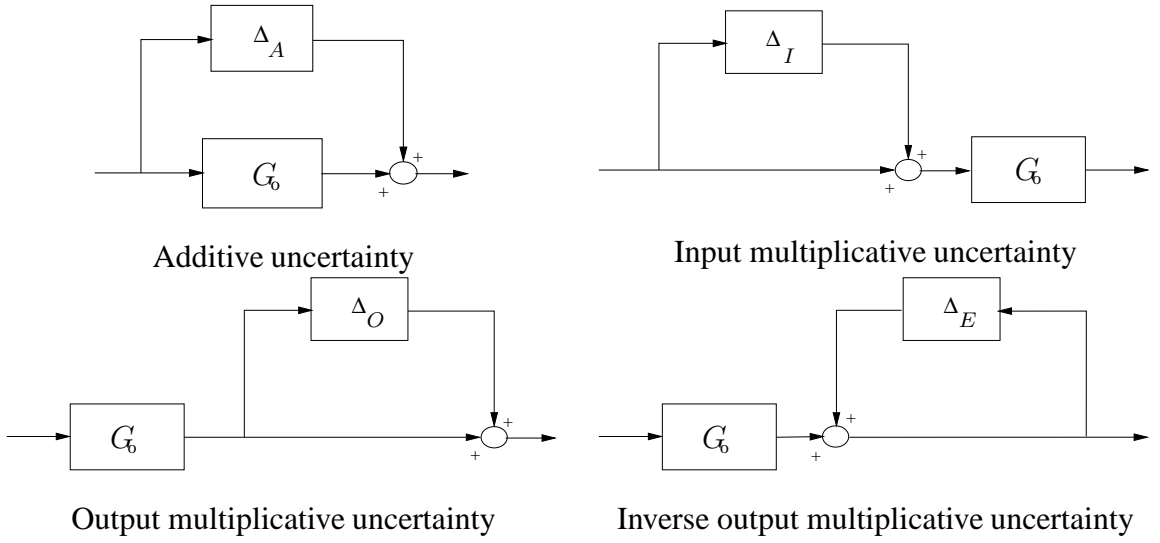


Figure 2.1: Common uncertainty representation [72]

$$G_P(s) = G_0(s) + \Delta_A(s) \quad (2.26)$$

$$G_P(s) = G_0(s) [I + \Delta_I(s)] \quad (2.27)$$

$$G_P(s) = [I + \Delta_O(s)] G_0(s) \quad (2.28)$$

$$G_P(s) = [I - \Delta_E(s)]^{-1} G_0(s) \quad (2.29)$$

$\Delta_A$  represents an *additive* uncertainty,  $\Delta_I$  an *input multiplicative* uncertainty,  $\Delta_O$  an *output multiplicative* uncertainty and  $\Delta_E$  represents *inverse output multiplicative* uncertainty. Additive uncertainty gives an account of absolute error between the actual dynamics and the nominal model, while the multiplicative represents the relative error. Such descriptions are generally classed as *lumped* uncertainty because they combine parametric variation and/or unmodelled dynamics combined into a single perturbation. Both, additive and multiplicative uncertainties, capture unmodelled dynamics and/or parametric variation to a reasonable level, however, they are mathematically problematic for capturing unstable perturbations

[72]. Also, with the Small Gain Theorem (details to follow) forming the basis of the results derived for these uncertainty types, it requires stability of these uncertainties. Thus restricting the class of uncertainty they represent.

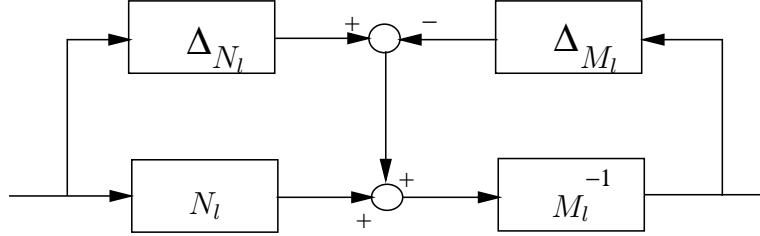


Figure 2.2: Coprime factor uncertainty configuration [72]

A solution to this is achieved by using the normalised coprime factorisation uncertainty description. This form is, at first glance, rather strange but is actually a more flexible way of representing uncertainty, especially those that arise in aerospace systems. This particular narrative will focus on the normalised *left* coprime factorisation as it leads directly to the chosen controller design methodology. Figure 2.2 depicts the left coprime factor uncertainty representation of a nominal plant,  $G_0 = M_l^{-1}N_l$  where  $M_l$  and  $N_l$  are *stable left coprime* factors of  $G_0$ .  $N_l$  is chosen to contain all the zeros of  $G_0$  with positive real parts, and  $M_l$  contains as zeros all the poles of  $G_0$  with positive real parts, thus ensuring stability of the two factors. These factors are also coprime because there are no common zeros between  $N_l$  and  $M_l$  which would result in pole-zero cancellations. The coprimeness of the above factors can also be assessed mathematically by showing the existence of stable transfer functions or matrices  $U_l$  and  $V_l$  that satisfy the following Bezout identity

$$N_l U_l + M_l V_l = I \quad (2.30)$$

Also important to note that satisfying the Bezout identity alone is not enough to guarantee uniqueness of a particular set of coprime factors. This individuality is only obtained by the so called *normalised* left coprime factorisation. The coprime factors,  $M_l$  and  $N_l$ , are said to be normalised if they also satisfy the following identity

$$M_l M_l^* + N_l^* N_l = I \quad (2.31)$$

where  $M_l^*$  and  $N_l^*$  are the complex conjugate transpose of  $M_l$  and  $N_l$  respectively. Numerically, for a nominal plant  $G_0$  that has the following state space realisation,

$$G_0 = \left[ \begin{array}{c|c} A_0 & B_0 \\ \hline C_0 & D_0 \end{array} \right] \quad (2.32)$$

the state space realisation (as shown in [86]) of the normalised left coprime factorisation is given by,

$$\left[ \begin{array}{c|c} N_l & M_l \end{array} \right] = \left[ \begin{array}{cc|c} A_0 + HC_0 & B_0 + HD_0 & H \\ \hline R^{-\frac{1}{2}}C_0 & R^{-\frac{1}{2}}D_0 & R^{-\frac{1}{2}} \end{array} \right] \quad (2.33)$$

where

$$H = -(B_0D_0^T + ZC^T)R^{-1}, R = I + D_0D_0^T$$

and  $Z$  is the unique positive definite solution to the algebraic Riccati equation

$$(A_0 - B_0S^{-1}D_0^TC)Z + Z(A_0 - B_0S^{-1}D_0^TC)^T - ZC_0^TR^{-1}C_0Z + B_0S^{-1}B_0^T = 0$$

and

$$S = I + D_0D_0^T$$

Now, for a system with normalised left coprime factorisation  $G_0 = M_l^{-1}N_l$ , the perturbed plant,  $G_P$ , is thus given by

$$G_P(s) = [M_l + \Delta_{M_l}]^{-1} [N_l + \Delta_{N_l}] \quad (2.34)$$

where  $\Delta_M$  and  $\Delta_N$  are stable unknown transfer function matrices. Also, coprime factorisation description has certain advantages that makes it ideally suited to represent uncertainties within helicopter systems.

1. It is evident from the definitions of additive and multiplicative uncertainty descriptions that these uncertainties must be *stable* matrices. They represent a set of plants where every perturbed plant has the same set of right half plane poles as the nominal plant. However, within a helicopter system a stable plant becoming open loop unstable due to parameter variation is a common occurrence and coprime factor uncertainty models are capable of modelling such variations [11].
2. Another phenomenon that is again quite common with helicopter systems is the case of lightly damped resonant poles. Using either additive or multiplicative type of description leads to either very large or unbounded uncertainty norms. Coprime factor uncertainty model allows sensible description of uncertainties that are caused due to this situation [11].

### 2.3.2 Small Gain Theorem

The Small Gain Theorem is an important element of  $\mathcal{H}_\infty$  optimal control due to its particular usefulness in studying stability of interconnected systems. Consider the system shown in Figure 2.3 that depicts a feedback interconnection of two systems,  $G_1$  and  $G_2$ . Suppose that both systems are finite gain  $\mathcal{L}_p$  stable, so that

$$\|y_1\| \leq \gamma_1 \|e_1\| \quad (2.35)$$

$$\|y_2\| \leq \gamma_2 \|e_2\| \quad (2.36)$$

where  $e_1, e_2 \in \mathcal{L}_p$  and

$$\|G_1\|_{i,p} = \gamma_1 \quad (2.37)$$

$$\|G_2\|_{i,p} = \gamma_2 \quad (2.38)$$

Also, suppose that the loop is well posed, i.e. for every pair of inputs  $u_1, u_2 \in \mathcal{L}_p$  there exists a unique output  $e_1, y_1, e_2, y_2 \in \mathcal{L}_p$ . The problem here is whether the feedback connection,

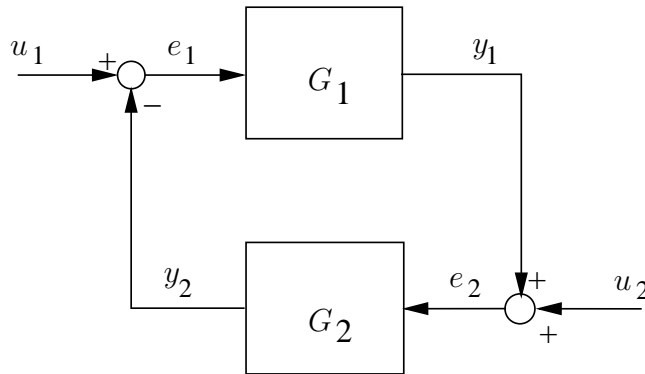


Figure 2.3: Small Gain Theorem [43]

when viewed as  $\begin{bmatrix} u_1 \\ u_2 \end{bmatrix} \mapsto \begin{bmatrix} y_1 \\ y_2 \end{bmatrix}$  is finite gain  $\mathcal{L}_p$  stable. The Small Gain Theorem gives a sufficient condition for finite gain  $\mathcal{L}_p$  stability of the feedback connection [43].

**Theorem 2.1** Small Gain Theorem: *The feedback connection in Figure 2.3 is finite gain  $\mathcal{L}_p$  stable if  $\gamma_1\gamma_2 < 1$ .*

The above feedback connection is often used to analyse feedback systems subject to model uncertainties where the nominal plant (closed loop plant dynamics) is well known and the uncertainty is not known, however the bounds on its norm are known.  $\mathcal{H}_\infty$  optimal control theory is devoted to the derivation of controllers which ensure that the  $\mathcal{H}_\infty$  norm of the closed loop system is small. Thus, making the closed loop system robust to as much uncertainty as possible.

### 2.3.3 $\mathcal{H}_\infty$ control problem

Systems that are subject to uncertain dynamic perturbations could be generalised into the standard  $M - \Delta$  configuration as illustrated in Figure 2.4, where  $M$  represents the stable nominal closed loop system which is dependent upon the particular problem to be solved, i.e. disturbance rejection, reference tracking, and  $\Delta$  represents norm bounded stable uncertainty [84]. The Small Gain Theorem effectively states that a given interconnection of two stable elements is stable if

$$\|M\|_\infty < \frac{1}{\|\Delta\|_\infty} \quad (2.39)$$

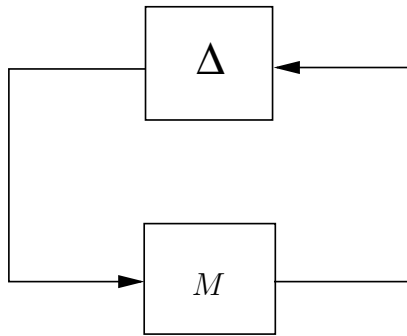


Figure 2.4:  $M - \Delta$  structure [72]

This inequality depicts an inverse relationship between the induced norms of the nominal closed loop system and the uncertainty and in order to maximise the norm bound of the uncertainty it is necessary to minimise the  $\mathcal{H}_\infty$  norm of the nominal closed loop system [84]. Accurate formulation of the control problem is critical for the correct functioning of the  $\mathcal{H}_\infty$  controller and it is useful to have a standard configuration into which any control problem could be manipulated and Figure 2.5 highlights the standard configuration as proposed by [16]. In this framework,  $P$  represents the generalised plant that includes the nominal plant (i.e. the system to be controlled) together with the weighting functions used to formulate the control problem (examples of this are shown later in the section).  $K$  is the controller designed at the nominal point that satisfies the design problem. The vector  $u$  represents the control signals to the generalised plant and the vector  $v$  includes the measured signals from the plant to the controller. The vector  $w$  represents the exogenous input vector (reference demand and disturbances). The vector signal  $z$ , represents the exogenous outputs and are the signals that are to be minimised and are selected to create performance and robustness objectives [72].

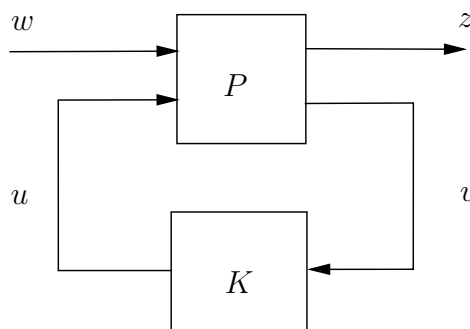


Figure 2.5: Standard feedback configuration [72]

The configuration shown in Figure 2.5 is described for all controllers  $K$  by,

$$\begin{bmatrix} z \\ v \end{bmatrix} = \left[ \begin{array}{c|c} P_{11} & P_{12} \\ \hline P_{21} & P_{22} \end{array} \right] \begin{bmatrix} w \\ u \end{bmatrix} \quad (2.40)$$

$$u = Kv \quad (2.41)$$

with a state-space realisation of  $P$  given by

$$P = \left[ \begin{array}{c|cc} A & B_1 & B_2 \\ \hline C_1 & D_{11} & D_{12} \\ C_2 & D_{21} & D_{22} \end{array} \right] \quad (2.42)$$

The closed loop transfer function matrix from  $w$  to  $z$  could be now described using the above relationships as

$$z = [P_{11} + P_{12}K(I - P_{22}K)^{-1}P_{21}]w \quad (2.43)$$

$$= F_l(P, K)w \quad (2.44)$$

$$= Mw \quad (2.45)$$

$F_l(P, K)$  is called the lower *linear fractional transformation* (LFT) of  $P$  and  $K$  and the  $\mathcal{H}_\infty$  optimal control problem is defined by

**Problem 2.1 ( $\mathcal{H}_\infty$  optimal control)** Find a stabilising controller  $K$  which minimises the  $\mathcal{H}_\infty$  norm of the closed loop system,  $F_l(P, K)$ .

$$\gamma_{min} = \min_K \|F_l(P, K)\|_\infty \quad (2.46)$$

This controller,  $K$ , is said to be optimum if it achieves the minimum value of  $\|F_l(P, K)\|_\infty$  i.e.,  $\gamma_{min}$ . However, this direct minimisation turns out to be a difficult problem, and in practice it is often sufficient to obtain a sub-optimal controller [72] and this problem is given as

**Problem 2.2 ( $\mathcal{H}_\infty$  sub-optimal control)** For a given  $\gamma > \gamma_{min}$ , to find a stabilising controller  $K$  which ensures

$$\|F_i(P, K)\|_\infty < \gamma \quad (2.47)$$

The solution to this problem could be achieved by using functions that are available in the MATLAB robust control toolbox [9], that utilises the algorithm proposed by [16, 25] that is based upon deriving the solutions of two algebraic Riccati equations. This solution yields a family of stabilising controllers that satisfies Equation (2.47) for some designer chosen value of  $\gamma$ . However, for the correct functioning of the optimisation process, certain assumptions are required about the generalised plant,  $P$ , and a detailed explanation of these assumptions and their significance is presented in [72]. More advanced solutions, such as the LMI based algorithm [24, 73], are also available that allow for some of these assumptions to be relaxed. Also, sensibly posed control problems generally tend to satisfy these assumptions and this shows that it is critical to pose the feedback problem correctly. The  $\mathcal{H}_\infty$  control synthesis algorithm provides  $\gamma$  iteration using the bisection method on the given value of  $\gamma$  in an effort to approach the optimal  $\mathcal{H}_\infty$  controller [25]. The iteration process checks the following conditions, explained in detail by [16, 25], to establish the success of a given  $\gamma$ :

1. There exists positive definite solutions to the two algebraic Riccati equations, i.e.

(a)  $\exists X \geq 0$  that solves the algebraic Riccati equation

$$A^T X + X A + C_1^T C_1 + X (\gamma^{-2} B_1 B_1^T - B_2 B_2^T) X = 0 \quad (2.48)$$

such that  $\text{Re } \lambda_i [A + (\gamma^{-2} B_1 B_1^T - B_2 B_2^T) X] < 0, \forall i$

(b)  $\exists Y \geq 0$  that solves the algebraic Riccati equation

$$A Y + Y A^T + B_1^T B_1 + Y (\gamma^{-2} C_1^T C_1 - C_2^T C_2) Y = 0 \quad (2.49)$$

such that  $\text{Re } \lambda_i [A + Y (\gamma^{-2} C_1^T C_1 - C_2^T C_2)] < 0, \forall i$

2. Spectral radius condition is satisfied, i.e.  $\rho(XY) < \gamma^2$

where  $\rho$  is the spectral radius ( $\rho(A) = \max_i |\lambda_i(A)|$ )

The outcome of the algorithm is usually a sub-optimal controller that is of the same order as the generalised plant,  $P$ . Thus far the discussion has presented the  $\mathcal{H}_\infty$  optimal control problem in a general setting. The focus will now be shifted towards two very commonly applied  $\mathcal{H}_\infty$  controller design methods:

1. Mixed sensitivity
2. Loop shaping

### Mixed sensitivity

For a given LTI plant,  $G$ , and a linear stabilising controller,  $K$ , the mixed sensitivity  $\mathcal{H}_\infty$  control problem involves the shaping of closed loop transfer functions such as the sensitivity function,  $S = (I + GK)^{-1}$ , along with one or more closed loop transfer functions such as the cosensitivity function,  $T = I - S$ , or  $KS$ . The selection of closed loop transfer functions along with the formulation of the generalised plant  $P$  and inclusion of signals in  $z(t)$  and  $w(t)$  are dependent on the specified design objectives [11, 72]. The illustration in Figure 2.6 considers one such formulation that looks at a general stacked  $S/T/KS$  problem where the aim is to bound  $\bar{\sigma}(S)$  for *disturbance rejection and command tracking*,  $\bar{\sigma}(T)$  for *robustness* and to reduce *sensitivity to noise*, and  $\bar{\sigma}(KS)$  to *penalise large control inputs* and to *provide robustness* with weighting function  $W_S$ ,  $W_T$  and  $W_{KS}$  respectively. Further to this, specifications based on the type of unstructured uncertainty (additional or input/output multiplicative) are also added. The  $\mathcal{H}_\infty$  optimal problem for this illustration is then to find a stabilising  $K$  which *minimises* the cost function,  $F_l(P, K)$

$$\|F_l(P, K)\|_\infty = \left\| \left[ \begin{array}{c} W_S S \\ W_T T \\ W_{KS} KS \end{array} \right] \right\|_\infty \quad (2.50)$$

where the generalised plant  $P$  from  $\begin{bmatrix} w & u \end{bmatrix}^T$  to  $\begin{bmatrix} z & v \end{bmatrix}^T$  has the following form

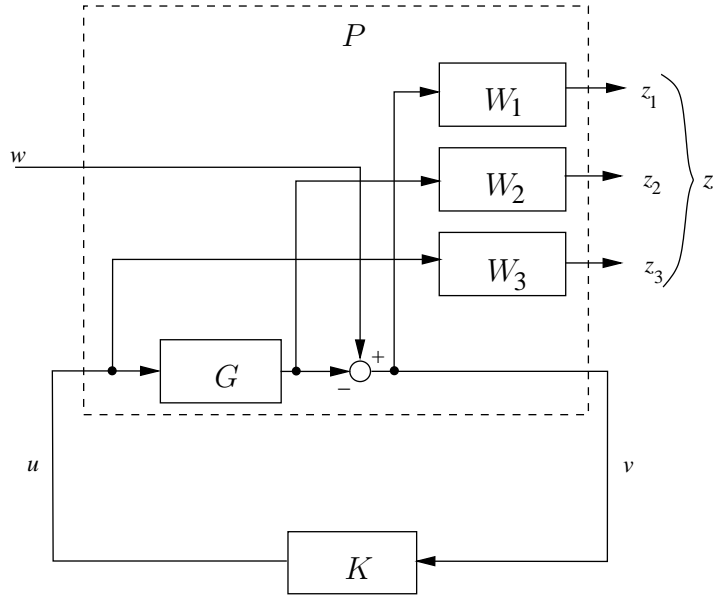


Figure 2.6: S/T/KS mixed sensitivity problem [72]

$$P = \left[ \begin{array}{c|c} W_S & -W_S G \\ 0 & W_T G \\ 0 & W_{KS} \\ \hline I & -G \end{array} \right] \quad (2.51)$$

The process of designing controller using the  $\mathcal{H}_\infty$  mixed sensitivity method revolves around iteratively modifying the weighting functions in order to shape the required closed loop transfer functions. It can be difficult to simultaneously satisfy all of the design requirements, however, this happens to be a fundamental nature of feedback design which involves managing trade-offs between conflicting design objectives. For example, disturbance rejection and command tracking generally requires  $\bar{\sigma}(S) \approx 0$ , reduction of control signal requires  $\bar{\sigma}(KS) \approx 0$  and attenuation of measurement noise requires  $\bar{\sigma}(T) \approx 0$ . In practice, this problem is made easier by the fact that different objectives are important over different frequency ranges. The situations where the three term cost function is needed are uncommon and in most, if not all, of the cases the design specifications could be satisfied using a two term cost function, e.g.  $S/KS$ ,  $S/T$  or  $T/KS$ , and the selection of weights is considered comparatively easier as the frequency requirements are usually complementary in principle. Therefore, simple and stable low and high pass filters are often sufficient to carry out the required shaping over frequencies [11]. This method has also been successfully applied to

the helicopter control problem in the past, see for example [84, 85, 88, 91].

## Loop shaping

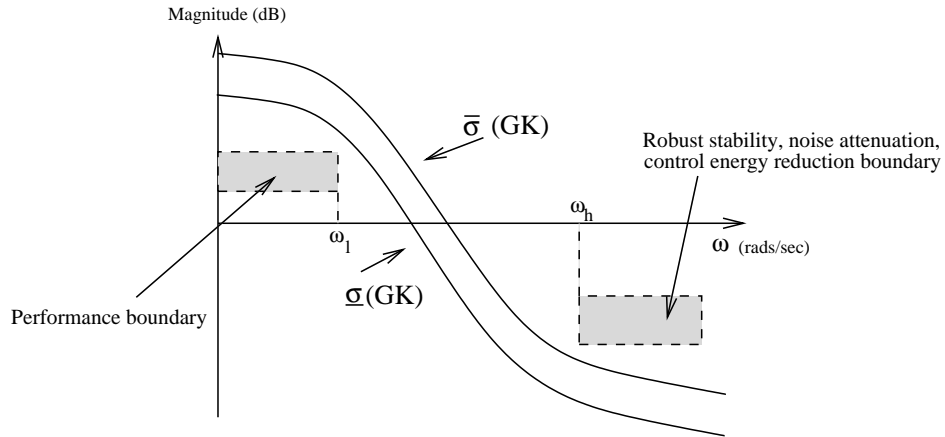


Figure 2.7: Design specification for singular values of  $GK$  [72]

This methodology combines classical loop shaping with  $\mathcal{H}_\infty$  optimisation and this was first introduced by [52]. This method has subsequently been developed and applied to a wide number of aerospace applications, see for example [10, 22, 37, 44, 63, 71, 75] and other non-aerospace applications, such as [80, 81]. Tuning is normally quite straightforward with this approach as it relies on the designer shaping the open loop singular values in a similar manner to the way the frequency response is shaped in classical control. Also, it allows robust stabilisation against normalised coprime factor uncertainty which is described earlier as a highly comprehensive uncertainty description. Frequency dependent trade-offs are applied to the required shape of the open loop singular values of  $GK$  as shown in Figure 2.7. Here, in a similar manner to the mixed sensitivity approach, requirements such as disturbance rejection and reference tracking are important at frequencies below the bandwidth frequency  $\omega_B$ , while noise attenuation and control signal reduction are more significant at frequencies above the bandwidth frequency [72]. These specifications are satisfied by shaping the singular values of the open loop transfer function so that  $\underline{\sigma}(GK)$  (minimum singular value) has a high gain at frequencies below  $\omega_l$  and  $\overline{\sigma}(GK)$  (maximum singular value) has a low gain at frequencies above  $\omega_h$ . Also desired are roll off rates of approximately  $20\text{dB}/\text{decade}$  at the desired bandwidth and higher rates of  $40\text{dB}/\text{decade}$  at higher frequencies in order to achieve a well damped closed-loop system. The shaping appears to be simpler here as it only

involves manipulation of open loop singular values, however, shaping the open loop singular values does not guarantee closed loop stability [53]. The approach adopted in  $\mathcal{H}_\infty$  loop shaping method is to first shape the singular values of  $G$  using a pair of pre ( $W_1$ ) and post ( $W_2$ ) compensator matrices to satisfy performance objectives without explicitly considering the issue of closed loop stability. The next stage of the  $\mathcal{H}_\infty$  loop shaping procedure involves using  $\mathcal{H}_\infty$  optimisation to compute the controller block  $K_\infty$  which robustly stabilises the shaped plant  $G_s = W_2GW_1$  against coprime factor uncertainty.

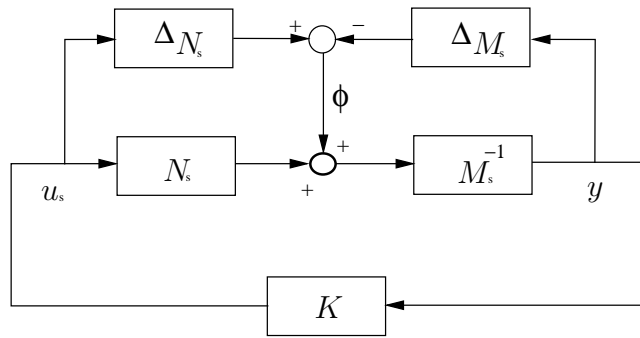


Figure 2.8: 1DOF loop shaping problem [72]

### 1DOF loop shaping

Now, the given shaped plant transfer function matrix  $G_s$  can be factorised to a pair of left-coprime transfer function matrices  $M_s$  and  $N_s$  such that  $G_s = M_s^{-1}N_s$  where  $M_s$  and  $N_s$  satisfy the normalisation equation  $M_sM_s^T + N_sN_s^T = I$  [52]. In  $\mathcal{H}_\infty$  loop shaping, the robustness of the system is measured with respect to perturbations of these coprime factors and the perturbed uncertain plant is represented as

$$G_p = [M_s + \Delta_{M_s}]^{-1} [N_s + \Delta_{N_s}]$$

As  $\Delta_{M_s}$  and  $\Delta_{N_s}$  (Figure 2.8) are assumed to be stable (hence bounded in their  $\mathcal{H}_\infty$  norm), and the Small Gain Theorem can be applied here. It then follows that an optimal robust controller is one that maximises the level of this type of uncertainty which can be tolerated before instability. It should be emphasized that although this type of uncertainty seems somewhat abstract, many common types of uncertainty (additive, multiplicative, etc.) can be interpreted in this manner and therefore, gives this representation a great deal of practical sense.

The complete class of perturbed plants,  $G_p$ , for the above uncertainty description is given by

$$G_p = \{(M_s + \Delta_{M_s})^{-1} (N_s + \Delta_{N_s}) : \|[\Delta_{N_s} \Delta_{M_s}]\|_\infty < \epsilon\}$$

and the objective of robust stabilisation is to stabilise this particular class. Now, the maximum of  $\epsilon$ ,  $\epsilon_{max}$ , that represents the largest possible class of such systems [52] and is given by

$$\gamma_{min} = \inf_K \left\| \begin{bmatrix} K (I - GK)^{-1} M^{-1} \\ (I - GK)^{-1} M^{-1} \end{bmatrix} \right\|_\infty \leq \frac{1}{\epsilon_{max}} \quad (2.52)$$

where  $\gamma_{min}$  is the stability margin and it should be noted that it is also the  $\mathcal{H}_\infty$  norm of the transfer function matrix from  $\phi$  to  $\begin{bmatrix} u_s & y \end{bmatrix}^T$  in Figure 2.8.

As this is a 1DOF design procedure, the controller may find it difficult to robustly stabilise and deliver adequate performance simultaneously. Although, for good command tracking a constant pre-filter could be implemented, however, there are many situations where a separate dynamic pre-filter is needed - hence came the inspiration for 2DOF loop-shaping.

## **2DOF loop shaping**

The original work of [52] focused on maximising robustness with respect to coprime factors type of uncertainty while also deriving bounds on the size which could be tolerated such that when the  $\mathcal{H}_\infty$  controller,  $K$ , was inserted into the open-loop, the singular values remained roughly the same as originally shaped by the designer. As it is well known that 2DOF controllers are able to give substantially better reference tracking performance without affecting robust stability or the feedback loop properties, [48] proposed a 2DOF loop shaping control structure in which the original robust stabilisation of [52] was augmented with an extra objective - minimisation of the  $\mathcal{H}_\infty$  norm of the transfer function representing the ideal closed-loop response of the system proposed by a reference model,  $T_{ref}$ , and the *actual* closed-loop response. The block diagram under consideration is shown in Figure 2.9. In this scenario, the optimal  $\mathcal{H}_\infty$  controller  $K_\infty = [K_1 \ K_2]$  for the shaped plant  $G_s = W_2 G W_1$ , with

a normalised coprime factorisation, is obtained by minimising the  $\mathcal{H}_\infty$  norm of the transfer function from  $\begin{bmatrix} r & \phi \end{bmatrix}^T$  to  $\begin{bmatrix} u_s & y & e \end{bmatrix}^T$ ,

$$\begin{bmatrix} u_s \\ y \\ e \end{bmatrix} = \begin{bmatrix} \rho(I - K_2 G_s)^{-1} K_1 & K_2(I - G_s K_2)^{-1} M_s^{-1} \\ \rho(I - G_s K_2)^{-1} G_s K_1 & (I - G_s K_2)^{-1} M_s^{-1} \\ \rho^2[(I - G_s K_2)^{-1} G_s K_1 - T_{ref}] & \rho(I - G_s K_2)^{-1} M_s^{-1} \end{bmatrix} \begin{bmatrix} r \\ \phi \end{bmatrix} \quad (2.53)$$

This problem could be formulated into the standard  $\mathcal{H}_\infty$  optimal control configuration (Figure 2.5) with the signal vectors  $\begin{bmatrix} w & u \end{bmatrix}^T$  and  $\begin{bmatrix} z & v \end{bmatrix}^T$  represented by  $\begin{bmatrix} r & \phi & | & u_s \end{bmatrix}^T$  and

$\begin{bmatrix} u_s & y & e & | & \beta & y \end{bmatrix}^T$  respectively. The generalised plant  $P$  is then defined as

$$P = \left[ \begin{array}{cc|c} 0 & 0 & I \\ 0 & M_s^{-1} & G_s \\ -\rho^2 T_{ref} & -\rho^2 M_s^{-1} & \rho G_s \\ \hline \rho I & 0 & 0 \\ 0 & M_s^{-1} & G_s \end{array} \right] \quad (2.54)$$

In this configuration,  $\rho$  is a scalar parameter that allows the designer to trade off between a pure robustness problem where  $\rho = 0$  (1DOF) and a model matching problem where  $\rho > 0$ . At  $\rho = 0$  the generalised plant from  $\begin{bmatrix} \phi & | & u_s \end{bmatrix}^T$  to  $\begin{bmatrix} u_s & y & | & y \end{bmatrix}^T$  reduces to

$$P = \left[ \begin{array}{c|c} 0 & I \\ M_s^{-1} & G_s \\ \hline M_s^{-1} & G_s \end{array} \right] \quad (2.55)$$

Now, the main steps of this design procedure are (as described in [72]):

1. Selection of the reference model,  $T_{ref}$ . This is typically chosen such that the reference model represents close to “ideal” behaviour.
2. Augmentation of the plant  $G$  by a pre-compensator,  $W_1$ , and a post-compensator,  $W_2$ , which are used by the designer to shape the open-loop singular values to the desired shape, i.e.

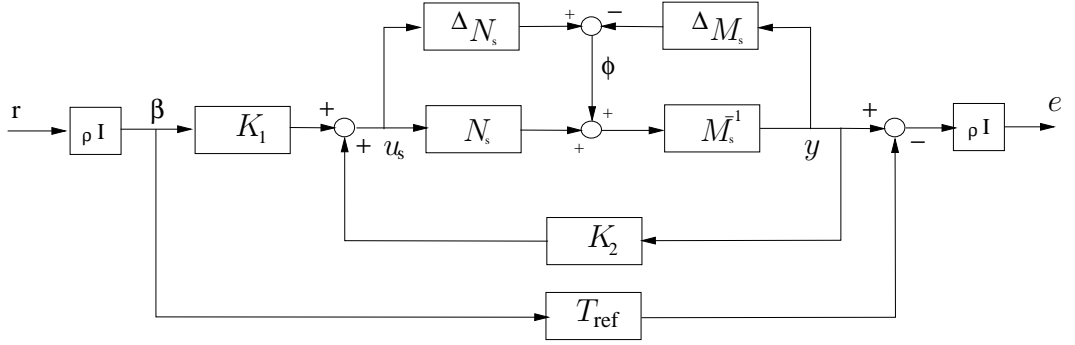


Figure 2.9: 2DOF loop shaping problem [72]

3. Synthesis of an optimal stabilising controller,  $K_\infty = [K_1 \ K_2]$  which minimises the  $\mathcal{H}_\infty$  norm of the transfer function, as given by Equation 2.53, associated with the closed-loop system's robust stability and performance. The controller is obtained using the 2DOF  $\mathcal{H}_\infty$  synthesis MATLAB code given in [72].

Once the  $\mathcal{H}_\infty$  controller,  $K_\infty$  has been constructed, the actual controller used for implementation has to be recovered. In the 2DOF case, the actual controller is obtained by incorporating the shaping functions into the controller and is given by

$$K = W_1 \begin{bmatrix} K_1 & K_2 W_2 \end{bmatrix}$$

### Advantages of 2DOF loop shaping approach

One of the major advantages of this method over the 1DOF loop shaping approach is the enhanced model matching properties ( $T_{ref}$ ), that gives the designer the power to specify an ideal response for the helicopter. Also, loop shaping methods are advantageous over the mixed sensitivity approach as it offers a clearer management of conflicting specifications, mainly around the crossover region, as the designer is only required to select weighting functions for the open loop plant that simultaneously shapes both the sensitivity and cosensitivity functions, thus avoiding the possibility of conflicting weights. Moreover, as this method maximises robustness to normalised coprime factor uncertainty, it provides robustness against unstable perturbations that are common to helicopter applications. Using coprime factor uncertainty also enables the controller to provide similar robustness and performance properties at both the plant input and output, whereas the mixed sensitivity approach

(that uses either the additive or multiplicative uncertainty description) provides robustness to either the plant input or the output [11]. These factors proved influential in making 2DOF loop shaping method an ideal choice for the FA controller design in this study.

## **2.4 Conclusion**

$\mathcal{H}_\infty$  optimal control problem was presented along with the two most commonly applied strategies to solve this - mixed sensitivity and loop shaping. The advantages of loop shaping method over mixed sensitivity approach, especially in terms of handling uncertain and multivariable systems, were also highlighted. Next chapter will review helicopter flight from a control theoretic perspective and justify the need for robust controller design methods within helicopters.

# Chapter 3

## Helicopter control problem

This chapter describes the three highly coupled pilot inputs that are utilised during helicopter flight and control. An in depth discussion about helicopter aerodynamics and modelling [61] is, however, beyond the scope of the current research and, although the author understands that they form a highly important component for ensuring that the controller delivers the precise performance, the dominant focus here is concerned with the design of automatic controllers for both FA and LA architectures. This chapter also presents the motivation for requiring an automatic control system along with the key factors that influence its design. Finally, the main elements of the ADS-33 handling qualities ratings specifications that are used to objectively quantify the controller's performance and stability are introduced.

### 3.1 Overview

Helicopters are highly nonlinear in nature and also exhibit inter-axis coupling modes that are dynamically unstable [83]. This requires the pilot to devote a large proportion of their time and attention to counter these modes, and controlling a helicopter thus becomes an extremely arduous task. The search for a solution to make this task easier has been a topic of research for many control engineers, but these intrinsic complexities have been a difficult obstacle to overcome [39, 69]. In the beginning, these solutions, for FA or LA systems, were based on single-loop-at-a-time classical control methods mainly due to their simplicity and ease of application and this is still the case with many helicopters (including the existing

EH101 LA control system). These solutions, however, did not decouple the interactions between the helicopter axes to a satisfactory level. Moreover, due to the requirement to meet the strict handling qualities criteria becoming more prominent in helicopter control design, there was a need to find more sophisticated solutions to this problem. Thus, over the last two decades or so, since the introduction of robust multivariable techniques and the improvements that these methods have shown within fixed-wing aircrafts study, helicopter control system design has received significant attention [84]. This led to a significant number of studies [6, 32, 46, 54, 89, 92, 94], that have successfully applied advanced methodologies to find a robust solution. However, most if not all, of the applications have been in the FA area and barring the study conducted by [85] there have not been other studies that have looked at the application of robust methods to the LA architecture. Hence, the aim of the study presented here is to expand the knowledge base of applying robust methods in LA architectures.

## 3.2 Helicopter flight

The EH101 helicopter has the most commonly observed helicopter configuration that utilises a horizontal propeller, called the *main rotor*, on the top of the aircraft that generates lift as it spins and a small rotor on its tail, called the *tail rotor*, that is used to balance the reaction torque produced by the main rotor. Modifying the inclination of the spinning main rotor allows the helicopter to *pitch* and *roll*. The relative difference in the torques generated by the main and tail rotor gives the helicopter a *yaw* motion. This basically means that the helicopter has four main types of motion: the three rotational degrees of freedom (pitch, roll, and yaw) and one vertical translation. From this it follows that in order to allow, in principle, each of these motions to be controlled independently, four control effectors are needed. In the helicopter, three of these control effectors are associated with the main rotor and motion is imparted through something known as the *swash plate* and the last degree of freedom is mainly controlled through the tail rotor. The control effectors available are

1. The *main rotor collective* lever or stick is located to the left of the pilot and this controls the main rotor collective actuator. The collective is used to change the main rotor

pitch at all points of the rotor blade rotation. The amount of movement (upwards or downwards) of the lever causes a simultaneous and equal change in blade inclination [4].

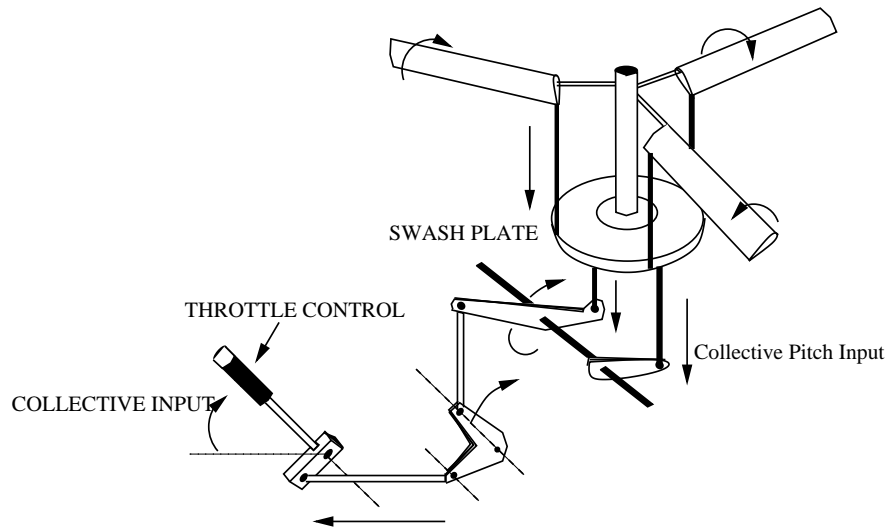


Figure 3.1: Collective control [5]

2. The *main rotor cyclic* controls the lateral and longitudinal cyclic actuators. The cyclic stick is mounted vertically from the cockpit floor, between the pilot's legs. It can be moved slightly in any direction from the vertical and with this control the pilot can move the helicopter in any direction horizontally - that is, for flying forward, aft, right or left. As the cyclic stick is moved in a given direction, the main rotor disc is tilted in the same direction causing movement of the helicopter in that direction. The tilt is achieved by altering the inclination of each blade in cycles, maximum-to-minimum-to-maximum, as the blade completes a full revolution [4].
3. Finally, the *tail rotor collective* control system is used to control the tail rotor collective actuator in order to - counter the torque produced by the main rotor and also to effect changes in heading (yaw). A set of pedals on the floor of the cockpit is used to produce this motion - right turn is produced when the right pedal is pushed down and similarly pushing down the left pedal produces a left turn [4].

The main problem with the open loop helicopter, from a control designer's perspective, is that the motions induced by the above three actuators are not independent as there is a significant

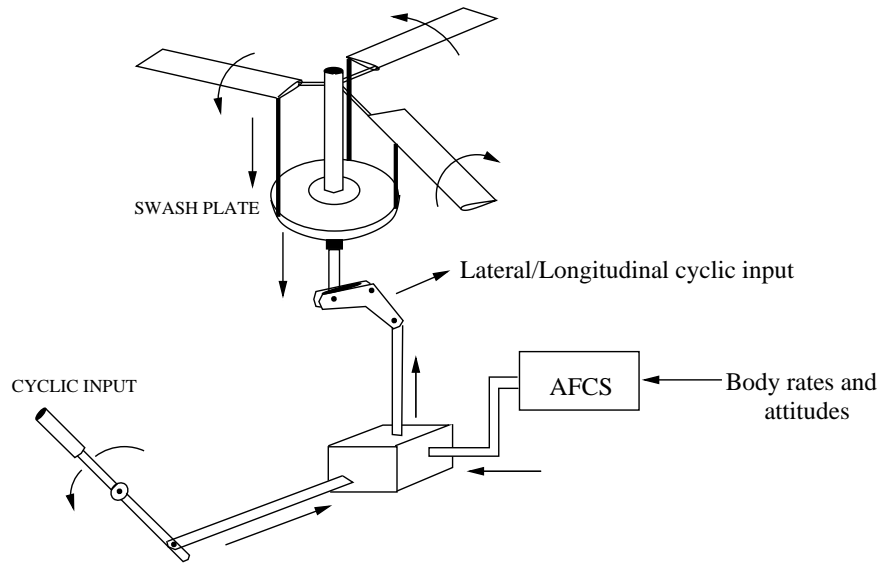
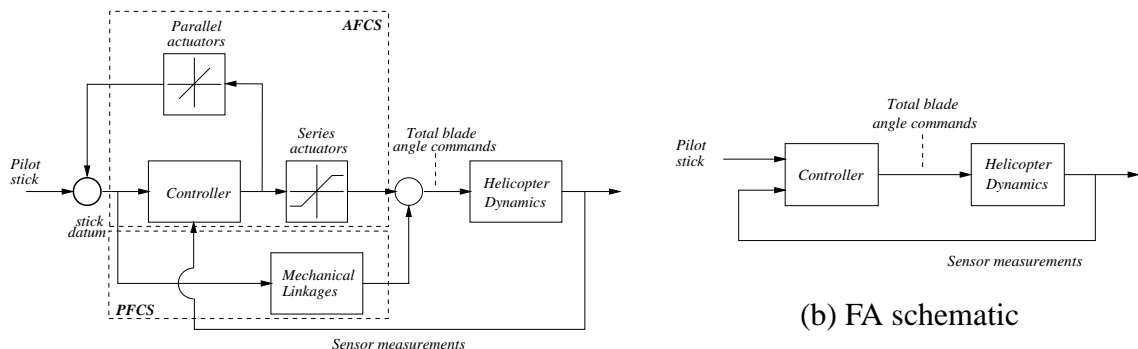


Figure 3.2: Cyclic control [5]

amount of coupling between the different open loop control channels. Helicopters are also open loop unstable, which means “hands-off” control is impossible in the open loop and that pilot workload is required to mainly stabilise the vehicle. Therefore, general opinion has it that, an efficient AFCS is required in order to efficiently manoeuvre a helicopter in a responsive fashion without excessive pilot workload.

### 3.3 Helicopter FCS architectures



(a) LA schematic

Figure 3.3: Helicopter flight control system architectures [84]

Traditionally, helicopters have utilised a LA control architecture, as shown in Figure 3.3(a), that features feed-forward mechanical linkages along with an electronic controller using

feedback for stability and control augmentation. The mechanical linkages connect the above cockpit controls directly to the swash plate actuation system. Augmentation of the basic handling qualities is then achieved through the electronic controller which provides the required command shaping and stabilisation. The control signals are often restricted by a limited authority/high rate *series* actuator (a typical example is shown in Figure 3.4) and in some architectures, including the one proposed in this study, a high authority/limited rate *parallel* actuators (a typical example is shown in Figure 3.5) are also included to prevent the premature saturation of series actuators [33] (a detailed discussion is provided Section 5.1). However, more recently designers have begun to favour the idea of giving the electronic controller greater authority. This leads to the notion of a FA control architecture, as shown in Figure 3.3(b), whereby the pilot demands are directly fed to the electronic controller, which in turn synthesises the appropriate collective and cyclic blade angle demands [84]. It is also believed that optimum handling qualities for all conditions are best achieved with the use of FA control architecture. However, as it would be sometime before all operational helicopters are upgraded to FA control systems there is an interim requirement for designing methods that would enable the functionality of a highly augmented FA control system to be sought within the structural bounds of the existing LA control architecture. This study goes some-way in presenting a possible solution to this problem.



Figure 3.4: Series Actuator [14]



Figure 3.5: Parallel Actuator [14]

### 3.4 Helicopter model

Whether the aim is to design either a FA or a LA controller, without a high fidelity helicopter model the design process is an extremely challenging problem. The complexities that are existent with the shape and motion of the helicopter impose difficulties while deriving a high quality model [29]. This complexity during modelling is relaxed by introducing some assumptions, such as constant moment of inertia, constant centre of gravity, constant rotor angular velocity and many more. Furthermore, the nonlinearities that are inherent to the helicopter due to variations in dynamics with changes to flight conditions and the cross-axis interactions between the four channels that are often poorly (theoretically) understood [51] add to the complexity of deriving a mathematical model. This, effectively, means that even the most sophisticated of models are subject to the presence of uncertainty [90] that would then predict inaccurate helicopter behaviour. These uncertainties are one of the main arguments that have advocated the usage of robust control methods to solve the helicopter control problem in the past and also during this study.

For this study, a highly comprehensive 38-state nonlinear model of the EH101 was made available. A 25-state linear model was obtained at various trim conditions using the linearisation routine provided by AgustaWestland. The linear model at the trim condition of 40kts/0ft/14200kg was further reduced to an 8-state model which then formed the basis for FA controller design because a lower order plant would result in a low order controller. This 8-state linearised model described a 6DOF rigid body motion of the helicopter and was further augmented with earth-axis attitudes (pitch ( $\theta$ ) and roll ( $\phi$ )) for attitude control. The model was expressed in the standard form as

Cockpit control	Axis influenced	Rotary movement	Translatory movement	Controlled variable
Main Rotor Collective	Vertical	NA	Heave ( $w$ )	NA
Longitudinal Cyclic	Longitudinal	Pitch rate( $q$ )	Longitudinal ( $u$ )	Pitch attitude ( $\theta$ )
Lateral Cyclic	Lateral	Roll rate( $p$ )	Lateral ( $v$ )	Roll attitude ( $\phi$ )
Tail Rotor Collective	Directional	Yaw rate( $r$ )	NA	Yaw rate ( $r$ )

Table 3.1: Helicopter structure overview

$$\begin{aligned} \dot{x} &= Ax + Bu \\ y &= Cx \end{aligned} \tag{3.1}$$

where the  $A, B$  and  $C$  matrices were obtained during the linearisation process. The state vector,  $x$ , consisted of rotational rate components ( $p, q, r$ ) and translational velocities ( $u, v, w$ ) together with pitch and roll attitude. The input vector,  $u$ , included the four cockpit controls. For the purpose of controller design, helicopters are thought of, roughly, as a four axis vehicle that exhibits a diagonally dominant structure. Each of the four inputs would primarily influence one of the axes as shown in Table 3.1 with significant interactions into the other channels [67] and not having an appropriate decoupling controller would result into poor helicopter behaviour and high pilot workload. Previous studies have indicated that pilots often prefer to control the vertical axis open-loop as the dynamics of this loop are fairly benign. Thus, within the scope of this study the EH101 helicopter system is sought as a  $3 \times 3$  system with the mathematical model featuring state variables, inputs and outputs as described in Table 3.2. Also, the states to be controlled are dependent on the control response type sought.

States	Description	Inputs	Description	Outputs	Description
$\theta$	Pitch attitude	$u_{ls}$	Longitudinal cyclic	$\theta$	Pitch attitude
$\phi$	Roll attitude	$u_{lc}$	Lateral cyclic	$\phi$	Roll attitude
$p$	Roll rate	$u_t$	Tail rotor collective	$r$	Yaw rate
$q$	Pitch rate				
$r$	Yaw rate				
$u$	Longitudinal velocity				
$v$	Lateral velocity				
$w$	Vertical velocity				

Table 3.2: Helicopter model variables

### 3.5 Control response types

Different environments and different mission types tend to require different response types from the helicopter [61]. The ADS-33 document [3] contains a detailed breakdown of these response types and the overlap between the mission types and response type.

1. *Attitude Command Attitude Hold (ACAH)*. In such a response type movement of the cyclic stick by a certain amount corresponds to a movement of helicopter attitude (i.e.  $\phi$  or  $\theta$ ) by a corresponding amount. For example, as the pilot pushes the cyclic stick forward a corresponding change in pitch attitude is expected and as the stick is centred the helicopter is expected to return to its attitude trim position.
2. *Rate Command Attitude Hold (RCAH)*. For this response type, the pilot commands rate instead of attitude and pilot's inputs should correspond to the helicopters rate being increased by a given amount. For example, if the pilot depresses the pedals (right or left) they expect to see a corresponding change in yaw rate. Also, when the pedals are released the rate is expected to fall to zero while maintaining the last attained attitude. A return to the attitude trim position is not expected.
3. *Translational Rate Command (TRC)*. In this response type cyclic stick movements control the lateral and forward velocities ( $u$  or  $v$ ) and is ideally useful while operating under poor flying conditions or when hovering close to ground or obstacles.

The controller designed in this study seeks to induce an ACAH type response in the longitudinal and lateral channels, and a RCAH type response in the directional channel.

### 3.6 Handling qualities

Although desktop simulations, especially the ones based upon nonlinear models, give a fairly comprehensive account of the controller's performance, in order to ascertain the success of a particular control strategy, controller designers refer to handling qualities returned by the pilot. Handling qualities represent "*the ease and precision by which a pilot is able to perform a given task*" [13] and it embodies more than just the dynamic response characteristics. Here, the pilot and the augmented rotorcraft combine to form a closed loop system which is driven by the piloting task and the above rating reflects both the accuracy in completing the task and the amount of effort required by the pilot in order to meet the necessary level of performance.

The ADS-33 document [3], US Army's Aviation System Command Specification, outlines the major criteria for handling qualities of rotorcrafts. This document meticulously specifies both qualitative (flight tests) and quantitative (desktop simulation) requirements and in addition defines the "levels" of performance. The pilot evaluation based on the qualitative ADS-33 criteria consists of two parts: pilot observational comments and pilot ratings. Comments are obtained by the pilots answering a series of structured questions regarding the controller's performance, and the pilot ratings are the end result of the evaluation process which associates a weight to the pilot comments (good or bad) and quantifies the overall performance quality. The Cooper-Harper scale [13] is one such quantitative weighting methodology and since its introduction in 1969, it has been used extensively during flight tests to quantify controller performance in terms of handling qualities ratings (HQRs). These ratings, in turn, are associated with different levels of performance as shown in Table 3.3. Controllers are designed to ideally achieve Level 1 rating that indicates a highly desirable performance which requires minimal, if any, amount of pilot effort (Cooper-Harper ratings between 1 and 3), however, many controllers struggle to achieve this level. Level 3, on the other hand, indicates a performance with major deficiencies and large amount of pilot effort is required to retain control (Cooper-Harper ratings between 7 and 9). Level 2 gives a measure of performance between these two extremes (Cooper-Harper ratings between 4 and 6).

<b>Rotorcraft characteristics</b>	<b>Demands on a pilot in selected task or operation</b>	<b>Cooper-Harper HQR</b>	<b>ADS Level</b>
Excellent Highly desirable	Pilot compensation not a factor for desired performance	1	1
Good Negligible deficiencies	Pilot compensation not a factor for desired performance	2	1
Fair but mildly unpleasant deficiencies	Minor pilot compensation is required for desired performance	3	1
Minor but annoying deficiencies	Desired performance requires moderate pilot compensation	4	2
Moderately objectionable deficiencies	Adequate performance requires considerable pilot compensation	5	2
Very objectionable but tolerable deficiencies	Adequate performance requires extensive pilot compensation	6	2
Major deficiencies	Adequate performance not attainable with maximum tolerable pilot compensation	7	3
Major deficiencies	Considerable pilot compensation is required for control	8	3
Major deficiencies	Intense pilot compensation is required to retain control	9	3
Major deficiencies	Control will be lost during some portion of required operation	10	n/a

Table 3.3: Cooper-Harper rating scale [13]

The ADS-33 document also contains various quantitative measures for assessing the controller performance that corresponds to one of the three performance levels, but are used on simulated responses to predict the handling quality level expected during flight tests. The ADS-33 analysis that will be presented in this thesis is based upon these quantitative criteria and the sections to follow will highlight the requirements so as to predict Level 1 handling qualities.

There are two main flight conditions in which the helicopter is said to operate - *hover* (< 15 kts) *to low speed* (15 – 45 kts) and *forward flight* (> 45 kts) [83]. The quantitative assessment criteria at each flight condition is divided into the following - *small amplitude demand response*, *moderate amplitude demand response*, *large amplitude demand response* and *inter-axis coupling*. These criteria are explained further in the following sections.

### Small amplitude

Small amplitude responses are further divided into - *short-* and *mid-term* responses. In the short-term analysis, a helicopter's handling qualities are assessed by linear tools which predict the helicopter's closed loop *bandwidth* and *phase delay*. The ADS-33 bandwidth,  $\omega_{BW}$ , of a closed loop system for an ACAH type response, as discussed in this thesis, is defined as the point where the phase response of the closed loop individual channel frequency response intersects the  $-135$  deg line. This is roughly a measure of the frequency range over which reasonably good tracking can be expected [3].

The phase delay is a measure of the high-frequency phase roll-off and is defined as the slope of the phase response between the phase crossover frequency,  $\omega_{180}$ , to twice that frequency. It roughly means, how quickly the handling qualities degrade at high frequency. The phase delay is also an individual channel measure and is found using the closed loop transfer function between the actuator input and the primary output (e.g. lateral cyclic to roll) [3]. If the phase lag at  $2\omega_{180}$  is measured as  $\Phi$  then the phase delay,  $\tau_p$ , is defined by

$$\tau_p = \frac{\Phi - \pi}{2\omega_{180}} \quad (3.2)$$

During the mid-term analysis, the handling qualities are assessed by the damping ratio,  $\eta$ , at frequencies below the bandwidth frequency. It is a measure of the controller's ability to reject unwanted oscillations caused by disturbances and high order dynamics. Level 1 ratings are achieved if  $\xi > 0.35$  [3].

### Moderate amplitude

At moderate amplitude demands the nonlinear dynamics of the helicopter becomes more prominent in the responses. *Attitude quickness* is an useful tool for measuring the HQR at such demands. For the pitch axis [65], attitude quickness parameter,  $\tau_r$ , is measured as the ratio

$$\tau_r = \frac{q_{peak}}{\Delta\theta_{peak}} \quad (3.3)$$

In Equation 3.3,  $q_{peak}$  defines the peak pitch rate and  $\Delta\theta_{peak}$  defines the peak pitch attitude change due to a pulse longitudinal cyclic input. Similarly for the roll axis attitude quickness is defined by  $\left(\frac{p_{peak}}{\Delta\phi_{peak}}\right)$ . This criteria is structured so that the under shoot characteristic of the attitude response is detrimental to the HQR level. However, the above parameter is generally expected to be slightly deteriorated for an ACAH response type as importance is given to stability over agility [54]. Therefore, this criterion would have a lesser impact over the success or failure of the controller designed in this study.

### Large amplitude

Large amplitude responses are also an important analysis tool as it indicates the ability to retain high levels of handling at situations where the nonlinearities are at their most severity. As the controller designed in this study is based on linear approximations of the EH101 it is thus desirable to analyse the controller at conditions where these approximations are no longer valid. Level 1 requirement, for ACAH responses type, is attained by achieving a stable response at  $\pm 30$  deg and  $\pm 60$  deg pitch attitude and roll attitude demand respectively, with minimal coupling into other channels. There is no such attitude limit for the yaw channel as they are expected to perform 360 deg rotations indefinitely, and as the controller in this study is designed to induce a RCAH type response in the yaw channel, the maximum demand for a Level 1 rating is required to be  $\pm 60$  deg/s [3]. It is important to note that these limits are specific to a high agility manoeuvres, such as *target acquisition* and *tracking*, and with moderate to limited agility manoeuvres like *hover* the limits are more relaxed.

### Inter-axis coupling

The manner in which the other channels respond when a demand is made to any one particular channel is known as inter-axis coupling. It is difficult to quantify this with a value as the discomfort experienced by the coupling is variable from one pilot to another. The criteria essentially states that the controller should be highly effective against these interactions, however, there are certain particular interactions that are quantified in the ADS-33 document, for example, the ratio of roll attitude due to pitch attitude demand and vice versa should not exceed 0.25 for a Level 1 rating [3].

## **3.7 Conclusion**

The requirement for robust multivariable controller design method to solve the uncertain and multivariable helicopter control problem has been established. The military design standard has also been described that allows to quantify the handling qualities of particular control system designs. Having justified the need for robust controller designs within helicopters, the following chapter will now present the application of 2DOF  $\mathcal{H}_\infty$  loop shaping methodology to design a FA controller for the EH101 helicopter.

# Chapter 4

## Full authority controller design

The primary aim of the study presented in this thesis is to derive a methodology to design a LA control system that would replicate the performance of a fully augmented FA control system. This chapter describes the design of a FA  $\mathcal{H}_\infty$  controller for the AgustaWestland EH101 helicopter along with an analysis of the resultant responses. The controller was designed using linear models extracted from a highly sophisticated nonlinear model provided by AgustaWestland. Details of the controller design are presented here, together with the frequency and linear time response analysis. The responses presented here thus form the baseline behaviour which the LA control system is expected to replicate. It should be noted that no other  $\mathcal{H}_\infty$  design for the EH101 has been published in the literature.

### 4.1 Introduction

A general unaugmented (open loop, except for the pilot) helicopter in either the hover (low speed) or forward flight condition demands a high workload from the pilot. Augmentation of the helicopter response, in order to ease this workload which also satisfies stringent handling quality requirements is thus considered desirable. Unfortunately, the highly nonlinear and cross-coupled nature of the typical single main rotor helicopter, such as the EH101, makes the design a difficult and challenging problem. A review of various approaches to the design of FA multivariable helicopter flight control systems ranging from classical (SISO) techniques, eigen-structure assignment methods, linear quadratic control, and  $\mathcal{H}_\infty$  optimisation

has been presented in Chapter 1. As  $\mathcal{H}_\infty$  control can systematically handle MIMO systems and the uncertainty present in them, it promises fast design of good performance-inducing augmentation. One of the most effective  $\mathcal{H}_\infty$  based designs is the  $\mathcal{H}_\infty$  loop shaping, which combines the traditional notions of bandwidth and loop gain together with modern ideas of robustness into a single framework. The particular advantages that make this method an ideal candidate for helicopter controller design have been highlighted in Chapter 2. The aim of this chapter is to describe, in some detail, the design of a controller for the EH101 helicopter based on the loop shaping ideology.

## 4.2 EH101 design model

The controller designs in this study are based on the EH101 model supplied by AgustaWestland and constructed in the NAOMI (New Aircraft Overall Modelling Initiative) framework, which is a modified AgustaWestland version of SIMULINK, specifically designed for rotorcraft applications and to meet AgustaWestland's own requirements [1]. The given EH101 SIMULINK model was a 38-state nonlinear flight mechanics model which is believed to capture the real helicopter's behaviour reasonably well. The model included **9** states describing the rigid body dynamics of the helicopter fuselage, **5** states representing the main rotor flap angles (1 average (coning), 2 first harmonic and 2 second harmonic), **5** states representing the main rotor lag angles (1 average, 2 first harmonic and 2 second harmonic), **5** states representing the main rotor inertial flap angle rates (1 average (coning rate), 2 first harmonic and 2 second harmonic), **5** states representing the main rotor inertial lag angle rates (1 average, 2 first harmonic and 2 second harmonic), **1** state for main rotor inflow, **1** state for tail rotor inflow, **5** states for defining the helicopter location (1 northerly, 1 easterly, 1 height, 1 longitude and 1 latitude), **1** state for rotor speed and **1** state for main rotor azimuth position. The NAOMI *trim* and *linearisation* routines [1] were used to derive the linear model at various flight conditions of different forward speeds (0 to 120 kts), altitudes (0, 2500 and 4500 ft) and masses (11000 and 14200 kg). During trimming each initial condition parameter was perturbed by a small amount and a Jacobian matrix was constructed which captured the influence of initial condition parameters variation on trim constraints. The optimisation algorithm within the routine then inverted the above matrix in order to translate known trim constraint

errors into initial condition parameter adjustments. Next, certain states were removed from the 38-state trimmed model - (a) second harmonics of the flap angle and rate and lag angle, and rate under the harmonic linearisation condition where higher harmonics are discarded during linearisation, (b) the northerly, easterly, longitudinal and latitudinal helicopter location states and the rotor azimuth state as they are not influential during the controller design process. Table 4.1 lists the states that represent the 25-state model that was then derived. The derived linear representation also features 5 plant inputs, (see Table 4.2 for complete details), and 20 plant outputs, (see Table 4.3 for complete details).

	<b>State</b>	<b>Unit</b>		<b>State</b>	<b>Unit</b>
<b>1</b>	Body axis velocity, ( $u$ )	$m/s$	<b>10-12</b>	Flap angles (average and first harmonic)	$rad$
<b>2</b>	Body axis velocity, ( $v$ )	$m/s$	<b>13-15</b>	Lag angles (average and first harmonic)	$rad$
<b>3</b>	Body axis velocity, ( $w$ )	$m/s$	<b>16-18</b>	Flap rate (average and first harmonic)	$rad/s$
<b>4</b>	Body axis velocity, ( $p$ )	$rad/s$	<b>19-21</b>	Lag rate (average and first harmonic)	$rad/s$
<b>5</b>	Body axis velocity, ( $q$ )	$rad/s$	<b>22</b>	Main rotor inflow	
<b>6</b>	Body axis velocity, ( $r$ )	$rad/s$	<b>23</b>	Tail rotor inflow	
<b>7</b>	Roll attitude, ( $\phi$ )	$rad$	<b>24</b>	Main rotor speed	$rad/s$
<b>8</b>	Pitch attitude, ( $\theta$ )	$rad$	<b>25</b>	Height above sea level	$m$
<b>9</b>	Heading, ( $\psi$ )	$rad$			

Table 4.1: EH101 plant states

One of the characteristics of 2DOF  $\mathcal{H}_\infty$  loop shaping methodology is that it produces controllers of magnitude equal to that of the generalised plant. Thus, to prevent high order controllers, and also to ease the process of synthesis and implementation, the 25-state linear model was further simplified. First, the height and heading ( $\psi$ ) states were removed from the model as neither variables were controlled nor were required for stabilisation. Furthermore, heading can be expressed in terms of the rigid body rates and  $\theta$  and  $\phi$ . In addition to the rigid body states, the remaining states in the 23 state model were those associated with the

	<b>Input</b>	<b>Unit</b>
<b>1</b>	Engine torque	$Nm$
<b>2</b>	Longitudinal cyclic	$deg$
<b>3</b>	Lateral cyclic	$deg$
<b>4</b>	Main rotor collective	$deg$
<b>5</b>	Tail rotor collective	$deg$

Table 4.2: EH101 plant inputs

	<b>Output</b>	<b>Unit</b>		<b>Output</b>	<b>Unit</b>
<b>1-3</b>	CG acceleration	$m/s^2$	<b>15</b>	Pitch attitude, ( $\theta$ )	$deg$
<b>4</b>	Main rotor yaw moment	$Nm$	<b>16</b>	Heading, ( $\psi$ )	$deg$
<b>5-7</b>	Fuselage attitude rates	$deg/s$	<b>17</b>	CG true air velocity	$m/s$
<b>8-10</b>	CG ground velocity	$m/s$	<b>18</b>	CG equivalent air velocity	$m/s$
<b>11-13</b>	CG angular velocity, ( $p,q,r$ )	$deg/s$	<b>19</b>	CG height above sea level	$m$
<b>14</b>	Roll attitude, ( $\phi$ )	$deg$	<b>20</b>	Rotorspeed	%

Table 4.3: EH101 plant outputs

rotor dynamics and are believed to be sufficiently fast to be replaced with their steady state values, thus the model was *residualised* to an 8-state model which consisted of simply the rigid body dynamics (i.e.  $u, v, w, p, q, r, \theta$  and  $\phi$ ). More discussion of this and other model reduction techniques can be found in [72] and [61]. In addition to the model order reduction, it was decided that only the pitch, roll and yaw axes would be controlled and that the collective channel would remain open-loop. This was partly due to safety reasons and partly due to previous knowledge of pilot preference. In the Bell 205 studies [75, 66, 65] and the LA AgustaWestland studies which preceded this work [85], the collective channel was left open-loop for these reasons. The states, inputs and outputs of the design model are shown in Tables 4.4 and 4.5.

### 4.2.1 Open loop characteristics

As mentioned earlier, the nonlinear model was linearised at a number of trim points to enable controller design and linear analysis. In addition the helicopter was also linearised at

	<b>State</b>	<b>Unit</b>
<b>1</b>	Body axis velocity, ( $u$ )	$m/s$
<b>2</b>	Body axis velocity, ( $v$ )	$m/s$
<b>3</b>	Body axis velocity, ( $w$ )	$m/s$
<b>4</b>	Body axis velocity, ( $p$ )	$rad/s$
<b>5</b>	Body axis velocity, ( $q$ )	$rad/s$
<b>6</b>	Body axis velocity, ( $r$ )	$rad/s$
<b>7</b>	Roll attitude, ( $\phi$ )	$rad$
<b>8</b>	Pitch attitude, ( $\theta$ )	$rad$

Table 4.4: EH101 8-state plant states

	<b>Input</b>	<b>Unit</b>		<b>Output</b>	<b>Unit</b>
<b>1</b>	Longitudinal cyclic	$deg$	<b>1</b>	Pitch attitude, ( $\theta$ ) (to be controlled)	$deg$
<b>2</b>	Lateral cyclic	$deg$	<b>2</b>	Roll attitude, ( $\phi$ ) (to be controlled)	$deg$
<b>3</b>	Tail rotor collective	$deg$	<b>3</b>	CG angular velocity, ( $r$ ) (to be controlled)	$deg/s$
			<b>4</b>	CG angular velocity, ( $q$ ) (for feedback only)	$deg/s$
			<b>5</b>	CG angular velocity, ( $p$ ) (for feedback only)	$deg/s$

Table 4.5: EH101 8-state plant inputs and outputs

different weights corresponding to a lightly loaded (11000kg) and heavily loaded (14200kg). These flight conditions are listed in Table 4.6. At all the points a 25-state and an 8-state model, as described above, were obtained. In order to assess the characteristics of the open-loop plant, the frequency response of these linearisations were examined. As the linear models are multivariable in nature, it is difficult to obtain an accurate picture of the plant's properties using standard Bode plots, so instead the singular value plots were used. Singular values give similar information as the Bode magnitude plots but they also account for coupling between the channels.

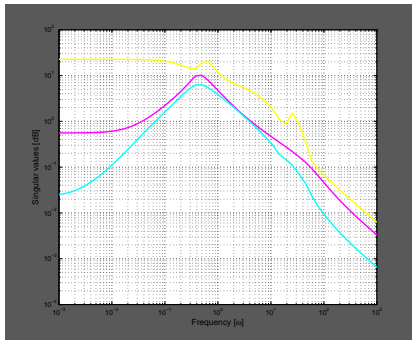
	<b>Helicopter mass - 11000 kg</b>		<b>Helicopter mass - 14200 kg</b>	
<b>Hover</b>	0kts, 0ft	0kts, 4500ft	0kts, 0ft	0kts, 2500ft
<b>Low speed</b>	10kts , 0ft	10kts , 4500ft	10kts , 0ft	10kts , 2500ft
	20kts , 0ft	20kts , 4500ft	20kts , 0ft	20kts , 2500ft
	30kts , 0ft	30kts , 4500ft	30kts , 0ft	30kts , 2500ft
<b>Medium speed</b>	40kts , 0ft	40kts , 4500ft	40kts , 0ft	40kts , 2500ft
	50kts , 0ft	50kts , 4500ft	50kts , 0ft	50kts , 2500ft
	60kts , 0ft	60kts , 4500ft	60kts , 0ft	60kts , 2500ft
	70kts , 0ft	70kts , 4500ft	70kts , 0ft	70kts , 2500ft
	80kts , 0ft	80kts , 4500ft	80kts , 0ft	80kts , 2500ft
<b>High speed</b>	90kts , 0ft	90kts , 4500ft	90kts , 0ft	90kts , 2500ft
	100kts , 0ft	100kts , 4500ft	100kts , 0ft	100kts , 2500ft
	110kts , 0ft	110kts , 4500ft	110kts , 0ft	110kts , 2500ft
	120kts , 0ft	120kts , 4500ft	120kts , 0ft	120kts , 2500ft

Table 4.6: EH101 trim points

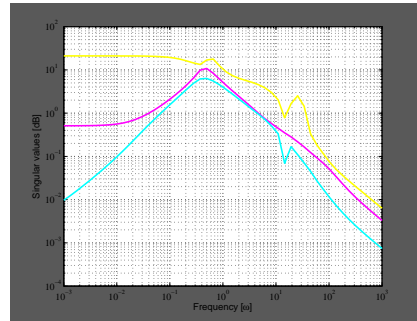
Figures 4.1 to 4.5 show the singular values (yellow - maximum singular value, blue - minimum singular value) of the 25-state linear rotorcraft model at selected flight conditions. The plots reveal variation in singular values from one flight condition to another across frequency, with dramatic variations at frequencies below 1 rad/s. It is of particular interest to note the difference in very low frequency behaviour of the minimum singular values which changes from being “derivative” like to constant as the flight conditions change. This variation in steady state behaviour implies that one LTI controller may find it difficult to achieve perfect steady state tracking at all the flight conditions. Also, the high 2-norm condition number defined as the ratio of maximum to minimum singular values (Table 4.7) at low frequency (0.1 rad/s) implies that the model is highly sensitive to changes to flight conditions.

<b>11000 kg</b>			<b>14200 kg</b>		
0kts/0ft	40kts/0ft	80kts/4500ft	0kts/0ft	40kts/0ft	80kts/2500ft
12.8	88.1	127.9	13.7	70.9	275.4

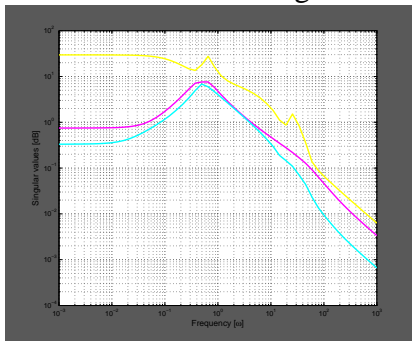
Table 4.7: Open loop condition number (0.1 rads/s)



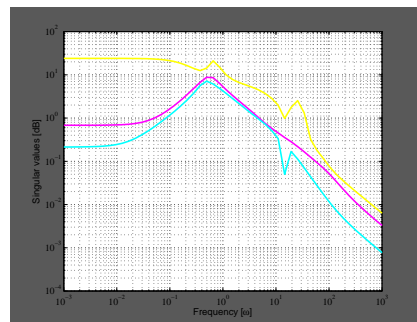
Hover/11000kg



Hover/14200kg

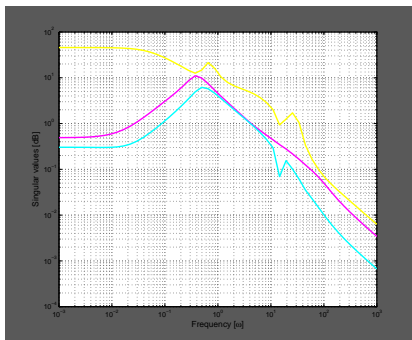


10kts/0ft/11000kg

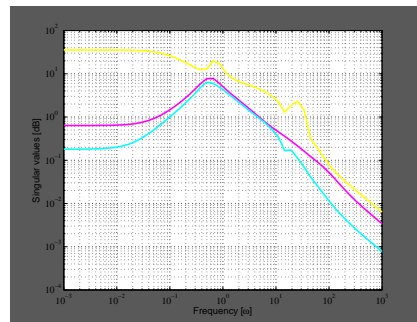


10kts/0ft/14200kg

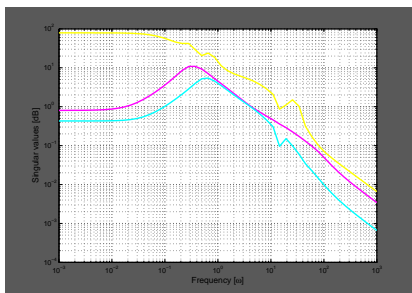
Figure 4.1: MIMO open-loop singular value comparison



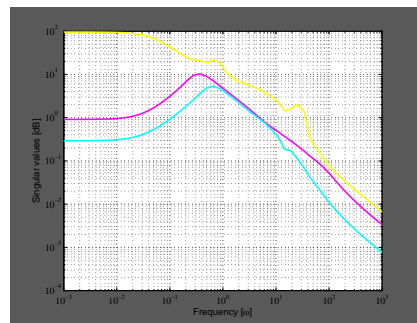
20kts/11000kg



20kts/14200kg



30kts/0ft/11000kg



30kts/0ft/14200kg

Figure 4.2: MIMO open-loop singular value comparison

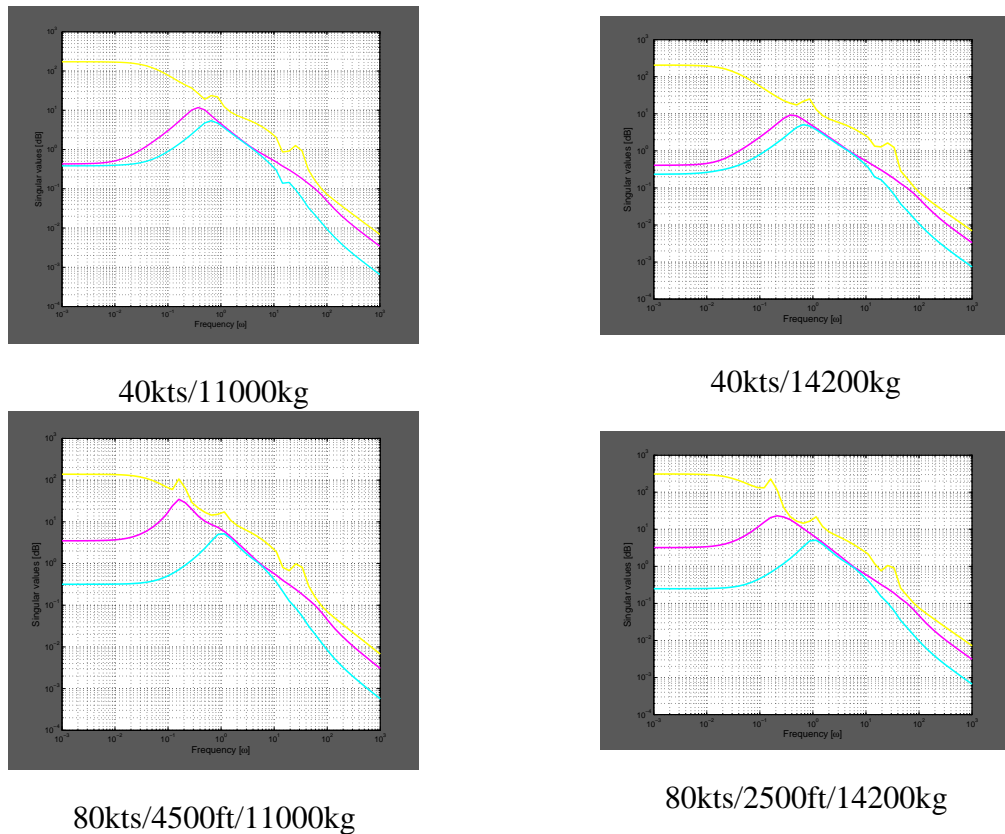
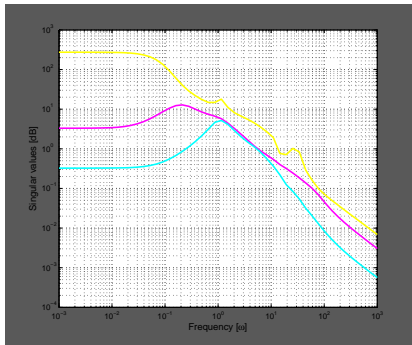


Figure 4.3: MIMO open-loop singular value comparison

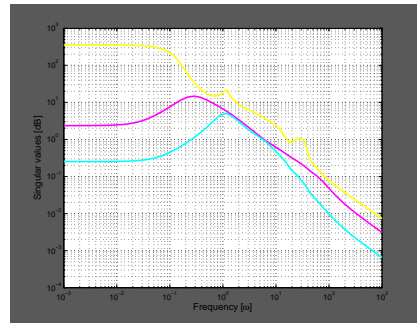
Prior to designing a controller using the lower order (8-state) plant it was important to validate the reduced order plant against the full order (25-state) plant. The plot in figure 4.6 compares the singular values of the reduced order (solid line) plant to that of the full order (dashed line) plant at the 40kts/0ft flight condition at both 11000 kg and 14200 kg mass cases. It was noted that the reduced order plant retains the frequency response features of the full order plant up to 10 rads/s and after this frequency the reduced order plant is not an accurate representation. This places an upper bound on the controller bandwidth of about 10 rads/s.

Tables 4.8 and 4.9 show the open loop poles of the reduced order plant at selected flight conditions. The presence of right-half plane poles is noted and this is particularly undesirable as it places lower bounds on the gain required to stabilise the system and complicates controller design. It should also be noted that the plant changes its stability properties with variation in flight condition and this partially justifies the use of loop shaping method as it specifically provides robustness against coprime factor uncertainty that are fully capable of representing such situations.

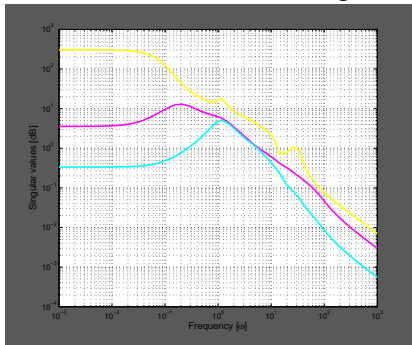
The two plots in Figure 4.7 show the variation in eigenvalues with changes to helicopter



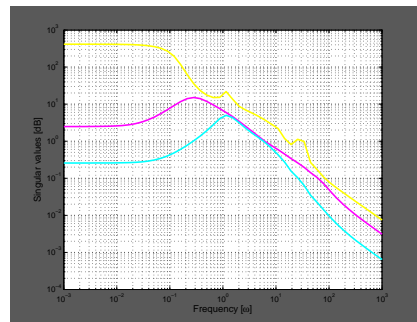
90kts/4500ft/11000kg



90kts/2500ft/14200kg

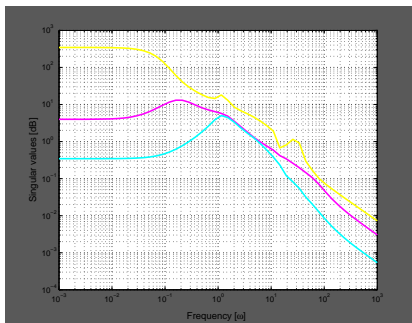


100kts/4500ft/11000kg

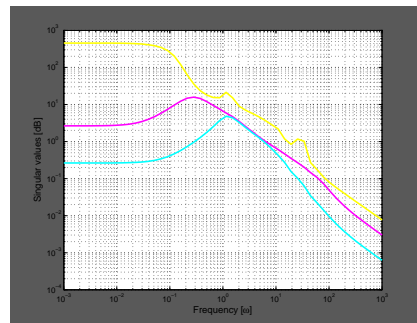


100kts/2500ft/14200kg

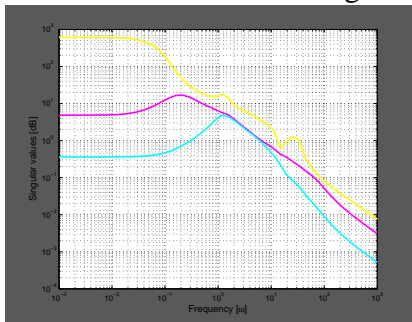
Figure 4.4: MIMO open-loop singular value comparison



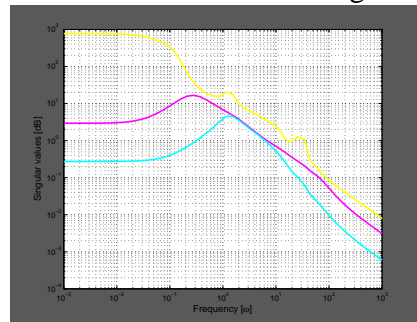
110kts/4500ft/11000kg



110kts/2500ft/14200kg

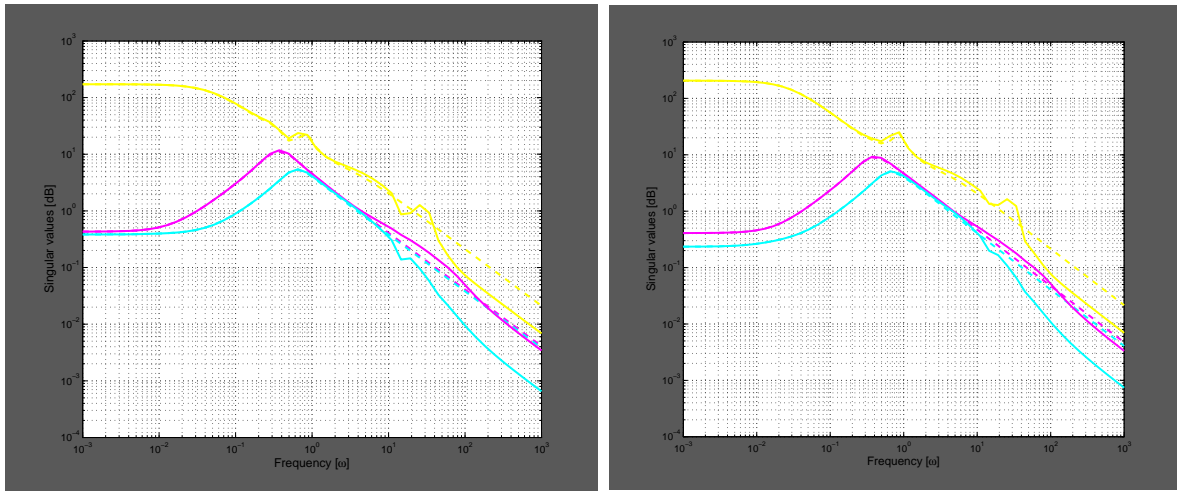


120kts/4500ft/11000kg



120kts/2500ft/14200kg

Figure 4.5: MIMO open-loop singular value comparison



11000kg

14200kg

Figure 4.6: Comparison between 8-state (dashed) and 25-state (solid) model

11000 kg					
0kts/0ft	0kts/4500ft	40kts/0ft	40kts/4500ft	80kts/0ft	80kts/4500ft
-3.29	-3.65	-3.08	-3.15	-2.28	-2.73
-0.86	-0.93	-1.15	-1.20	-0.24 + 1.08i	-0.24 + 1.09i
0.24 + 0.38i	-0.05 + 0.60i	-0.17 + 0.78i	-0.16 + 0.86i	-0.24 - 1.08i	-0.24 - 1.09i
0.24 - 0.38i	-0.05 - 0.60i	-0.17 - 0.78i	-0.16 - 0.86i	-0.72 + 0.57i	-0.69 + 0.83i
-0.16 + 0.56i	0.13 + 0.13i	0.12 + 0.32i	0.08 + 0.28i	-0.72 - 0.57i	-0.69 - 0.83i
-0.16 - 0.56i	0.13 - 0.13i	0.12 - 0.32i	0.08 - 0.28i	-0.06 + 0.08i	-0.02 + 0.18i
-0.19	-0.18 + 0.12i	-0.29	-0.20	-0.06 - 0.08i	-0.02 - 0.18i
-0.22	-0.18 - 0.12i	0.05	0.04	0.05	-0.05

Table 4.8: Open loop poles - 8-state plant (11000kg)

forward speed at altitudes of 0ft and 2500ft. Analysis of the plots show that the EH101, like most conventional helicopters, depicts the commonly observed longitudinal and lateral modes. At both altitudes, for speeds of upto 30kts the eigenvalue plot shows the presence of a low frequency unstable *phugoid* mode, low frequency stable *dutch roll* mode, slow critically damped stable *spiral, heave*, faster *pitch subsidence* and fastest *roll subsidence* modes. As the speed increases to 70kts, the heave mode becomes *marginally* unstable and the pitch and roll subsidence modes also reduce in frequency. At speeds greater than 70kts, the heave mode returns to stability and the critically damped mode of pitch subsidence changes to a

14200 kg					
0kts/0ft	0kts/2500ft	40kts/0ft	40kts/2500ft	80kts/0ft	80kts/2500ft
-4.01	-3.73	-3.49	-3.53	-2.62	-2.81
-1.04	-1.03	-1.33	-1.36	-0.20 + 1.10i	-0.21+ 1.13i
0.23 + 0.39i	-0.05 + 0.64i	-0.17 + 0.82i	-0.16 + 0.92i	-0.20 - 1.10i	-0.21- 1.13i
0.23 - 0.39i	-0.05 - 0.64i	-0.17 - 0.82i	-0.16 - 0.92i	-0.66 + 0.49i	-0.65 + 0.49i
-0.17 + 0.54i	0.15 + 0.19i	0.18 + 0.36i	0.14 + 0.34i	-0.66 - 0.49i	-0.65 - 0.49i
-0.17 - 0.54i	0.15 - 0.19i	0.18 - 0.36i	0.14 - 0.34i	-0.08 + 0.11i	-0.02 + 0.19i
-0.18	-0.19 + 0.06i	-0.23	-0.18	-0.08 - 0.11i	-0.02 - 0.19i
-0.22	-0.19 - 0.06i	0.03	0.02	0.08	-0.03

Table 4.9: Open loop poles - 8-state plant (14200kg)

*pitch/roll short period* mode. This trend was also observed at the 11000kg linearisations (Figure 4.8).

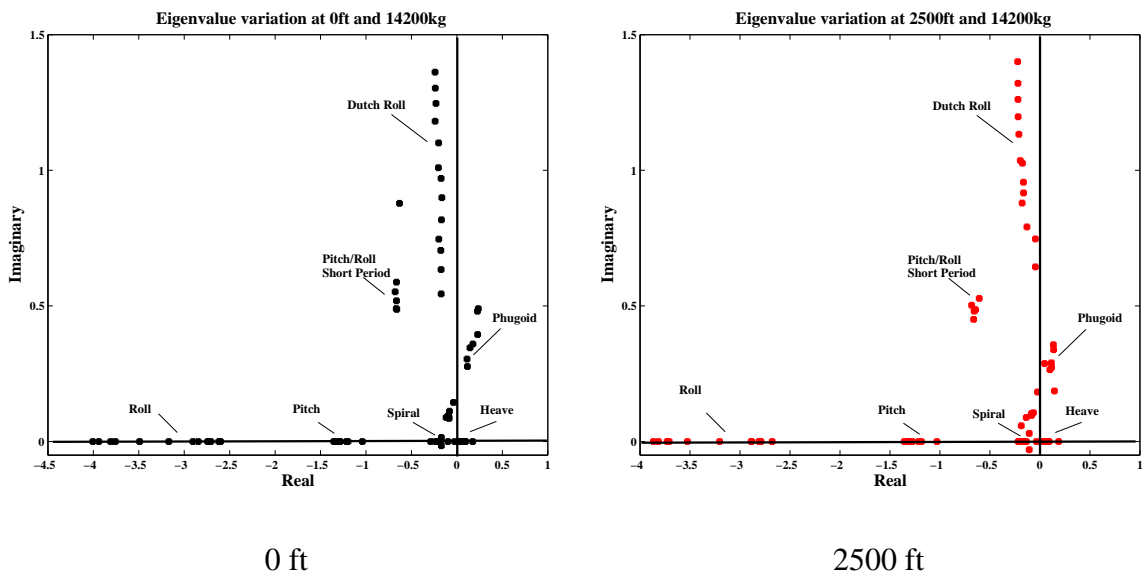


Figure 4.7: Eigen value variation as a function of speed (0 - 120kts) for 14200kg

Table 4.10 shows the transmission zeros of the EH101 at low speed flight conditions. Note that for the 40kts/0ft 8-state model, all the zeros are in the left half plane, but for forward speeds of 20kts or less, the linearisations contained non minimum phase zeros around the origin. Positive zero limits the achievable controller performance and robustness by restricting the controller bandwidth and system gain margin respectively [30]. Also, an odd number

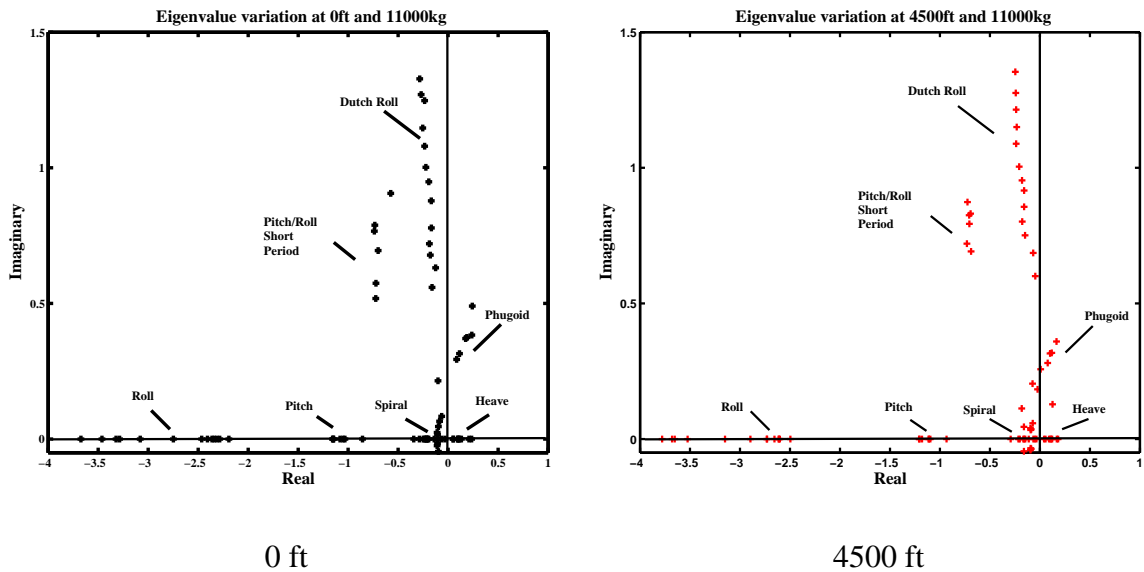


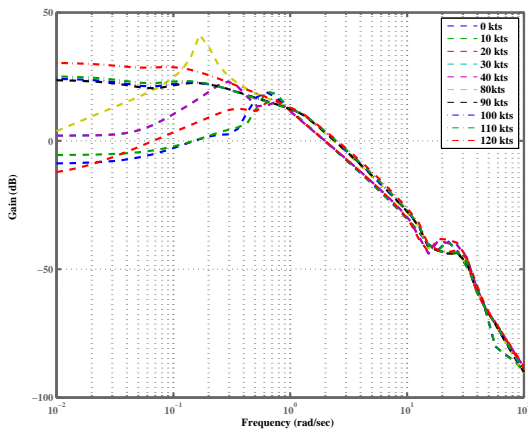
Figure 4.8: Eigen value variation as a function of speed (0 - 120kts) for 11000kg

of non-minimum phase zero cause an initial undershoot which makes the helicopter go in the opposite direction to the asymptotic value and this then slows the helicopter response. These factors strongly discouraged the use of other flight conditions for controller design.

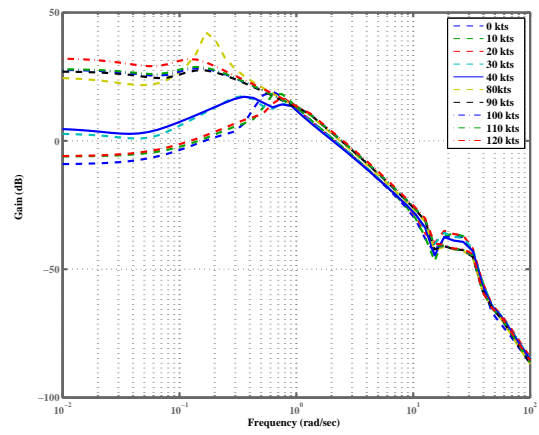
10kts/0ft	20kts/0ft	40kts/0ft
-0.1661	<b>0.0430</b>	-0.2837
<b>0.0513</b>	-0.0203	-0.0143
-0.0180	-0.1617	-0.0404

Table 4.10: Open loop zeros - 8-state plant

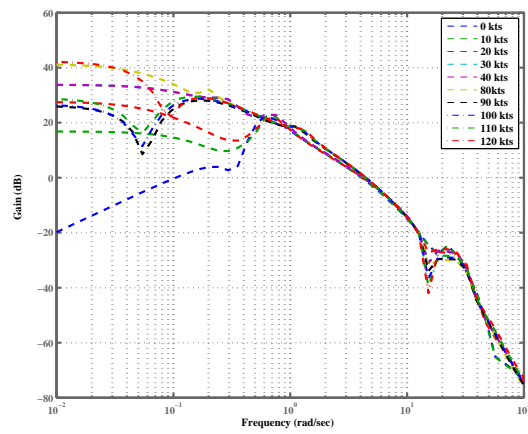
In order to obtain specific information about the frequency responses of each channel, standard on-axis Bode plots of the pitch attitude, roll attitude and yaw rate were also plotted. The magnitude portions of these Bode plots for all the flight conditions are shown in Figure 4.9. The information from the singular values is confirmed with large variations observed in pitch and roll axes plots with changes in flight condition. The large low frequency variations make designing controllers which provide the same level of tracking at each flight condition difficult. The yaw axis shows less frequency variation but there are some troublesome mid-frequency resonances and anti-resonances which change with flight condition and could cause stability problems. Assessment of these plots showed that the magnitude values for the 40kts/0ft/14200kg flight condition was approximately at the centre of the cluster in all three channels and selecting this as the nominal plant would require a lower uncertainty margin to



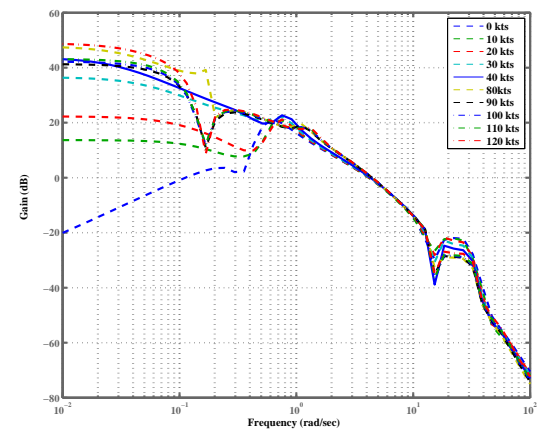
Gain variation - pitch axis at 11000kg



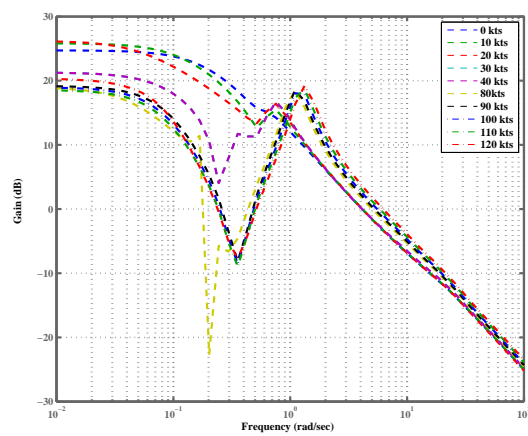
Gain variation - pitch axis at 14200kg



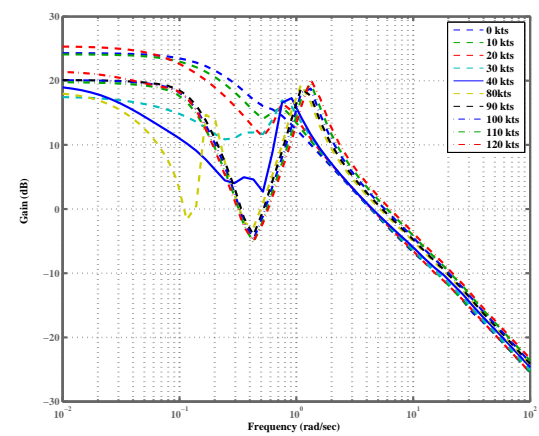
Gain variation - roll axis at 11000kg



Gain variation - roll axis at 14200kg



Gain variation - yaw axis at 11000kg



Gain variation - yaw axis at 14200kg

Figure 4.9: Bode magnitude plots

cover the full flight envelope.

The above discussion lists the challenges that would be encountered while designing a controller for the EH101 - changing characteristics with flight conditions, i.e. RHP poles and RHP zeros, and high frequency uncertainty. 2DOF  $\mathcal{H}_\infty$  loop shaping methodology with its robust uncertainty management ability and multivariable nature was chosen to design the MIMO FA controller.

## 4.3 Controller design

The 2DOF  $\mathcal{H}_\infty$  loop shaping procedure proposed by [48] and as explained in Chapter 2 consists of three steps:

1. Selection of reference model
2. Augmentation of open loop plant with weighting functions
3. Controller synthesis (using  $\mathcal{H}_\infty$  optimisation)

### 4.3.1 Selection of reference model

Selecting a reference model provides the ability to amend the rotorcraft response to fit a desired model. The controller was designed to seek a ACAH (Attitude Command/Attitude Hold) type response in the pitch and roll channels, and a RC (Rate Command) type response in the yaw channel. The reference model,  $T_{ref}$ , was chosen as a second order linear model of unity gain in each channel in order to induce second order type of behaviour in the responses. The second order model was used in order to provide the input-output behaviour that meets the ADS-33 criteria [3] and such models have shown success in previous helicopter studies, for eg. [31], [88], [91] and [93] and these studies also provided guidelines to design the reference model. As reference tracking in pitch, roll and yaw axes was sought, the reference model has the following diagonal structure to induce decoupled responses:

$$T_{ref} = \begin{bmatrix} T_{pitch} & 0 & 0 \\ 0 & T_{roll} & 0 \\ 0 & 0 & T_{yaw} \end{bmatrix} \quad (4.1)$$

where

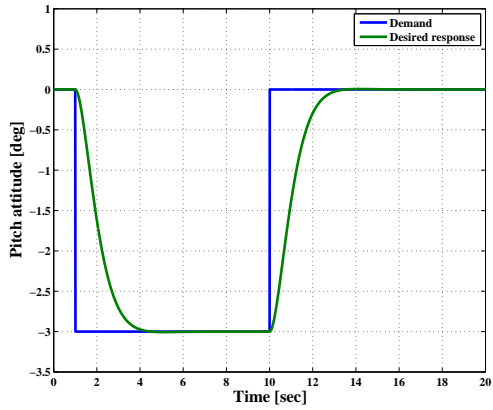
$$\begin{aligned} T_{pitch} &= \frac{2.89}{s^2 + 3.06s + 2.89} \\ T_{roll} &= \frac{6.25}{s^2 + 4.0s + 6.25} \\ T_{yaw} &= \frac{49}{s^2 + 28.0s + 49} \end{aligned} \quad (4.2)$$

Figure 4.10 shows the responses that are induced into the respective channels of EH101 due to the above reference models. Table 4.11 shows the respective natural frequency ( $\omega_n$ ) and the damping ratio ( $\xi$ ) for the reference models listed above along with the corresponding rise time ( $t_r$ ) that was expected in each channel.

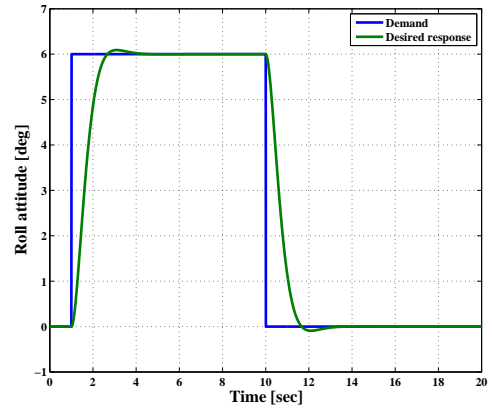
Reference Model	Natural frequency ( $\omega_n$ )	Damping ratio ( $\xi$ )	Expected rise time ( $t_r$ )
$T_{pitch}$	1.7	0.9	1.5
$T_{roll}$	2.5	0.8	1.0
$T_{yaw}$	7.0	2.0	0.5

Table 4.11: Reference model description

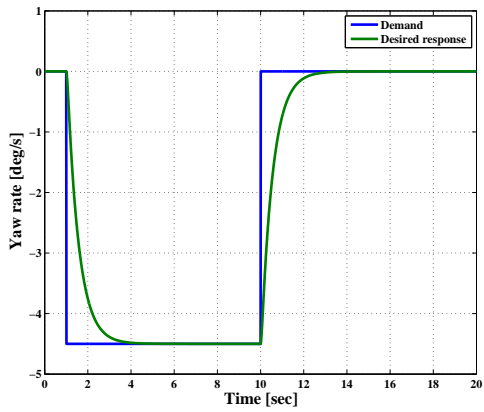
The above model ensures well-damped attitude responses with smooth rates in longitudinal and lateral channels and a fast response in the directional channel. The use of second order reference model is open to discussion with the observation that first order reference model will produce a lower order controller. However, using the second order reference model provides the designer with an extra degree of freedom to improve the responses. The availability of controller order reduction methods, that assist in obtaining a lower order controller which maintains the capability of the high order controller supports the usage of second order reference model. Also, second order models with slight overshoot can sometimes be better than first order since many pilot inputs are not true steps and thus the overshoot is not observed



Desired Pitch Response



Desired Roll Response



Desired Yaw Response

Figure 4.10: Desired responses from each channel

but faster tracking of the demand can be achieved. Although  $\theta$ ,  $\phi$  and  $r$  were the three controlled outputs (i.e. matched to reference models), measurement of pitch and roll rate ( $q$  and  $p$  respectively) were also fed back into the controller as they are able to increase the system's damping and provide a stabilising effect to the overall system [94].

### 4.3.2 Loop shaping and controller synthesis

The open loop plant is augmented by a pre- ( $W_1$ ) and post-compensator  $W_2$  to give a desired shape to the open loop frequency response (in terms of singular values). The nominal plant  $G$  and the shaping functions  $W_1$  and  $W_2$  are combined to form the desired plant,  $G_s$  where  $G_s = W_2GW_1$ . This is normally aimed to achieve high gain at low frequencies, roll off rates of approximately 20dB/decade at the desired bandwidth and higher rates at high frequen-

cies. There is usually some trial and error involved in this process and it is normally fairly straightforward to find a reasonably good loop shape, and the design procedure is somewhat iterative.  $W_2$  is effectively chosen as a constant, reflecting the relative importance of outputs to be controlled and other measurements being fed back to the controller and  $W_1$  contains the either non-dynamic or dynamic shaping. The final controller order is directly proportional (proportionality constant of two) to the order of the weights employed and this advocates the case of applying non-dynamic weights, provided the required shape is attained. Keeping this in mind three designs are discussed here - the first (Design 1) using non-dynamic shaping, the second (Design 2) using additional dynamic shaping to which further iteration was performed to achieve the final shape (Design 3).

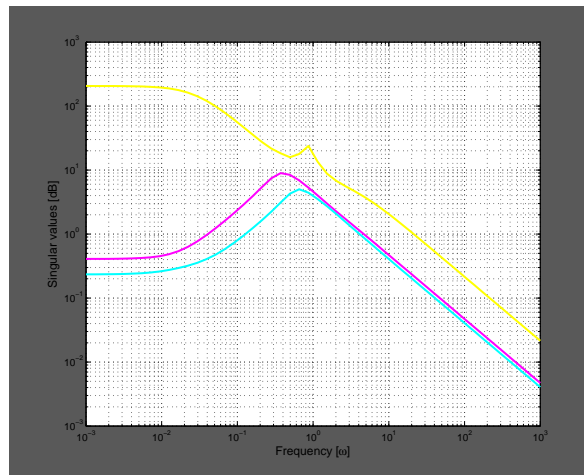


Figure 4.11: Open loop singular values - Nominal

### Design 1

The open loop singular values of the nominal plant are shown in Figure 4.11 and it is evident from inspection of the maximum singular value that high additional gain was not necessary on certain channels as the open loop bandwidth was already close to 10 rad/s. The following non-dynamic shaping function  $W_1$  with low gains along the leading diagonal was employed

$$W_1 = \text{diag}(4, 7, 8) \quad (4.3)$$

and the post-compensator  $W_2$  was chosen as

$$W_2 = \text{diag}(1, 1, 1, 1, 1) \quad (4.4)$$

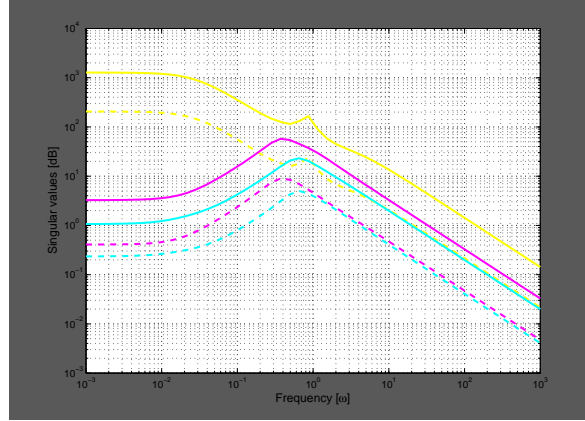


Figure 4.12: Shaped open loop singular values - Design 1

The plot in Figure 4.12 shows the shaped (solid) and the nominal singular values (dashed). The shaped plant frequency response shows that the non-dynamic functions have not been able to produce the required shape. Although, one of the required characteristic of low loop gain, i.e.  $\bar{\sigma}(G_s) \ll 1$ , at high frequency values was observed. However, at the other end for low frequency values high loop gain, i.e.  $\underline{\sigma}(G_s) \gg 1$ , requirement was not produced. Also, the closed loop bandwidth was found to be 100 rads/s and was higher than the limit of 10 rads/s set for this system. Increasing the gain values could improve the low frequency gain, however that would compromise the high frequency gain requirement. This shows the relative weakness of non-dynamic weights for this particular model.

A (14<sup>th</sup>) order  $\mathcal{H}_\infty$  controller  $K_\infty = \begin{bmatrix} K_1 & K_2 \end{bmatrix}$  was synthesised with the value for  $\rho$  for reference model matching set to 2. The controller had an uncertainty margin of  $\epsilon = 0.35$  ( $\gamma = 2.86$ ), which was within the range considered acceptable in [72]. This indicated approximately 35% allowable uncertainty in  $N_s$  and  $M_s$  at the cross-over frequency range.

The final 2DOF controller  $K = W_1 \begin{bmatrix} K_1 & K_2 W_2 \end{bmatrix}$  also had 14 states. The frequency response of the loop transfer function  $GW_1 K_2 W_2$  is given in Figure 4.13. The shape of the open loop singular values is quite poor but similar to Figure 4.12, which is essential in attaining closed loop design objectives. However, gain ( $\underline{\sigma}(GW_1 K_2 W_2)$ ) at low frequency value was not as high as desired and the low loop gain ( $\bar{\sigma}(GW_1 K_2 W_2)$ ) was not as low as

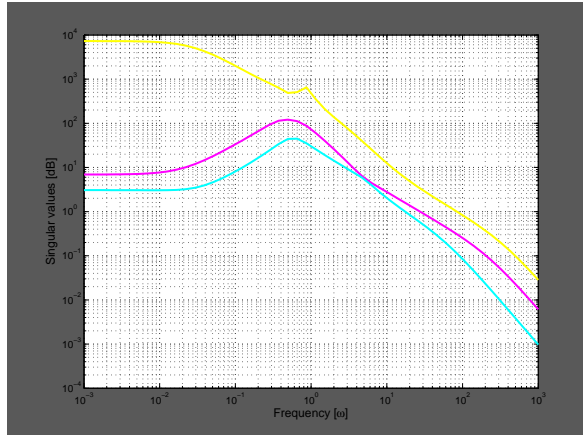
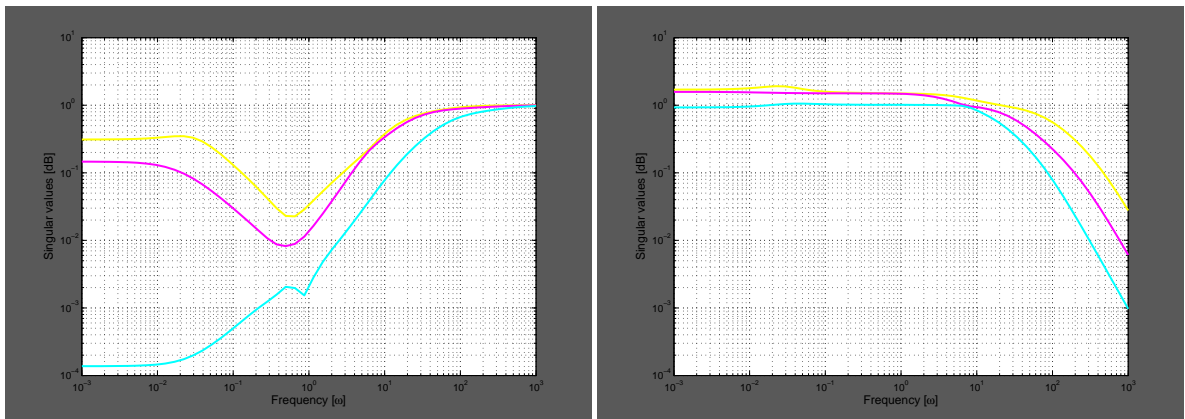


Figure 4.13: Stabilised open loop singular values - Design 1

desired at high frequency. Also, closed loop bandwidth  $\omega_B$  was found to be  $80 \text{ rad/s}$ , which was too high to be used in practice.



Sensitivity plot

Cosensitivity plot

Figure 4.14: Closed loop frequency response - Design 1

The sensitivity  $(I + GW_1K_2W_2)^{-1}$  and cosensitivity  $GW_1K_2W_2(I + GW_1K_2W_2)^{-1}$  singular value plots are shown in Figure 4.14. The sensitivity plot shows strange behaviour, with small singular values between 0.1 and 10 rad/s corresponding to good mid frequency tracking. However low frequency tracking (for at least some inputs) will be poor due to the relatively high low frequency singular values. In addition, a closed-loop bandwidth (from the sensitivity perspective)  $\omega_B$  of 20 rad/s would result in poor robustness within the flight envelope. The cosensitivity function also has a fairly attractive shape, with high frequency roll off, although again, the closed-loop bandwidth  $\omega_{BT}$  is approaching a high 100 rad/s. The resultant controller also showed poor performance when applied to the full order model

(not shown here). Overall the above controller provided a good uncertainty margin and both the open and the closed loop singular values showed the capability of achieving the desired shape which would make this an apt choice, however the large closed loop bandwidth and poor low frequency performance suggested that further iteration was required.

## Design 2

In order to improve the low frequency performance and to reduce the closed loop bandwidth the shaping function was replaced by the following dynamic function

$$W_1 = \text{diag} \left( \frac{(s + 7.0)}{5s}, \frac{3(s + 8.5)}{10s}, \frac{2(s + 9)}{s} \right) \quad (4.5)$$

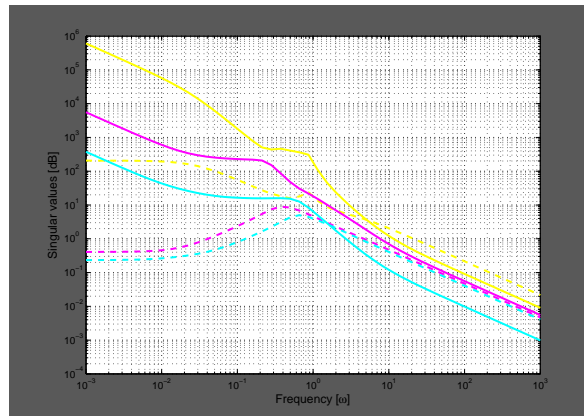


Figure 4.15: Shaped open loop singular values - Design 2

and the post compensator  $W_2$  was unchanged.  $W_1$  is basically a bank of PI type controllers. The integral action was added to improve the low frequency performance such as disturbance rejection and steady state tracking. The phase lead part of the compensator was adjusted to ensure that the open-loop bandwidth was sufficiently high for adequate manoeuvring capability and also around the cross-over point the slope of the singular value curves is relatively shallow. Recall that high-phase lag is associated with steep gradients so an approximate way of avoiding the critical Nyquist point in the multivariable loop shaping is to ensure small gradients near the cross-over point. The process of multivariable loop shaping is something of an art and the values given in Equation 4.5 were arrived at by an iterative tuning and simulation in order to obtain good open-loop shapes. The singular values of the shaped system (solid)

along with the nominal system (dashed) is illustrated in Figure 4.15. The low frequency gain is significantly larger compared to the shaped plant singular values (Figure 4.12) obtained in Design 1. In addition the open loop bandwidth has reduced to 9 rads/s which would still be considered a little high in practice, however an improvement from Design 1 is clearly evident.

With the value of  $\rho$  unchanged, a 17<sup>th</sup> order controller  $K_\infty$  with a slightly lower uncertainty margin of  $\epsilon = 0.24$  ( $\gamma = 4.17$ ) was obtained after the optimisation process. This value of  $\epsilon$  relates to 24% of tolerable uncertainty in  $N_s$  and  $M_s$  at the cross-over frequency range.

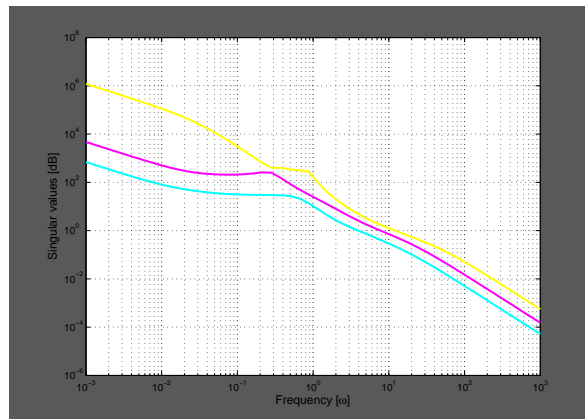
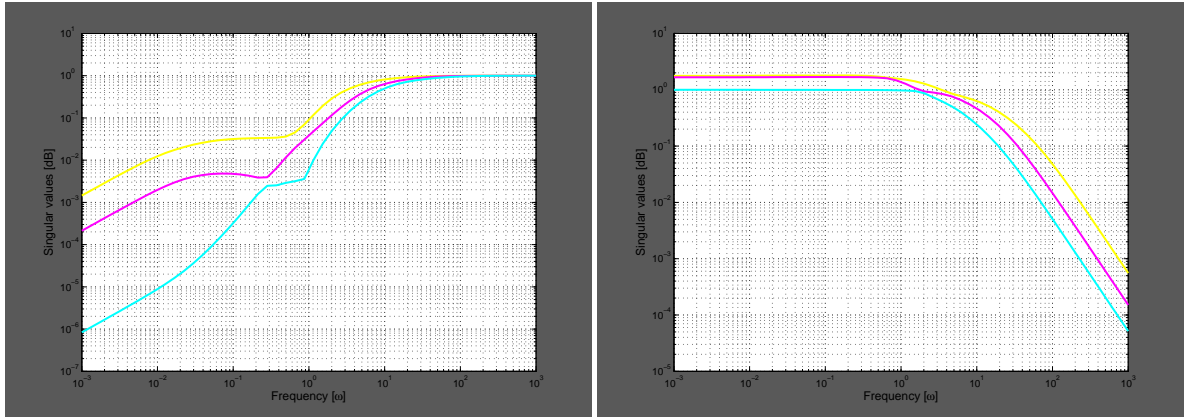


Figure 4.16: Stabilised open loop singular values - Design 2

The actual 2DOF controller,  $K$ , derived by combining the shaping function with the above controller,  $K_\infty$ , was of the order 20. In order to analyse the closed loop frequency response the feedback part of this controller,  $W_1K_2W_2$ , was then connected in series with the nominal plant. The singular value plot of the resultant loop transfer function,  $GW_1K_2W_2$ , is shown in Figure 4.16.

The corresponding sensitivity and cosensitivity singular value plots are illustrated in Figure 4.17. A closed loop bandwidth of 8 rads/s was found from the loop transfer function frequency response. Loop transfer function had the desired text book shape with high loop gain at low frequencies below the gain crossover frequency and this guarantees good low frequency disturbance rejection and good steady state command following. This was further confirmed by the sensitivity plot with the maximum singular value  $\bar{\sigma}((I + GW_1K_2W_2)^{-1}) \ll 1$  at frequencies below about 0.5 rads/s. At frequencies above the crossover frequency the open-loop transfer function had the desirable low loop gain, ensuring attenuation of mea-



Sensitivity plot

Cosensitivity plot

Figure 4.17: Closed loop frequency response - Design 2

surement noise and the cosensitivity plot confirms this further with high roll off rate at high frequencies. There was also a significant improvement in the closed loop bandwidth ( $\approx 10$  rads/s from the cosensitivity perspective), however, as it was effectively the same as the upper limit set by the open loop singular values and as this would cause performance deterioration (as shown in the time domain results in Figures 4.35, 4.36 and 4.37), further iterations were conducted.

### Design 3

Subsequently the following pre-compensator  $W_1$  was finalised

$$W_1 = \text{diag} \left( \frac{(s + 2.5)}{4s}, \frac{(s + 2.5)}{4s}, \frac{(s + 5)}{2s} \right) \quad (4.6)$$

and as before the post compensator  $W_2$  was unchanged. The shaped (solid) singular values along with the nominal (dashed) are presented in Figure 4.18. The effect of the shaping function is clearly evident as the shaped plant now has the desired shape of high loop gain at low frequency and low loop gain at high frequency. Crucially, the open-loop bandwidth is now noted to be a low and acceptable 4.5 rads/s (9 rads/s with Design 2).

The value of  $\rho$  was left constant and the  $\mathcal{H}_\infty$  optimal control problem was solved. As a result a 17<sup>th</sup> order controller,  $K_\infty$ , with a slightly lower uncertainty margin of  $\epsilon = 0.23$  ( $\gamma = 4.33$ ) was produced.

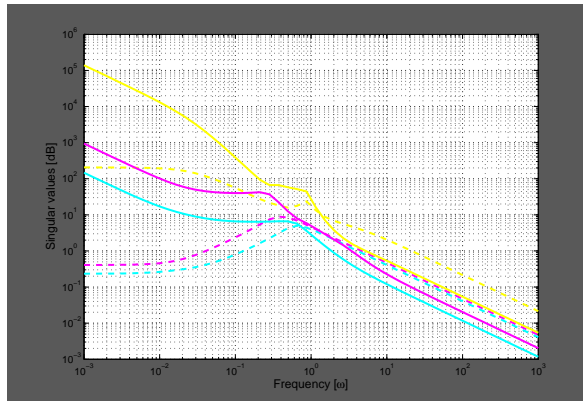


Figure 4.18: Shaped open loop singular values - Design 3

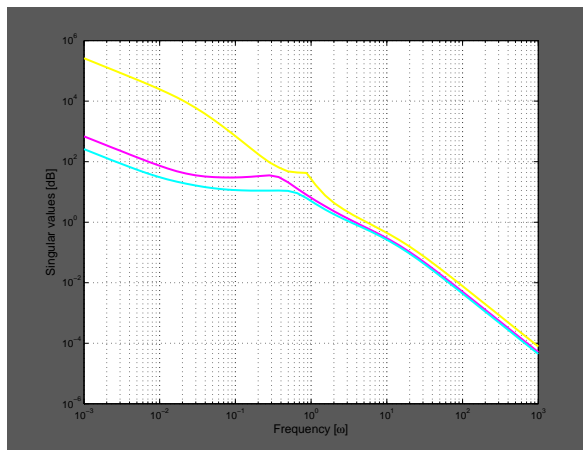
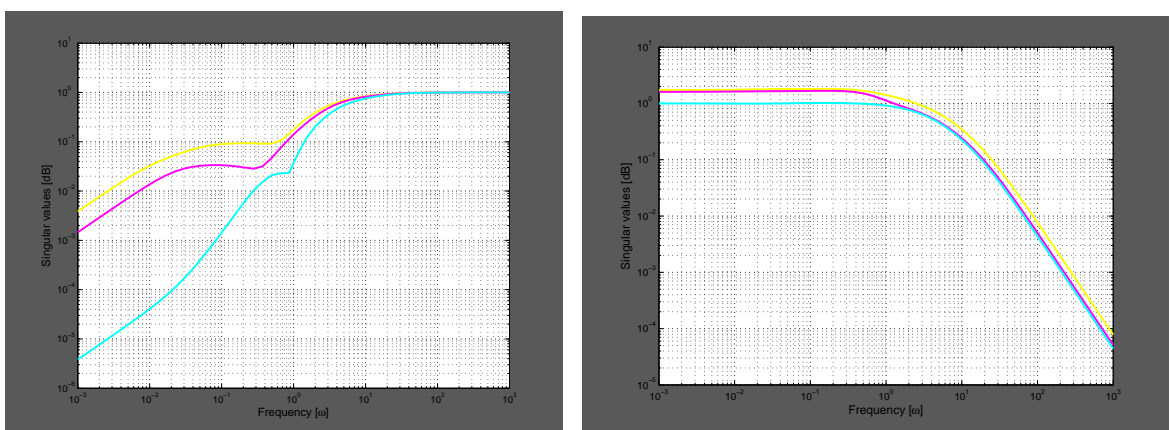


Figure 4.19: Stabilised open loop singular values - Design 3



Sensitivity plot

Cosensitivity plot

Figure 4.20: Closed loop frequency response - Design 3

The final 2DOF controller  $K = W_1 \begin{bmatrix} K_1 & K_2 W_2 \end{bmatrix}$  was then derived from the above controller and similarly to Design 2, produced a 20<sup>th</sup> order controller. The loop frequency

response (Figure 4.19) showed a comparatively higher low frequency gain and also the bandwidth of 6 rads/s, which is less than the limit set by the open loop singular values. The larger low frequency gain would guarantee performance and lower controller bandwidth would guarantee stability against variation in flight conditions. The corresponding sensitivity and cosensitivity plots are shown in Figure 4.20. These plots further confirm the above results with maximum singular value  $\bar{\sigma}((I + GW_1K_2W_2)^{-1}) \ll 1$  at low frequencies in the sensitivity plot and  $\bar{\sigma}(GW_1K_2W_2(I + GW_1K_2W_2)^{-1}) \ll 1$  at high frequencies in the cosensitivity plot. Also, the plots also show a lower closed loop bandwidth of 5 rads/s observed from the cosensitivity plot.

## 4.4 Linear simulation results

The controller design discussed in the previous section was assessed using both linear (presented here) and nonlinear (presented in Chapter 7) time domain simulation. While the frequency domain analysis gives a rough indication of the effectiveness of a given controller design, as it is based mainly on singular value analysis, it is not precise enough to yield sufficient information about the level of coupling and transient behaviour of the system. Thus the time domain results presented here give a vital counterpart to the frequency domain analysis. For simplicity, all simulation results given in this section consider axis-by-axis pulse input demands. While a little artificial, such analysis gives a good indication of the level of coupling and transient response of the aircraft, although the long term responses must be interpreted with care. For both the frequency and time domain analysis, the controller was implemented as shown in Figure 4.21,

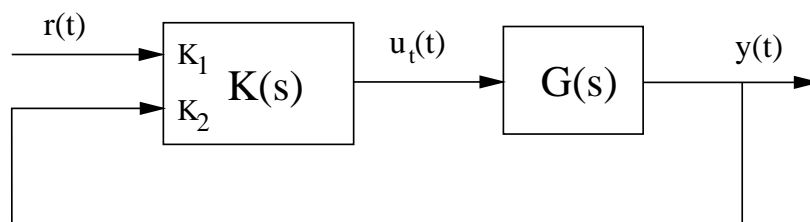


Figure 4.21: 25-state SIMULINK model for time domain analysis

where

- $r(t) = \begin{bmatrix} \theta_{dem} \\ \phi_{dem} \\ r_{dem} \end{bmatrix} = \text{Pilot demand}$
- $y(t) = \begin{bmatrix} \theta \\ \phi \\ r \\ q \\ p \end{bmatrix} = \text{System output}$
- $\begin{bmatrix} K_1 & K_2 \end{bmatrix} = W_1 \begin{bmatrix} K_1 & K_2 W_2 \end{bmatrix} = \text{2DOF controller}$
- $u_t(t) = \begin{bmatrix} \textit{Longitudinal cyclic} \\ \textit{Lateral cyclic} \\ \textit{Tail rotor collective} \end{bmatrix} = \text{Control effector}$

Recall that the controller was designed using a reduced order 8-state linear plant at a 40kts /0ft/14200kg trim condition. However, the linear plant used to assess its time domain performance was the full 25-state linear model. A variety of trim points (Table 4.6) were tested, although only a selection are presented here. The trim points shown here are 0kts/0ft/11000kg, 40kts /0ft/11000kg, 80kts/4500ft/11000kg, 0kts/0ft/14200kg, 40kts/0ft/14200kg and 80kts /2500ft/14200kg. Also, at each trim point the demands of  $-20$  deg,  $20$  deg and  $-10$  deg/s were applied one by one to the pitch, roll and yaw channel respectively.

#### 4.4.1 Longitudinal response

Pitch attitude responses at the listed flight conditions are illustrated in Figure 4.26. Linear pitch attitude response at the design point is fast and smooth as that predicted by the second order reference model with little coupling into other channels and certainly less than the 25% limit specified by the ADS-33 standard. The pitch rate also appears smooth and predictable. The responses at the off-trim points also maintain the general form of the on-trim response, however minor degradations were observed. The response at 40kts/0ft/11000kg flight condition shows minimal degradation. The response was faster by 0.2 s with an overshoot of

1.5% and coupling was similar to that at the design point. At the hover condition, it can be seen that there is slightly more “steady state” coupling than at the design point, however, no major degradations were observed in the performance. Also, there is a slight “wash-out” in the response leading to a “steady state” error of around 1 deg. At the 80kts/2500ft/14200kg condition, the response is slightly slower compared to the design point and has an overshoot of 4%. Off-axis responses at this flight condition were generally good, although there was some initial roll transients of a significant magnitude. Similar response was achieved at the flight condition 80kts/4500ft/11000kg. Figures 4.27 and 4.28 illustrate the variations in on-axis pitch attitude response with changes to flight conditions. It was observed that the single MIMO controller was highly effective at all flight conditions, with the exception of 10kts forward speed.

#### **4.4.2 Lateral response**

Figure 4.29 shows the roll attitude response at the above flight conditions. At each of the flight conditions, the response is very similar with a swift and smooth transient response in roll attitude and effectively no steady state error. Off-axis responses appear very good, with only the 80 kts flight condition showing a slight long-term off-set in pitch attitude. Damping in all cases appears good with an overshoot of zero. Figures 4.30 and 4.31 illustrate the variations in on-axis roll attitude response with changes to flight conditions. However, unlike the longitudinal channel the MIMO controller was effective at all flight conditions.

#### **4.4.3 Directional response**

Yaw rate responses are shown in Figure 4.32. As with the pitch and roll attitude responses, the yaw rate response is best at the design point. On-axis response is good, being swift and well-damped, and off-axis response is acceptable but with some steady state coupling into pitch. Recall, that the singular values did not display “ideal” integrator behaviour at low frequencies. At the other flight conditions, the on-axis yaw response was broadly similar apart from a slight steady state error of about 1 deg at hover and overshoot of approximately 4% at high speed flight condition, although remember that this is in yaw rate which is difficult for a pilot to detect. Most of the off-trim degradation in responses manifested itself

as increased coupling into other axes. The hover condition is particularly noticeable with coupling reaching just below 20% transiently in most off-axis variables. However, this level of coupling was thought to be acceptable as it was within the 25% tolerance specified by the ADS-33 document. Figures 4.33 and 4.34 illustrate the variations in on-axis yaw rate response with changes to flight conditions. The single MIMO controller was again seen to be highly effective against variations in flight conditions.

#### **4.4.4 Comparison to Design 2**

The relative weakness of Design 2 can also be illustrated by the time responses presented in Figures 4.35 (pitch), 4.36 (roll) and 4.37 (yaw). Comparing the pitch attitude response from Design 2 to Design 3 shows a similar on-axis performance at the design point as well as the off-trim flight conditions. However, the off-axis behaviour at each of the condition show minor deteriorations. There is a development of a “kink” in pitch rate response at high velocity flight condition and appears to allow an oscillatory transient behaviour in roll axis. While this was not thought to be too much of a problem it is noted as a deficiency of this design which might cause pilot complaint. Effectively this “kink” in pitch rate manifests itself as an abrupt acceleration of the rotorcraft that appears as a “jerk” to the pilot. The roll attitude response shows minor deterioration in the on-axis performance, especially at high velocity flight conditions, and there is a significant amount of degradation in roll rate response with an exaggerated presence of several uncomfortable “kinks”. Again, these kinks cause “jerky” accelerations of the helicopter that could cause discomfort to the pilot. Yaw rate responses, in terms of on-axis performance show minor degradation and off-axis responses show the presence of an oscillatory transient behaviour which would be deemed uncomfortable by the pilot. These high-order dynamics in Design 2 were mainly due to the closed loop controller bandwidth ( $\approx 10$  rads/s) being very close to the bandwidth limit set by the model reduction process. Due to its close proximity to the limit, it made the controller highly sensitive to the variation in flight conditions. In terms of countering inter-axis coupling, both controllers are equally capable of keeping it below the prescribed 25% mark. However, the responses have shown, comparatively, a lot more off-axis oscillation with Design 2 and that would suggest that the controller derived using Design 3 is more suited to the EH101 system. The main

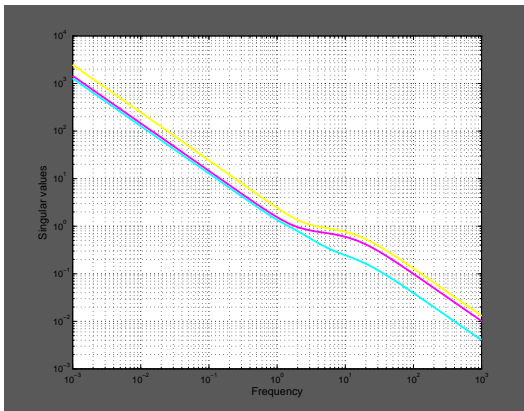
on-axis time response features are presented in Tables 4.13, 4.14 and 4.15. While these tables do not indicate much difference between Designs 2 and 3, the “jerky” rate behaviour is a notable weakness in Design 2 and was the main reason for iterating until Design 3 was obtained.

#### 4.4.5 Controller order reduction

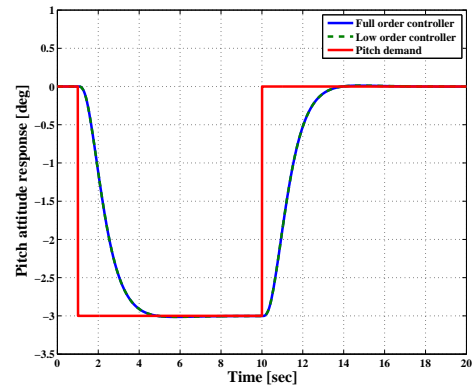
The above 2DOF  $\mathcal{H}_\infty$  loop shaping design methodology provided a feasible way of producing a robust FA controller. The resulting controller, however, was noted to be complicated with a high order ( $20^{th}$  in this case), making it difficult to be implemented in practice. Methods such as *truncation*, *residualisation*, *Hankel norm approximation*, are available in robust control toolbox that allow to reduce this order. These methods required either a balanced or a minimal realisation of the controller. As the above controller was noted to be marginally unstable with three eigenvalues at the origin, the normalised coprime factorisation was applied to the controller in order to obtain a balanced realisation and the controller order was then reduced by applying residualisation. There is a measure known as the  $\nu$ -gap that allows to measure the deviation of the reduced controller from the original full order controller. Table 4.12 shows the expected increase in this measure with reduction in controller order. Figures 4.22 to 4.25 shows the variation in controller performance (longitudinal channel) as the controller order is reduced. These plots show that a lower order controller (upto  $4^{th}$  in this case) is more or less capable of matching the full order controller performance. Despite these encouraging results, it was decided to work with the original full order  $\mathcal{H}_\infty$  controllers. Although from an implementation perspective, it indeed would be possible to replace the full order controllers with the reduced order versions of significantly less complexity, and because the thesis did not attempt to implement any controllers, this avenue of research was not pursued any further. Furthermore, the results obtained later in the thesis are not dependent on the controller order and hence in principle can be applied to any linear-based controller design. Thus, while it is acknowledged that in practice, the reduced order controllers would be preferable to implement, the  $\mathcal{H}_\infty$  controllers used throughout the remainder of the thesis are all of full order.

Controller order	$\nu - gap$
16	0.002
12	0.013
8	0.08
4	0.4

Table 4.12: Controller order  $\nu - gap$  variation

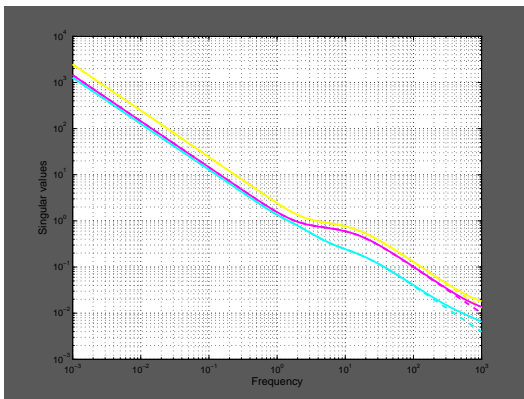


Frequency domain comparison

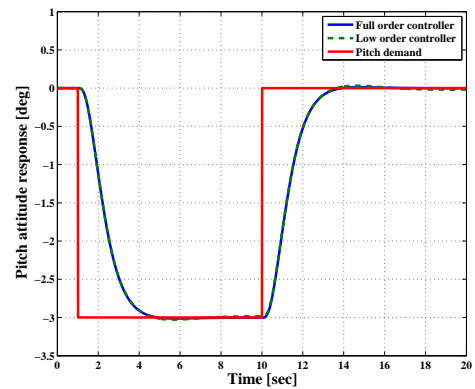


Controller performance

Figure 4.22: 16<sup>th</sup> order controller



Frequency domain comparison

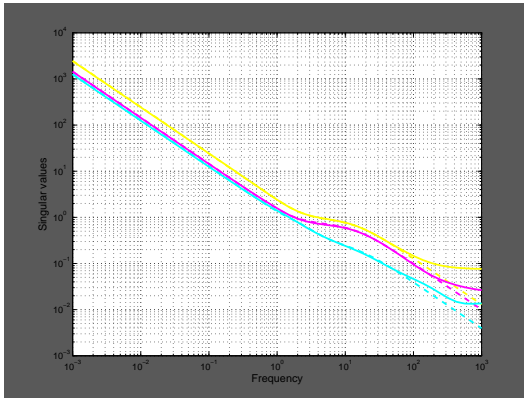


Controller performance

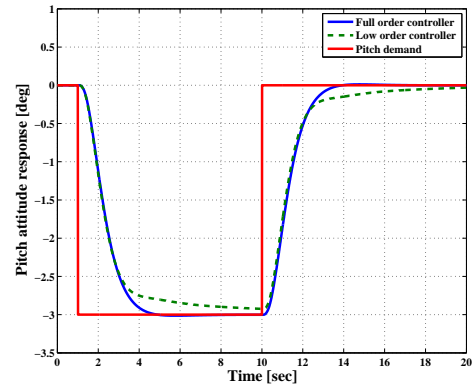
Figure 4.23: 12<sup>th</sup> order controller

## 4.5 Conclusion

The design of a multivariable FA controller using 2DOF  $\mathcal{H}_\infty$  loop shaping design procedure has been described. The methodology is systematic and fairly easy to tune, with the designer

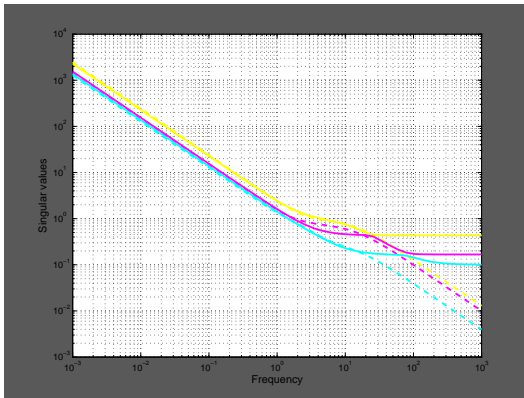


Frequency domain comparison

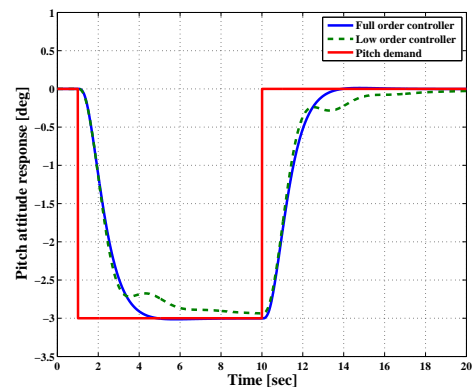


Controller performance

Figure 4.24: 8<sup>th</sup> order controller



Frequency domain comparison



Controller performance

Figure 4.25: 4<sup>th</sup> order controller

only having to select weighting functions for controller re-design. The controllers described in this chapter were LTI controllers, designed at an operating point of 40kts/0ft/14200kg and featured no scheduling. Three different designs were proposed and it was concluded that Design 1 with non-dynamic weights was the weakest amongst them with poor frequency and time response features. Designs 2 and 3 with the dynamic weighting functions were both satisfactory at the design point and both performed well at other conditions within the flight envelope. However, the fragility of Design 2 became apparent with poor off-axis performances, particularly at off-trim flight conditions. Design 3 produced satisfactory results at all the tested flight conditions with minimal degradation in performance at both on and off-trim points. Design 2 contained higher singular value bandwidths (in terms of sensitivity and cosensitivity function) than necessary thus making Design 3 clearly the preferred con-

troller, both as a standalone FA controller, and as the basis from which the LA controller could be constructed. The following chapter presents LA architecture proposed in this study along with the state-space based formulae to transform the FA controller derived here so that it is fully functional in the proposed LA architecture.

Flight condition	Rise Time (sec)		Overshoot (%)	
	Design 3	Design 2	Design 3	Design 2
40kts/0ft/14200kg	1.8	1.8	0.5	0.5
40kts/0ft/11000kg	1.6	1.6	1.5	1.5
Hover/14200kg	2.0	2.0	0.0	0.0
Hover/11000kg	1.8	1.8	0.0	0.0
80kts/2500ft/14200kg	2.1	2.0	4.0	2.0
80kts/4500ft/11000kg	2.0	1.9	4.5	2.5

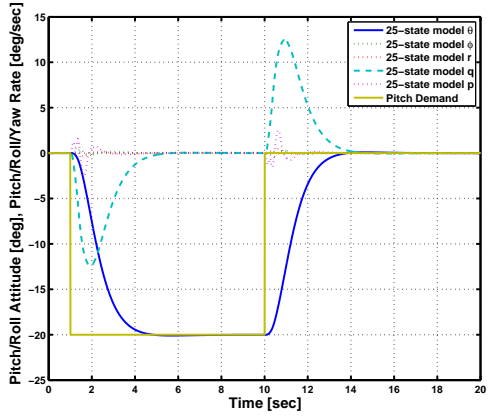
Table 4.13: Pitch attitude time response features

Flight condition	Rise Time (sec)		Overshoot (%)	
	Design 3	Design 2	Design 3	Design 2
40kts/0ft/14200kg	1.4	1.4	0.2	0.0
40kts/0ft/11000kg	1.4	1.4	1.0	0.5
Hover/14200kg	1.4	1.4	0.5	0.5
Hover/11000kg	1.4	1.4	0.3	0.3
80kts/2500ft/14200kg	1.4	1.4	1.6	0.8
80kts/4500ft/11000kg	1.4	1.4	2.0	1.0

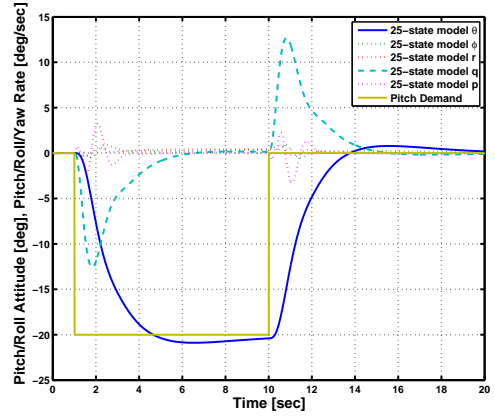
Table 4.14: Roll attitude time response features

Flight condition	Rise Time (sec)		Overshoot (%)	
	Design 3	Design 2	Design 3	Design 2
40kts/0ft/14200kg	0.8	0.7	0.5	0.0
40kts/0ft/11000kg	0.8	0.7	0.8	0.0
Hover/14200kg	0.7	0.7	3.0	0.0
Hover/11000kg	0.7	0.7	3.9	0.0
80kts/2500ft/14200kg	1.0	1.0	0.0	0.0
80kts/4500ft/11000kg	1.0	1.0	0.0	0.0

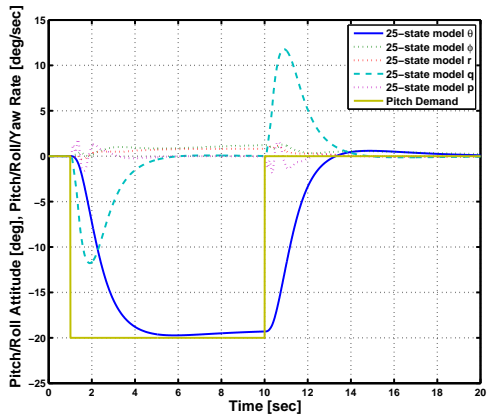
Table 4.15: Yaw rate time response features



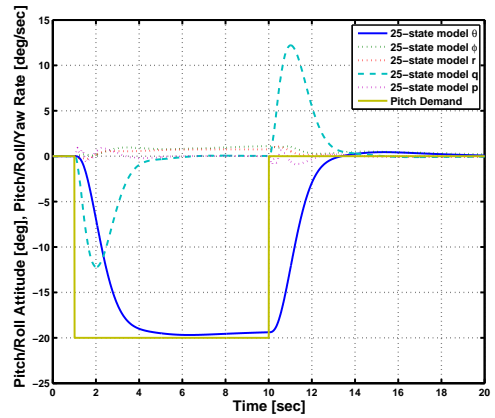
40kts/0ft/14200kg (Design point)



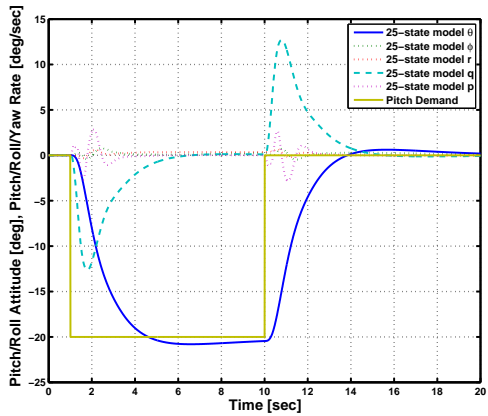
40kts/0ft/11000kg



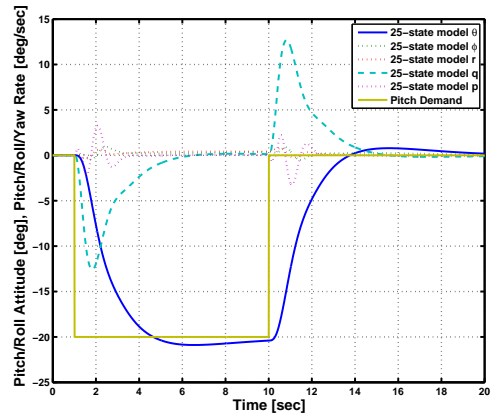
Hover/14200kg



Hover/11000kg

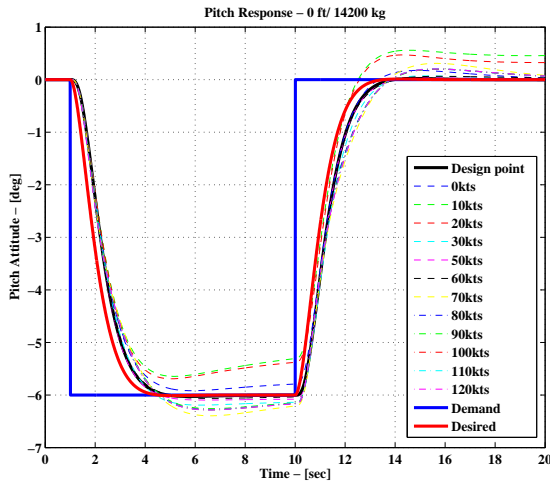


80kts/2500ft/14200kg

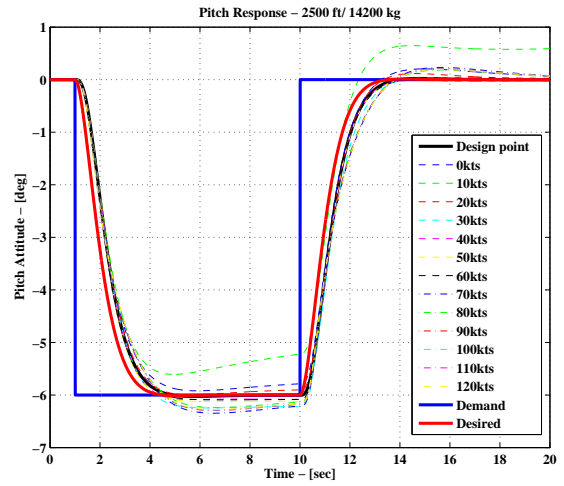


80kts/4500ft/11000kg

Figure 4.26: Pitch attitude time response - Design 3

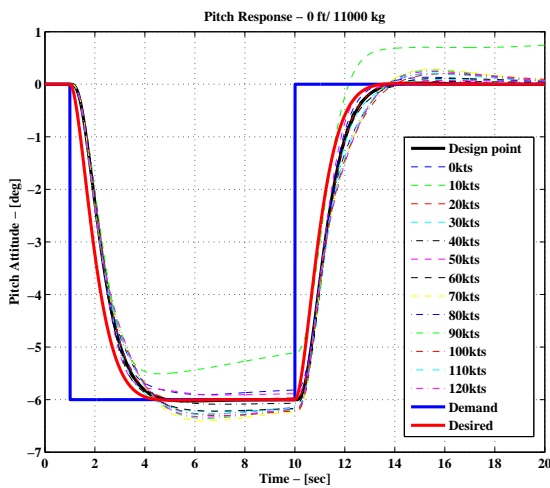


0 ft

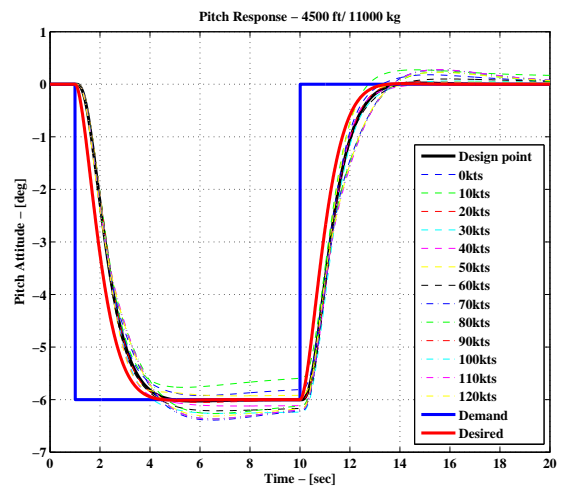


2500 ft

Figure 4.27: Variation in longitudinal response with flight condition (14200kg)

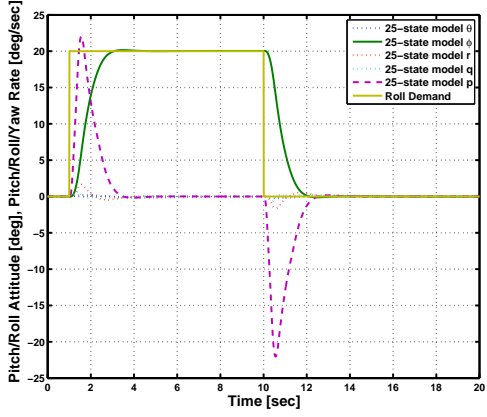


0 ft

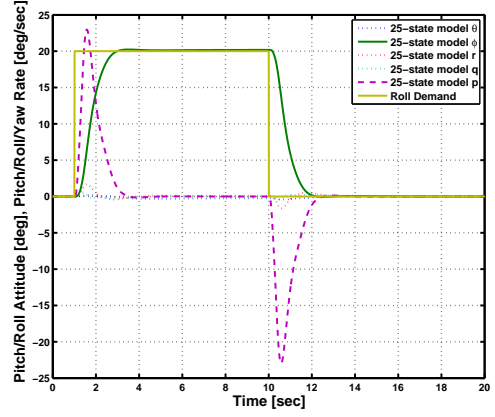


4500 ft

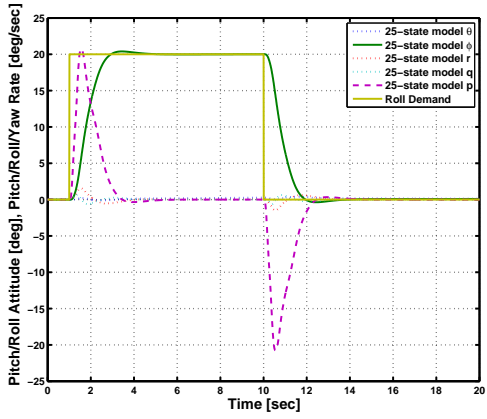
Figure 4.28: Variation in longitudinal response with flight condition (11000kg)



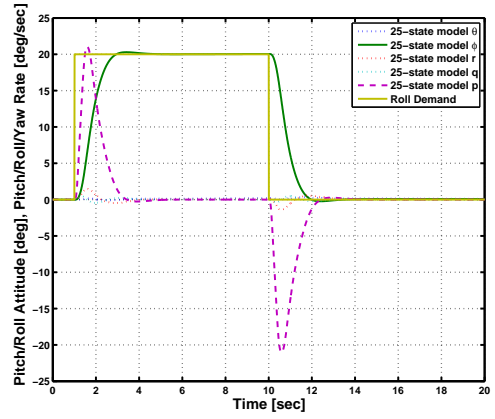
40kts/0ft/14200kg (Design point)



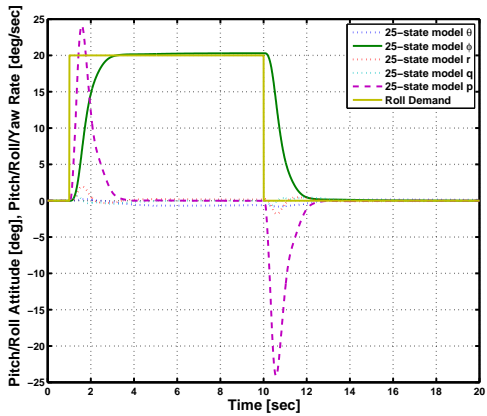
40kts/0ft/11000kg



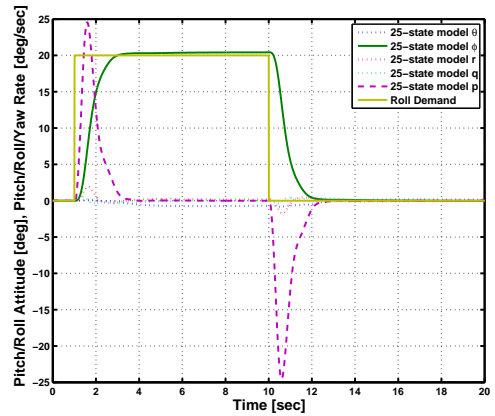
Hover/14200kg



Hover/11000kg

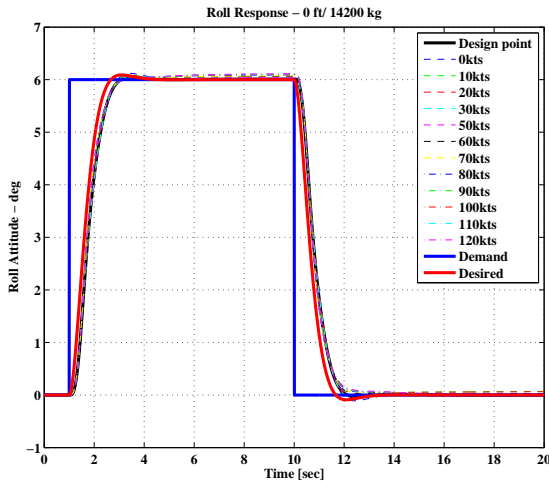


80kts/2500ft/14200kg

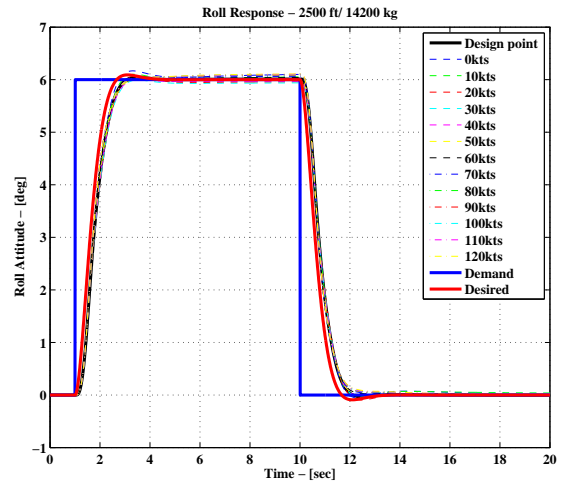


80kts/4500ft/11000kg

Figure 4.29: Roll attitude time response - Design 3

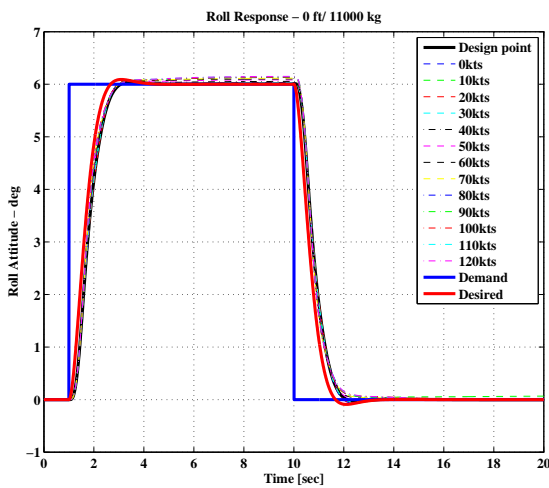


0 ft

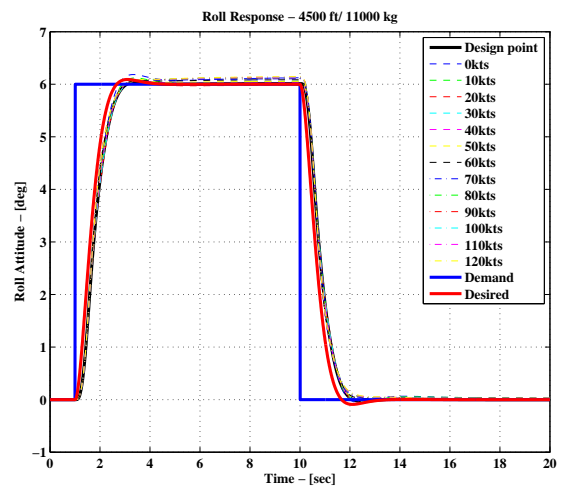


2500 ft

Figure 4.30: Variation in lateral response with flight condition (14200kg)

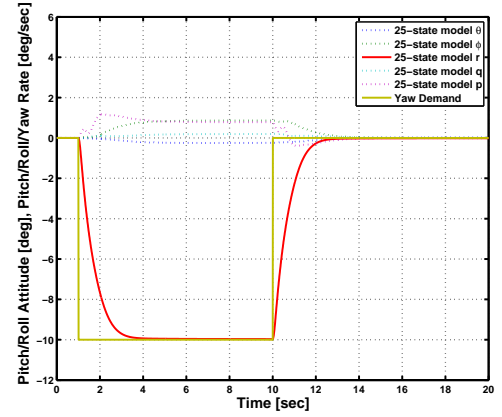
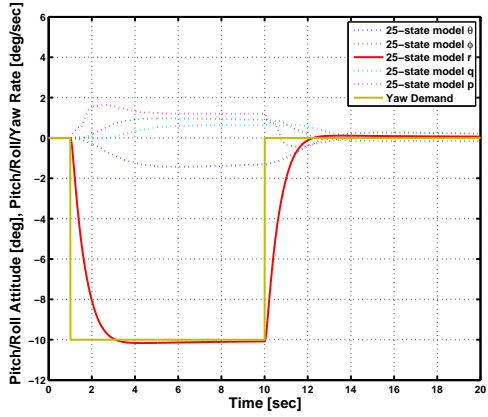


0 ft



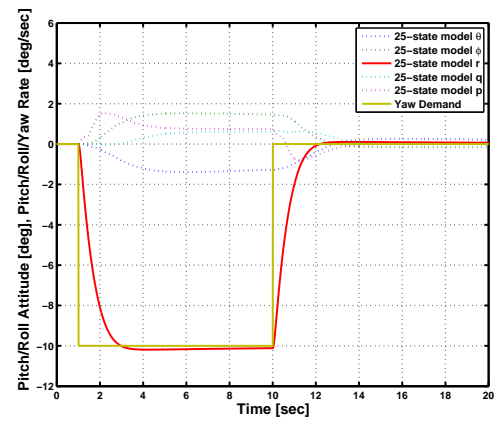
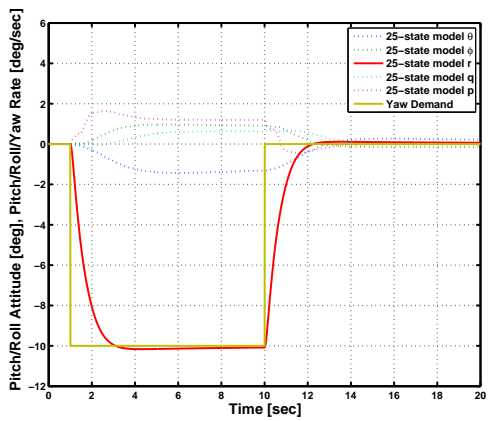
4500 ft

Figure 4.31: Variation in lateral response with flight condition (11000kg)



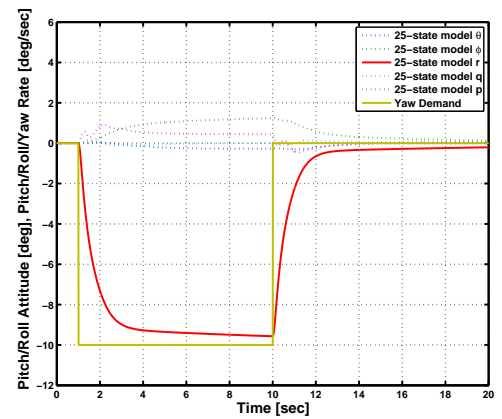
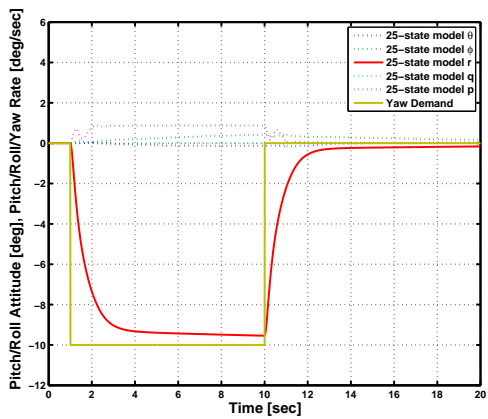
40kts/0ft/14200kg (Design point)

40kts/0ft/11000kg



Hover/14200kg

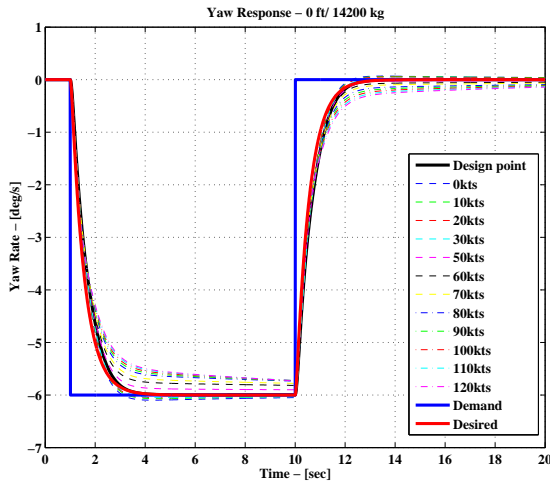
Hover/11000kg



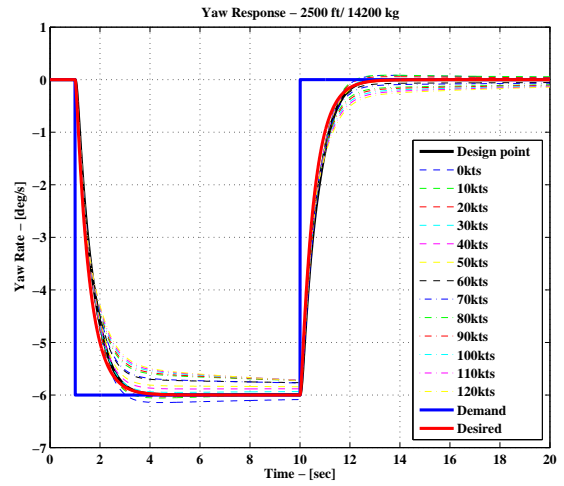
80kts/2500ft/14200kg

80kts/4500ft/11000kg

Figure 4.32: Yaw rate time response - Design 3

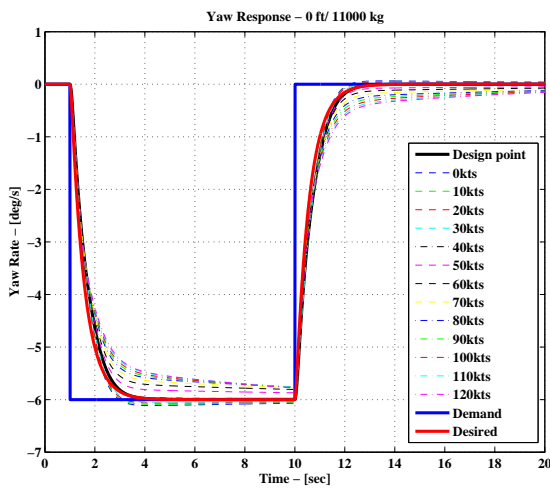


0 ft

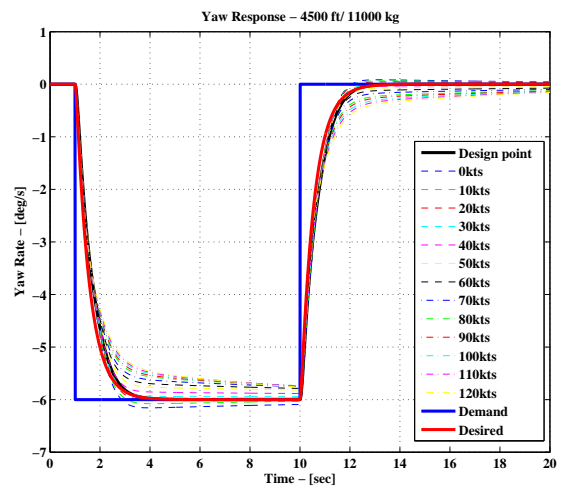


2500 ft

Figure 4.33: Variation in directional response with flight condition (14200kg)

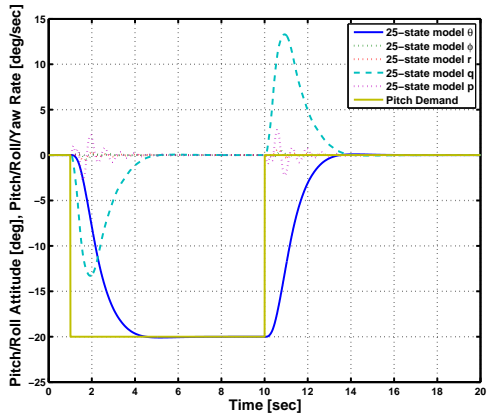


0 ft

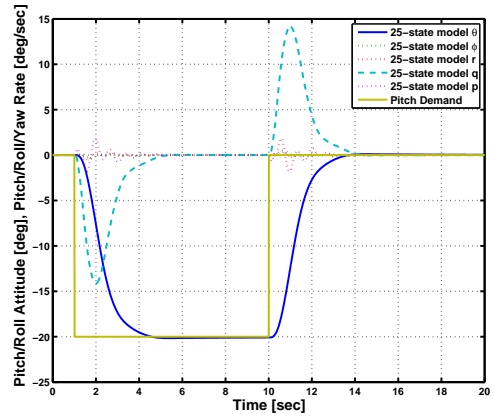


4500 ft

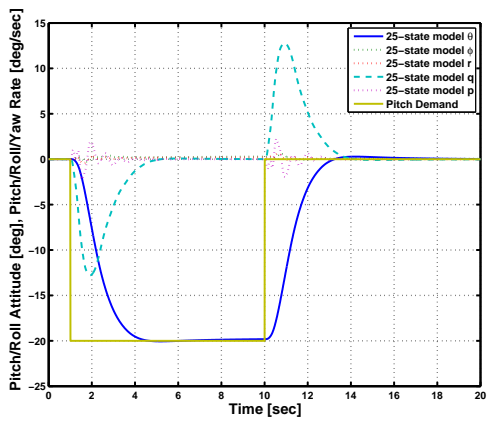
Figure 4.34: Variation in directional response with flight condition (11000kg)



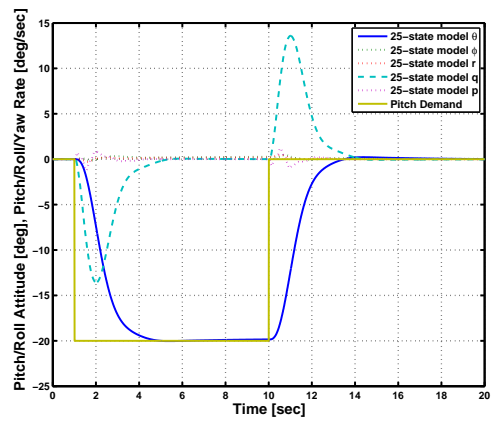
40kts/0ft/14200kg (Design point)



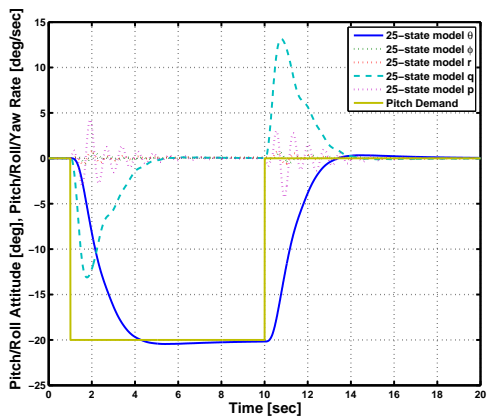
40kts/0ft/11000kg



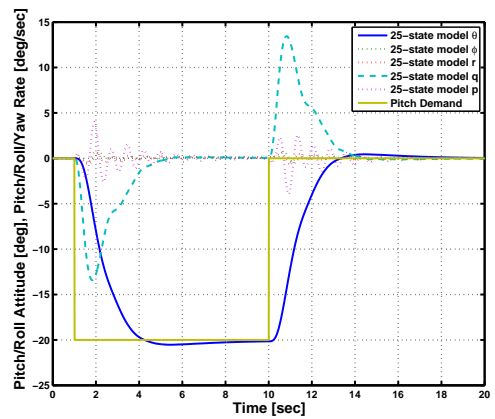
Hover/14200kg



Hover/11000kg

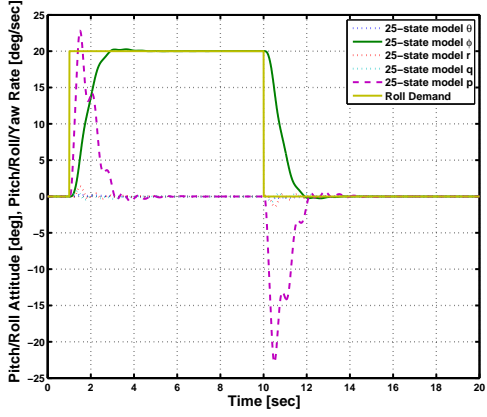


80kts/2500ft/14200kg

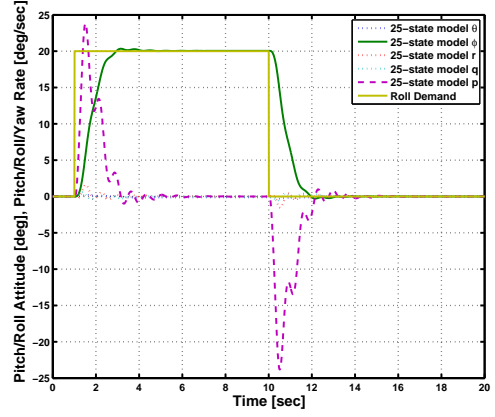


80kts/4500ft/11000kg

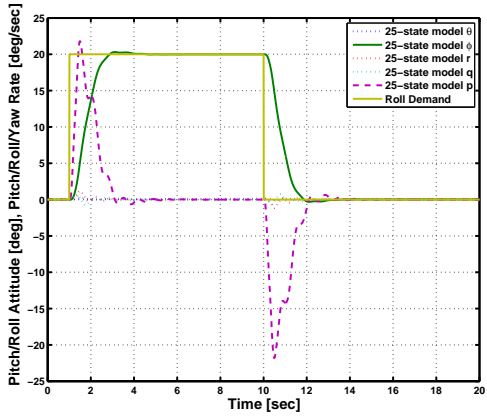
Figure 4.35: Pitch attitude time response - Design 2



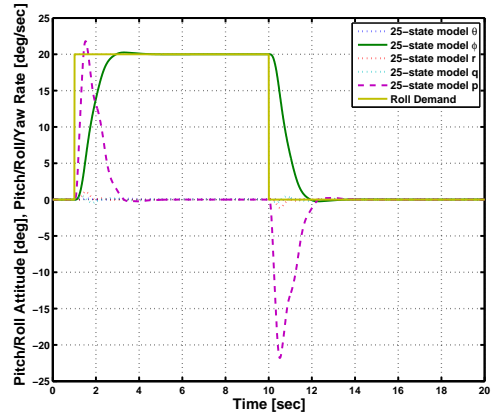
40kts/0ft/14200kg (Design point)



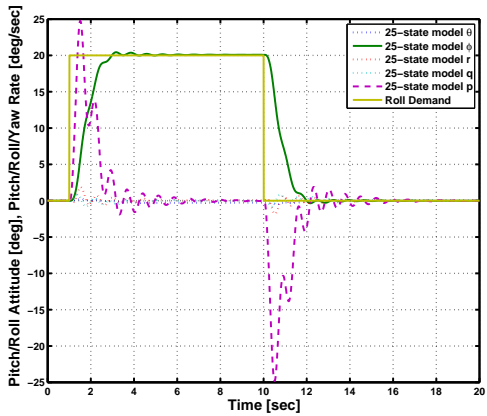
40kts/0ft/11000kg



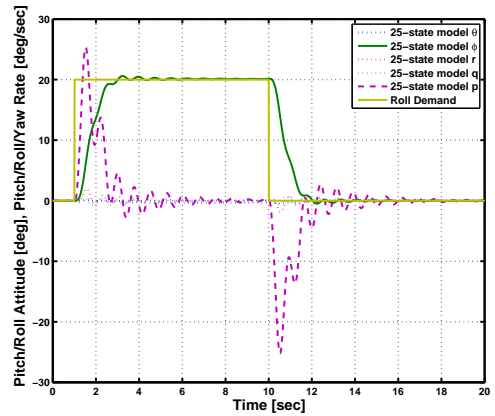
Hover/14200kg



Hover/11000kg

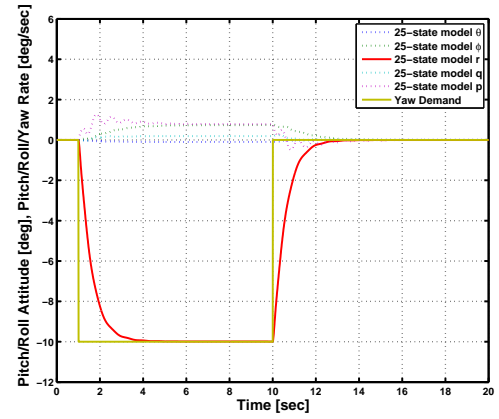
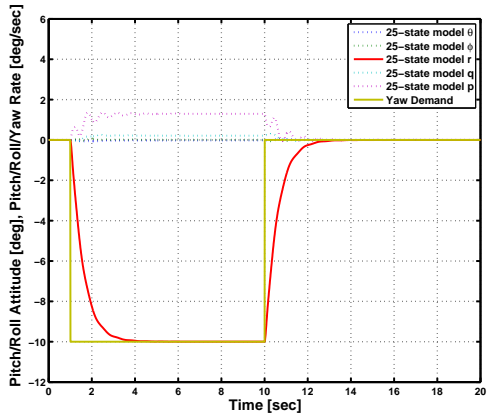


80kts/2500ft/14200kg



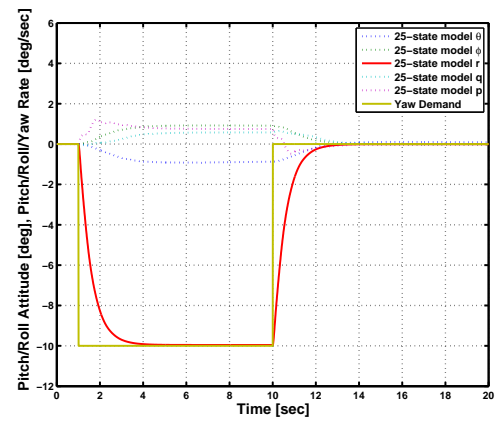
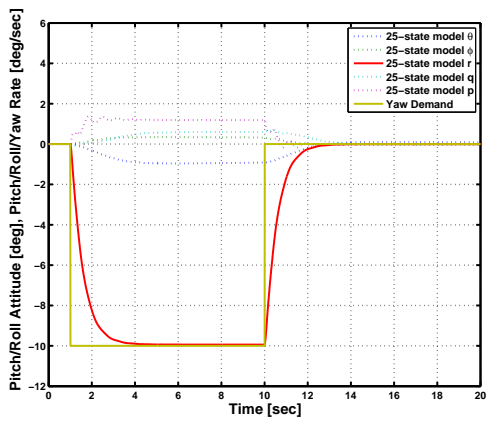
80kts/4500ft/11000kg

Figure 4.36: Roll attitude time response - Design 2



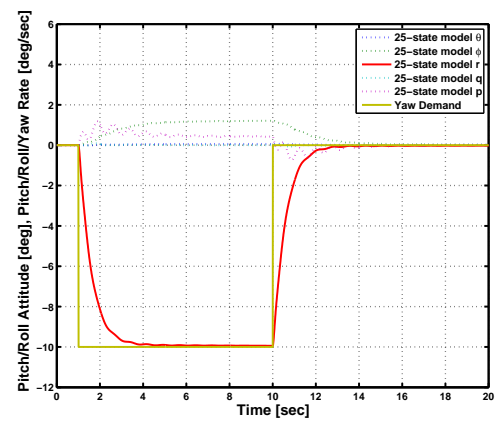
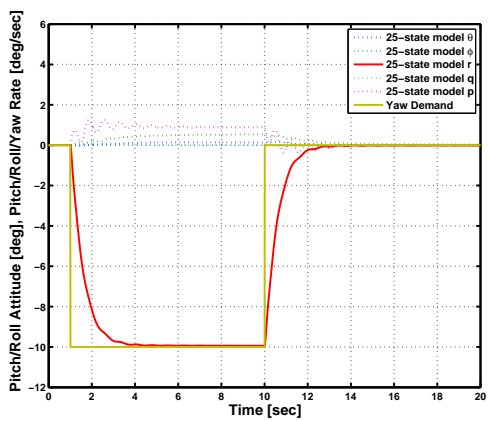
40kts/0ft/14200kg (Design point)

40kts/0ft/11000kg



Hover/14200kg

Hover/11000kg



80kts/2500ft/14200kg

80kts/4500ft/11000kg

Figure 4.37: Yaw rate time response - Design 2

# Chapter 5

## Transformation to limited authority controllers

The findings of Chapter 4 suggest that a well-designed FA controller can bestow desirable characteristics on a helicopter as coupled and nonlinear as the EH101. However, as mentioned in Chapter 1, there is a desire to realise FA performance within the LA framework. This chapter discusses the architecture of LA controllers and identifies some of the system theoretic problems which arise in their design. In particular, the implications of injecting reference demands to the controller are discussed in detail. A state space based formulae is also developed that would then translate an arbitrary FA controller into a LA architecture that would produce identical FA performance.

### 5.1 Limited authority control systems

In LA architectures, the FCS is a combination of a mechanical and an electronic system. The mechanical system consists of hydraulic interlinks with which the pilot has total control over the swash plates. The electronic system consists of the stabilisation strategy that achieves augmentation of basic handling qualities either via the limited authority, high rate series actuators alone or via the combination of series actuators with the high authority, limited rate parallel actuators.

Recent years have seen significant progress in the application of modern control techniques

to helicopter FA FCS design. However, there is still a lack of rigorous, systematic theory to assist the engineer in the construction of LA control systems. Moreover, with the arrival of digital FBW (fly-by-wire) technology there is the possibility of constructing more advanced control systems to deliver improved performance and functionality. Despite this, even state of the art contributions have tended to gloss over a crucial issue in LA control system design: the transpositions of a FA system into a LA one. Although the harmonious functionality of series and parallel actuators are mentioned to some extent in [31], the parallel actuator control systems appear more as retro fits to predominantly a series actuator based design rather being an integral part of a more holistic design. It is important to remark that, from a control perspective at least, the LA architecture can be seen as a problem because it is rather different to the control system architectures found in standard texts on control system design, where FA architectures are assumed to be the norm. The aim of this chapter, which also is a significant contribution of this study, is to develop a method which provides a systematic way of translating a FA controller, which may be designed using any standard method, into a LA architecture. It ensures that the small signal performance of the original FA controller are matched by the resulting LA.

In order to comprehend the functionality of a LA control system, it is best to refer to Figure 5.1. The total control input to the swash plate comprises a direct mechanical link between the pilot's stick and the swash plates, plus a contribution from the *series actuators*, the input of which is generated from the electronic controller. The reference for the electronic controller is generated by the stick datum. In turn this is influenced by the pilot's stick position and the *parallel actuators* which are also driven by the electronic controller. It should be noted at this stage that the electronic controller only has authority over the series and parallel actuators and their correct use is crucial to the functionality of a LA control system. Thus the total control signal delivered to the helicopter's swash plate is dependent on the direct pilot command through the mechanical interlinks, the series and the parallel actuators. Depending on which combination of these devices is used the type of control system achieved is classified as:

1. **Manual control** : This operation utilises full control authority mechanical system that is influenced by the absolute stick datum and allows the pilot to influence the swash plates independently to the electronic controller. However helicopters are inherently unstable machines and pilot workload can be high when operating under difficult flying

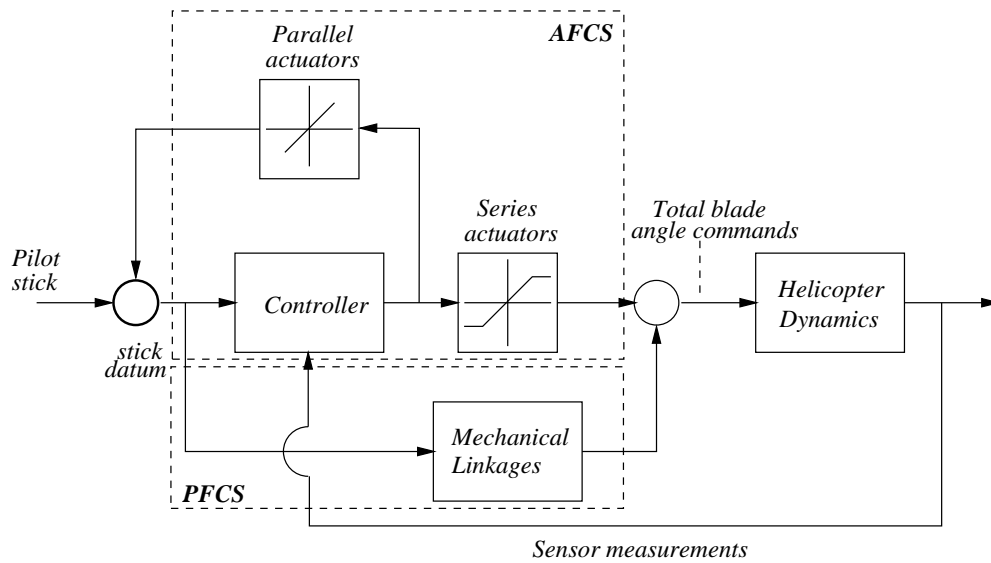


Figure 5.1: LA schematic [85]

conditions. Therefore, the FCS is improved by additional operations to ease pilot workload and to permit better performance.

2. **Auto-stabilisation :** In order to reduce the pilot workload and to improve handling qualities, LA architectures utilise an auto-stabilisation loop. The stabilisation corrections are made by means of electrically driven fast *series actuators*. They operate with a limited control authority in order to protect against hardover failures [41], i.e. not allowing the actuators to be driven to extreme positions. These actuators receive stabilisation signals from the electronic controller and then provide fast input to the swashplates without feeding back to the pilot's control stick, hence they are said to be in series with the pilot. Now, their key feature, from a control designers perspective is that they are modelled as a saturation element. This essentially limits the *magnitude* of the output. As the saturation level is set to a small percentage of the total control authority, for large stick inputs or aggressive manoeuvring, these actuators have the tendency to saturate.
3. **Autopilot :** The auto-stabilisation function sends small high frequency control inputs to the swashplates, whereas the autopilot function is used send slowly varying control inputs. The autopilot function is achieved by means of *parallel actuators* that can either be activated by the pilot's trim switch or by feedback. Along with slowly changing the swashplate these actuators are also reflected at the stick, hence they are said to be

in parallel to the pilot. The parallel actuators also have limited control authority, but unlike the series actuators, their dominant feature is that their *rate* is limited. Their rate is limited in order to protect the helicopter against excessive transient that arise in the event of a trim malfunction [41]. However, this limited rate does makes them prone to rate saturation and they are unable to react to sudden control signal changes, although their output can attain fairly large magnitudes.

Note that for low aggression pilot stick movements (i.e. low magnitude, low rate), the series actuators will not saturate and the parallel actuators will not rate-limit. However, as soon as more aggressive pilot commands are input, saturation in either magnitude (series actuators), rate (parallel actuators) or both is likely to occur. This makes the system nonlinear and unpredictable and is often a source for system stability problems and consequently degraded handling qualities. Effectively the saturation causes the helicopter to attain a more open loop type behaviour, transferring the task of stabilisation to the pilot and thereby increasing workload which then has a detrimental effect on the aircraft's handling qualities [35]. Another important feature to notice about the LA architecture is the way in which the parallel actuators appear, causing there to be an "inner loop" in the controller. Obviously care has to be taken to ensure that this itself is stable, as well as the overall outer loop involving the aircraft dynamics.

### **5.1.1 EH101 interlinks model**

In the work thus far, the interlinks between the absolute stick datum and the swashplate have been considered to be purely linear and constant. Similarly, the links between the series actuators and the swashplate have been assumed to be part of the plant model, as depicted in Figure 5.1. However, the EH101 interlinks model which was used in this study was supplied in a form which was somewhat different as shown in Figure 5.2. Considering Figure 5.2, it is evident that the interlinks provide a mapping from the series actuator commands, absolute stick datum commands and, main rotor torque and speed to cyclic, collective and engine torque. In particular, for the EH101, the series actuator command is split (equally) among two different physical actuators and thus the control architecture needs slight modification to account for this. This section describes how the EH101 configuration can be addressed

using the approach proposed in this thesis. It is assumed that the series actuator command will have the form,  $u'_s(t) = \begin{bmatrix} p'_s(t) & r'_s(t) & y'_s(t) \end{bmatrix}^T$ , where

- $p'_s(t)$  = Longitudinal series actuator command
- $r'_s(t)$  = Lateral series actuator command
- $y'_s(t)$  = Directional series actuator command

and the series actuator command in each channel is also equally divided, i.e.

$$p'_s(t) = \begin{bmatrix} \frac{1}{2}p'_s(t) & \frac{1}{2}p'_s(t) \end{bmatrix}^T, r'_s(t) = \begin{bmatrix} \frac{1}{2}r'_s(t) & \frac{1}{2}r'_s(t) \end{bmatrix}^T \text{ and } y'_s(t) = \begin{bmatrix} \frac{1}{2}y'_s(t) & \frac{1}{2}y'_s(t) \end{bmatrix}^T.$$

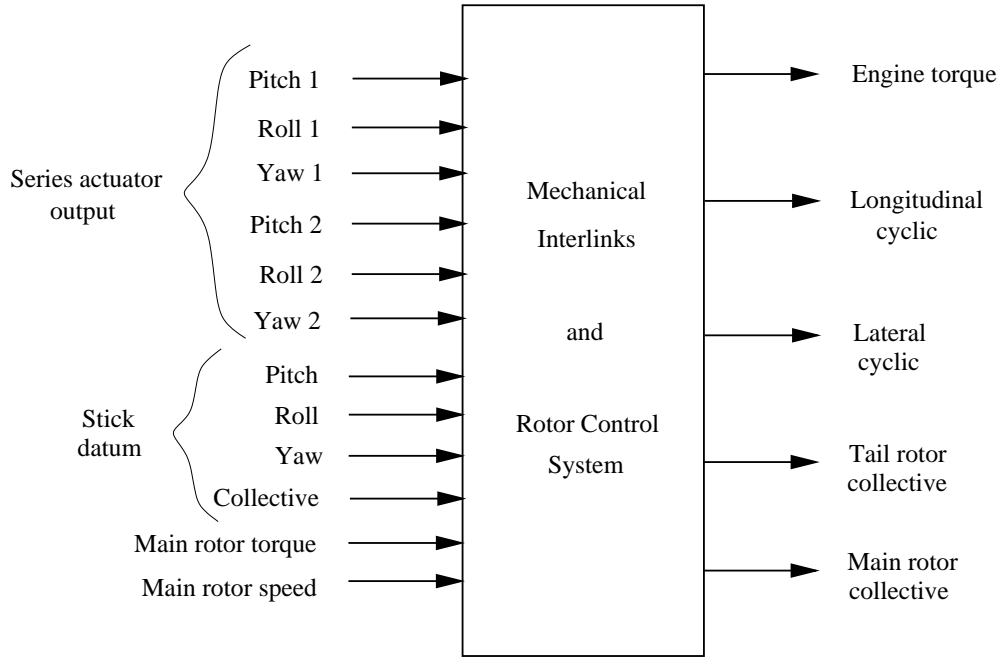


Figure 5.2: EH101 interlinks

The behaviour of this interlink is highly nonlinear and tends to vary with flight condition, thus presenting another complication to the controller design process. In order to simplify this process, the interlinks model is linearised at the same operating point at which the FA controller was designed and this produces a  $5 \times 12$  linear model. Next, the main rotor collective channel is left open-loop (pilot preference), the main rotor torque and speed are assumed to be constant and the engine torque is considered to have minimal influence during linear analysis. This effectively results in truncating the linearised model to a  $3 \times 9$  system which is then further divided into two subsystems:  $M$ , a  $3 \times 3$  system denoting the map

from stick datum commands to the cyclics and collectives and  $\hat{L}$ , a  $3 \times 6$  system denoting the map from the series actuator commands to the cyclics and collectives. As they both exhibited sufficiently fast poles, the subsystems were then simplified to their respective DC gain matrices. This produced matrices  $M \in \mathbb{R}^{3 \times 3}$  and  $\hat{L} \in \mathbb{R}^{3 \times 6}$ . It was further noted, that matrix  $\hat{L}$  (after some re-arrangement) consisted of two equal matrices, i.e.  $\hat{L} = \begin{bmatrix} L & L \end{bmatrix}$  where  $L \in \mathbb{R}^{3 \times 3}$ . Now, the total controller output,  $u_t(t)$ , was given by

$$u_t = \begin{bmatrix} L & L & M \end{bmatrix} \begin{bmatrix} \frac{1}{2}u'_s \\ \frac{1}{2}u'_s \\ r + u_p \end{bmatrix} \quad (5.1)$$

where,

- $r(t)$  = Pilot command
- $u_p(t)$  = Parallel actuator command
- $r(t) + u_p(t)$  = Absolute stick datum command

The above equation further simplifies to

$$u_t = \begin{bmatrix} L & M \end{bmatrix} \begin{bmatrix} u'_s \\ r + u_p \end{bmatrix} \quad (5.2)$$

This effectively meant that the linear LA architecture design and analysis could be simplified by replacing the matrix  $\hat{L}$  and the signal vector

$$u'_s(t) = \left[ \frac{1}{2}p'_s(t) \quad \frac{1}{2}r'_s(t) \quad \frac{1}{2}y'_s(t) \quad \frac{1}{2}p'_s(t) \quad \frac{1}{2}r'_s(t) \quad \frac{1}{2}y'_s(t) \right]^T \quad (5.3)$$

with matrix  $L$  and signal vector

$$u'_s(t) = \left[ p'_s(t) \quad r'_s(t) \quad y'_s(t) \right]^T \quad (5.4)$$

## 5.2 Proposed limited authority architecture

Perhaps the most important aspect of LA control system is to find a way in which the series and parallel actuators work together effectively and harmoniously. They are complementary in the sense that the series actuators are useful for fast, low magnitude control signals and the parallel actuators are useful for slow, large magnitude control activity. This, however, is a simplistic view and a number of ways of harnessing series and parallel actuators effectively have been proposed. Many are discussed in [31] and they range from simply using parallel actuators to trim the aircraft, to complementary filter approaches and more abstruse nonlinear schemes involving blending. In this study the architecture depicted in 5.3 is followed. In this architecture,

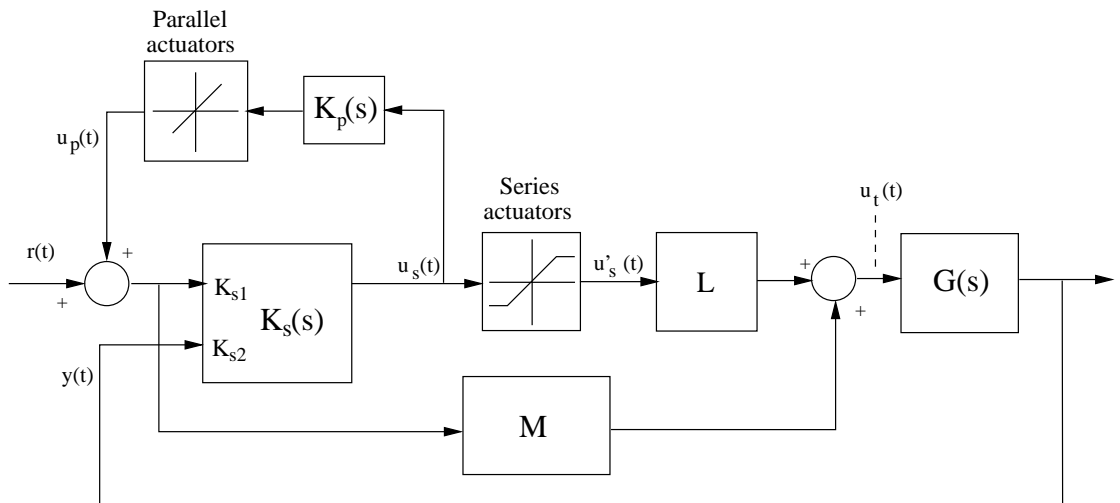


Figure 5.3: Proposed LA control architecture

- $u_s(t)$  = Series actuator input
- $u'_s(t)$  = Series actuator command
- $u_p(t)$  = Parallel actuator command
- $u_t(t)$  = Total controller output
- $G$  = Helicopter dynamics
- $M = 3 \times 3$  interlinks gain between stick datum to swash plate

- $L = 3 \times 3$  interlinks gain between series actuator command to swash plate
- $r(t) =$  Pilot command
- $y(t) =$  System output
- $K_s(s) = \begin{bmatrix} K_{s1} & K_{s2} \end{bmatrix} =$  Series component of LA controller
- $K_p(s) =$  Parallel component of LA controller

This architecture is in sync with the existing helicopter LA control system and is similar to that used in [35] and [85] in which the series actuator output is generated by the difference between an “ideal” control output and the mechanical linkage activity. The parallel actuators are then used to off-load the series actuators and ideally reduce their steady state output to zero, thus preventing long term saturation. The advantage of viewing the LA architecture in this manner is that it effectively partitions the electronic controller in two: the primary part is used for driving the series actuators to deliver responsive control activity and the secondary part of the controller is used purely for parallel actuator control which is used to influence the behaviour in a much slower manner and to off-load the series actuators, hopefully preventing their long-term steady state saturation. The following section will now present an analysis of this particular architecture and describe the formulae that would enable the transformation of the FA 2DOF controller described in the previous chapter.

### 5.3 Developing the state-space formulae

For small pilot demands, a LA controller should not cause the series or parallel actuators to encounter position or rate-limits and, in principle should operate in an essentially linear manner. However, there appears to be no wide agreement of how, precisely, a LA controller should be designed for such small signal behaviour. One can view an equivalent FA design as representing the “ideal” small signal behaviour. Then the problem becomes one of transposing the FA design (of arbitrary linear architecture) into a LA design, which has a restricted architecture due to the mechanical interlinks and the partitioning of the various control elements. In this section, state-space formulae which enable this transposition to be carried out systematically are given.

### 5.3.1 Small signal analysis

The proposed LA architecture is redrawn in Figure 5.4, where it is assumed that the series and parallel actuator control signals are sufficiently small such that position and rate-limits are not violated, and that the mechanical interlink components may be considered to be linear.  $r(t)$  is a three dimensional vector with elements  $r_i(t) \in [-50, 50]$  which represent the pilot forward/aft and left/right stick demands and the pedal demands respectively, where +50 (−50) indicates the maximum positive (negative) displacement of the inceptor.  $u_s(t)$  and  $u_p(t)$  denote the series and parallel actuator control signals, respectively, while  $u_t(t)$  denotes the total control signal appearing at the swash plate.  $y(t)$  is the vector of measurements fed back to the controller. For the purposes of this analysis it is assumed that  $M$  and  $L$  are purely static elements, although in reality they have high bandwidth linear dynamics. An informal statement of the LA control problem would be:

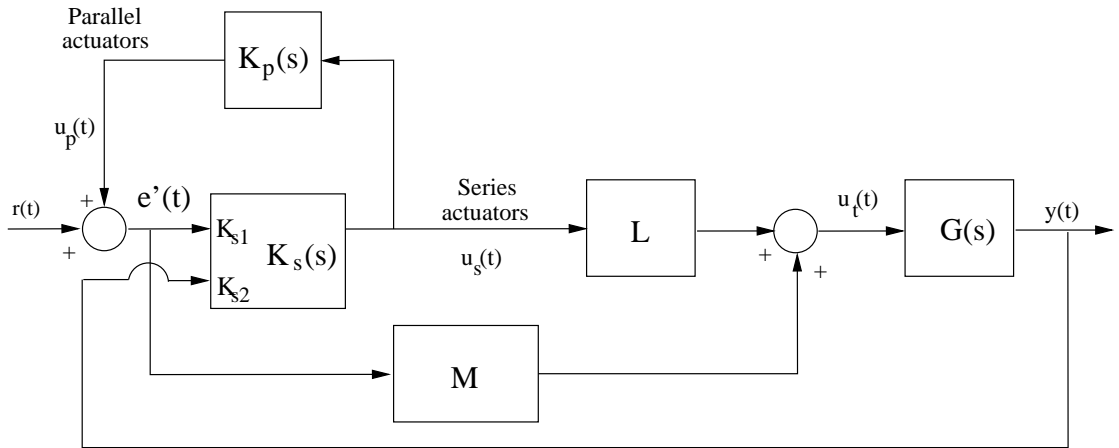


Figure 5.4: Unconstrained LA architecture

**Problem 5.1 LA control problem:** Given  $G(s)$ ,  $L$  and  $M$ , design  $K_s(s)$  and  $K_p(s)$  such that the outputs  $y$  due to stick  $r$  are desirable.

It is interesting to compare this to the FA problem, depicted in Figure 5.5, where the relationship between  $\begin{bmatrix} r \\ y \end{bmatrix}$  and  $u_t$  is simply given by  $K = \begin{bmatrix} K_1 & K_2 \end{bmatrix}$ . Informally the FA controller problem given by:

**Problem 5.2 FA control problem:** Given  $G(s)$ , design  $K(s)$  such that the outputs  $y$  due to stick  $r$  are desirable.

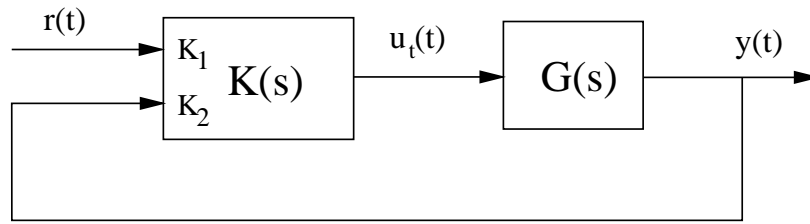


Figure 5.5: FA architecture

Note that both the LA control problem and the FA control problem seek controllers which give a relationship between  $\begin{bmatrix} r \\ y \end{bmatrix}$  and  $u_t$ , but the LA problem is *more constrained*. From a control theoretic perspective, in the FA control problem the controller's internal architecture is allowed to be *unconstrained*, whereas in the LA problem the controller architecture is forced to have structural disadvantages.

### 5.3.2 Translation to limited authority

There are many systematic methods available by which one can design FA control systems and indeed the vast majority of control theory concentrates on this. However there are few, if any, *systematic* methods for designing LA control systems of the architecture depicted in Figure 5.7. It therefore seems logical to determine whether an *arbitrary* FA controller (Figure 5.6 can be implemented as the LA architecture in Figure 5.7 and to derive the relationship between the various control elements. This was investigated previously in [58] and a formula which allowed the translation of an arbitrarily structured FA control law into a LA form was derived using transfer functions. However, this formula was restricted to SISO control laws when in reality helicopter control laws may have extra measurements available to them and also may have the flexibility to manipulate more than one control input. In addition, the transfer function approach tends to lead to rather high order controllers. It would therefore be helpful, if expressions for the series control law elements could be given which allow lower order control laws to be obtained for general multivariable controllers.

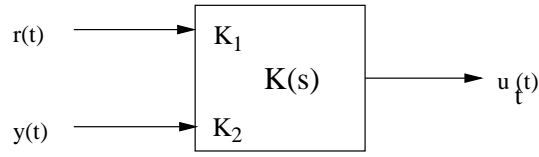


Figure 5.6: FA controller

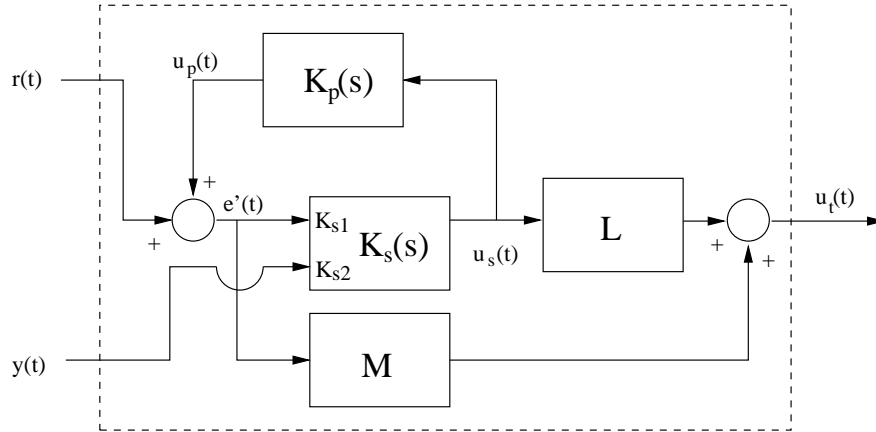


Figure 5.7: LA controller

### A transfer function based representation

The first step in the derivation of state-space formulae is to derive a transfer function relationship (for multivariable systems) between the FA and LA control architectures. The total control activity for the FA case in Figure 5.6 is given by

$$u_t = \begin{bmatrix} K_1 & K_2 \end{bmatrix} \begin{bmatrix} r \\ y \end{bmatrix} \quad (5.5)$$

The above FA controller is to be implemented in the LA architecture of Figure 5.7 and the aim here is to derive an expression for  $\begin{bmatrix} K_{s1} & K_{s2} \end{bmatrix}$  such that the transfer function for

$\begin{bmatrix} r \\ y \end{bmatrix} \rightarrow u_t$  is identical for the two architectures. Now, from Figure 5.7:

$$\begin{aligned} e' &= r + K_P \left[ K_{s1} e' + K_{s2} y \right] \\ e' &= [I - K_P K_{s1}]^{-1} [r + K_P K_{s2} y] \end{aligned} \quad (5.6)$$

Also,

$$u_s = K_{s1} e' + K_{s2} y$$

$$\begin{aligned}
u_s &= K_{s1} [I - K_P K_{s1}]^{-1} [r + K_P K_{s2} y] + K_{s2} y \\
u_s &= K_{s1} [I - K_P K_{s1}]^{-1} r + [K_{s1} [I - K_P K_{s1}]^{-1} K_P + I] K_{s2} y \quad (5.7)
\end{aligned}$$

Applying the “push through” rule [12] to Equation (5.7) the following expression is derived:

$$u_s = K_{s1} [I - K_P K_{s1}]^{-1} r + [I - K_{s1} K_P]^{-1} K_{s2} y \quad (5.8)$$

Now, the total control signal ( $u_t$ ) can be represented as,

$$u_t = L u_s + M e' \quad (5.9)$$

By replacing for  $u_s$  and  $e'$  from Equations (5.7) and (5.6) respectively gives,

$$\begin{aligned}
u_t &= L K_{s1} [I - K_P K_{s1}]^{-1} r + L [I - K_{s1} K_P]^{-1} K_{s2} y + \\
&\quad M [I - K_P K_{s1}]^{-1} r + M [I - K_P K_{s1}]^{-1} K_P K_{s2} y \\
u_t &= [L K_{s1} + M] [I - K_P K_{s1}]^{-1} r + [L + M K_P] [I - K_{s1} K_P]^{-1} K_{s2} y \quad (5.10)
\end{aligned}$$

Comparing Equation (5.10) to the expression for total control activity in the FA system (Equation (5.5)) gives the following expression for  $K_{s1}$ ,

$$\begin{aligned}
K_1 &= [L K_{s1} + M] [I - K_P K_{s1}]^{-1} \\
K_1 [I - K_P K_{s1}] &= [L K_{s1} + M] \\
K_1 - M &= [L + K_1 K_P] K_{s1} \\
K_{s1} &= [L + K_1 K_P]^{-1} [K_1 - M] \quad (5.11)
\end{aligned}$$

and for  $K_{s2}$ :

$$\begin{aligned}
K_2 &= [L + M K_P] [I - K_{s1} K_P]^{-1} K_{s2} \\
K_{s2} &= [I - K_{s1} K_P] [L + M K_P]^{-1} K_2 \quad (5.12)
\end{aligned}$$

Substituting for  $K_{s1}$  from Equation (5.11) in Equation (5.12):

$$\begin{aligned}
K_{s2} &= K_2 [I - [L + K_1 K_P]^{-1} [K_1 - M] K_P] [L + M K_P]^{-1} \\
K_{s2} &= K_2 [L + K_1 K_P]^{-1} [L + K_1 K_P - [K_1 - M] K_P] [L + M K_P]^{-1} \\
K_{s2} &= [L + K_1 K_P]^{-1} K_2 \quad (5.13)
\end{aligned}$$

### Complexity of the inner loop

The parallel actuators, in this architecture, drive both the mechanical system from the stick datum through the mechanical linkages, and also provide part of the reference to the electronic controller which then drives both the series and parallel actuators - giving rise to this complex loop within the controller itself. Also, notice that the expressions for both  $K_{s1}$  and  $K_{s2}$  feature the parameter  $K_P$  which is the control element used primarily to control the parallel actuators. Therefore, given an expression for  $K_P$ , Equations (5.11) and (5.13) represent an *explicit* way of translating a FA design into a LA one which delivers identical small signal performance. An appealing way of choosing  $K_P$  is so that it reduces the steady state output of the series actuators to zero, thus avoiding any long term saturation problems. This can be achieved easily and for this part of the analysis,  $K_{s1}$ ,  $K_{s2}$  and  $K_P$  are assigned the following representations,

$$K_{s1} = \frac{1}{d_s} \hat{K}_{s1} \quad (5.14)$$

where  $\hat{K}_{s1}$  is a  $3 \times 3$  matrix,

$$K_{s2} = \frac{1}{d_s} \hat{K}_{s2} \quad (5.15)$$

where  $\hat{K}_{s2}$  is a  $3 \times 5$  matrix, and

$$K_P = \frac{1}{d_p} \hat{K}_P \quad (5.16)$$

where  $\hat{K}_P$  is a  $3 \times 3$  diagonal matrix (as one parallel actuator per channel).

Also,  $d_s$  and  $d_p$  are the characteristic equation of the transfer function matrices  $K_s$  and  $K_P$  respectively. Applying the push through rule to Equation 5.8, modifies the expression for series actuator control signal,  $u_s$ , to

$$u_s = [I - K_{s1}K_P]^{-1} [K_{s1}r + K_{s2}y] \quad (5.17)$$

and applying the definitions from Equations (5.14), (5.15) and (5.16) to the above representation,

$$\begin{aligned}
u_s &= \left[ I - \frac{1}{d_s d_p} \hat{K}_{s1} \hat{K}_P \right]^{-1} \left( \frac{1}{d_s} \hat{K}_{s1} r + \frac{1}{d_s} \hat{K}_{s2} y \right) \\
&= d_p \left[ d_s d_p I - \hat{K}_{s1} \hat{K}_P \right]^{-1} \left( \hat{K}_{s1} r + \hat{K}_{s2} y \right)
\end{aligned} \tag{5.18}$$

Therefore, by selecting  $d_p = s$ , and assuming that  $\det \left| \left( d_s d_p I - \hat{K}_{s1} \hat{K}_P \right) \right|_{s=0} \neq 0$ , it follows that the transfer function matrix from  $\begin{bmatrix} r \\ y \end{bmatrix}$  to  $u_s$

$$\lim_{s \rightarrow 0} d_p \left[ d_s d_p I - \hat{K}_{s1} \hat{K}_P \right]^{-1} \begin{bmatrix} \hat{K}_{s1} & \hat{K}_{s2} \end{bmatrix} = 0 \tag{5.19}$$

This implies that provided the control loop is stable, the series actuator control signals will tend to zero at steady state, thus preventing long-term saturation. An additional problem, as mentioned earlier, caused by the above LA structure, is the presence of this complex ‘‘inner’’ control loop due to the parallel actuators. It transpires that in order to stabilise this inner loop, the transfer function matrix

$$K_{s1} [I - K_P K_{s1}]^{-1} = d_p \left[ d_s d_p I - \hat{K}_{s1} \hat{K}_P \right]^{-1} \hat{K}_{s1} \tag{5.20}$$

must be stable. This can be accomplished by ensuring the stability of the matrix,  $\left[ d_s d_p I - \hat{K}_{s1} \hat{K}_P \right]$ .

With

$$\hat{K}_P = \begin{bmatrix} \gamma_p & 0 & 0 \\ 0 & \gamma_r & 0 \\ 0 & 0 & \gamma_y \end{bmatrix} \tag{5.21}$$

conventional approaches were used to determine an appropriate gain value, i.e.  $\gamma_p$ ,  $\gamma_r$  and  $\gamma_y$ . Applying SISO techniques such as Routh-Hurwitz criterion [36], it was possible to guarantee stability of the inner loop for all positive gain values [58] (irrespective of the channel). Within the scope of this study, the parallel actuators available in the EH101 helicopter were slow actuators, that were primarily used to off-load the series actuators to prevent long-term saturation. Based on the above derivation, in order to drive the series actuator error to zero, the parallel actuator controller was chosen as a bank of integrators. The parallel actuator controller plays a crucial role in determining the range of pilot demand that would produce identical FA responses. This was dependent upon the scaling  $\gamma_p$ ,  $\gamma_r$  and  $\gamma_y$  and there was

certain amount of tuning involved in this. It will be shown in Chapter 6 that very low gain values would lead to minimal off-loading of the series actuators and hence would result in premature saturation of series actuators even at relatively small pilot demands. Conversely, too high a gain value would mean a highly active parallel actuators that resulted in rate saturation that produced undesirable responses.

### State space realisation of the LA controller

Using Equations 5.11 and 5.13, the series actuator component of the LA controller can be written as follows,

$$\begin{aligned} \begin{bmatrix} K_{s1} & K_{s2} \end{bmatrix} &= \begin{bmatrix} (L + K_1 K_P)^{-1}(K_1 - M) & (L + K_1 K_P)^{-1}K_2 \end{bmatrix} \\ \begin{bmatrix} K_{s1} & K_{s2} \end{bmatrix} &= (L + K_1 K_P)^{-1} \begin{bmatrix} K_1 - M & K_2 \end{bmatrix} \end{aligned} \quad (5.22)$$

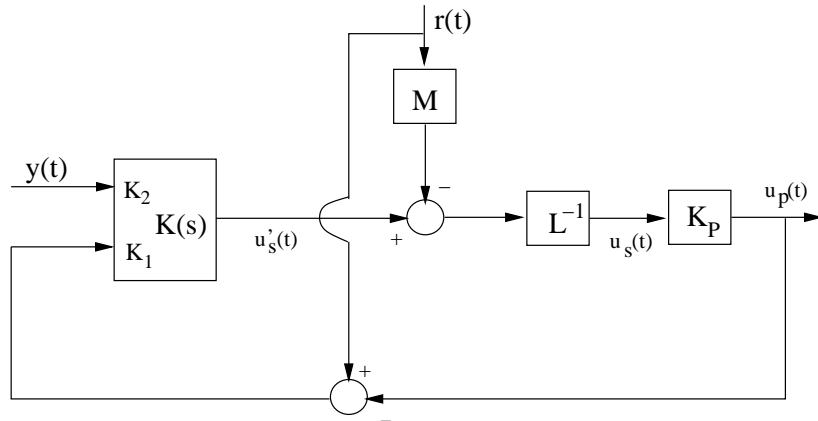


Figure 5.8: Block diagram realisation

The above equation can be pictorially represented by the block diagram in Figure 5.8.

$$\begin{aligned} u_s &= L^{-1} [K_2 y + K_1 [r - K_P u_s] - M r] \\ [L + K_1 K_P] u_s &= K_2 y + (K_1 - M) r \\ u_s &= [L + K_1 K_P]^{-1} \begin{bmatrix} K_1 - M & K_2 \end{bmatrix} \begin{bmatrix} r \\ y \end{bmatrix} \end{aligned} \quad (5.23)$$

Equation 5.23 validates the block diagram representation. Now, the next step in the deriving the state space realisation of  $K_s(s)$  is to assign  $K(s)$  and  $K_P(s)$  the following state-space

realisations (based on the above block diagram),

$$K(s) \sim \begin{cases} \dot{x}_c & = A_c x_c + [B_{cr} \ B_c] \begin{bmatrix} (r - u_p) \\ y \end{bmatrix} \\ y_c = \dot{u}_s & = C_c x_c + [D_{cr} \ D_c] \begin{bmatrix} (r - u_p) \\ y \end{bmatrix} \end{cases} \quad (5.24)$$

$$K_P(s) \sim \begin{cases} \dot{x}_p & = A_p x_p + B_p L^{-1} \begin{bmatrix} \dot{u}_s - Mr \end{bmatrix} \\ y_p = u_p & = C_p x_p + D_p L^{-1} \begin{bmatrix} \dot{u}_s - Mr \end{bmatrix} \end{cases} \quad (5.25)$$

It should be noted at this stage that the matrices  $M$  and  $L$  are assumed to be static and nonsingular. Now, substituting for  $u_p$  from Equation (5.25) in to the output equation in Equation (5.24),

$$\begin{aligned} \dot{u}_s &= C_c x_c + D_{cr} \left[ r - C_p x_p - D_p L^{-1} \begin{bmatrix} \dot{u}_s - Mr \end{bmatrix} \right] + D_c y \\ \dot{u}_s [I + D_{cr} D_p L^{-1}] &= C_c x_c + D_{cr} r - D_{cr} C_p x_p + D_{cr} D_p L^{-1} M r + D_c y \\ \dot{u}_s &= [I + D_{cr} D_p L^{-1}]^{-1} \\ &\quad [C_c x_c + D_{cr} [I + D_p L^{-1} M] r - D_{cr} C_p x_p + D_c y] \end{aligned} \quad (5.26)$$

By defining

$$\Delta = [I + D_{cr} D_p L^{-1}]^{-1} \quad (5.27)$$

Equation (5.26) can now be simplified further to,

$$\dot{u}_s = \Delta C_c x_c - \Delta D_{cr} C_p x_p + \Delta D_{cr} [I + D_p L^{-1} M] r + \Delta D_c y \quad (5.28)$$

Now, by substituting for  $\dot{u}_s$  from Equation (5.28) in to the output equation in Equation (5.25),

$$\begin{aligned} u_p &= C_p x_p + D_p L^{-1} \begin{bmatrix} \dot{u}_s - Mr \end{bmatrix} \\ u_p &= C_p x_p + D_p L^{-1} [\Delta C_c x_c + \Delta D_{cr} [I + D_p L^{-1} M] r - \Delta D_{cr} C_p x_p + \Delta D_c y - Mr] \\ u_p &= D_p L^{-1} \Delta C_c x_c + (C_p - D_p L^{-1} \Delta D_{cr} C_p) x_p \\ &\quad + D_p L^{-1} (\Delta D_{cr} [I + D_p L^{-1} M] - M) r + D_p L^{-1} \Delta D_c y \end{aligned} \quad (5.29)$$

Analysing the following extract from Equation (5.29),

$$\begin{aligned}
D_p L^{-1}(\Delta D_{cr}(I + D_p L^{-1}M) - M) &= D_p L^{-1}\Delta D_{cr} + D_p L^{-1}(\Delta D_{cr}D_p L^{-1} - I)M \\
&= D_p L^{-1}\Delta D_{cr} \\
&\quad + D_p L^{-1}\Delta (D_{cr}D_p L^{-1} - I - D_{cr}D_p L^{-1})M \\
&= D_p L^{-1}\Delta (D_{cr} - M) \tag{5.30}
\end{aligned}$$

Thus, simplifying Equation (5.29) to,

$$\begin{aligned}
u_p &= D_p L^{-1}\Delta C_c x_c + (C_p - D_p L^{-1}\Delta D_{cr}C_p) x_p \\
&\quad + D_p L^{-1}\Delta (D_{cr} - M)r + D_p L^{-1}\Delta D_c y \tag{5.31}
\end{aligned}$$

Next, using the state equation from Equation (5.24) and by substituting for  $u_p$  from Equation (5.31),

$$\begin{aligned}
\dot{x}_c &= A_c x_c + B_{cr}r - B_{cr}D_p L^{-1}\Delta C_c x_c - B_{cr}(C_p - D_p L^{-1}\Delta D_{cr}C_p) x_p \\
&\quad - B_{cr}D_p L^{-1}\Delta (D_{cr} - M)r - B_{cr}D_p L^{-1}\Delta D_c y + B_c y \\
\dot{x}_c &= (A_c - B_{cr}D_p L^{-1}\Delta C_c) x_c + B_{cr}(D_p L^{-1}\Delta D_{cr}C_p - C_p) x_p \\
&\quad + B_{cr}(I - D_p L^{-1}\Delta (D_{cr} - M))r + (B_c - B_{cr}D_p L^{-1}\Delta D_c) y \tag{5.32}
\end{aligned}$$

and by substituting for  $u_s$  from Equation (5.28) in the state equation in Equation (5.25),

$$\begin{aligned}
\dot{x}_p &= A_p x_p + B_p L^{-1} \left[ \Delta C_c x_c + \Delta D_{cr} [I + D_p L^{-1}M] r - \Delta D_{cr} C_p x_p + \Delta D_c y - Mr \right] \\
\dot{x}_p &= B_p L^{-1}\Delta C_c x_c + (A_p - B_p L^{-1}\Delta D_{cr}C_p) x_p + B_p L^{-1}\Delta (D_{cr} - M)r + B_p L^{-1}\Delta D_c y \tag{5.33}
\end{aligned}$$

The above two equations (5.32 and 5.33) forms the state equation for the series actuator controller and,

$$\begin{aligned}
u_s &= L^{-1}(u_s - Mr) \\
u_s &= L^{-1}(\Delta C_c x_c - \Delta D_{cr}C_p x_p + \Delta D_{cr}[I + D_p L^{-1}M]r + \Delta D_c y) - Mr \\
u_s &= L^{-1}\Delta C_c x_c - L^{-1}\Delta D_{cr}C_p x_p + L^{-1}\Delta (D_{cr} - M)r + L^{-1}\Delta D_c y \tag{5.34}
\end{aligned}$$

Equation 5.34 forms the output equation for the series actuator controller. Furthermore, using the expression for  $\Delta$  and applying the push-through rule, the following extract from Equation (5.32),

$$B_{cr} (D_p L^{-1} \Delta D_{cr} - I) C_p \quad (5.35)$$

can be written as,

$$\begin{aligned} & B_{cr} (D_p L^{-1} (I + D_{cr} D_p L^{-1})^{-1} D_{cr} - I) C_p \\ = & B_{cr} ((I + D_p L^{-1} D_{cr})^{-1} D_p L^{-1} D_{cr} - I) C_p \end{aligned} \quad (5.36)$$

Next, by defining

$$\tilde{\Delta} = (I + D_p L^{-1} D_{cr})^{-1} \quad (5.37)$$

Equation (5.36) simplifies to,

$$B_{cr} (\tilde{\Delta} (D_p L^{-1} D_{cr} - I - D_p L^{-1} D_{cr})) C_p = -B_{cr} \tilde{\Delta} C_p \quad (5.38)$$

Similarly, another extract from Equation (5.32) simplifies to,

$$B_{cr} (I - D_p L^{-1} \Delta (D_{cr} - M)) = B_{cr} (\tilde{\Delta} + D_p L^{-1} \Delta M) \quad (5.39)$$

The above two extracts are then replace by their simplifications in Equation (5.32) to obtain,

$$\begin{aligned} \dot{x}_c &= (A_c - B_{cr} D_p L^{-1} \Delta C_c) x_c - B_{cr} \tilde{\Delta} C_p x_p \\ &+ B_{cr} (\tilde{\Delta} + D_p L^{-1} \Delta M) r + (B_c - B_{cr} D_p L^{-1} \Delta D_c) y \end{aligned} \quad (5.40)$$

Thus, obtaining the following state space realisation

$$\begin{bmatrix} \dot{x}_c \\ \dot{x}_p \\ u_s \end{bmatrix} = \begin{bmatrix} A_c - B_{cr} D_p L^{-1} \Delta C_c & -B_{cr} \tilde{\Delta} C_p & B_{cr} (\tilde{\Delta} - D_p L^{-1} \Delta M) & (B_c - B_{cr} D_p L^{-1} \Delta D_c) \\ B_p L^{-1} \Delta C_c & (A_p - B_p L^{-1} \Delta D_{cr} C_p) & B_p L^{-1} \Delta (D_{cr} - M) & B_p L^{-1} \Delta D_c \\ L^{-1} \Delta C_c & -L^{-1} \Delta D_{cr} C_p & L^{-1} \Delta (D_{cr} - M) & L^{-1} \Delta D_c \end{bmatrix} \begin{bmatrix} x_c \\ x_p \\ r \\ y \end{bmatrix} \quad (5.41)$$

The above state-space formula gives a concise description of the series actuator controller which is necessary to replicate the small-signal behaviour of  $K$ . Moreover, assuming no pole-zero cancellations in the transfer function in Equation (5.23) then the order of  $K_s$  as described above should be minimal.

### Large signal performance

Although the above analysis is useful for small-signal matching of FA and LA designs, when actuator saturation occurs and the system therefore becomes nonlinear, it does not hold. In fact for large pilot demands, the series actuator experiences saturation that makes the system unpredictable and may degrade the handling qualities. Although the parallel actuators are used in the architecture to offload the series actuator by driving their output to zero in steady state, the parallel actuators themselves are subject to rate-limiting that introduces another nonlinearity into the system, which may degrade performance further. It therefore becomes critical to assess how far the LA control system could be pushed before the helicopter becomes unstable and difficult to control. In order to form a complete picture, LA controller's large signal performance was also analysed during both linear and non-linear simulation.

## **5.4 Alternative reference demand injection**

In LA control architectures, the way in which the pilot reference is injected into the control system is of critical importance. This is partly because the point in which the reference is fed into the control system alters the configuration of the control loops and hence adjusts the complex “internal” controller loop, which of course has stability consequences as shown in the previous section. The point at which the reference is injected also has associated large signal stability and performance implications when the series or parallel actuators saturate. The way in which the reference is fed into the control system, ultimately alters the reference signal which the electronic portion ( $K_s(s)$ ) of the controller “sees”. The architecture seen thus far has shown the pilot reference being altered by the parallel actuator output,  $u_p$ . This architecture has the important advantage that it conforms to the architecture seen within current generation of helicopters, however, it contains small signal stability intricacies due to the complex internal loop that required careful treatment as was shown in the above derivation. Another potential obstacle is that the pilot's stick is back-driven by the parallel actuators which might also be unsettling. However, quite often to avoid this back drive the parallel channel is only activated once the stick is centred (this again has its own stability and performance limitations).

In this section, an alternative more architecturally appealing method is presented. This method considers the architecture as shown in Figure 5.9, where:

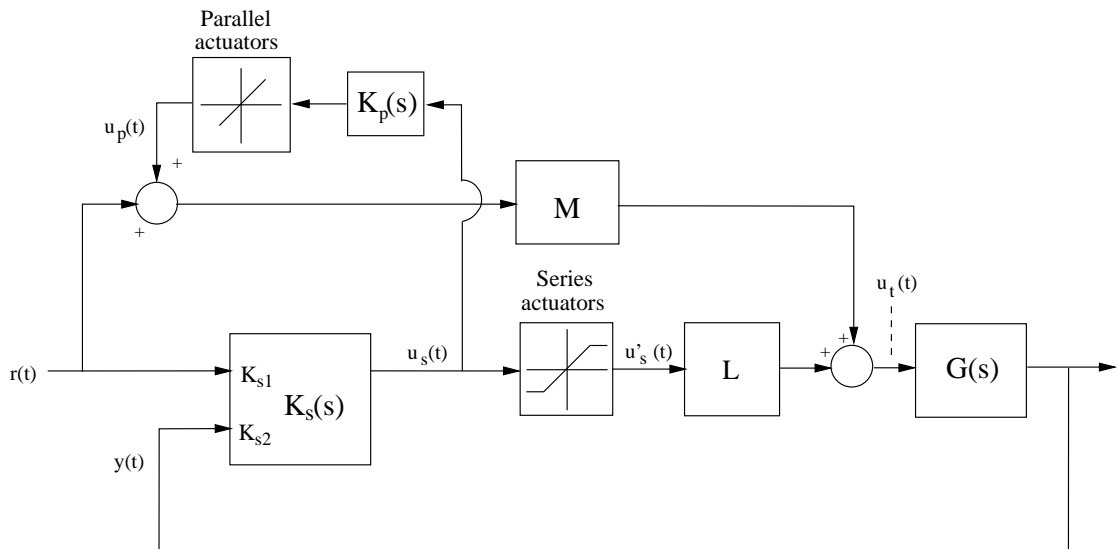


Figure 5.9: Alternate LA architecture

- $u_s(t)$  = Series actuator input
- $u'_s(t)$  = Series actuator command
- $u_p(t)$  = Parallel actuator command
- $u_t(t)$  = Total controller output
- $G$  = Helicopter dynamics
- $M = 3 \times 3$  interlinks gain between stick datum to swash plate
- $L = 3 \times 3$  interlinks gain between series actuator command to swash plate
- $r(t)$  = Pilot command
- $y(t)$  = System output
- $K_s(s) = \begin{bmatrix} K_{s1} & K_{s2} \end{bmatrix}$  = Series component of LA controller
- $K_p(s)$  = Parallel component of LA controller

It should be noted from the schematic that the pilot command,  $r(t)$ , is fed directly into the controller without modification, however, the signal into mechanical linkages is modified by parallel actuator command,  $u_p(t)$ . Note in particular that the parallel actuators *do not influence* the reference which the series actuator controller “sees”. Although such a scheme would be difficult to implement in current generation helicopters, it could be implemented as a purely electronic version of a LA controller in future aircraft. There are certain advantages for this way of generating references:-

1. The control architecture is simpler
2. Stability problems are more easily avoided as there are no complicated “inner loops” which affect stability.
3. The pilot’s stick is not “back driven” by the parallel actuators, meaning that the pilot would not experience unsettling non-commanded movement of the cyclic stick datum.

However, as the helicopter trim is normally delivered by the parallel actuators, this may mean that the pilot loses track of the aircraft’s trim. In order to present a complete picture, a small signal analysis was also conducted for this scheme in a similar manner to the proposed architecture and this is presented below.

### Analysis

From Figure 5.9 it can be seen that for small pilot demands where the saturation elements are assumed as unity gain

$$\begin{aligned} u_t &= Lu_s + M(r + u_p) \\ u_t &= (L + MK_p)u_s + Mr \end{aligned} \tag{5.42}$$

as  $u_p = K_P u_s$

Also,

$$u_s = (K_{s1}r + K_{s2}y) \tag{5.43}$$

Now, replacing  $u_s$  in Equation (5.42) using the above relation,

$$\begin{aligned}
 u_t &= (L + MK_p) [(K_{s1}) r + (K_{s2}) y] + Mr \\
 u_t &= [(L + MK_p) K_{s1} + M] r + \\
 &\quad (L + MK_p) (K_{s2}) y
 \end{aligned}
 \tag{5.44}$$

This total control output was equated to the FA total control signal in Equation (5.5), thus providing the following expression for  $\begin{bmatrix} K_{s1} & K_{s2} \end{bmatrix}$  as

$$\begin{aligned}
 K_1 &= (L + MK_p) (K_{s1} + M) \\
 K_{s1} &= (L + MK_p)^{-1} (K_1 - M)
 \end{aligned}
 \tag{5.45}$$

and

$$\begin{aligned}
 K_2 &= (L + MK_p) K_{s2} \\
 K_{s2} &= (L + MK_p)^{-1} K_2
 \end{aligned}
 \tag{5.46}$$

Equations (5.45) and (5.46) describe the transfer function based transformation formulae that, once applied to the FA controller, would produce the series actuator compensator component  $(K_s)(s)$  for this alternative LA architecture. In order to obtain the state space based solution the block diagram in Figure 5.10 was constructed.

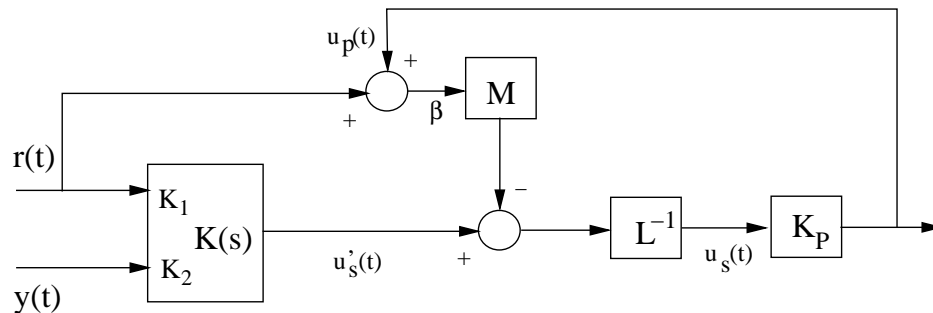


Figure 5.10: Block diagram realisation - alternative scheme

and the following analysis was conducted to assess its validity.

$$\begin{aligned}
u_s &= L^{-1} [K_2 y + K_1 r - M (r + K_P u_s)] \\
[L + MK_P] u_s &= K_2 y + (K_1 - M) r \\
u_s &= [L + MK_P]^{-1} \begin{bmatrix} K_1 - M & K_2 \end{bmatrix} \begin{bmatrix} r \\ y \end{bmatrix}
\end{aligned} \tag{5.47}$$

Also, the following state-space realisations are assigned

$$K(s) \sim \begin{cases} \dot{x}_c &= A_c x_c + \begin{bmatrix} B_{cr} & B_c \end{bmatrix} \begin{bmatrix} r \\ y \end{bmatrix} \\ y_c = \dot{u}_s &= C_c x_c + \begin{bmatrix} D_{cr} & D_c \end{bmatrix} \begin{bmatrix} r \\ y \end{bmatrix} \end{cases} \tag{5.48}$$

$$K_P(s) \sim \begin{cases} \dot{x}_p &= A_p x_p + B_p L^{-1} \begin{bmatrix} \dot{u}_s - M\beta \end{bmatrix} \\ y_p = u_p &= C_p x_p + D_p L^{-1} \begin{bmatrix} \dot{u}_s - M\beta \end{bmatrix} \end{cases} \tag{5.49}$$

It can be seen from Figure 5.10 and the output equation of Equation 5.49,

$$\begin{aligned}
\beta &= u_p + r \\
\beta &= (I + D_p L^{-1} M)^{-1} [C_p x_p + D_p L^{-1} \dot{u}_s + r]
\end{aligned} \tag{5.50}$$

The output equation part of the series actuator compensator is given by

$$\begin{aligned}
u_s &= L^{-1} (\dot{u}_s - M\beta) \\
u_s &= L^{-1} \left( \dot{u}_s - M (I + D_p L^{-1} M)^{-1} [C_p x_p + D_p L^{-1} \dot{u}_s + r] \right) \\
u_s &= L^{-1} (I + D_p L^{-1} M)^{-1} (\dot{u}_s - M (C_p x_p + r))
\end{aligned} \tag{5.51}$$

and by replacing for  $\dot{u}_s$  from Equation 5.48

$$\begin{aligned}
u_s &= L^{-1} (I + D_p L^{-1} M)^{-1} \left[ C_c x_c + [D_{cr} \ D_c] \begin{bmatrix} r \\ y \end{bmatrix} - M (C_p x_p + r) \right] \\
u_s &= L^{-1} (I + D_p L^{-1} M)^{-1} [C_c x_c - M C_p x_p + (D_{cr} - M) r + D_c y] \quad (5.52)
\end{aligned}$$

Similarly, by replacing for  $\beta$  and  $u_s$  in the state equation in Equation 5.49 results in

$$\begin{aligned}
\dot{x}_p &= A_p x_p + B_p [L^{-1} \Lambda [C_c x_c - M C_p x_p + (D_{cr} - M) r + D_c y]] \\
\dot{x}_p &= B_p L^{-1} \Lambda C_c x_c + (A_p - B_p L^{-1} \Lambda M C_p) x_p + \\
&\quad B_p L^{-1} \Lambda (D_{cr} - M) r + B_p L^{-1} \Lambda D_c y \quad (5.53)
\end{aligned}$$

where  $\Lambda = (I + D_p L^{-1} M)^{-1}$

Finally, the last state equation that represents the series actuator compensator is

$$\dot{x}_c = A_c x_c + [B_{cr} \ B_c] \begin{bmatrix} r \\ y \end{bmatrix} \quad (5.54)$$

$$(5.55)$$

Thus, resulting in the following state space realisation for the series actuator compensator

$$\begin{bmatrix} \dot{x}_c \\ \dot{x}_p \\ u_s \end{bmatrix} = \left[ \begin{array}{cc|cc} A_c & 0 & B_{cr} & B_c \\ \hline B_p L^{-1} \Lambda C_c & (A_p - B_p L^{-1} \Lambda M C_p) & B_p L^{-1} \Lambda (D_{cr} - M) & B_p L^{-1} \Lambda D_c \\ L^{-1} \Lambda C_c & -L^{-1} \Lambda M C_p & L^{-1} \Lambda (D_{cr} - M) & L^{-1} \Lambda D_c \end{array} \right] \begin{bmatrix} x_c \\ x_p \\ r \\ y \end{bmatrix} \quad (5.56)$$

## 5.5 Conclusion

This chapter has proposed two approaches for transforming FA schemes into LA schemes, and associated state-space formulae which allow these transformations have been developed.

The key idea behind these transformations is that the LA schemes are considered as “standard” control schemes but with *constrained* internal architectures (dictated by the series and parallel actuators). The first transformation is useful in helicopters of today as most of their LA systems are configured as assumed in the first scheme. Extensive use of the transformation will be made in the remainder of the thesis. The second transformation is appealing conceptually and while it is not appropriate for current LA configurations it may be of interest for future LA configuration, particularly LA systems which are implemented purely “electronically”.

# Chapter 6

## Linear limited authority simulation

This chapter describes the analysis and computer-based linear simulation of a LA controller for the EH101 helicopter. These simulation results are tagged as linear because they are conducted using the linear 25-state model of the EH101, although there are nonlinear elements (i.e. magnitude and rate saturation) present in this architecture. It demonstrates the application of the transformation formulae derived in Chapter 5 and shows how they can be used to successfully realise a given FA controller in a LA architecture. Also, it explores the importance of parallel actuators in a LA control system. In order to appreciate the importance of parallel actuator controller  $K_p$ , the LA controller was analysed and compared *with* and *without* the parallel actuator controller,  $K_p$ . The chapter's main contribution is the extensive simulation testing of the LA controller using high-fidelity linear models.

### 6.1 Modifications to the full authority controller

Recall from Chapter 4, that the FA controller was multivariable and designed using the 2DOF  $\mathcal{H}_\infty$  loop shaping technique as discussed in Chapter 2. The nonlinear flight mechanics model was trimmed and linearised at several different design points throughout the flight envelope and the 40kt/0ft/14200kg trim point was used for controller design. The controller was an ACAH controller in the pitch and roll channels and a RC controller in the yaw channel, and the collective was left open-loop. The FA controller functioned well over the portion of the flight envelope tested (0-120kts speed, 0-4500ft altitude, 11000-14200kg mass). The

controller did not require scheduling with flight condition and, although its responses degraded at points distant from the design point, it still enabled reasonably good responses to be obtained.

Note that FA helicopters are driven by a reference, which is generated by the pilot's inceptor (i.e. stick or pedals). In practice this means that there must be a "scaling" or a gain which takes the stick or pedal input and converts it into an appropriate reference demand for a FA controller. For example if the pilot pushes the stick forward as much as possible, this must then be converted to a maximum pitch attitude command for the helicopter by a scaling in the controller. In block diagram terms, this means that an extra block is inserted at the input of the FA controller to generate  $r$  from the stick/pedal displacements.

In LA architectures the situation is slightly more complex because the pilot's stick/pedal inputs act as both the *reference demand generator* for the series actuator controller, and a direct swash-plate command via its connection to the mechanical interlinks. It is therefore vital to ensure that the gain (or scaling) which converts stick/pedal displacement to reference acts harmoniously with the capabilities of the mechanical interlinks. As the pilot stick/pedal inputs to values in the range  $\pm 50\%$  in each channel (pitch, roll, yaw) it was decided that the reference scaling gain would associate  $\pm 50\%$  to  $\mp 30$  deg in pitch,  $\pm 60$  deg in roll and  $\mp 45$  deg/s in yaw rate. These input ranges in each channel are based upon the EH101 capability and it effectively means that a 50% pilot input is equal to  $-30$  deg,  $60$  deg and  $-45$  deg/s demand in longitudinal, lateral and directional channel respectively. Now, the FA controller has the following state space realisation

$$\begin{aligned} \dot{x}_c &= A_c x_c + \begin{bmatrix} B_{cr} & B_c \end{bmatrix} \begin{bmatrix} r \\ y \end{bmatrix} \\ y_c &= C_c x_c + \begin{bmatrix} D_{cr} & D_c \end{bmatrix} \begin{bmatrix} r \\ y \end{bmatrix} \end{aligned} \quad (6.1)$$

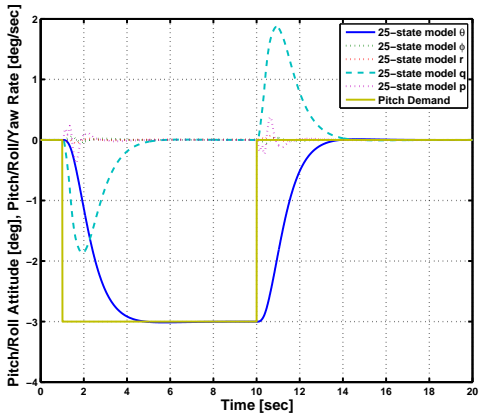
and by incorporating the below diagonal matrix

$$K_{ref} = \begin{bmatrix} -0.6 & 0 & 0 \\ 0 & 1.2 & 0 \\ 0 & 0 & -0.9 \end{bmatrix}$$

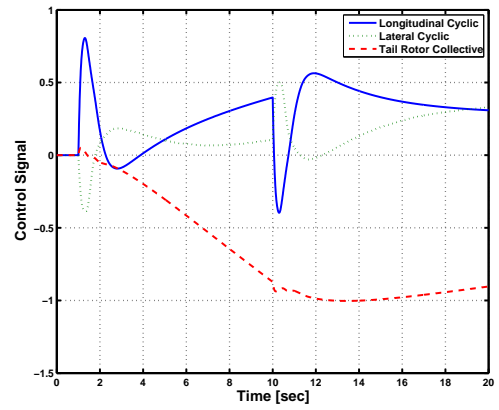
into Equation 6.1, the FA controller is modified to

$$\begin{aligned}\dot{x}_c &= A_c x_c + \begin{bmatrix} B_{cr} K_{ref} & B_c \end{bmatrix} \begin{bmatrix} r \\ y \end{bmatrix} \\ y_c &= C_c x_c + \begin{bmatrix} D_{cr} K_{ref} & D_c \end{bmatrix} \begin{bmatrix} r \\ y \end{bmatrix}\end{aligned}\quad (6.2)$$

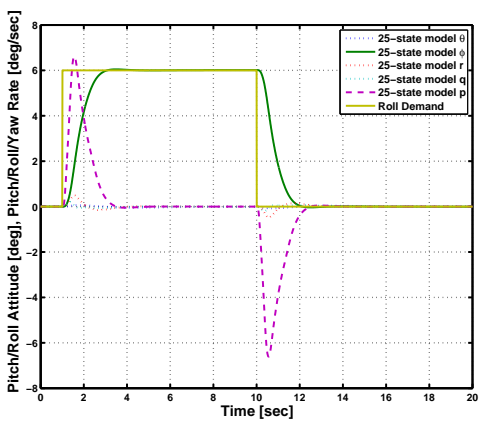
This above FA controller was used to obtain the time responses along with the total control activity to a 5% (-3 deg pitch attitude, 6 deg roll attitude and -4.5 deg/s yaw rate) demand in each channel (one channel at a time) and these are presented in Figures 6.1 (design point), 6.2, 6.3, 6.4, 6.5 and 6.6 (off trim points). These plots provide the baseline set of small signal FA responses that the LA architecture is desired to replicate. The control activity in these plots is evidence of the high level of inter-axis coupling that is present in the helicopter model with each inceptor being active even when not excited by the pilot. This activity shows the decoupling capability of the controller and the degree of inceptor activity depends upon the level of inter-axis coupling which in turn is related to the flight condition that helicopter is operating at.



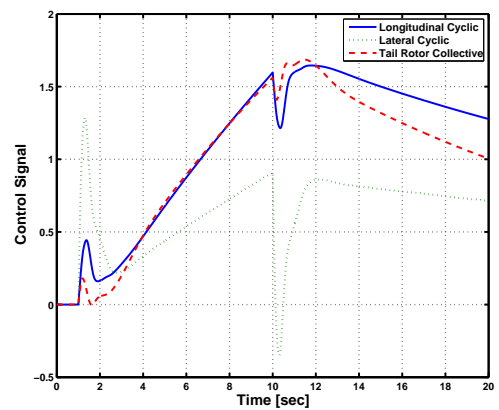
Longitudinal response



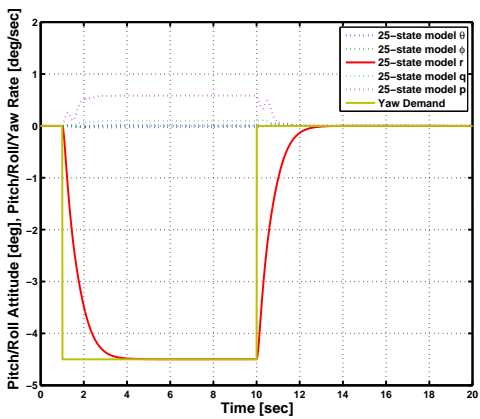
Total control activity



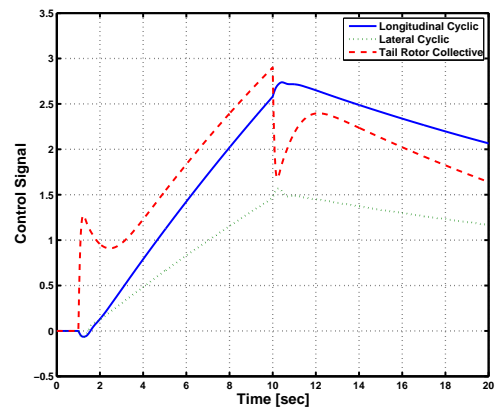
Lateral response



Total control activity

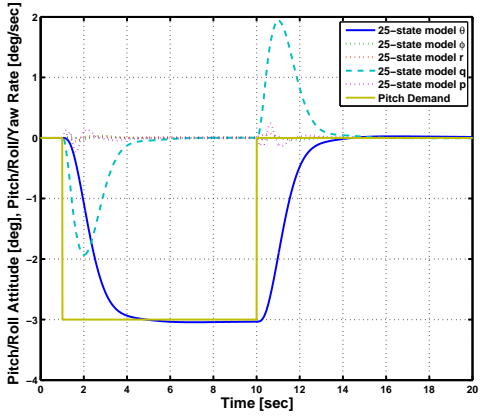


Directional response

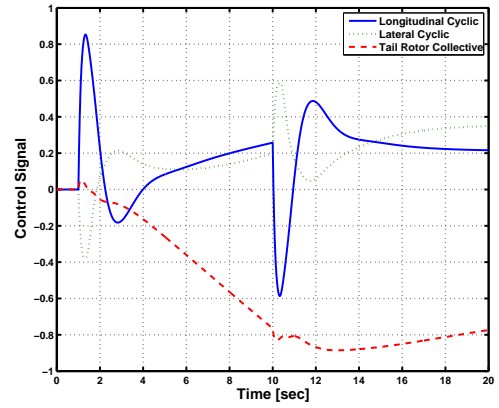


Total control activity

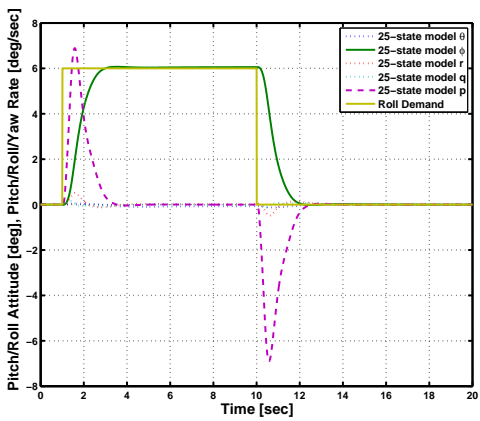
Figure 6.1: FA response - 40kts/0ft/14200kg (Design point)



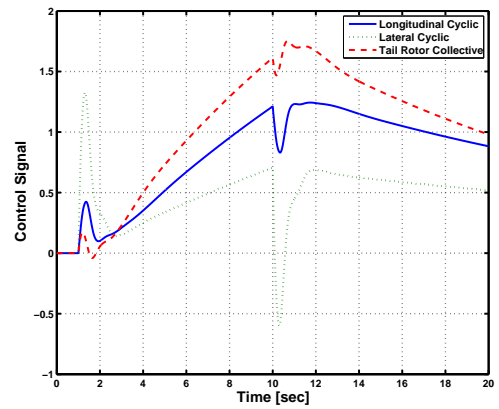
Longitudinal response



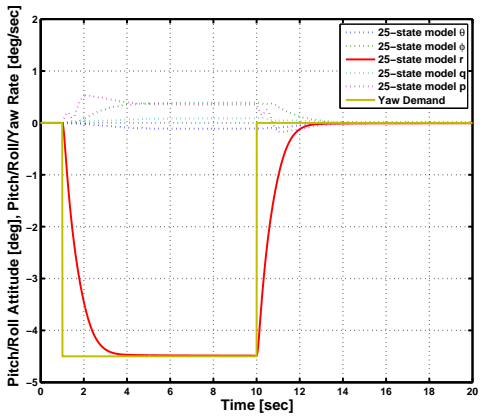
Total control activity



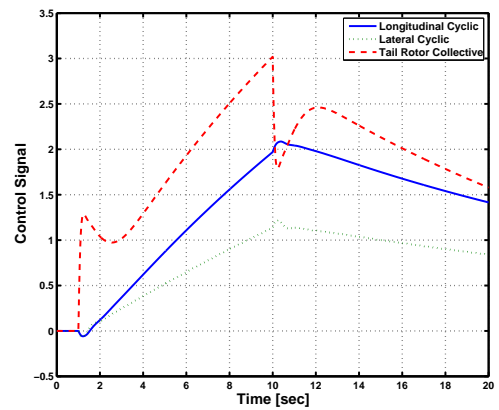
Lateral response



Total control activity

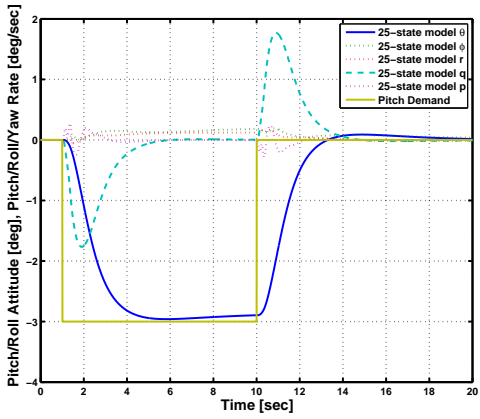


Directional response

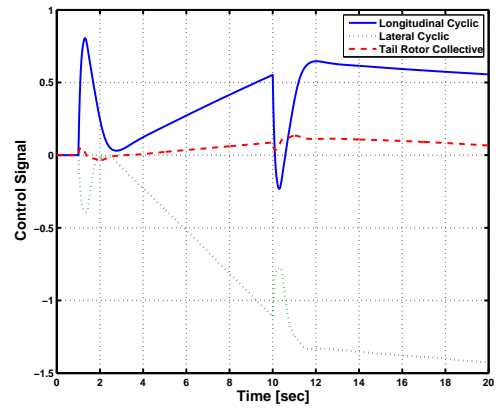


Total control activity

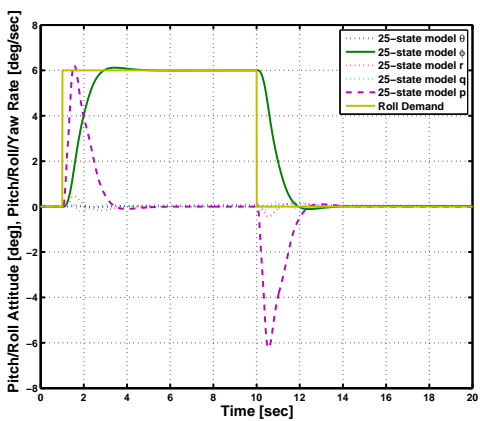
Figure 6.2: FA response - 40kts/0ft/11000kg



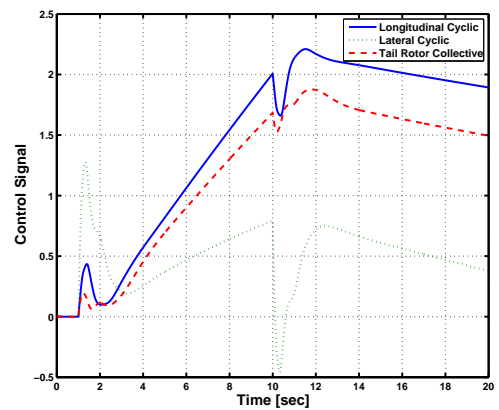
Longitudinal response



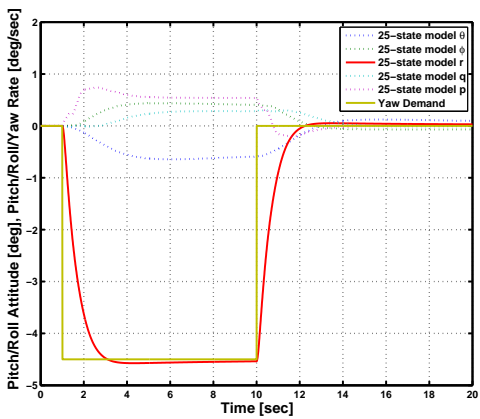
Total control activity



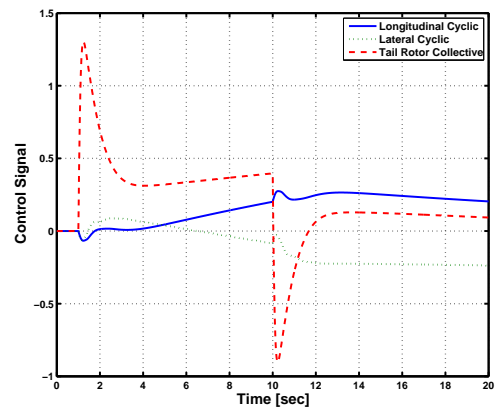
Lateral response



Total control activity

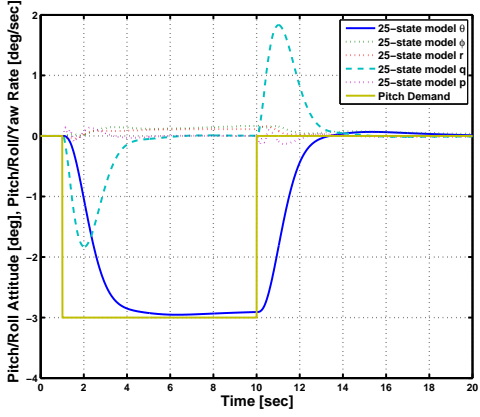


Directional response

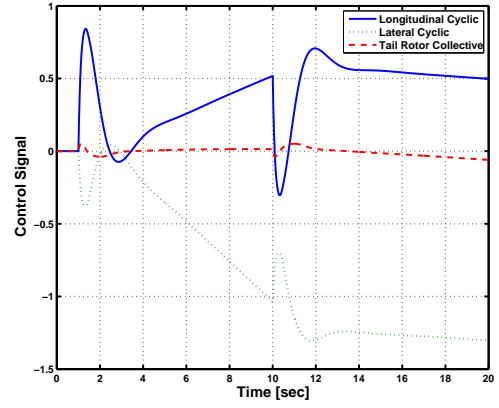


Total control activity

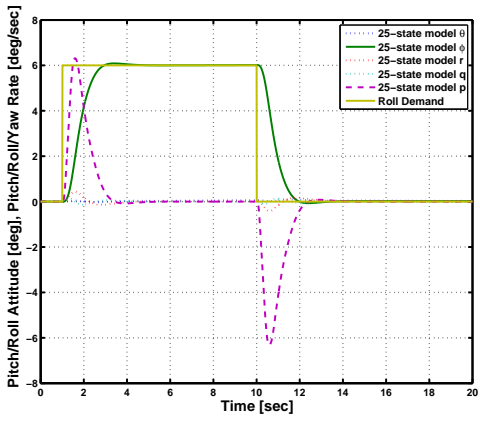
Figure 6.3: FA response - Hover/14200kg



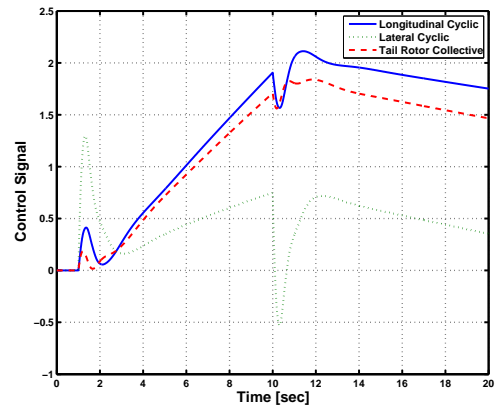
Longitudinal response



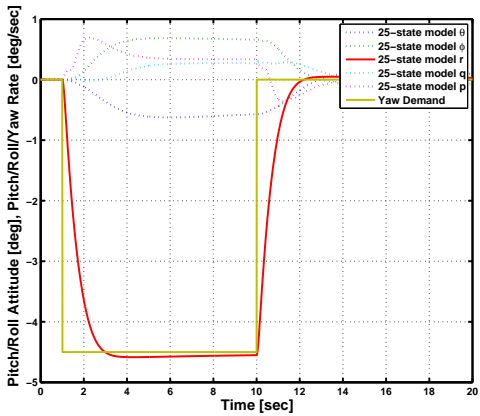
Total control activity



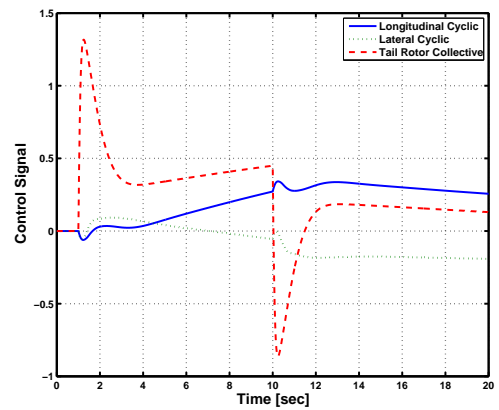
Lateral response



Total control activity

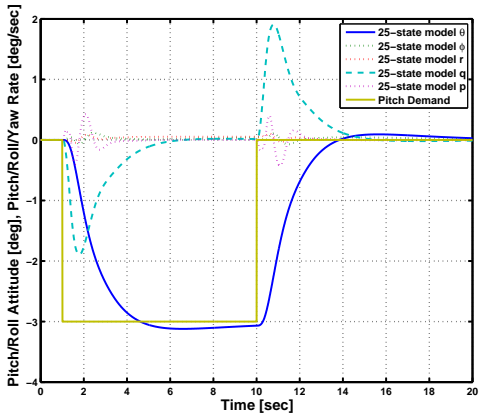


Directional response

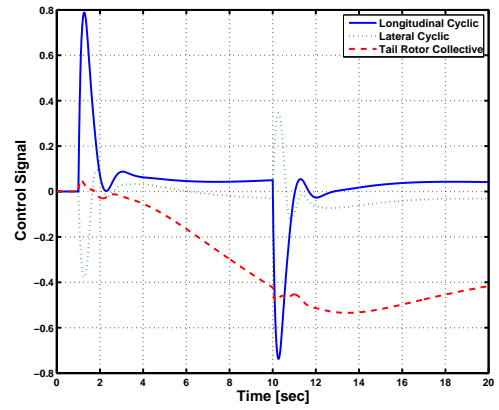


Total control activity

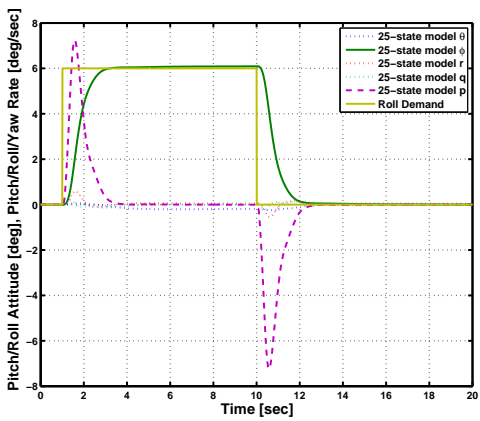
Figure 6.4: FA response - Hover/11000kg



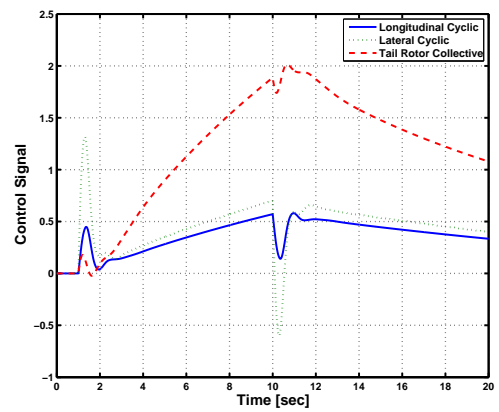
Longitudinal response



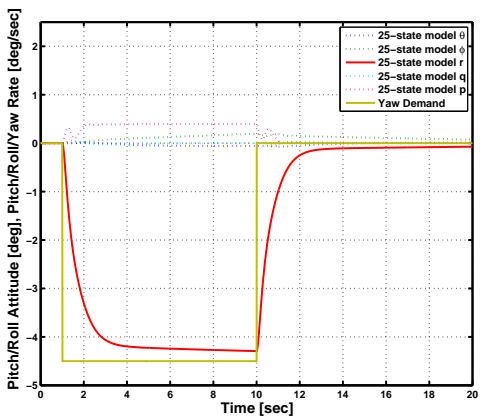
Total control activity



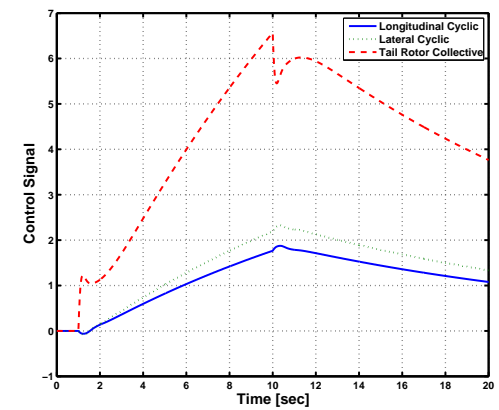
Lateral response



Total control activity

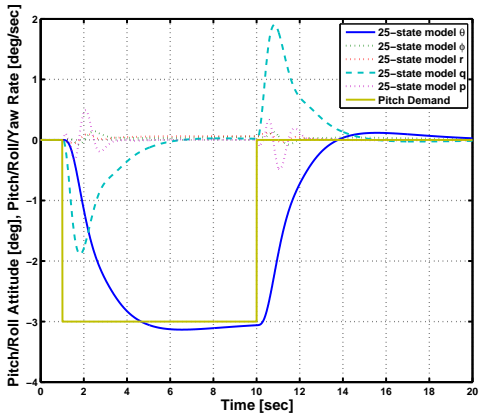


Directional response

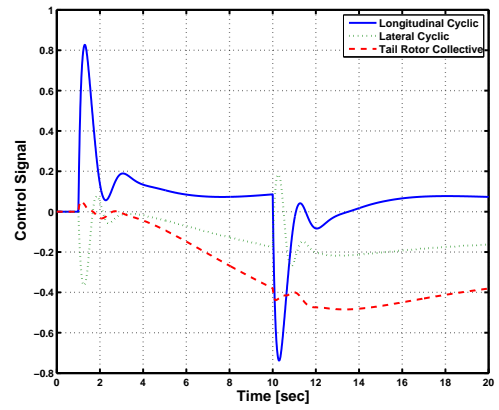


Total control activity

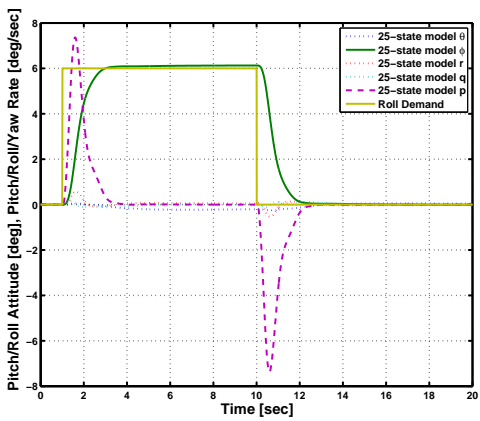
Figure 6.5: FA response - 80kts/2500ft/14200kg



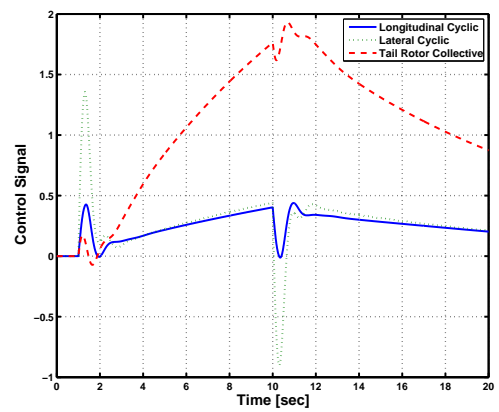
Longitudinal response



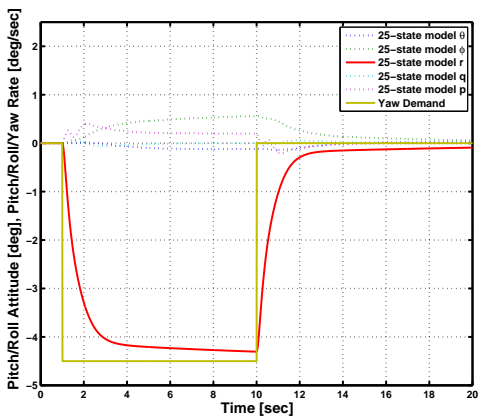
Total control activity



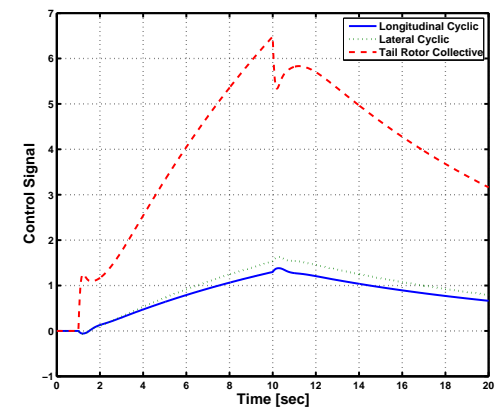
Lateral response



Total control activity



Directional response



Total control activity

Figure 6.6: FA response - 80kts/4500ft/11000kg

## 6.2 Linear simulation

This section describes the results of a series of simulations carried out using linear models of the EH101 augmented with the proposed LA control system. The nonlinear elements were the series actuator saturation limits and the parallel actuators rate limits. These limits are tabulated in Table 6.1 and it should be noted that they are given in percentages for consistency and as required by the model. Although purely linear, these simulations give a good idea of what can be expected in the nonlinear model and give a rough idea of the range in which the LA functions well.

Variable	Limit
Series actuator position limits (all channels)	$\pm 50\%$
Pitch channel parallel actuator rate limit	$\pm 4.5\%$
Roll channel parallel actuator rate limit	$\pm 5.0\%$
Yaw channel parallel actuator rate limit	$\pm 5.0\%$
Stick limits (all channels)	$\pm 50\%$

Table 6.1: Limits for the nonlinear elements

As mentioned earlier, the FA controller was designed at the 40kts/0ft/14200kg flight condition and therefore the LA controller was also expected to perform best at this point. Most results are presented for this flight condition, although for comparison purposes a small selection of results at other flight conditions are also presented. Figure 5.3 shows the schematic of the SIMULINK model that was used to obtain the results, where  $G(s)$  represents the linear helicopter dynamics,  $M$  and  $L$  represent the mechanical interlinks components as described previously, and  $K_s(s)$  and  $K_P(s)$  represent the series and parallel components of the LA controller respectively. The stick inputs,  $r(t)$  (interpreted as reference demands), were chosen to be fairly clinical pulse inputs which gives a rough idea of the performance of the control system.

The results were not only compared to the FA results but also to a LA controller which only uses series actuation. This would assist in understanding the limitations of the series-actuator only architecture and strengthens the case for the inclusion of parallel actuators in the architecture.

## 6.2.1 Series actuation only

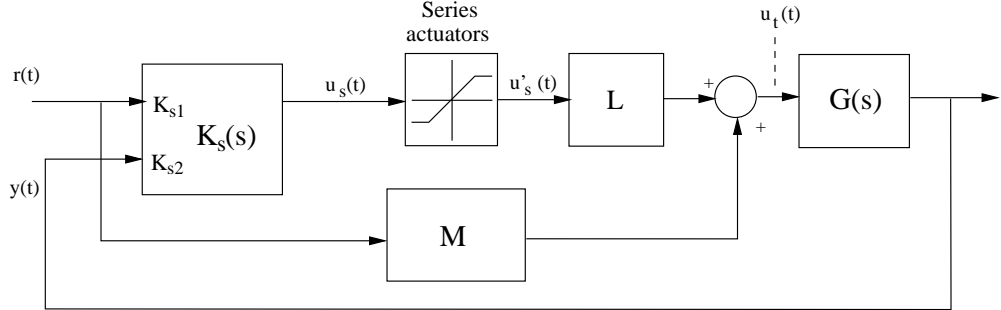


Figure 6.7: LA architecture - series actuators only

One of the issues that was highlighted in the previous chapter was that parallel actuators in this architecture back drives the stick which could cause discomfort to the pilot. Thus, for the purpose of comparing, it would be interesting to discover what a LA control system equipped only with that series actuators (Figure 6.7) could achieve. This particular architecture (with no parallel actuators) was also quite heavily used by [35, 33] and QinetiQ in their various PAFCA trials and is comparatively simpler to implement. The expression for the series actuator controller can be obtained simply by setting the parallel actuator controller,  $K_P(s)$ , to zero. Thus, the expressions for  $\begin{bmatrix} K_{s1} & K_{s2} \end{bmatrix}$  reduces to

$$K_{s1} = (L)^{-1} (K_1 - M) \quad (6.3)$$

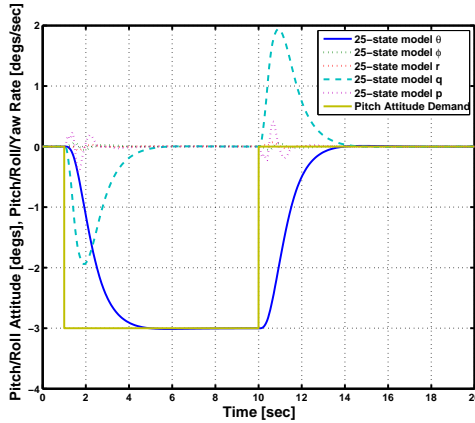
$$K_{s2} = (L)^{-1} (K_2) \quad (6.4)$$

with the following state space realisation

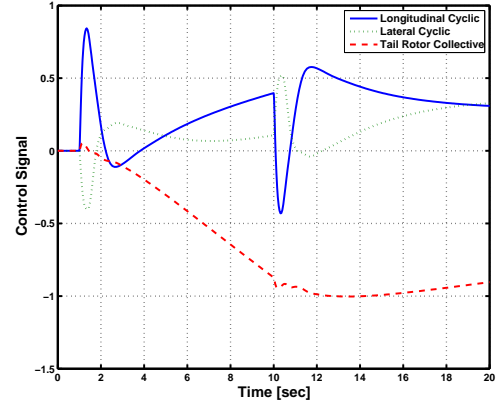
$$\begin{bmatrix} \dot{x}_c \\ u_s \end{bmatrix} = \begin{bmatrix} A_c & B_{cr}\tilde{\Delta} & B_c \\ L^{-1}\Delta C_c & L^{-1}\Delta(D_{cr} - M) & L^{-1}\Delta D_c \end{bmatrix} \begin{bmatrix} x_c \\ r \\ y \end{bmatrix} \quad (6.5)$$

Note, that this arrangement means that the total blade angle demand is still the sum of the mechanical control signal and the series actuator control signal, but, importantly, the parallel actuators are not present to off-load the series actuators and this must be done solely by the pilot. However, it is important to point out that the PAFCA trials illustrated some success with this LA architecture.

## Longitudinal Response

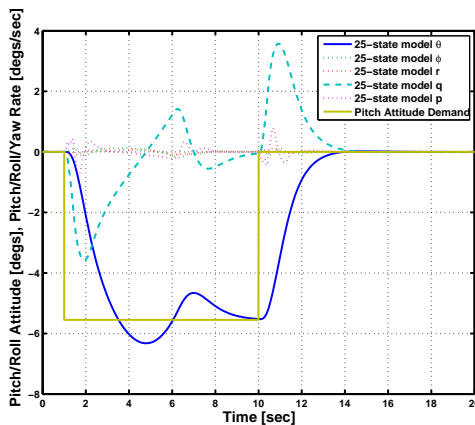


Longitudinal response (5%)

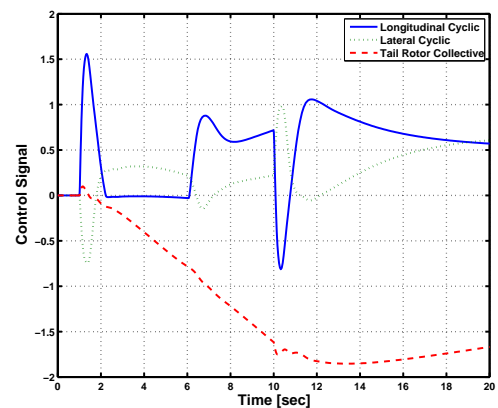


Total control activity (5%)

Figure 6.8: Longitudinal Response (5%)



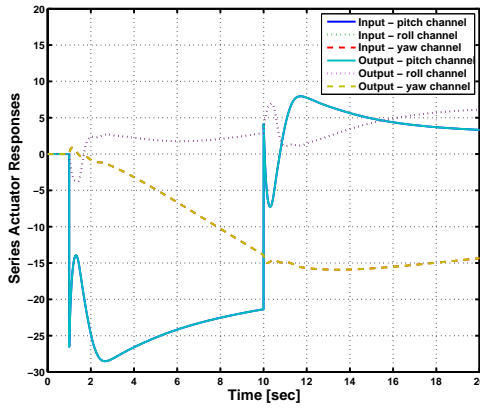
Longitudinal response (9.25%)



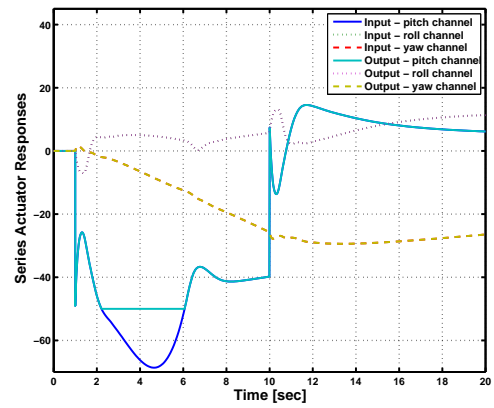
Total control activity (9.25%)

Figure 6.9: Longitudinal Response (9.25%)

The LA controller designed with only series actuation was able to retain identical responses to that of the FA controller for inputs of up to  $\pm 8.5\%$  ( $\mp 5.1$  deg) in the longitudinal axis. In Figure 6.8 an example response to a pulse demand of  $5.0\%$  ( $-3.0$  deg) is shown, that confirms small signal behaviour matching. When the pilot demand is increased beyond  $\pm 8.5\%$ , the performance degrades sharply and, excessive series actuator saturation causes the response to become intolerable when input demands greater than  $\pm 9.25\%$  ( $\mp 5.55$  deg) are applied. An example response in Figure 6.9 to a demand of  $\pm 9.25\%$  ( $\mp 5.55$  deg) and the corresponding series actuator behaviour is shown in Figure 6.10. These plots confirm that the degradation is due to the longer periods of series actuator saturation.

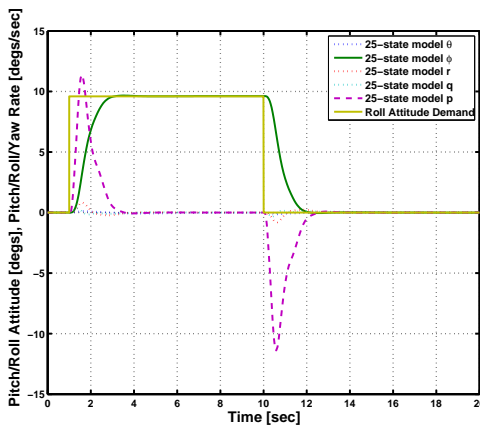


Series actuator response (5%)

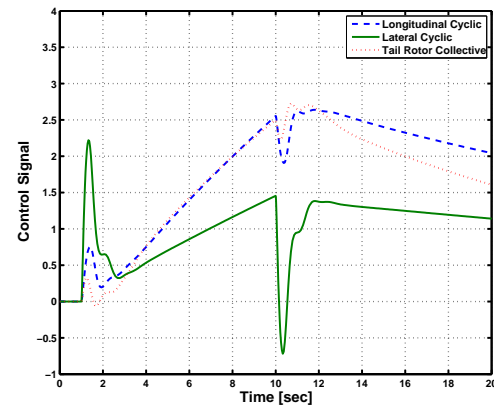


Series actuator response (9.25%)

Figure 6.10: Series Actuator Response - Pitch channel



Lateral response (8%)

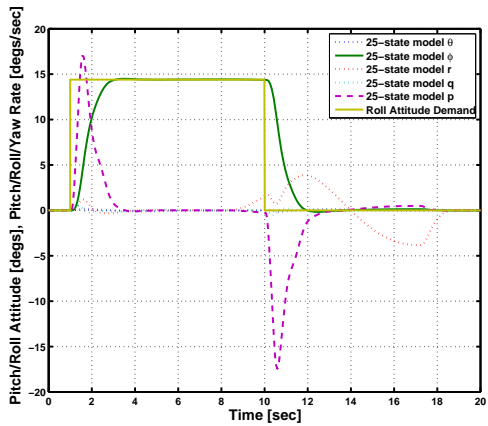


Total control activity (8%)

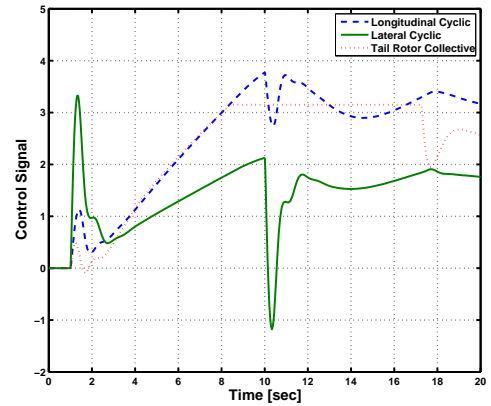
Figure 6.11: Lateral Response (8%)

## Lateral Response

This architecture showed similar behaviour in the lateral channel, however, with two important differences: (i) performance identical to the FA architecture was preserved for a larger stick deflection ( $\pm 10.5\%$  /  $\pm 12.6$  deg); and (ii) the degradation from identical response to intolerable response was more gradual, with the system able to tolerate reference demands of up to about  $\pm 20.0\%$  before instability. This was mainly due to the lateral channel requiring a low series actuator compensator activity compared to the longitudinal channel. This resulted in the lateral channel series actuators not saturating as early as the longitudinal channel series actuator. It is noted that this feature of the limited authority system is not surprising because the series actuator limits are approximately the same in the roll channel as the pitch channel,

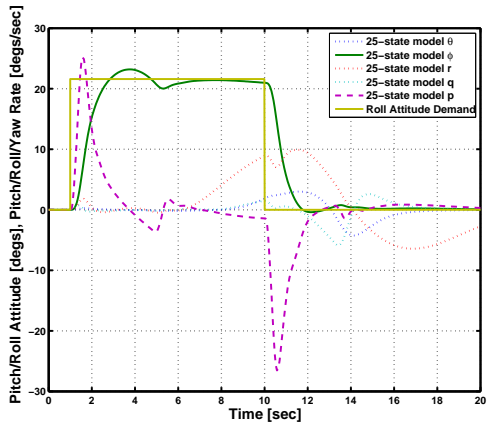


Lateral response (12%)

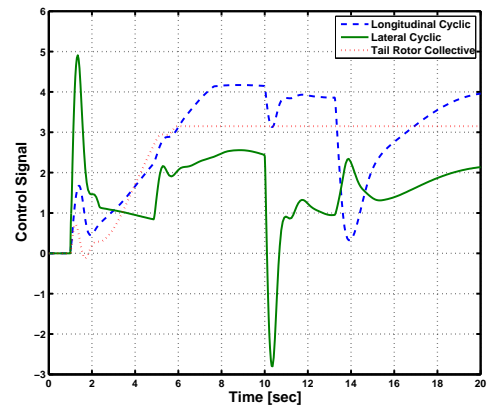


Total control activity (12%)

Figure 6.12: Lateral Response (12%)



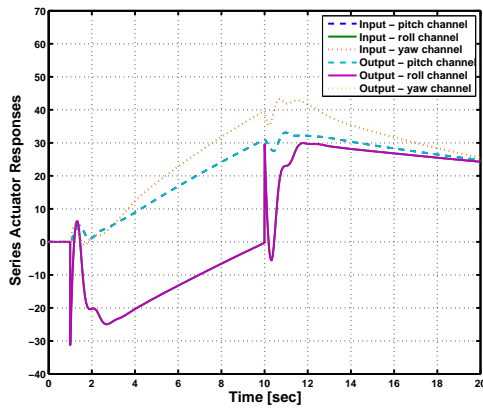
Lateral response (18%)



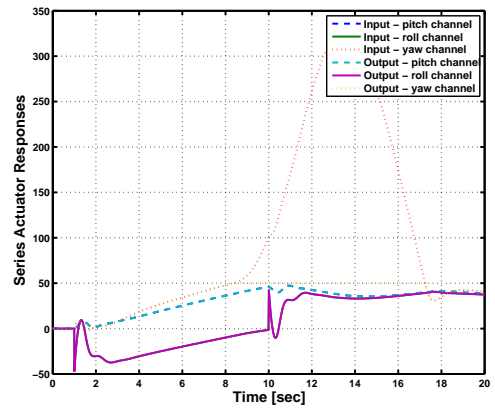
Total control activity (18%)

Figure 6.13: Lateral Response (18%)

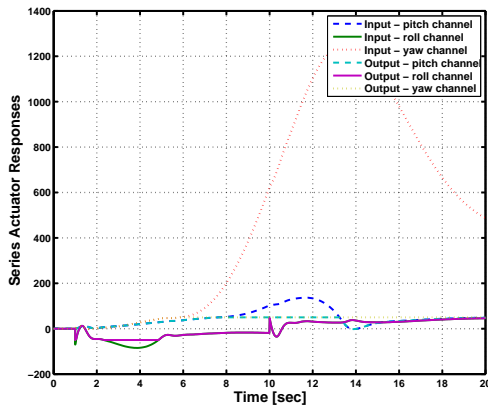
despite the inertia in the pitch axis being much greater than the roll axis. This effectively means that rolling the helicopter requires much less actuator activity than pitching the aircraft, meaning that the series actuator saturates for higher pilot demands in the roll channel than the pitch channel. Example of an identical FA response is shown in Figure 6.11 where a stick demand of 8.0% (9.6 deg) is applied. Degradation in the off-axis response, in particular yaw rate, began to appear as the inputs were increased beyond  $\pm 10.5\%$ . Figures 6.12 and 6.14 show the response due to a lateral stick input of 12.0% (14.4 deg). Note the largely unaffected roll response with degradation in yaw rate response due to saturation of directional channel series actuator. The roll attitude response is only affected by the directional channel series actuator saturation when demands exceeding  $\pm 17.0\%$  ( $\pm 20.4$  deg) are applied.



Series actuator response (8%)



Series actuator response (12%)



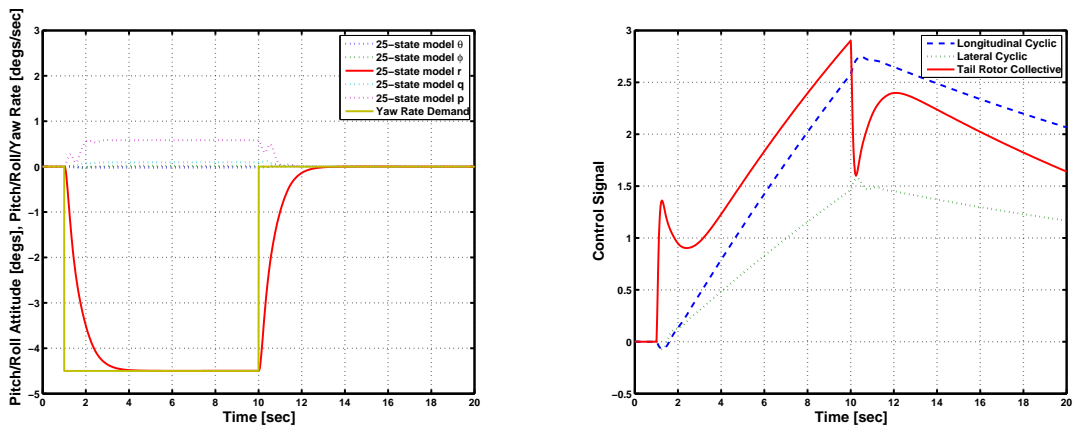
Series actuator response (18%)

Figure 6.14: Series Actuator Response - Roll channel

Here both the directional and lateral channel series actuators experience saturation and this is shown in Figures 6.13 and 6.14 that show response due to a roll attitude demand of 18.0% (21.6 deg). Recall, that the helicopter is a highly coupled vehicle with the roll and yaw axes showing significant coupling. The controller is designed to decouple these responses, but when actuator saturation occurs, the vehicle displays a combination of open and closed loop properties and thus some of the cross coupling is exposed. The roll controller was designed to ensure roll commands were followed with negligible impact on the yaw of the aircraft. However, such behaviour required significant yaw actuator input since the helicopter naturally yaws when it rolls. Thus, for a roll demand there is activity in both actuators and hence, when the yaw series actuator saturated, the decoupling between the yaw and roll channels was reduced, as may be expected.

## Directional Response

In the directional axis, identical response to FA system was observed up to a yaw rate demand of  $\pm 7.0\%$  ( $\mp 6.3$  deg/s) and as the demands are increased beyond this, degradation in both the on- and off-axis responses are observed. The example plot in Figure 6.15 shows the yaw rate response and the total control activity to a pilot demand of  $5.0\%$  ( $\mp 4.5$  deg/s) and the corresponding series actuator activity is shown in Figure 6.17. Similar to the other two axes, identical responses are seen in the directional channel as long as the series actuator is unsaturated. As the pilot demand is increased above the  $\pm 7.0\%$  limit, the actuator begins to saturate and this directly starts to degrade the system yaw rate response. An example of this shown in the yaw rate response (Figure 6.16) and the corresponding series actuator activity (Figure 6.17) to a pilot demand of  $\pm 9.0\%$  ( $\mp 8.1$  deg/s), and confirms that the degradation in the responses is directly associated to the series actuator saturation.



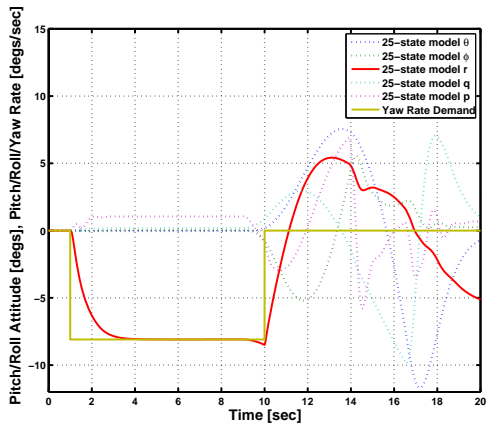
Directional response (5%)

Total control activity (5%)

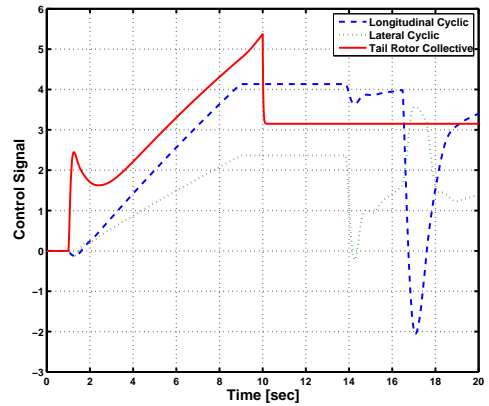
Figure 6.15: Directional Response (5%)

## Summary

The maximum pilot demand in the longitudinal, lateral and directional channel that produced identical FA response was  $\pm 8.5\%$  ( $\mp 5.1$  deg),  $\pm 10.5\%$  ( $\pm 12.6$  deg) and  $\pm 7.0\%$  ( $\mp 6.3$  deg/s) respectively. The relatively low value for the maximum value was due to the series actuators being loaded with all the work, causing premature saturation of these actuators. These results showed the weakness of this particular design and also presented a problem that required



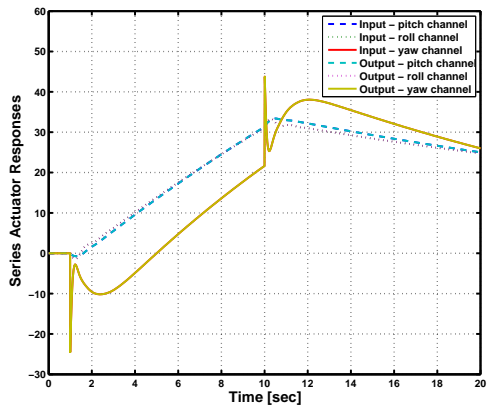
Directional response (9%)



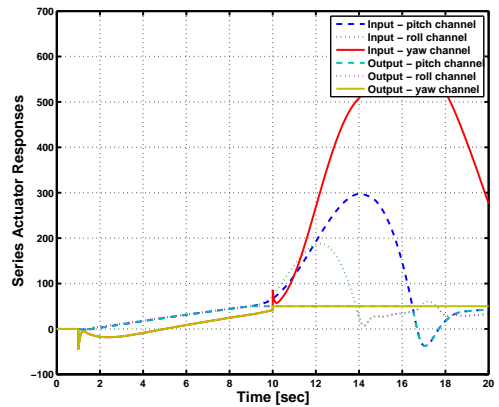
Total control activity (9%)

Figure 6.16: Directional Response (9%)

careful addressing. The following section shows the enhancement that was made to the architecture by the introduction of the parallel actuator and the parallel actuator compensator.



Series actuator response (5%)



Series actuator response (9%)

Figure 6.17: Series Actuator Response - Yaw channel

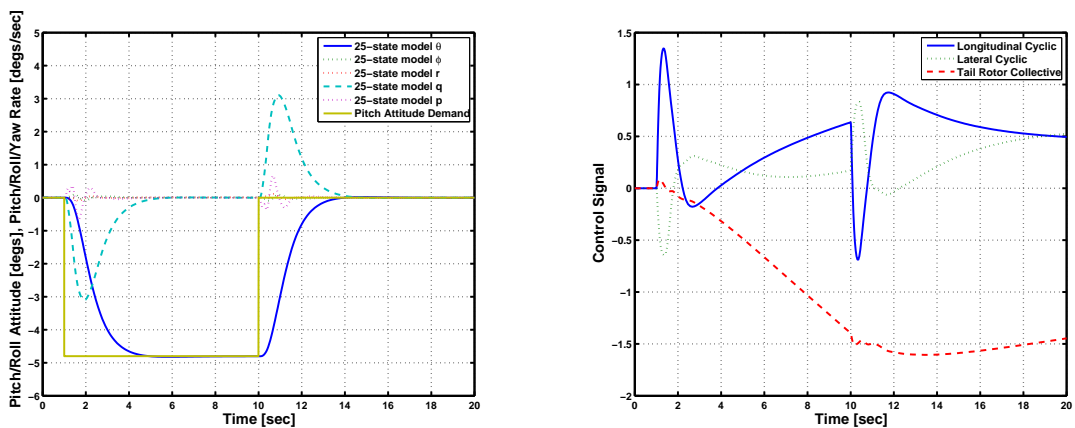
## 6.2.2 Limited authority controller with series and parallel actuation

This section focuses on the application of the theoretical results presented in Chapter 5 to the EH101. In this case, the parallel actuators and an accompanying controller are included in the LA framework. For this study, the parallel actuator controller was chosen as a scaled integrator in each channel, in order to drive the series actuator outputs to zero and in common with some of the other LA architectures. Parallel actuator compensator are given the following state-space realisation

$$\begin{aligned} \dot{x}_p &= \begin{bmatrix} 1 & 0 & 0 \\ 0 & 1 & 0 \\ 0 & 0 & 1 \end{bmatrix} \hat{u}_p \\ y_p &= \alpha \begin{bmatrix} 1 & 0 & 0 \\ 0 & 1 & 0 \\ 0 & 0 & 1 \end{bmatrix} x_p \end{aligned} \quad (6.6)$$

where  $\hat{u}_p$  represents the input to the compensator. The choice of  $\alpha$  is of significant importance as it has a strong implication towards the success of this architecture. To begin with  $\alpha$  was chosen as 0.05.

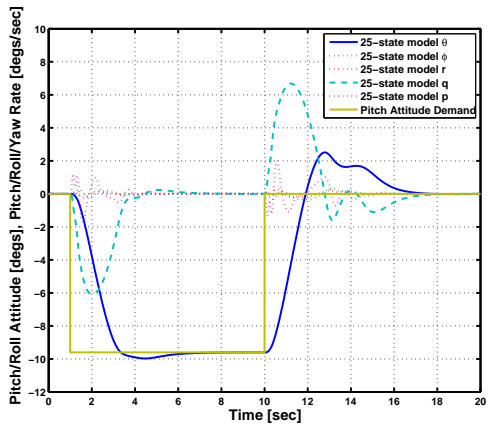
### Longitudinal Response



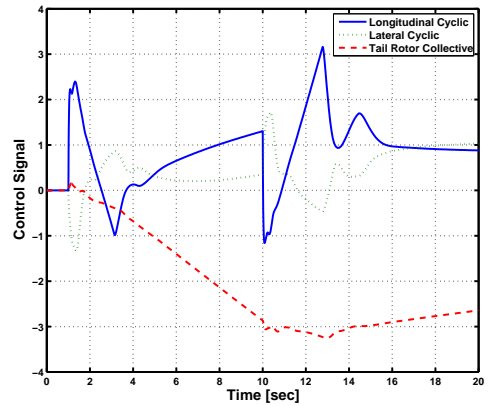
Longitudinal response

Total control activity

Figure 6.18: Longitudinal Response (8%)

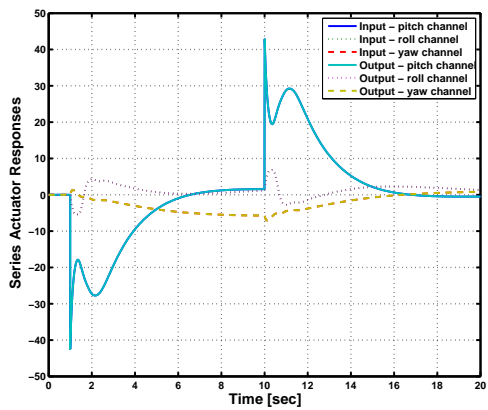


Longitudinal response

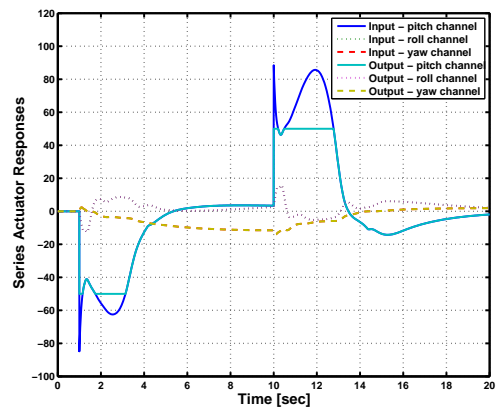


Total control activity

Figure 6.19: Longitudinal Response (16%)



Series actuator response (8%)

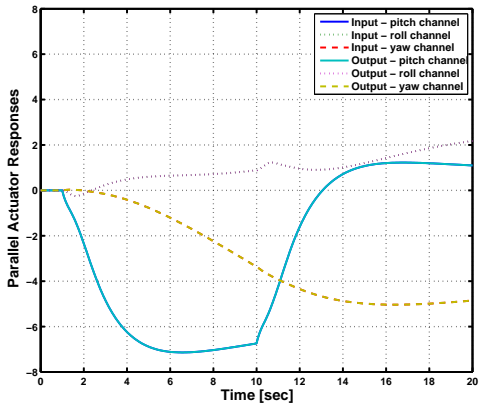


Series actuator response (16%)

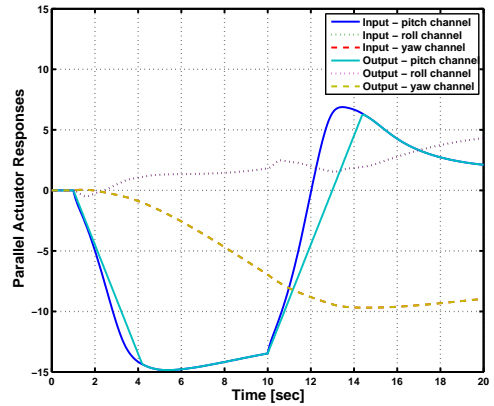
Figure 6.20: Series Actuator Response

The presence of the parallel actuators increased both the range of pilot input that produced identical FA system response, and the range of input that could be tolerated before the response becomes unstable. These increased from  $\pm 8.5\%$  to  $\pm 12\%$  ( $\mp 7.2$  deg) and from  $\pm 9.25\%$  to  $\pm 20\%$  ( $\pm 12$  deg) respectively. An example of the response for small input demand (8% ( $-4.8$  deg)) is shown in Figure 6.18 and the corresponding series and parallel actuator activities are presented in Figures 6.20 and 6.21. At this pitch magnitude, the series actuators are active only for a short period of time. Also, note that the parallel actuator, through its integral action, drives the mechanical links to become consistent with such a demand and hence in steady state the series actuators are inactive.

Figures 6.19, 6.20 and 6.21 show the response to a larger demand of 16% ( $-9.6$  deg). Note



Parallel actuator response (8%)

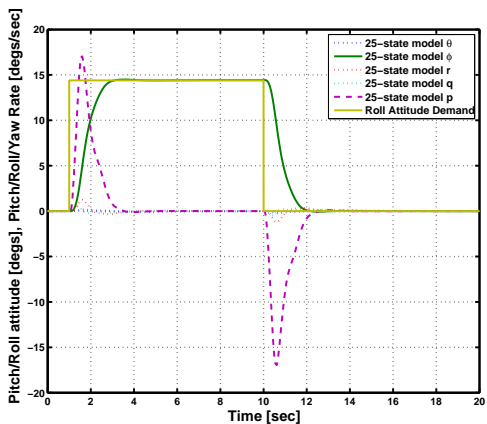


Parallel actuator response (16%)

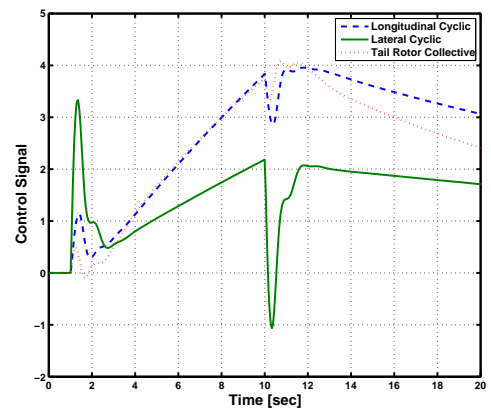
Figure 6.21: Parallel Actuator Response

that for this stick demand, the series and parallel actuators are saturated and rate-limited respectively for longer and hence the response deteriorates. In particular, note that the rate-limit of the parallel actuators prevent the swift off-loading of the series actuators and the transient response suffers as a result. As the stick demand is increased, the series and parallel actuators experience their respective saturations for longer periods of time, and the helicopter reverts to open-loop type behaviour.

### Lateral Response



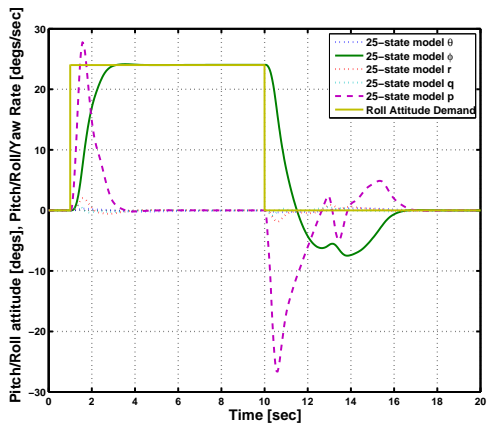
Lateral response



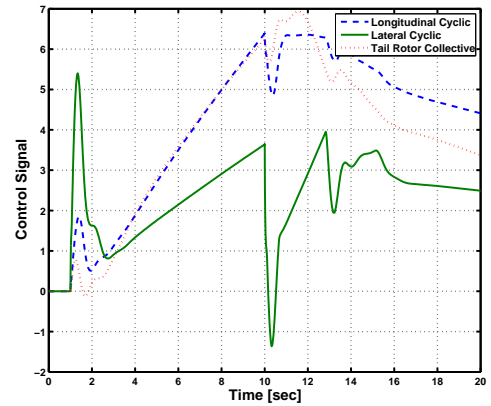
Total control activity

Figure 6.22: Lateral Response (12%)

The behaviour of the roll-axis with the LA controller was similar to the pitch axis, but larger

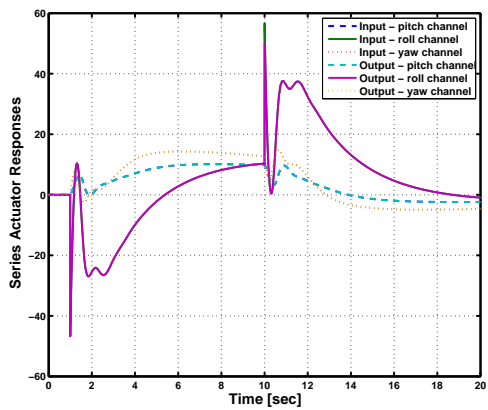


Lateral response

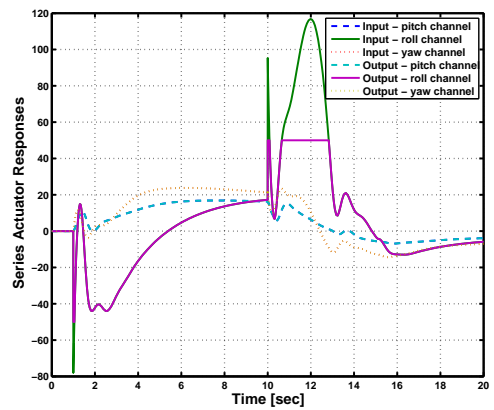


Total control activity

Figure 6.23: Lateral Response (20%)



Series actuator response (12%)

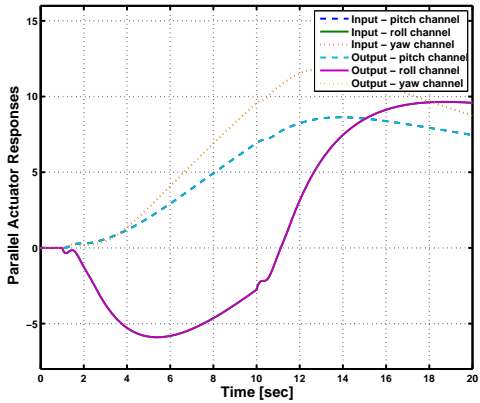


Series actuator response (20%)

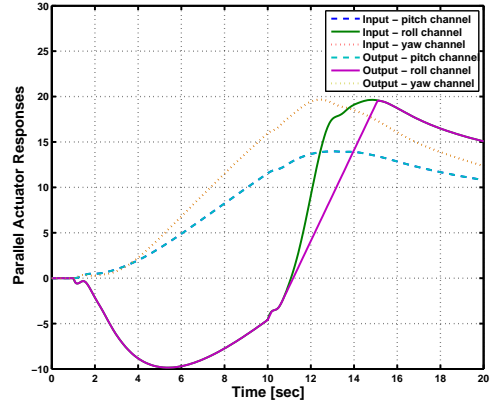
Figure 6.24: Series Actuator Response

stick demands were tolerated before the response became unstable. The maximum stick demand which could be applied to the system before minor deterioration started to appear increased from  $\pm 10.5\%$  (with series-actuation-only) to  $\pm 17\%$  ( $\pm 20.4$  deg). For demands above  $\pm 17\%$ , the deterioration in the response became worse, but these deteriorations are bearable until a stick input of around  $\pm 26\%$  ( $\pm 31.2$  deg).

Figures 6.22, 6.24 and 6.25 show the response of the system with a stick input of 12% (14.4 deg). The workload is shared between the series and parallel actuators in a similar manner to the longitudinal channel with the series actuators being heavily activated in the first few seconds, followed by a slower parallel actuator response to gradually drive the series actuator control signal to zero. Note that, the yaw series actuator saturation which caused off-axis



Parallel actuator response (12%)



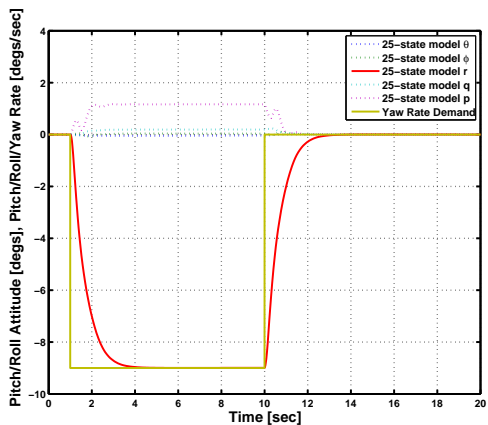
Parallel actuator response (20%)

Figure 6.25: Parallel Actuator Response

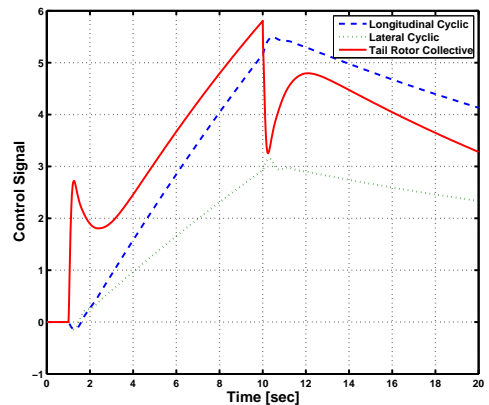
coupling for the series-only LA controller is mitigated by the parallel actuators in the current control scheme.

Figures 6.23, 6.24 and 6.25 show the response to a stick demand of 20% (26 deg). The slight degradation in the response is explained by the series actuator saturation. It is also noted that the parallel actuators experience rate-saturation for this level of stick demand, causing a prolonged period of series saturation (as they are unable to drive the output to zero as quickly as desired) and hence weakened performance.

### Directional Response

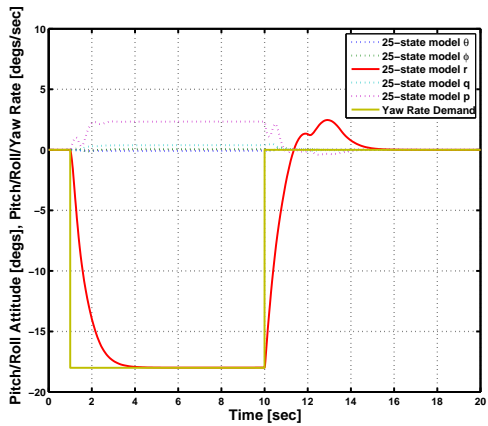


Directional response

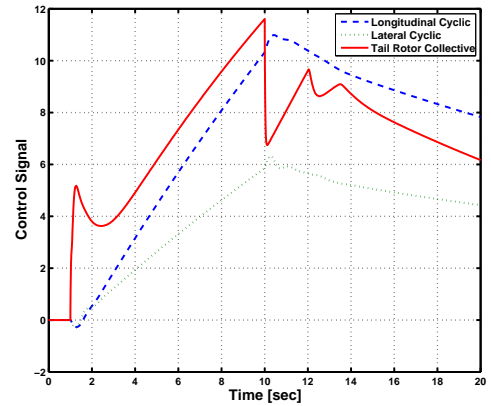


Total control activity

Figure 6.26: Directional Response (10%)

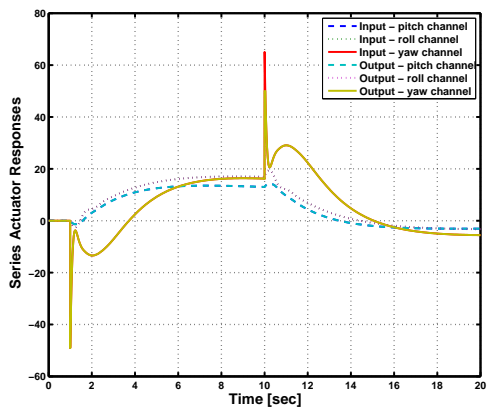


Directional response

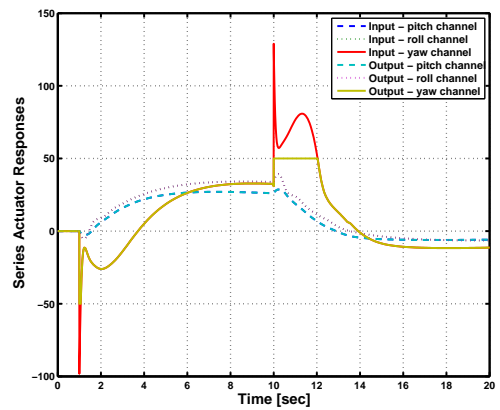


Total control activity

Figure 6.27: Directional Response (20%)



Series actuator response (10%)

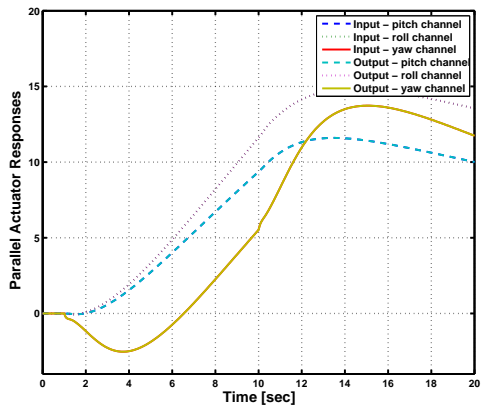


Series actuator response (20%)

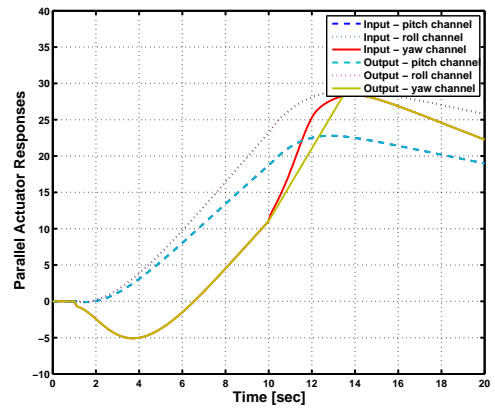
Figure 6.28: Series Actuator Response

The directional responses due to pedal inputs follow a similar pattern to the longitudinal and lateral responses due to stick inputs. Using the parallel actuators allowed the maximum pedal inputs applicable before response deterioration to be increased from  $\pm 7\%$  to  $\pm 15\%$  ( $\mp 13.5$  deg/s); a three-fold improvement. Also, the responses only become intolerable after pedal inputs of  $\pm 27\%$  ( $\mp 24.3$  deg/s) are applied.

An example of a the system's response to a low amplitude pedal input is shown in Figures 6.26, 6.28 and 6.29. Despite some saturation of the series actuators, the parallel actuators allow the LA controllers response to match the FA response. Without the parallel actuators, the series actuators would remain in saturation much longer and would lead to instability for much smaller pedal inputs.



Parallel actuator response (10%)



Parallel actuator response (20%)

Figure 6.29: Parallel Actuator Response

An example of a larger pedal input is shown in Figures 6.27, 6.28 and 6.29. During this larger input, there is rapid series actuator activity leading to saturation. However, due to the parallel actuator rate-limits this activity cannot be attenuated as quickly by the parallel actuators and hence persists for longer, leading to deterioration of the response. As the pedal inputs are increased, the periods of series and parallel actuation magnitude and rate saturation increase, respectively, and performance deteriorates further.

### Design point results summary

The above results show that the inclusion of the parallel actuators in the LA architecture in the manner proposed in this study leads to increased ranges of stick/pedal inputs that can be applied without leading to grossly deteriorated response. Table 6.2 and 6.3 shows the summary of these results. Note, the range of inputs which lead to responses identical to that of the FA system has also increased. It is also interesting to observe that the roll and yaw channels appear to preserve tolerable rotorcraft behaviour for much higher levels of pilot stick/pedal demands than the pitch channel mainly due to the larger amount of saturation in the pitch channel.

Actuation	Max pilot demand		
	Pitch attitude $\%(\text{deg})$	Roll attitude $\%(\text{deg})$	Yaw rate $\%(\text{deg}/s)$
Series	$\pm 8.5(\mp 5.1)$	$\pm 10.5(\pm 12.6)$	$\pm 7(\mp 6.3)$
Series plus parallel	$\pm 12(\mp 7.2)$	$\pm 17(\pm 20.4)$	$\pm 15(\mp 13.5)$

Table 6.2: Maximum pilot input for identical FA response

Actuation	Max pilot demand		
	Pitch attitude $\%(\text{deg})$	Roll attitude $\%(\text{deg})$	Yaw rate $\%(\text{deg}/s)$
Series	$\pm 9(\mp 5.4)$	$\pm 17(\pm 20.4)$	$\pm 10(\mp 9.0)$
Series plus parallel	$\pm 20(\mp 12)$	$\pm 26(\pm 31.2)$	$\pm 27(\mp 24.3)$

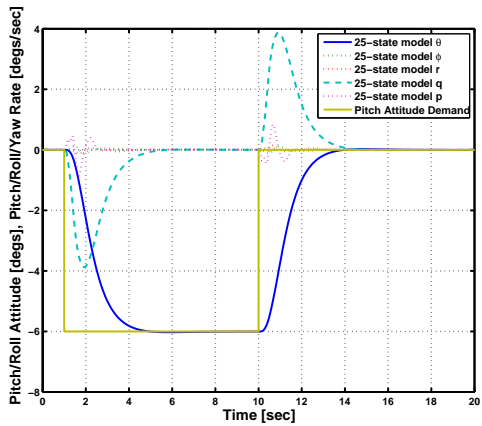
Table 6.3: Maximum pilot input for stable LA response

### 6.2.3 Other choices for parallel actuator controller

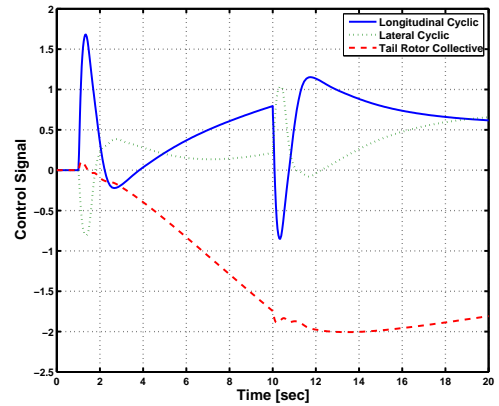
The parallel actuator controller,  $K_P(s)$  is crucial for deciding the workload split between the series and parallel actuators. Large gain values of  $K_P(s)$  imply that the parallel actuator will attempt to off-load the series actuators as swiftly as possible, but also implies increased instances of parallel actuator rate-limiting. Excessive parallel actuator activity can also be irritating to the pilot. On the other hand, low parallel actuator gains imply that the series actuator is responsible for most of the control and stabilising task and is likely to saturate more due to less assistance from the parallel actuator. This section investigates the effect of different values of  $\alpha$ .

#### Output Matrix Gain $\alpha > 0.05$

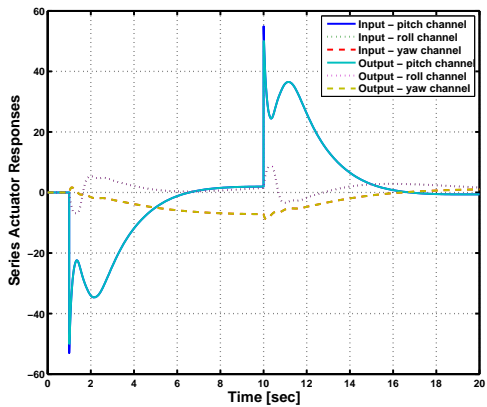
For this set of results  $\alpha$  was set to 0.5 which meant that the parallel actuators are expected to be more active and also try to off-load the series actuators more rapidly than before. Figure 6.31 shows an example response using this value of  $\alpha$  for a longitudinal stick demand of 10% (-6 deg). The parallel actuator was observed to be working in their saturated (rate-limited) state from the start of this manoeuvre and due to this the series actuators were also, although momentarily, pushed above their saturation limit. The oscillations in the pitch attitude response when compared to the response obtained for  $\alpha = 0.05$  (Figure 6.30) were



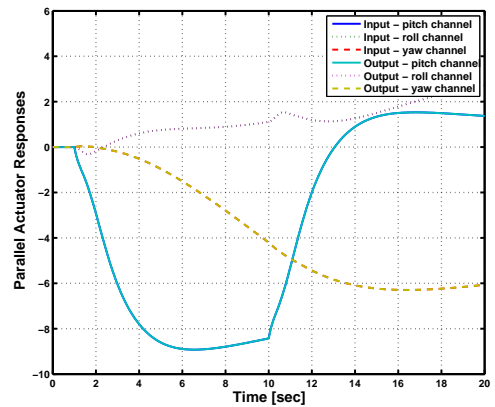
Longitudinal response



Total control activity



Series actuator response



Parallel actuator response

Figure 6.30: Longitudinal Response (10%) ( $\alpha = 0.05$ )

predominantly due to parallel actuator saturation. This also meant that the range of pilot demands that produced identical or stable FA response was smaller than when  $\alpha$  was set to 0.05.

### Output Matrix Gain $\alpha < 0.05$

Lower gain values meant that the parallel actuator controller was slower at off-loading the series actuator. This set of results was generated by setting  $\alpha$  to 0.005. In the limit as  $\alpha \rightarrow 0$ , this scheme naturally approaches the series actuator only scheme. The lower gain value was also analysed for the same 10% stick demand in the longitudinal axis as before and is shown in Figure 6.32 along with the series/parallel actuator activity. Again, the helicopter response is degraded compared to when  $\alpha$  is set to 0.05. This was mainly due to the series actuators

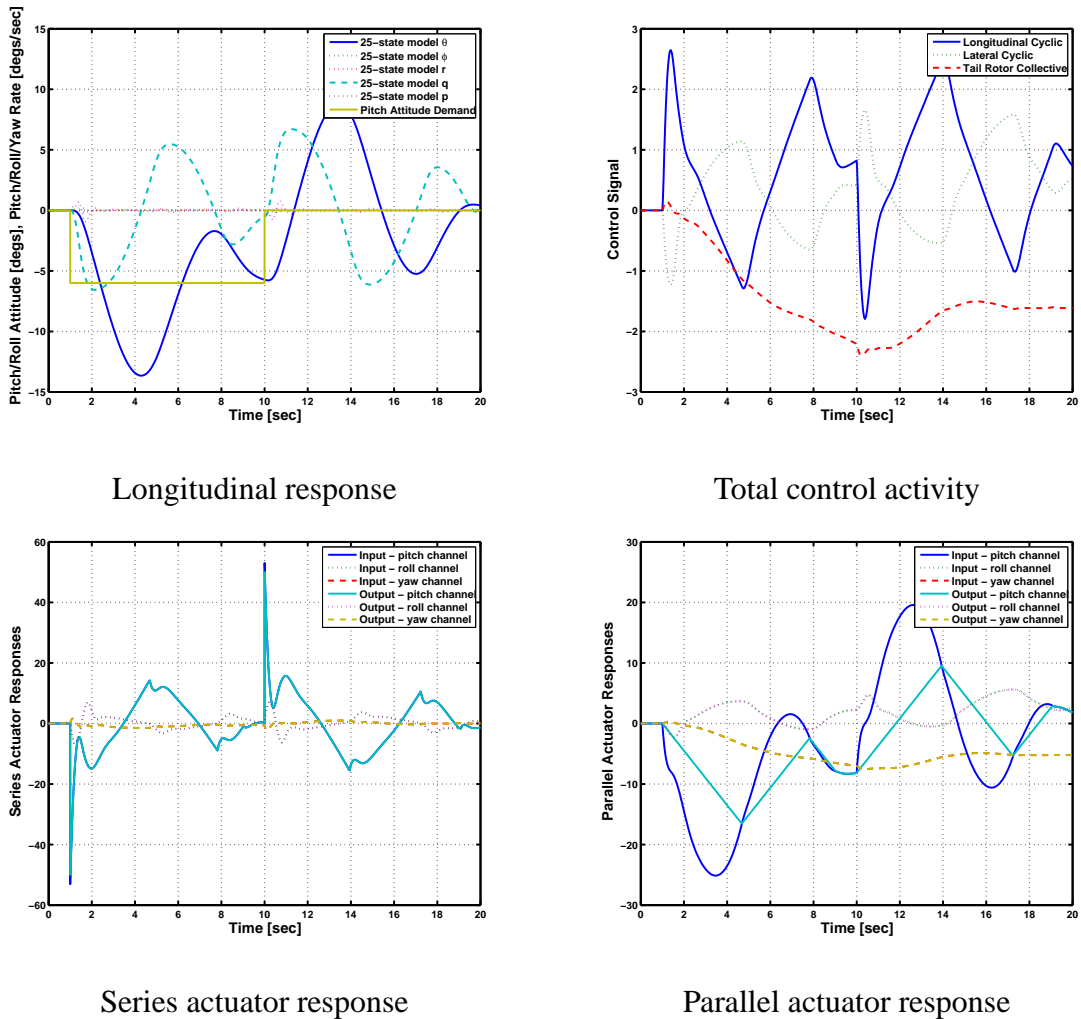
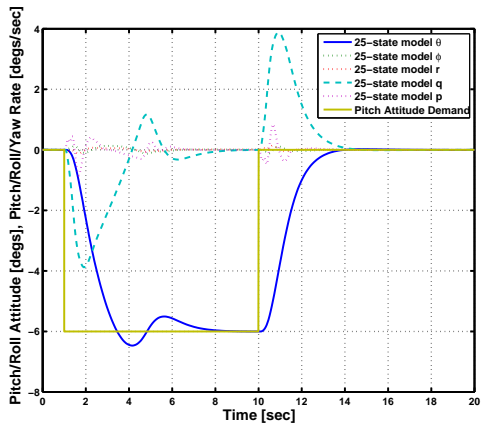


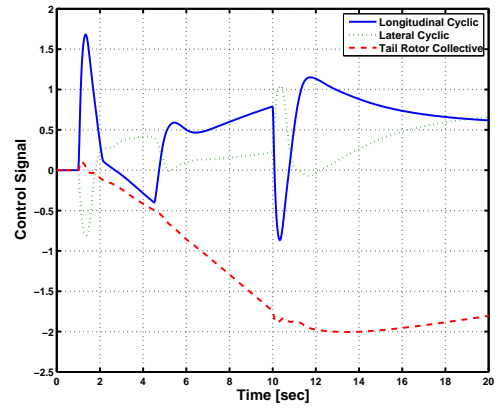
Figure 6.31: Longitudinal Response (10%) ( $\alpha = 0.5$ )

experiencing longer saturation periods as the parallel actuator was slower in returning the series actuator signal to zero.

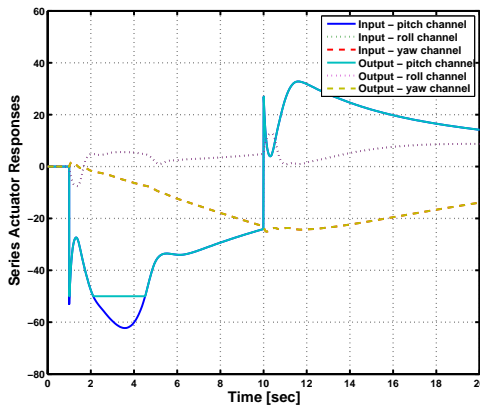
Similar patterns as the longitudinal channel were also observed with the lateral and directional channels. A summary of these results is presented in Table 6.4. High gain values gave the parallel actuators more workload that made them prone to rate saturation, whereas a low gain value meant that the series actuators were more prone magnitude saturation due to excessive workload. The above explanation justifies the choice of  $\alpha$  value as 0.05 a good compromise that provides a satisfactory division of work to both series and parallel actuators without making either of them susceptible to premature saturation. This of course does not take into account whether the pilot is comfortable with this level of parallel actuator interference, and would have to be tuned from helicopter to helicopter.



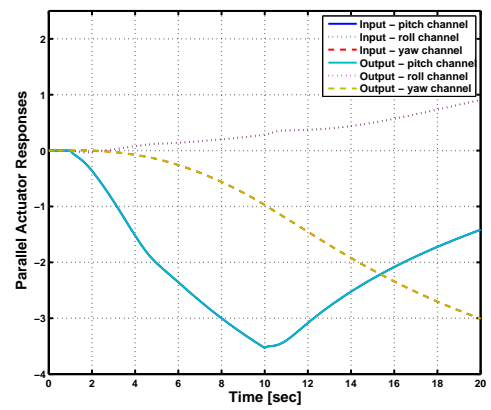
Longitudinal response



Total control activity



Series actuator response



Parallel actuator response

Figure 6.32: Longitudinal Response (10%) ( $\alpha = 0.005$ )

Value of $\alpha$	Max pilot demand		
	Pitch attitude $\%(\text{deg})$	Roll attitude $\%(\text{deg})$	Yaw rate $\%(\text{deg/s})$
0.005	$\pm 9(\mp 5.4)$	$\pm 12(\pm 14.4)$	$\pm 8(\mp 7.2)$
<b>0.05</b>	$\pm 12(\mp 7.2)$	$\pm 17(\pm 20.4)$	$\pm 15(\mp 13.5)$
0.5	$\pm 4.5(\mp 2.7)$	$\pm 5(\pm 6)$	$\pm 10(\mp 9)$

Table 6.4: Maximum pilot input for a identical response with variation to value of  $\alpha$

## 6.2.4 Robustness

In a similar manner to the FA analysis, in order to form a broader understanding of the robustness property of LA controller, it was essential to simulate the LA controller at different flight conditions. The controller was analysed at various flight conditions and a few of those

conditions are discussed here, they are:

1. Low speed, low altitude, light - 40kts/0ft/11000kg.
2. Hover, light - 0kts/0ft/11000kg.
3. Hover, heavy - 0kts/0ft/14200kg.
4. High speed, high altitude, light - 80kts/4500ft/11000kg.
5. High speed, high altitude, heavy - 80kts/2500ft/14200kg.

Initially the LA architecture with only series actuation was analysed. Throughout the flight envelope, identical FA responses were observed in both the longitudinal and the lateral channels for approximately similar magnitude range of pitch and roll attitude demands respectively. The only discrepancy was seen in the directional channel, where the range increased from  $\pm 6.3$  deg/s at low speed/low altitude to  $\pm 10.8$  deg/s at hover and dropped significantly to  $\pm 2.43$  deg/s at the high speed/high altitude condition. A similar pattern was noticed after the inclusion of parallel actuator with both longitudinal and lateral channels producing identical FA responses for approximately the same range of pilot demands as at the design point. However, the directional channel again showed a reduction to the range of pedal demand that could be applied for an identical FA response at high speed/high altitude condition from  $\pm 13.5$  to  $\pm 8.1$  deg/s. Overall, it could be concluded that the above LA controller is fairly robust towards flight condition changes especially in the longitudinal and lateral channel. A summary of these results are presented in Tables 6.5 and 6.6.

Figures 6.33, 6.34, 6.35, 6.36 and 6.37 present the LA responses to a pulse demand of 5%, i.e.  $-3$  deg in longitudinal,  $6$  deg in lateral and  $-4.5$  deg/s in directional, to each of the channel one at a time. These responses confirm LA controller's ability to reproduce the FA responses, not only at the design point but also at other trim conditions and this was observed by comparing these to the FA responses presented earlier in the chapter (Figures 6.2 to 6.6). The baseline FA controller presented in Chapter 4 was designed using  $\mathcal{H}_\infty$  loop shaping methodology that guarantees robustness against coprime factor uncertainty which is believed to be a highly comprehensive type of uncertainty description. The transformation methodology presented in Chapter 5 has assisted to obtain a LA controller that has retained the robustness property of this baseline FA controller.

Flight Condition	Max pilot demand		
	Pitch attitude $\%(\text{deg})$	Roll attitude $\%(\text{deg})$	Yaw rate $\%(\text{deg}/\text{s})$
40kts/00ft/14200kg	$\pm 8.5(\mp 5.1)$	$\pm 10.5(\pm 12.6)$	$\pm 7(\mp 6.3)$
40kts/00ft/11000kg	$\pm 8.7(\mp 5.22)$	$\pm 10.2(\pm 12.24)$	$\pm 7(\mp 6.3)$
Hover/14200kg	$\pm 9.8(\mp 5.88)$	$\pm 9.4(\pm 11.28)$	$\pm 11.5(\mp 10.35)$
Hover/11000kg	$\pm 9.3(\mp 5.58)$	$\pm 9.6(\pm 11.52)$	$\pm 12(\mp 10.8)$
80kts/2500ft/14200kg	$\pm 9.4(\mp 5.64)$	$\pm 9(\pm 10.8)$	$\pm 2.5(\mp 2.25)$
80kts/4500ft/11000kg	$\pm 9.5(\mp 5.70)$	$\pm 8.75(\pm 10.5)$	$\pm 2.3(\mp 2.07)$

Table 6.5: Series actuation robustness and summary

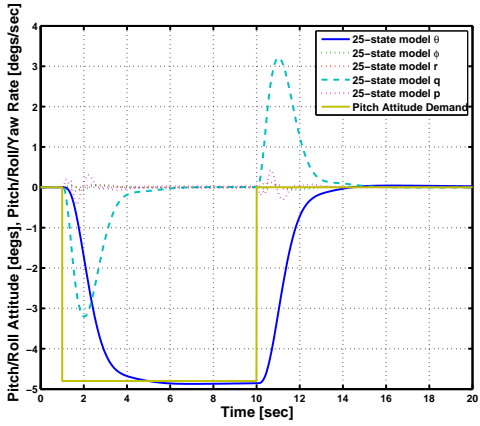
Flight Condition	Max pilot demand		
	Pitch attitude $\%(\text{deg})$	Roll attitude $\%(\text{deg})$	Yaw rate $\%(\text{deg}/\text{s})$
40kts/00ft/14200kg	$\pm 12(\mp 7.2)$	$\pm 17(\pm 20.4)$	$\pm 15(\mp 13.5)$
40kts/00ft/11000kg	$\pm 12(\mp 7.2)$	$\pm 16(\pm 19.2)$	$\pm 14(\mp 12.6)$
Hover/14200kg	$\pm 12(\mp 7.2)$	$\pm 18(\pm 21.6)$	$\pm 16(\mp 14.4)$
Hover/11000kg	$\pm 12(\mp 7.2)$	$\pm 17(\pm 20.4)$	$\pm 15(\mp 13.5)$
80kts/2500ft/14200kg	$\pm 12(\mp 7.2)$	$\pm 15(\pm 18)$	$\pm 9.5(\mp 8.55)$
80kts/4500ft/11000kg	$\pm 12(\mp 7.2)$	$\pm 12(\pm 14.4)$	$\pm 9(\mp 8.1)$

Table 6.6: Series and parallel actuation robustness summary

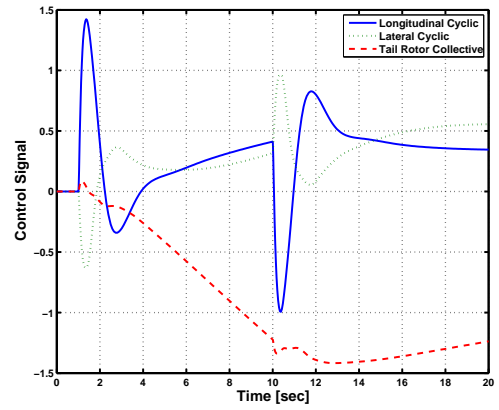
## 6.3 Conclusion

This chapter has described the responses achieved using the 25-state linear model after the transformation formulae was applied. The results from an architecture that utilises only the series actuator activity were also shown to illustrate the advantages of using parallel actuators in LA architectures. The maximum pilot demand in the longitudinal, lateral and directional channel using series actuation alone was observed to be  $\pm 8.5(\mp 5.1 \text{ deg})$ ,  $\pm 10.5(\pm 12.6 \text{ deg})$  and  $\pm 7(\mp 6.3 \text{ deg/s})$  respectively. Applying the parallel actuators improved upon the limit on the maximum pilot demand that could be applied for an identical FA response by 135%, 148% and 200% in the pitch, roll and yaw channel respectively. It was also observed that maximum pilot input that ensured a stable, not identical, response improved by a further 25% and 38% in the longitudinal and lateral stick deflections respectively and 81% in the

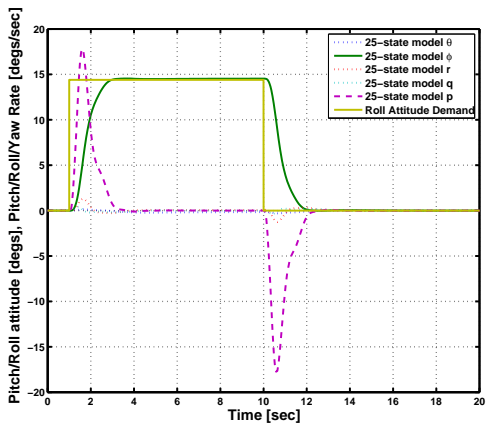
pedal demand. The results in this chapter showed a more than satisfactory functioning of the proposed LA architecture throughout the flight envelope. These responses allowed for a fair prediction of the helicopter performance and are further substantiated by the nonlinear and handling qualities evaluation presented in the next chapter.



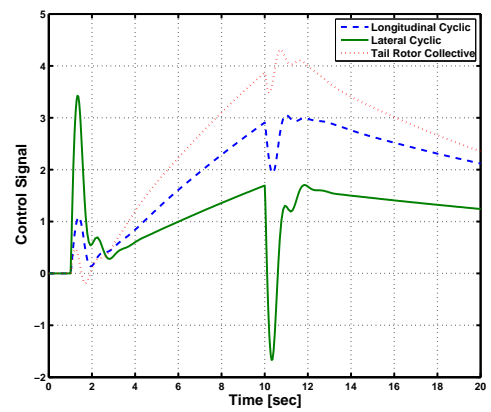
Longitudinal response



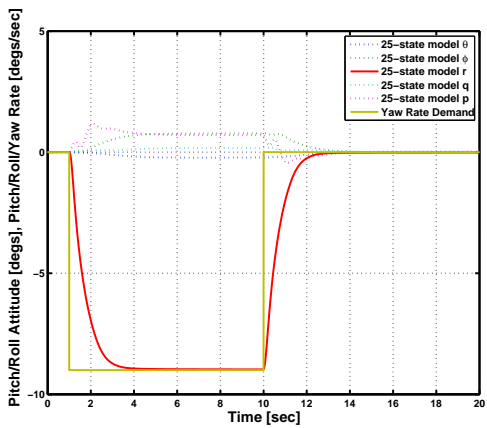
Total control activity



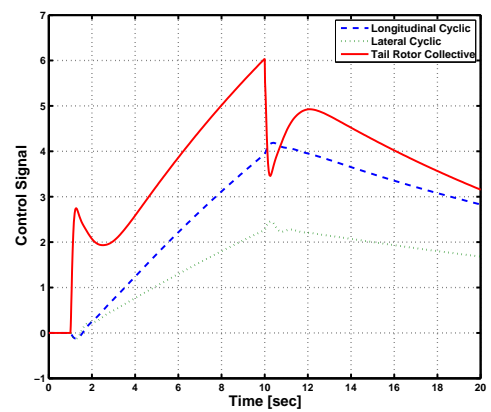
Lateral response



Total control activity

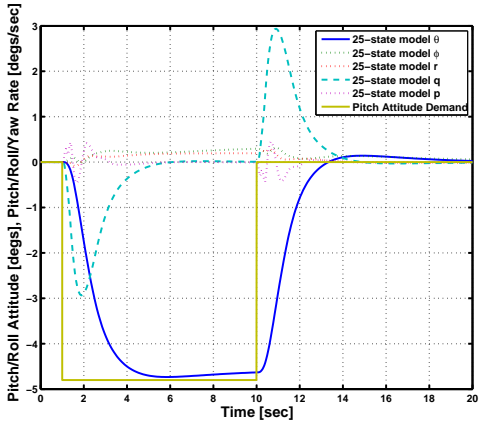


Directional response

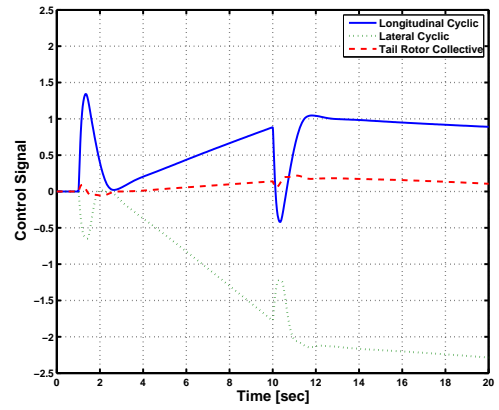


Total control activity

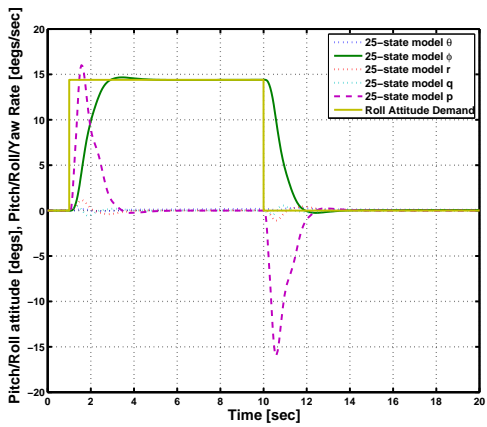
Figure 6.33: LA response - 40kts/0ft/11000kg



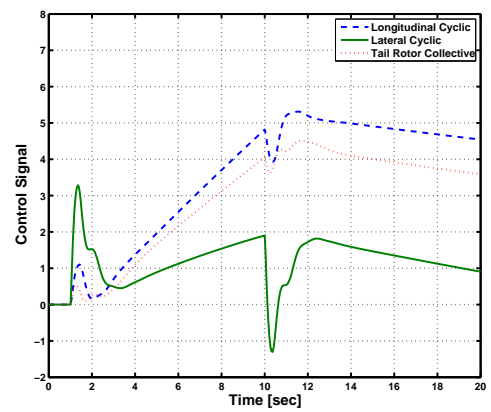
Longitudinal response



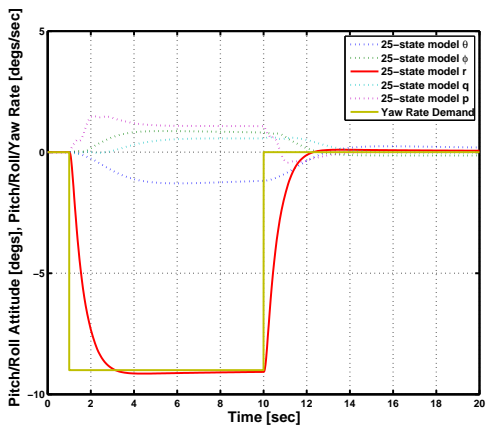
Total control activity



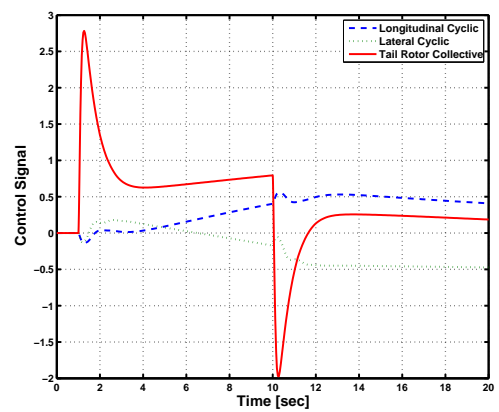
Lateral response



Total control activity

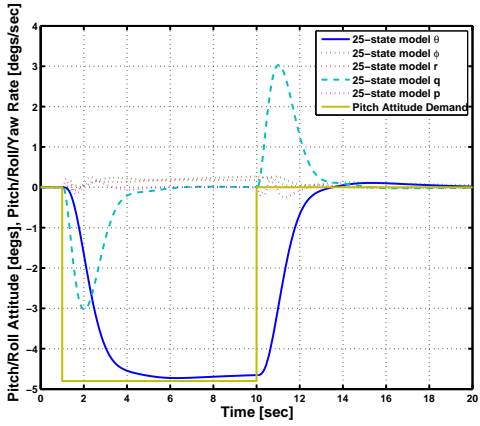


Directional response

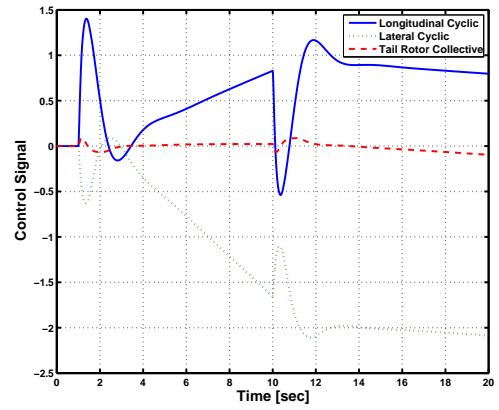


Total control activity

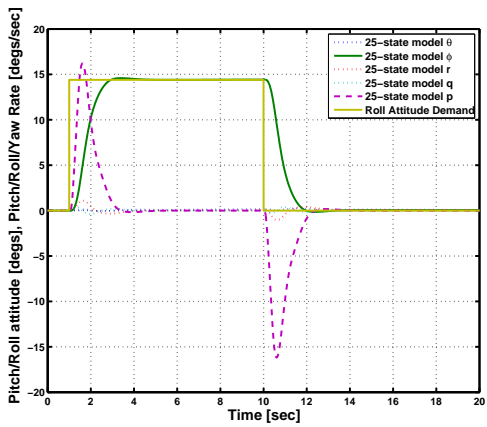
Figure 6.34: LA response - Hover/14200kg



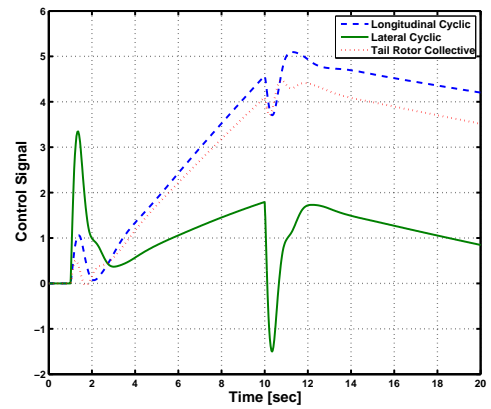
Longitudinal response



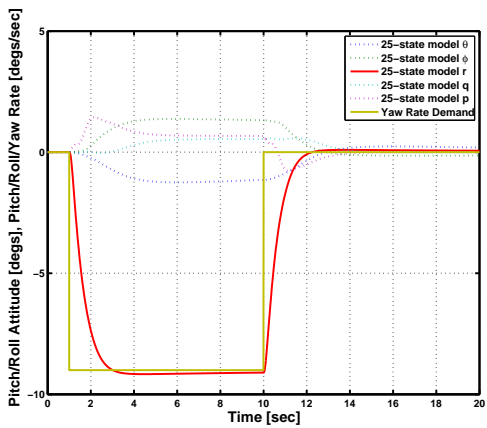
Total control activity



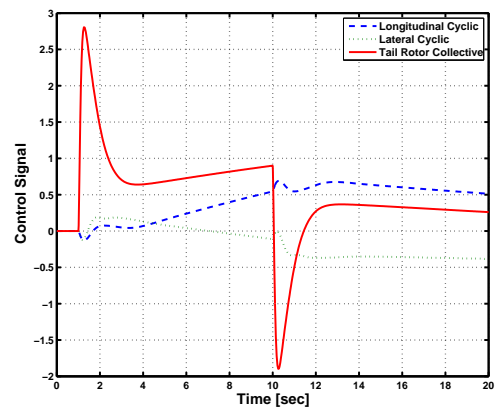
Lateral response



Total control activity

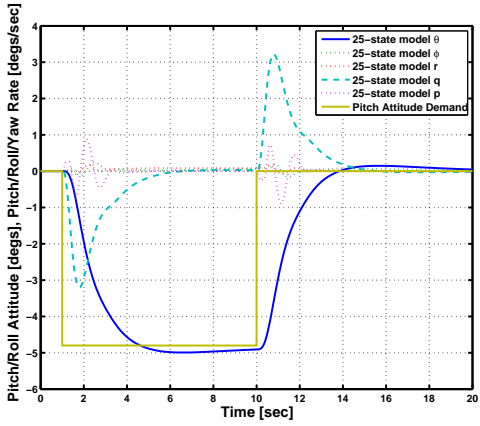


Directional response

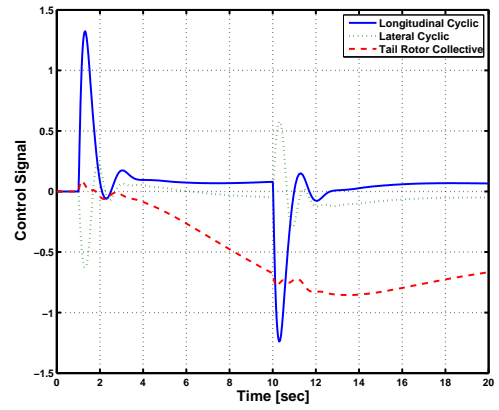


Total control activity

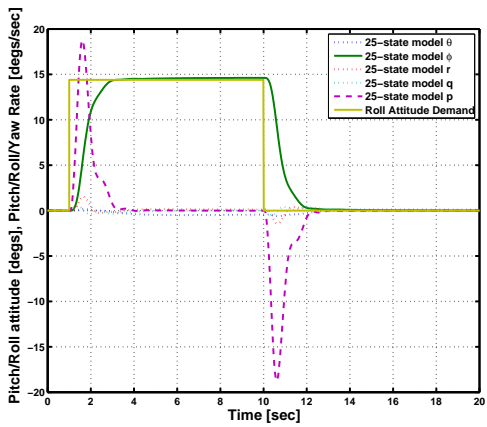
Figure 6.35: LA response - Hover/11000kg



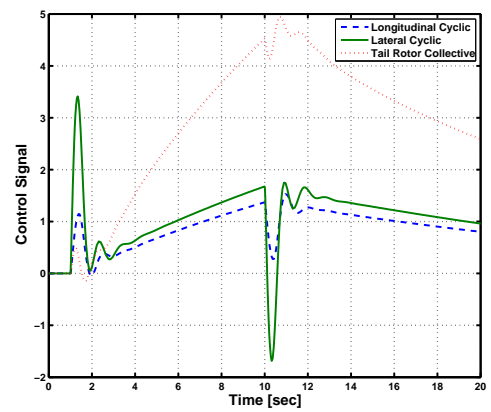
Longitudinal response



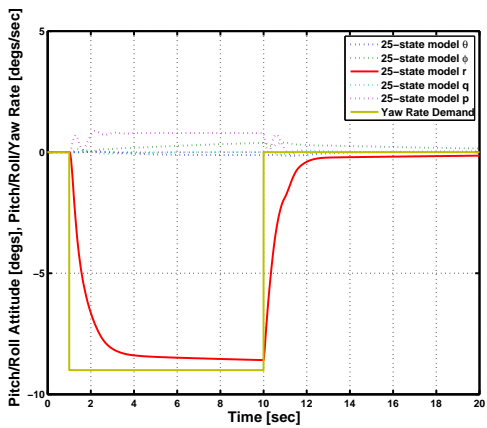
Total control activity



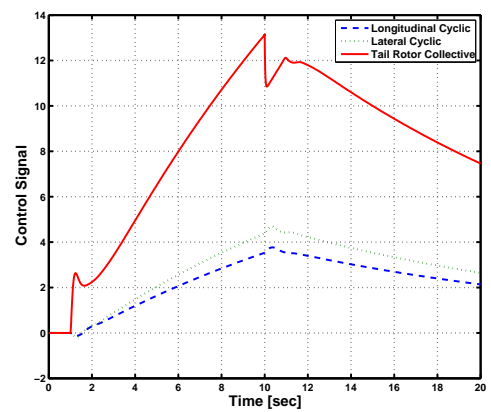
Lateral response



Total control activity

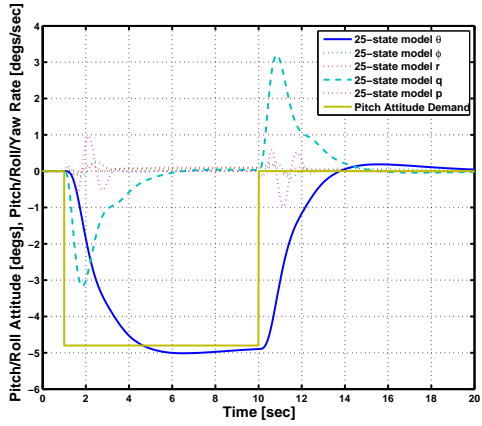


Directional response

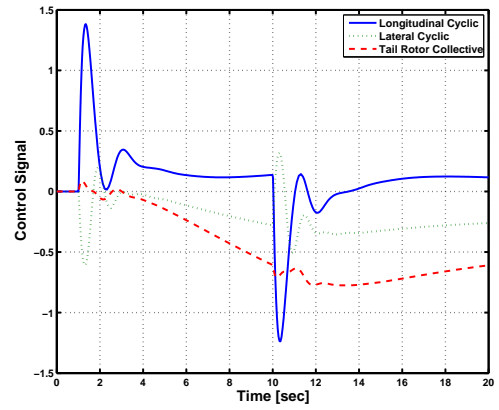


Total control activity

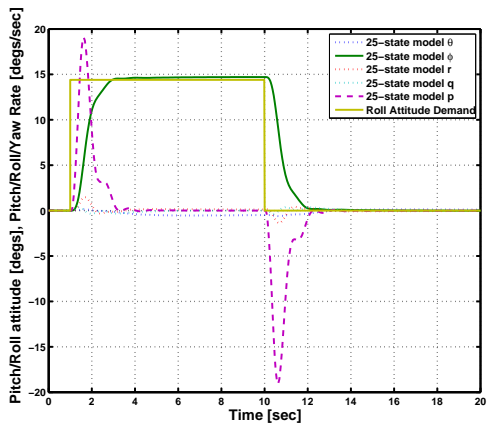
Figure 6.36: LA response - 80kts/2500ft/14200kg



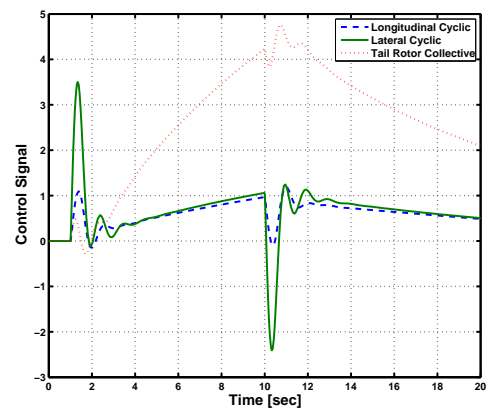
Longitudinal response



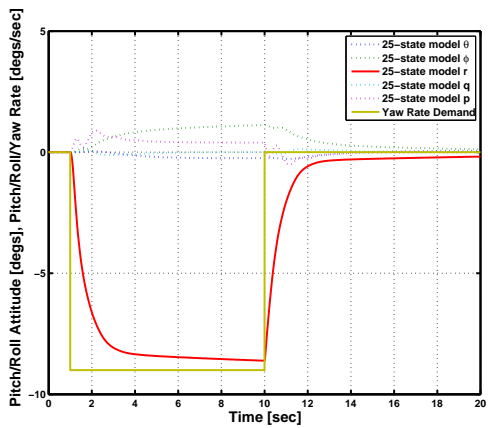
Total control activity



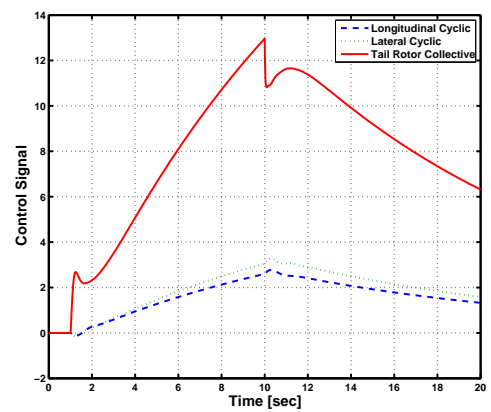
Lateral response



Total control activity



Directional response



Total control activity

Figure 6.37: LA response - 80kts/4500ft/11000kg

# Chapter 7

## Nonlinear simulation and quantitative ADS-33 analysis

The results presented thus far have been based on the 25-state linear model and while they do represent the EH101's behaviour to a certain extent, and provide a good initial assessment of both the FA and LA controller's performance, the large signal results in particular may be somewhat inaccurate. This chapter presents the results obtained using the nonlinear EH101 model which should assist to make a more accurate appraisal of both controller's performance. These are further complemented by an evaluation of quantitative handling qualities information against the design standard ADS-33.

### 7.1 Full authority simulation results

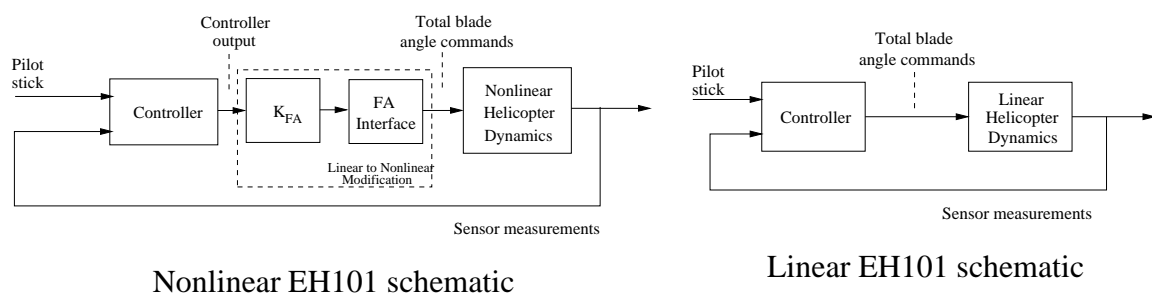


Figure 7.1: Linear and Nonlinear FA architecture comparison

This section describes the nonlinear simulation results obtained with the FA controller de-

scribed in Chapter 4. The structure of the control system is essentially the same as in the linear case, with some slight differences due to the inclusion of a mechanical mixer, or “FA interface” in the nonlinear model. In addition, because the nonlinear simulation is inherently a four-axis simulation model, the collective stick - which was not considered in the earlier linear simulations - was included in the simulation set-up, although was set to zero. Thus the main difference between the linear and non linear model is the FA interface which is a nonlinear device, that converts rotor jack positions into the corresponding blade angle commands. Thus, for the nonlinear simulation the controller must generate demands in terms of jack positions rather than blade angle commands.

The way in which the linear controllers are adjusted for nonlinear implementation is shown in Figure 7.1. The right hand figure shows the situation in the linear case. The left hand figure shows the nonlinear set-up. In the left hand figure  $K_{FA}$  represents a matrix gain which converts the controller output (blade angle commands) into jack commands, which are accepted by the FA interface.  $K_{FA}$  represents the inverse of the steady-state gain of the linearised FA interface. Note, that because the dynamics are fast, at small blade angle commands,  $K_{FA}^{-1}$  is a very good approximation of the FA interface and thus the components in the dashed box in the left hand diagram of Figure 7.1 are essentially equal to the identity and thus the linear controller functions virtually identical to the linear case. However, for larger blade angle demands, the nonlinearity of the FA interface means that some differences between the linear and nonlinear simulations are evident.

Based on the linearisation of the FA interface,  $K_{FA}$  was thus chosen as

$$K_{FA} = \begin{bmatrix} -2.74 & 0.53 & -3.03 & 0 \\ 1.01 & 2.59 & -3.03 & 0 \\ 2.37 & -1.46 & -3.03 & 0 \\ 0 & 0 & 0 & -3.14 \end{bmatrix} \quad (7.1)$$

During the nonlinear analysis, the linear controller was not only tested for varying flight conditions but also for different magnitude and direction of pilot demands. While it is not possible to present an analysis of all flight conditions and all inputs, this section describes simulation results from several differing flight conditions for the heavier EH101 configuration (14200kg) - 0kts/0ft (hover), 40kts/0ft (design point) and 80kts/2500ft (high speed/high

altitude). The trim values at these flight conditions are listed in Table 7.1.

	Trim values								
Trim point	$\theta_0$	$\phi_0$	$\psi_0$	$q_0$	$p_0$	$r_0$	$u_0$	$v_0$	$w_0$
0kts/0ft	6.8	-3.4	0	0	0	0	0	0	0
40kts/0ft	7.4	-1.2	0	0	0	0	20	0	2.6
80kts/2500ft	5.1	0	0	0	0	0	42	2.4	3.7

Table 7.1: Trim points and variables values

### 7.1.1 Longitudinal response (pitch-down)

The nonlinear analysis of the longitudinal channel began with a series of pitch-down pulse demands of varying magnitudes that were applied in a similar way as in Chapter 4. Figure 7.2 shows the helicopter responses at the controller design point due to pitch attitude demands of 5% (−3 deg), 20% (−12 deg) and 50% (−30 deg). Not surprisingly, the response to small amplitude pilot demands (up to 15% (−9 deg) are identical to those predicted by the linear simulation in Chapter 4. As the pilot demands increase to moderate amplitude (up to 30% (−18 deg), the helicopter behaviour is broadly similar to that predicted by the linear behaviour especially the short term response. The long term response, however, is little “bumpier” than predicted with slow low amplitude ( $\approx 1$  deg) “bumps” in the pitch attitude response. The response at larger demands does not deteriorate dramatically, but there are noticeable differences in the finer behaviour. One such difference is the development of a “kink” in the pitch rate response that resulted in a higher degree of coupling than predicted by the linear response.

### 7.1.2 Lateral response (roll-right)

Next, the lateral axis was tested for a range of roll-right pulse demands. The responses to inputs of 5% (6 deg), 20% (24 deg) and 40% (48 deg) at the design point are shown in Figure 7.3. Overall, the on-axis responses were in good agreement with the linear simulations in terms of their time response features. The roll attitude and the off-axis responses for a small

demand of up to 10 deg are clearly in agreement to the linear predictions. As the demand increases up to 30 deg, the coarse behaviour is similar to the linear prediction. However, roll rate response develops the previously highlighted “kink” which could be discomforting for the pilot. At 48 deg roll demand, the on-axis response shows minimum deterioration with only the long term response showing some discrepancy. However, the “kink” is more prominent and could cause the pilot further discomfort.

### **7.1.3 Directional response (right pedal forward)**

Finally, the directional channel was analysed for a range of yaw rate demands. The responses to pulse demands of 5% ( $-4.5$  deg/s), 20% ( $-18$  deg/s) and 50% ( $-45$  deg/s) at the design point are presented in Figure 7.4. For small amplitude demand, the yaw rate response is in broad agreement with the linear prediction, however, minor discrepancies in terms of the larger overshoot and the higher degree of coupling are observed. The response did not show any significant deterioration up to pedal demands of  $-10$  deg/s, however at larger pedal inputs,  $-20$  deg/s and greater, minor deterioration in tracking were observed.

#### **Design point results summary**

Overall, the responses at the design point have shown that for low magnitude stick/pedal inputs, the nonlinear small signal responses were essentially true to their linear predictions. At larger pilot demands minor deteriorations began to appear, but mainly in the off-axis responses. Also, inter-axis coupling was similar to that observed during the linear analysis for low amplitude signals and was severe at large pilot inputs. These discrepancies in the nonlinear responses were mainly due to the differences between the linearised 25-state model of the EH101 and the full nonlinear dynamics of the helicopter.

### **7.1.4 Robustness**

Apart from the design point, the controller was also analysed at other flight conditions. It is of definite interest to investigate how the robust stability indications, obtained from linear analysis, affected the robust performance of the nonlinear system. Figures 7.5, 7.6 and

7.7 illustrates the pulse demand responses in the longitudinal, lateral and directional channel respectively at the hover condition. For consistency, the off-design point responses are also shown for the same range of pilot demands as the design point. In the longitudinal channel, the responses for small amplitude pitch demands matched the corresponding linear predictions. The helicopter's behaviour at larger pilot demands was broadly similar, particularly in terms of short period response features, to their respective linear prediction. The long term behaviour, on the other hand, showed slightly "bumpier" activity than that seen at the design point. In the lateral channel, the responses for low amplitude roll demand were again in agreement with their predictions. As the roll demand was increased up to 25% (30 deg), degradations were mainly noticeable with off-axis responses, especially with roll rate response. The tail rotor collective input begins to saturate beyond 30 deg roll attitude demand, however, the on-axis response remains satisfactory and saturation mainly results to exaggerated coupling into yaw and pitch rate responses. In complete contrast to the above two channels, the directional channel responses at hover condition did not see any deterioration with changes in the yaw rate demand, although, an overshoot larger than the linear responses was observed.

Figures 7.8, 7.9 and 7.10 illustrate the pulse input responses in the longitudinal, lateral and directional channel respectively at the high speed/high altitude flight condition. The longitudinal responses for small pitch demands were again identical to their linear prediction. On-axis gross attitude acquisition deteriorates as the demands increase in magnitude. Off-axis responses, mainly pitch rate, also showed an exaggerated presence of the discomforting "kink", as observed at other flight conditions. Lateral channel responses remain, by and large, in agreement with the linear prediction at all the tested roll demands, particularly the on-axis response. Off-axis response, mainly roll rate, showed a greater deterioration as the roll demand is increased from 5% (6 deg) to 40% (48 deg). The directional channel on-axis response, for small yaw rate demands, were also in agreement to their predictions, whereas the off-axis responses showed significantly more coupling than their prediction. Tail rotor collective saturation occurred as yaw rate demand was increased to 20% (-18 deg/s) which effectively caused a sharp transient in the on-axis response as well as some corresponding deviation in the off-axis responses. Generally, the off-axis was observed to be quite poor even without the above saturation.

Overall, small signal analysis of the nonlinear model showed that the helicopter's coupling characteristics were in agreement with linear predictions, but for larger inputs significantly higher cross coupling was observed. For instance, a demand of 50% (−30 deg) in the longitudinal channel showed an increment from 12% to 28% (Figure 7.2) in roll rate response. In the lateral case, a maximum coupling of 32% (Figure 7.6) was observed at the hover condition for a roll attitude demand of 40% (48 deg). The directional channel showed the highest degree of coupling during the high speed/high altitude flight condition analysis ((Figure 7.10) where a maximum coupling of 35% was observed. Overall, the linear controller was highly effective against inter-axis coupling, although there were instances, such as the ones mentioned above, where performance degraded and the level of coupling could be discomforting for the pilot.

### **7.1.5 Note on symmetry**

Helicopter behaviour has the tendency to vary from one flight condition to another predominantly due to the variation in dynamics. The analysis presented thus far had examined the helicopter responses for *positive* pilot demands, however, due to their nonlinear nature, subtle differences were expected between these responses and those obtained for *negative* pilot demands. This section will present the set of responses obtained for negative pilot demands and analyse their symmetry to those obtained in the previous sections.

#### **Longitudinal response (pitch-up)**

At low magnitude stick deflections, up to 5%, the off-axis response characteristics for pitch-up demands were found to be symmetrical to the pitch-down demands. On-axis responses were comparable in terms of their rise time and overshoot characteristics, however, there was a small error in terms of fine response tracking behaviour. As the pitch-up demand was increased to 20% (12 deg) the fine tracking feature suffered further acquiring slightly oscillatory type behaviour. At increased pitch demand magnitudes, i.e. from 20% (12 deg) to 50% (30 deg), the on-axis response showed improvement with the magnitude of the above oscillations notably reduced. The symmetry in responses for low magnitude pilot demand and the asymmetry at larger magnitudes were observed at the other flight conditions as well.

Although the responses for positive and negative pilot demands were found to be asymmetrical in their fine tracking behaviour, the linear FA controller was capable of producing stable responses with a good rise time and minimal overshoot for the full set of pitch attitude demand ( $-30$  to  $+30$  deg). A sample of pitch-up responses along with pitch-down response of the same magnitude is presented in Figures 7.11, 7.12 and 7.13.

### **Lateral response (roll-left)**

At low magnitudes of roll attitude demands, both the on- and off-axis performances had similar time response features for roll-left and roll-right situations. As the magnitude was increased to 20% (24 deg), small discrepancies with fine tracking began to appear in roll-left responses. The off-axis performance remained symmetrical for both roll-left and right demands. Increasing the demand magnitude further saw a greater amount of discrepancy with the roll-left responses which showed larger overshoot along with an exaggerated presence of the “kink” that was observed in roll rate response during the linear analysis. This trend of symmetrical responses for low magnitude demands and asymmetrical response at larger magnitudes was observed at other flight conditions as well. A sample of these responses is presented in Figures 7.14, 7.15 and 7.16.

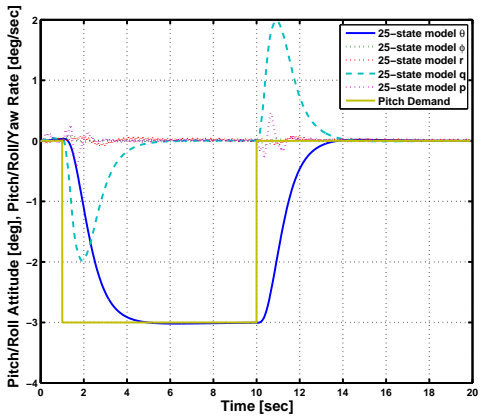
### **Directional response (left pedal forward)**

The yaw rate responses to left pedal demands are shown in Figures 7.17, 7.18 and 7.19. These responses remained broadly symmetrical to the right pedal demands in terms of their short term features, with a few notable discrepancies in their fine tracking properties. Coupling into other channels due to left pedal demands was observed to be significantly more than right pedal demands. The analysis was also extended to other flight conditions and it was observed that at the hover flight condition, the responses to left pedal demands were symmetrical to the right pedal demands up to a magnitude of 35% (31.5 deg/s). During the high speed/high altitude flight condition analysis, it was noted that the responses for low magnitude left pedal input remained broadly symmetrical to right pedal inputs with minor discrepancies in fine tracking properties. At a left pedal input of 20 deg/s a sharp transient is observed in the on-axis response due to the saturation of tail-rotor collective signal and this behaviour is

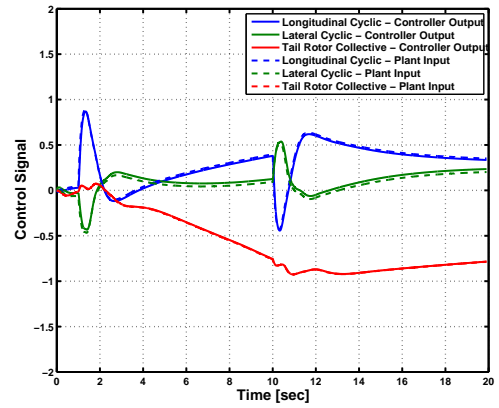
symmetric to the on-axis response for a right pedal demand of 20 deg/s. As the demand is increased to the maximum pedal press the quality of response is degraded with the tail-rotor collective signal saturating for longer periods.

### **7.1.6 Summary**

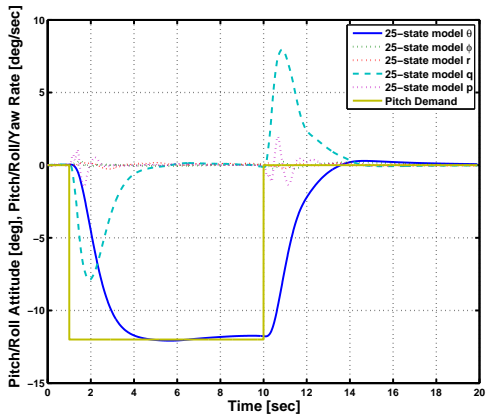
The above results have shown good, but not perfect, agreement between the linear predictions from Chapter 4 and the actual nonlinear FA controller performance. It was also noticed that, in the simulations very small (e.g. less than 0.1 unit peak to peak) persistent oscillations occurred in variables such as sensed CG acceleration, rotor speed and angular velocity ( $r$ ). This does not appear to be an instability associated with the controller, however, it is believed that these oscillations are most likely a manifestation of the rotor passing frequency, as the rotor is modelled as an individual blade rotor rather than with the disc approximation normally used. The controller's robustness and counter cross-coupling properties extended to the nonlinear realm as well and satisfactory results were obtained at the tested flight conditions. In terms of symmetry in responses, the linear controller was able to adapt to the variation in helicopter characteristics and maintained consistent time response features for both positive and negative demands.



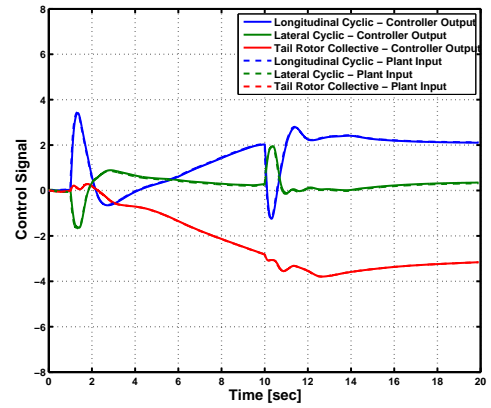
Longitudinal response (5%)



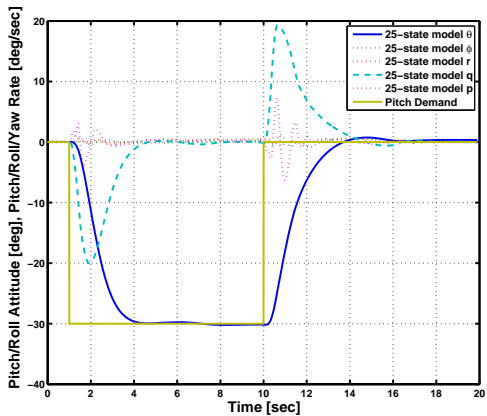
Total control activity (5%)



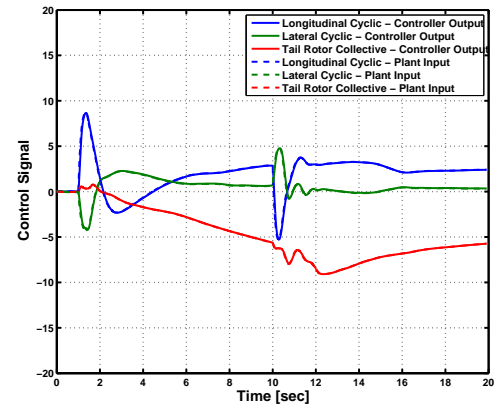
Longitudinal response (20%)



Total control activity (20%)

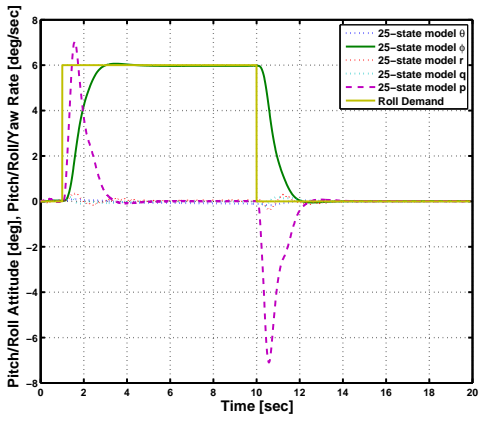


Longitudinal response (50%)

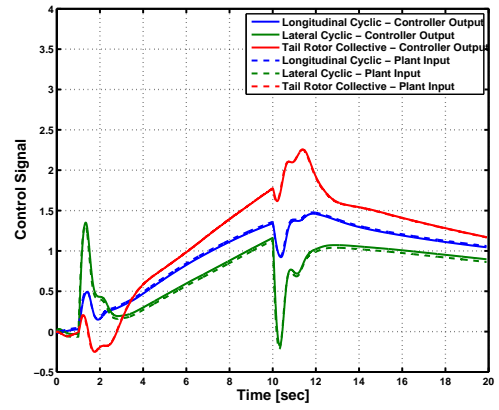


Total control activity (50%)

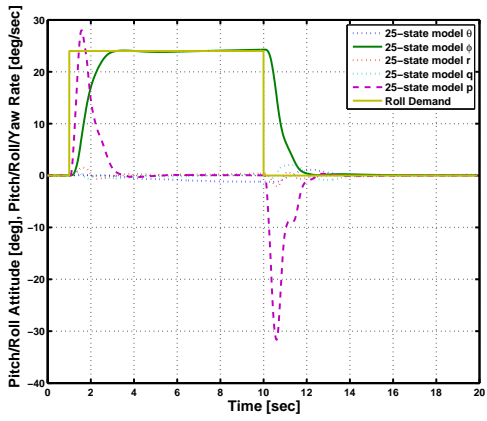
Figure 7.2: Nonlinear pitch attitude response - 40kts/0ft



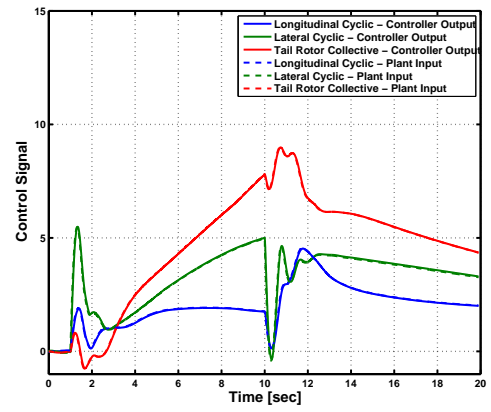
Lateral response (5%)



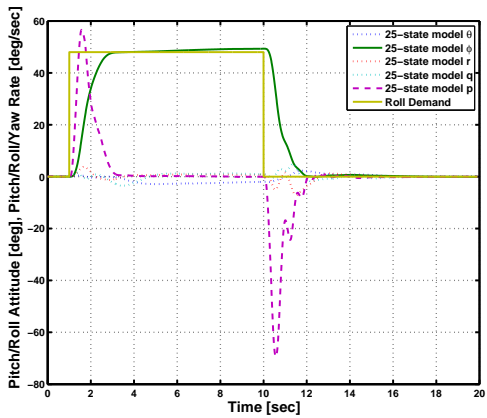
Total control activity (5%)



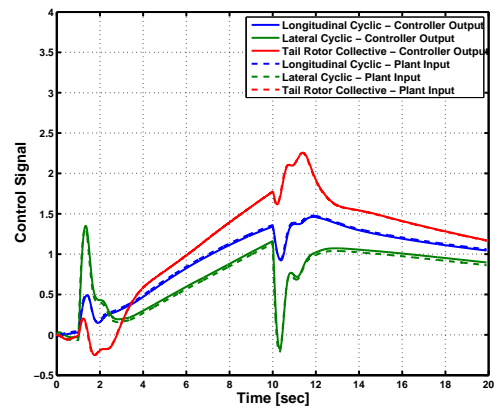
Lateral response (20%)



Total control activity (20%)

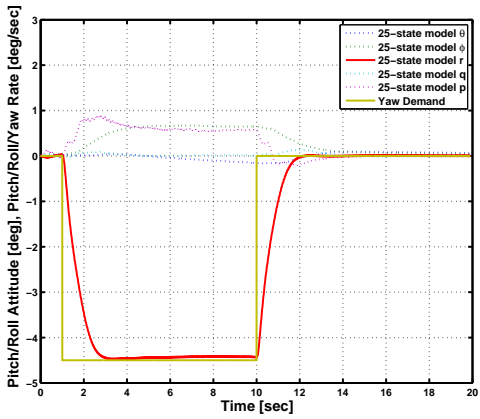


Lateral response (40%)

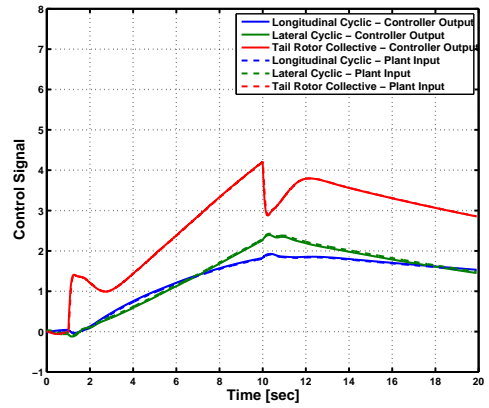


Total control activity (40%)

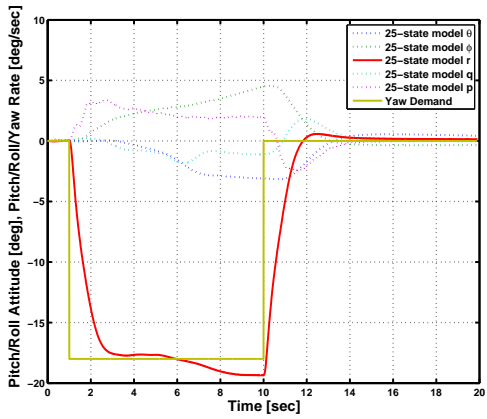
Figure 7.3: Nonlinear roll attitude response - 40kts/0ft



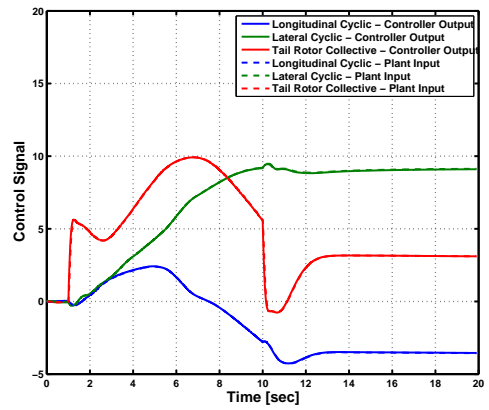
Directional response (5%)



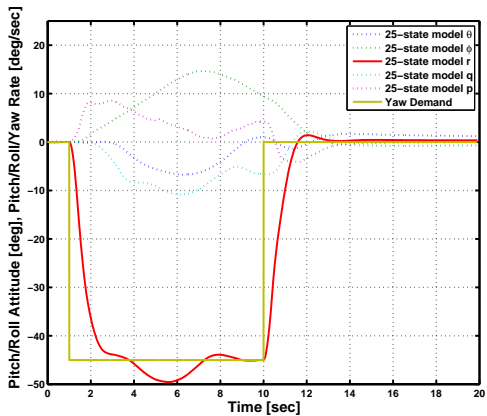
Total control activity (5%)



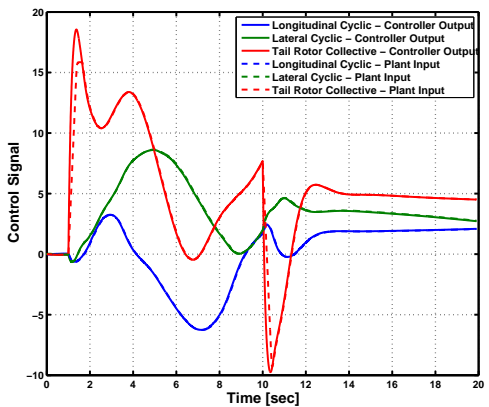
Directional response (20%)



Total control activity (20%)

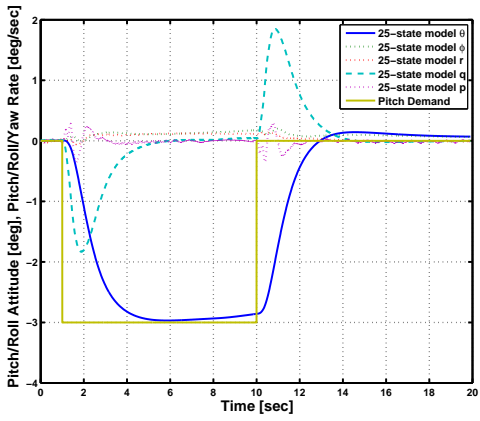


Directional response (50%)

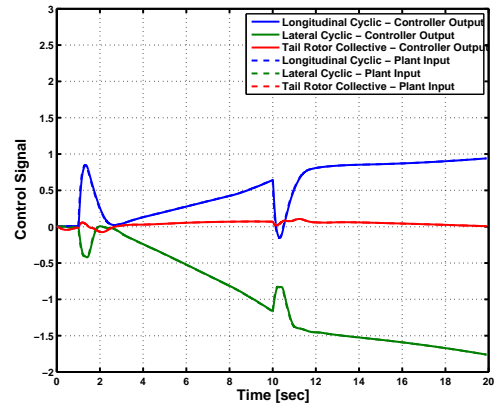


Total control activity (50%)

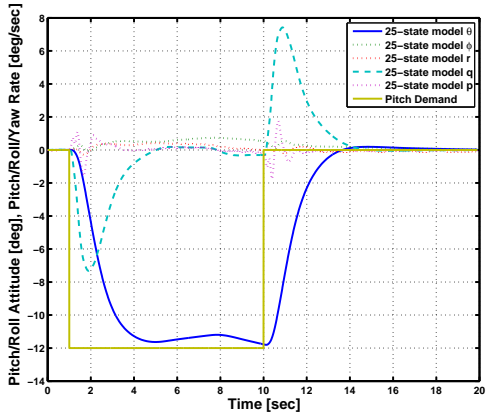
Figure 7.4: Nonlinear yaw rate response - 40kts/0ft



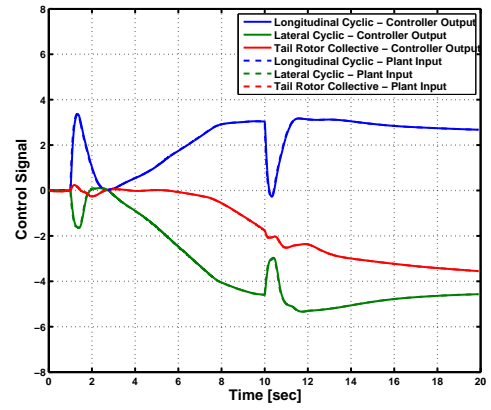
Longitudinal response (5%)



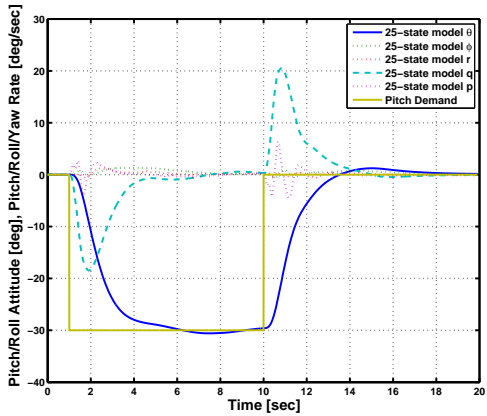
Total control activity (5%)



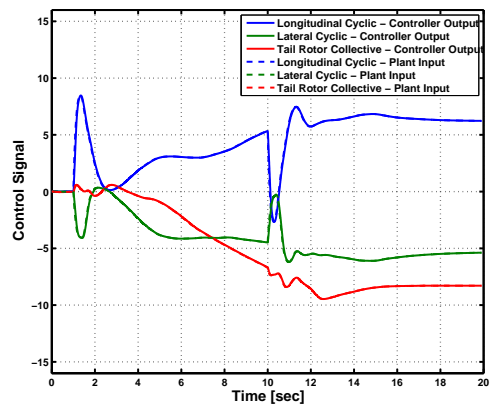
Longitudinal response (20%)



Total control activity (20%)

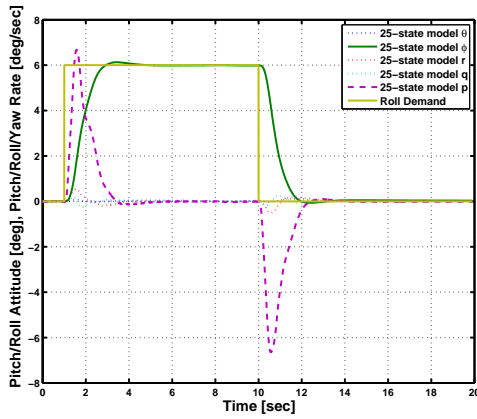


Longitudinal response (50%)

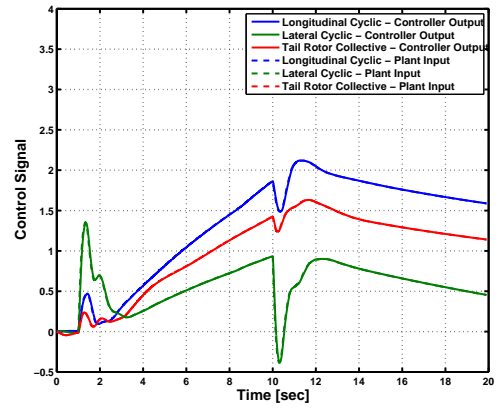


Total control activity (50%)

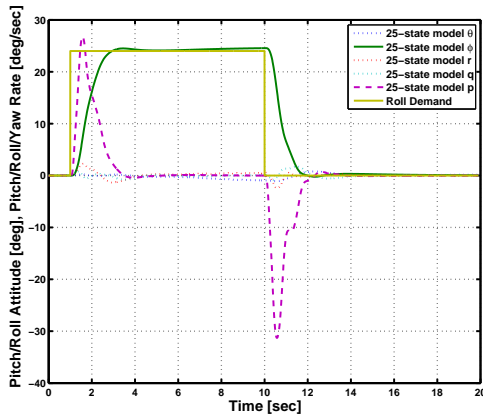
Figure 7.5: Nonlinear pitch attitude response - 0kts/0ft



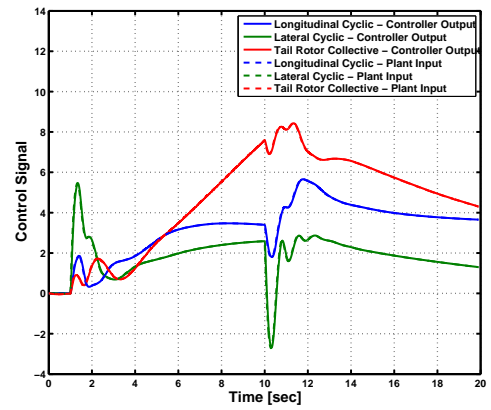
Lateral response (5%)



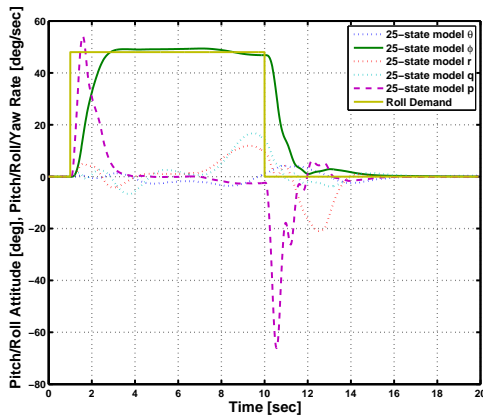
Total control activity (5%)



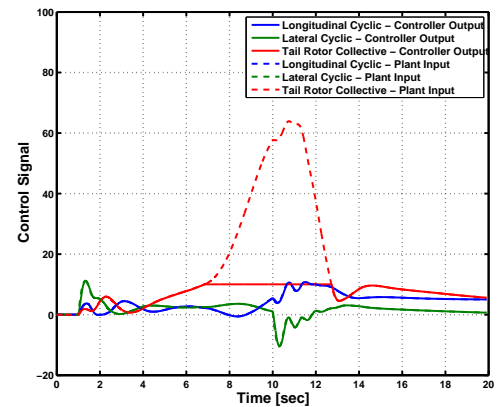
Lateral response (20%)



Total control activity (20%)

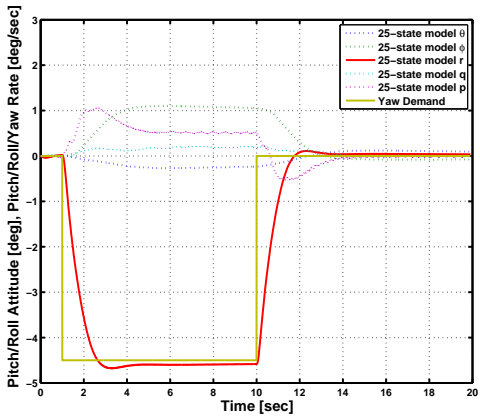


Lateral response (40%)

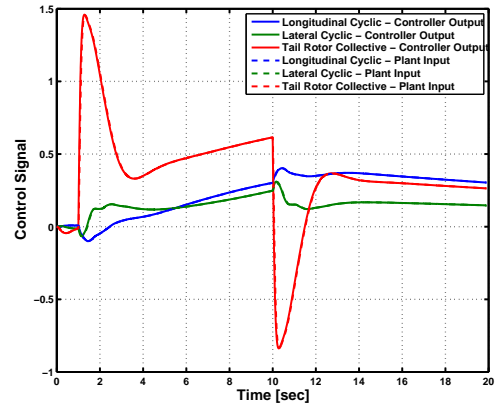


Total control activity (40%)

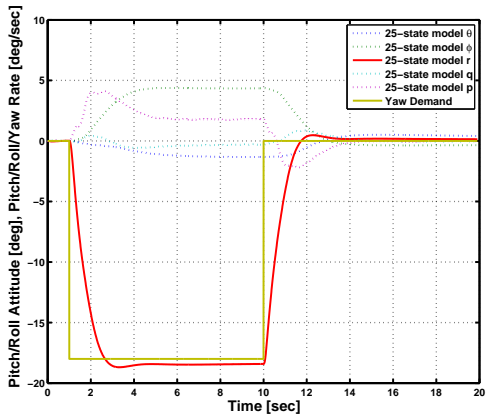
Figure 7.6: Nonlinear roll attitude response - 0kts/0ft



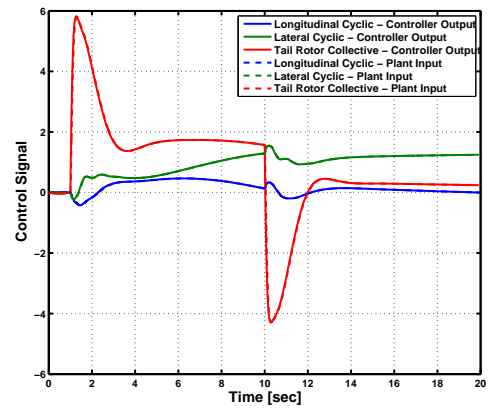
Directional response (5%)



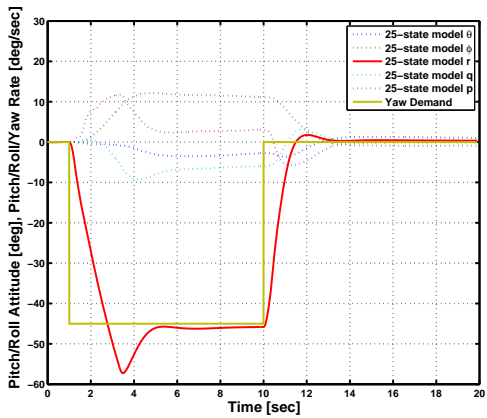
Total control activity (5%)



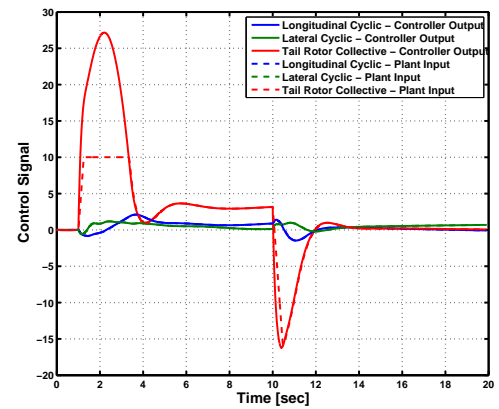
Directional response (20%)



Total control activity (20%)

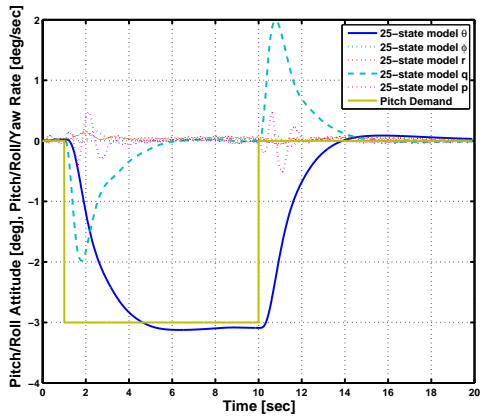


Directional response (50%)

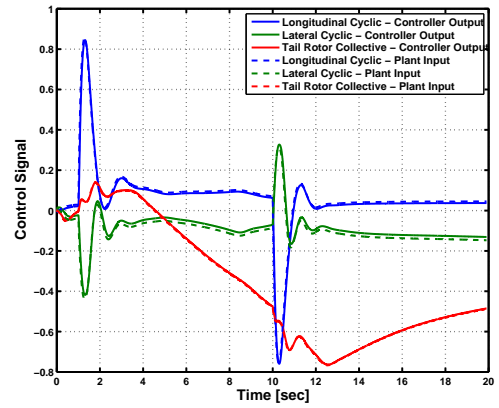


Total control activity (50%)

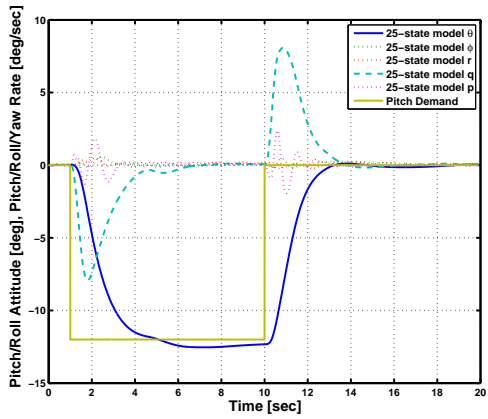
Figure 7.7: Nonlinear yaw rate response - 0kts/0ft



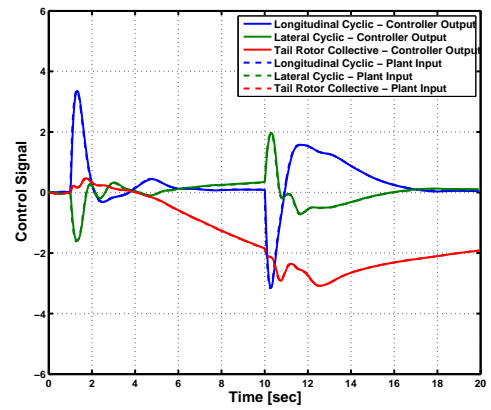
Longitudinal response (5%)



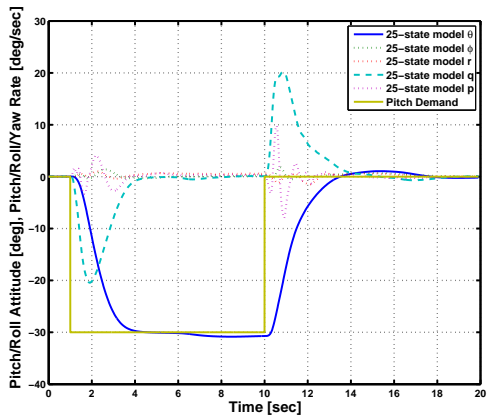
Total control activity (5%)



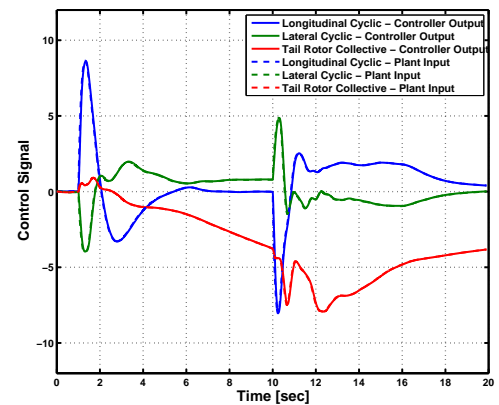
Longitudinal response (20%)



Total control activity (20%)

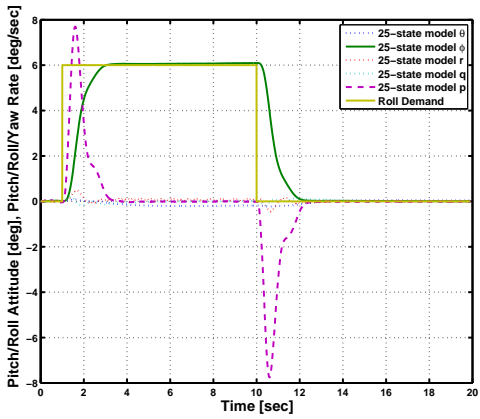


Longitudinal response (50%)

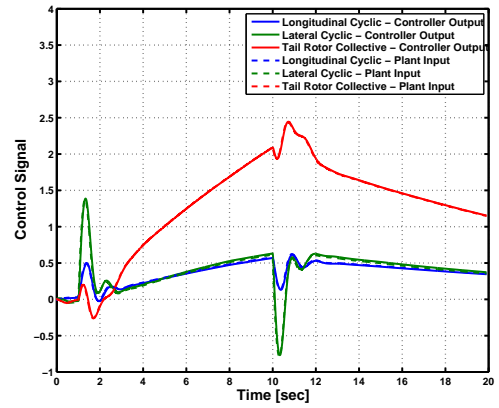


Total control activity (50%)

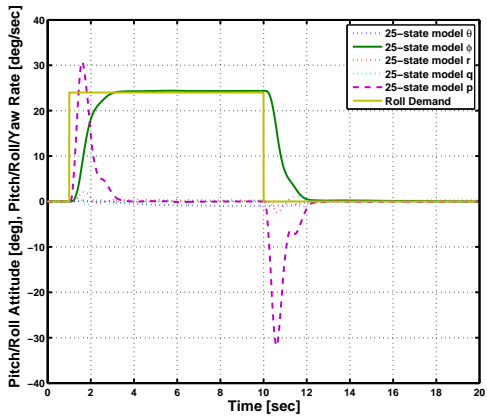
Figure 7.8: Nonlinear pitch attitude response - 80kts/2500ft



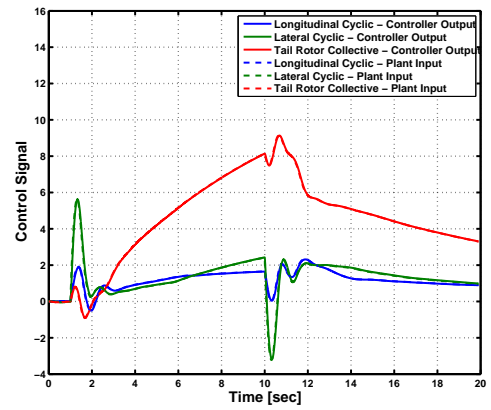
Lateral response (5%)



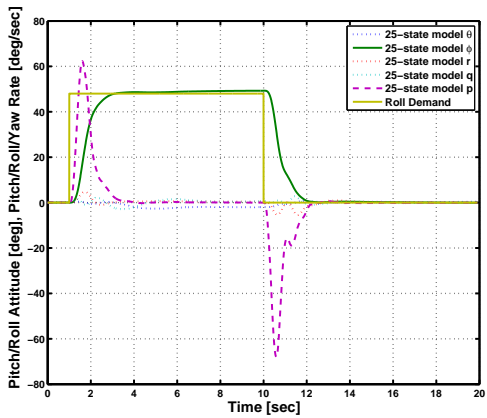
Total control activity (5%)



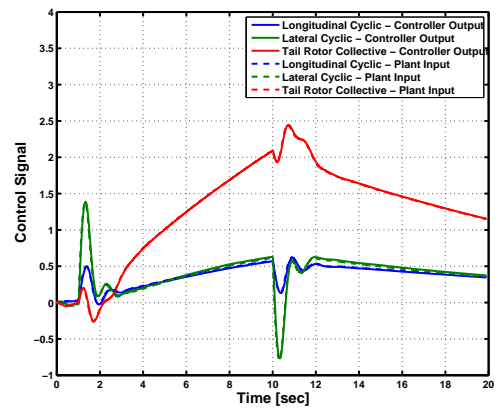
Lateral response (20%)



Total control activity (20%)

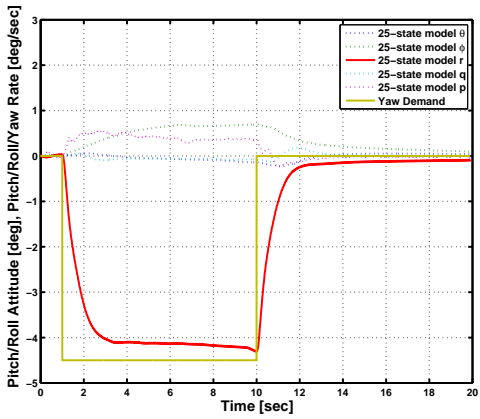


Lateral response (40%)

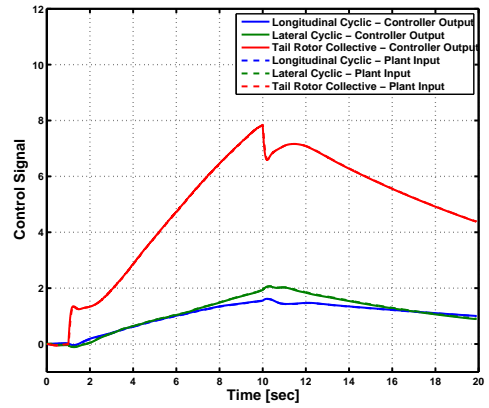


Total control activity (40%)

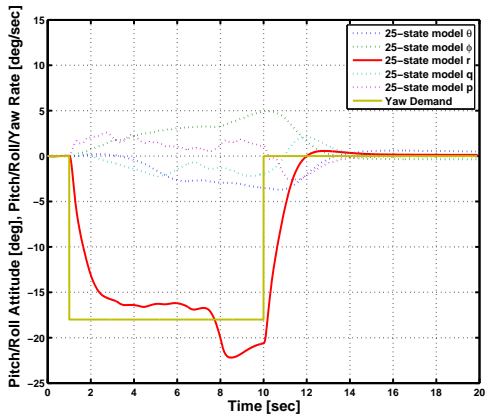
Figure 7.9: Nonlinear roll attitude response - 80kts/2500ft



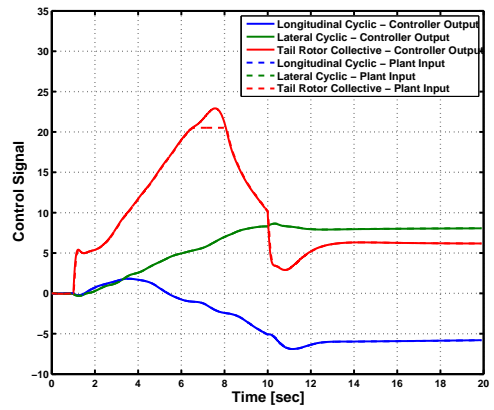
Directional response (5%)



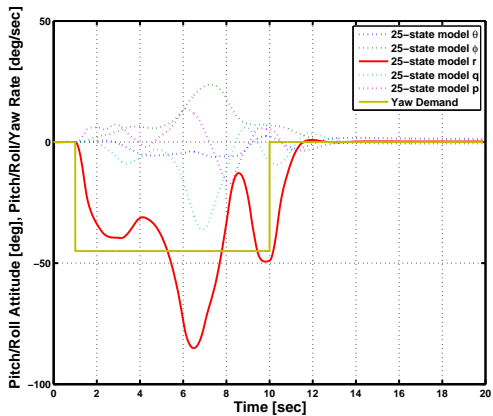
Total control activity (5%)



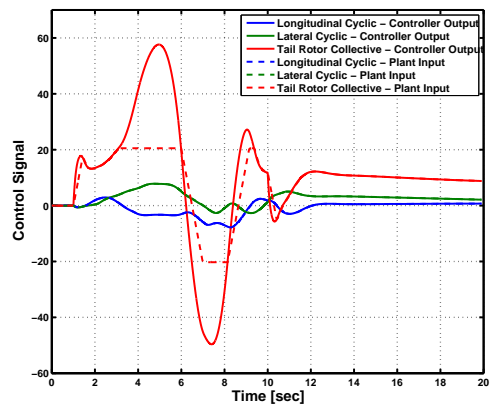
Directional response (20%)



Total control activity (20%)

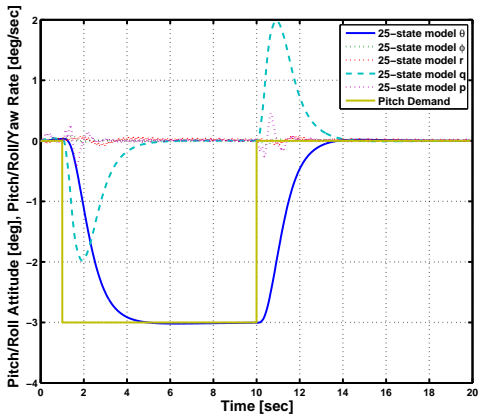


Directional response (50%)

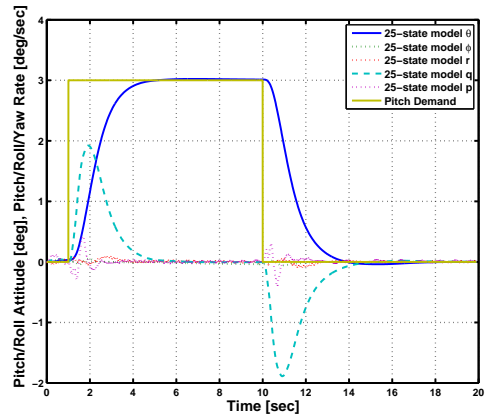


Total control activity (50%)

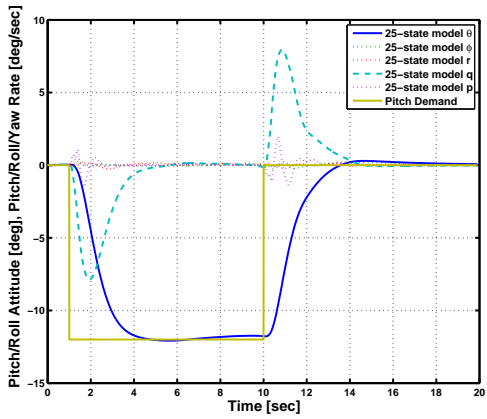
Figure 7.10: Nonlinear yaw rate response - 80kts/2500ft



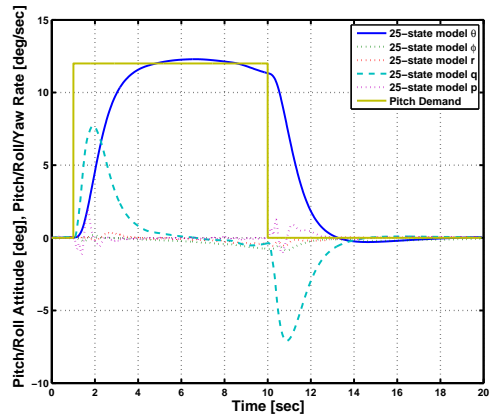
Longitudinal response (5%)



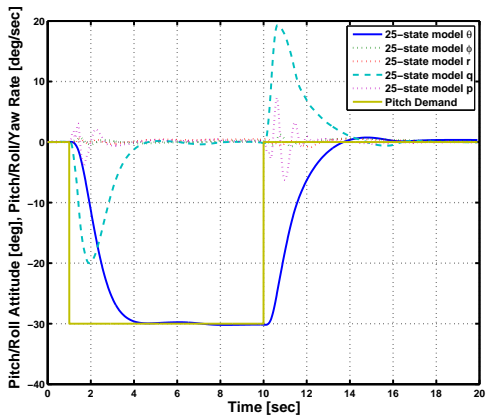
Longitudinal response (-5%)



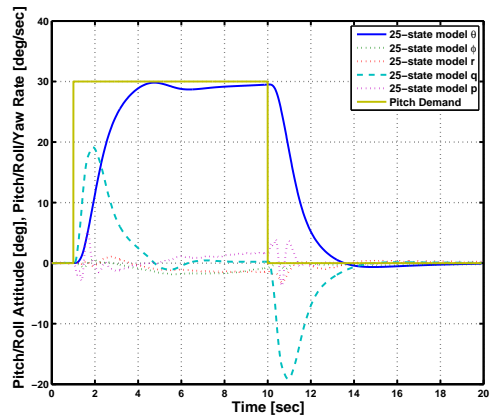
Longitudinal response (20%)



Longitudinal response (-20%)

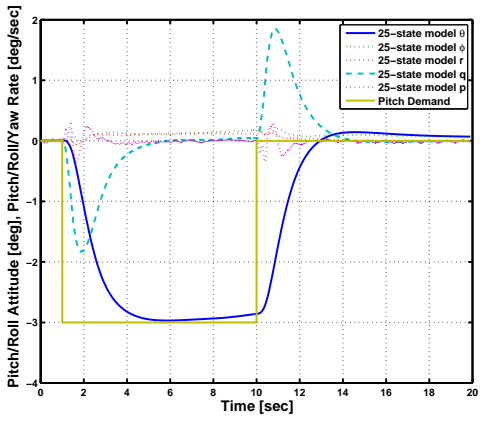


Longitudinal response (50%)

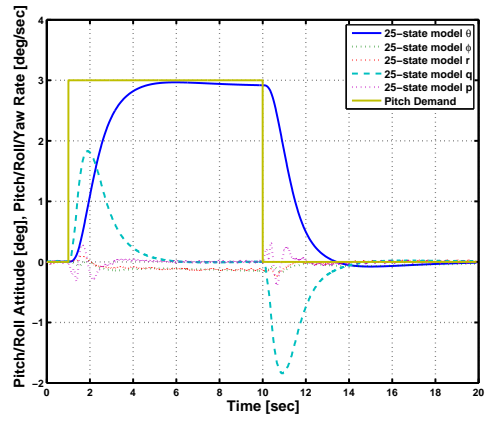


Longitudinal response (-50%)

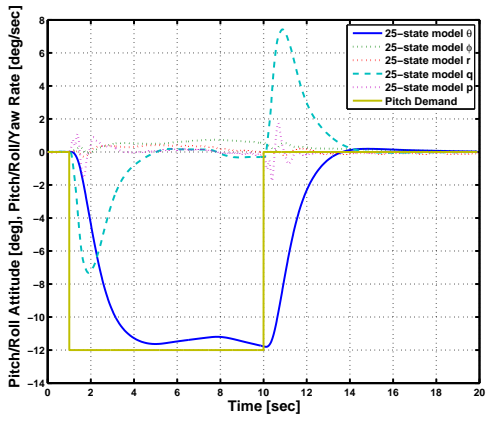
Figure 7.11: Nonlinear pitch attitude symmetry - 40kts/0ft



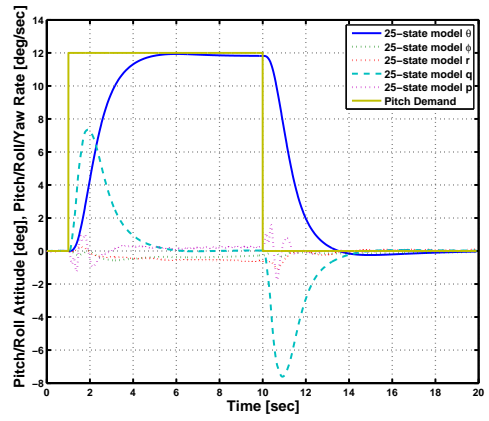
Longitudinal response (5%)



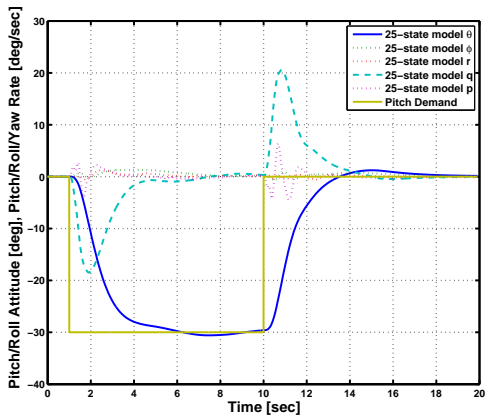
Longitudinal response (-5%)



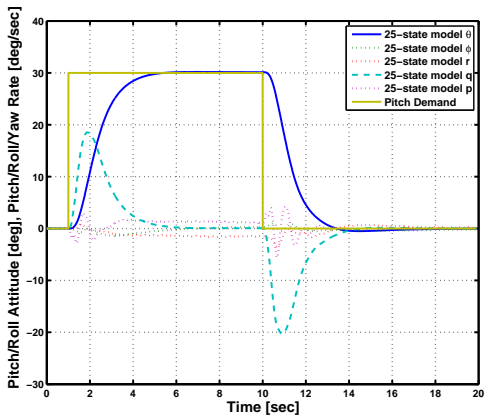
Longitudinal response (20%)



Longitudinal response (-20%)

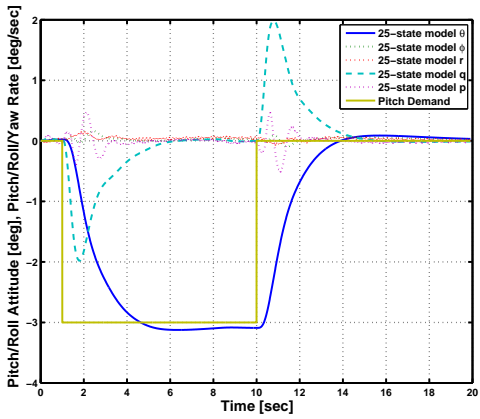


Longitudinal response (50%)

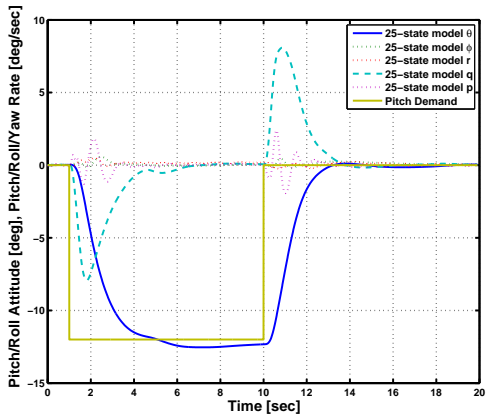


Longitudinal response (-50%)

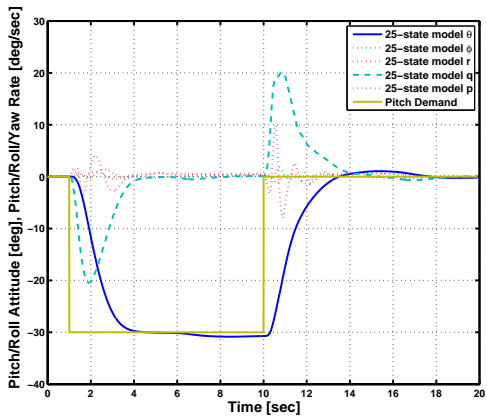
Figure 7.12: Nonlinear pitch attitude symmetry - 00kts/0ft



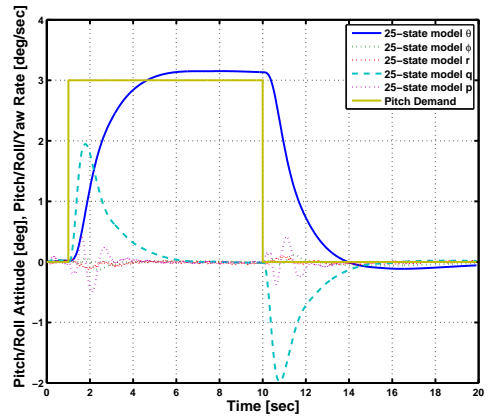
Longitudinal response (5%)



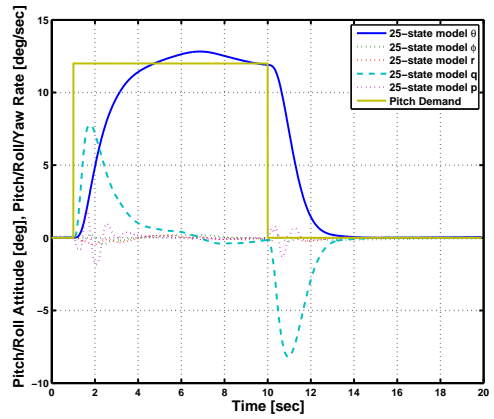
Longitudinal response (20%)



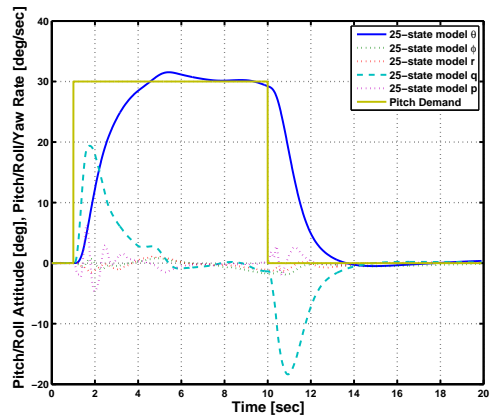
Longitudinal response (50%)



Longitudinal response (-5%)

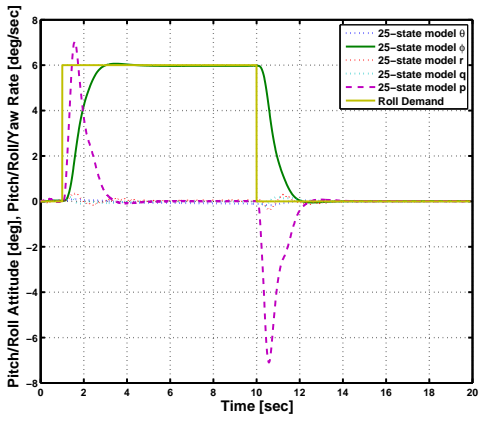


Longitudinal response (-20%)

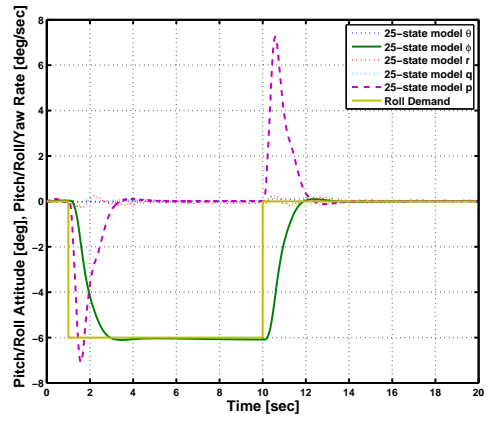


Longitudinal response (-50%)

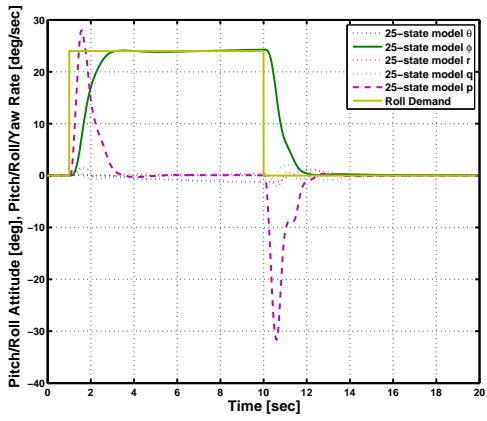
Figure 7.13: Nonlinear pitch attitude symmetry - 80kts/2500ft



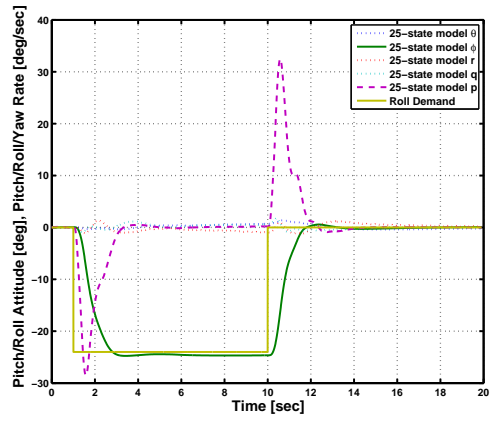
Lateral response (5%)



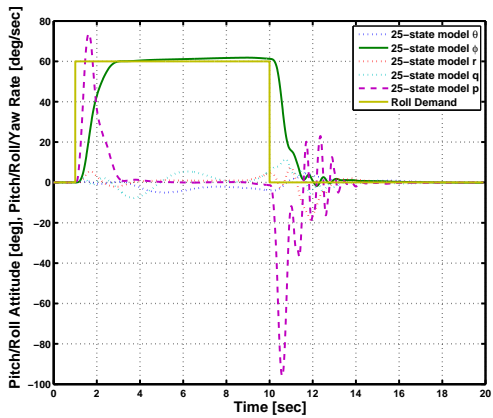
Lateral response (-5%)



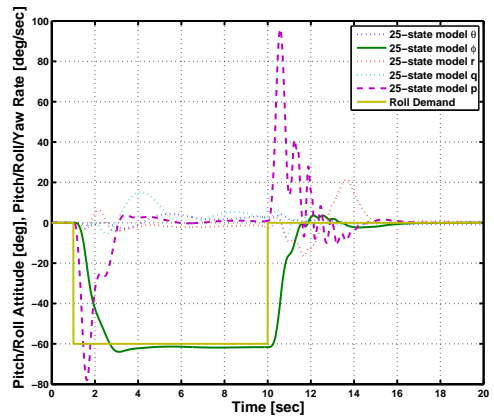
Lateral response (20%)



Lateral response (-20%)

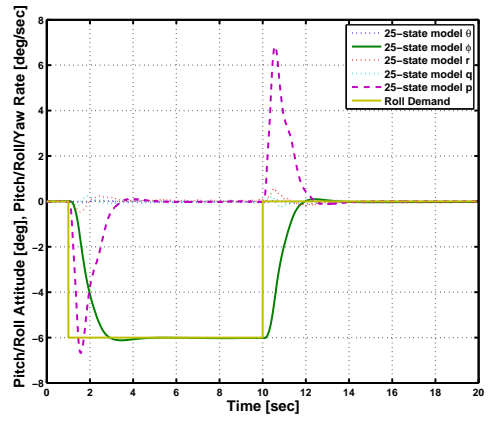
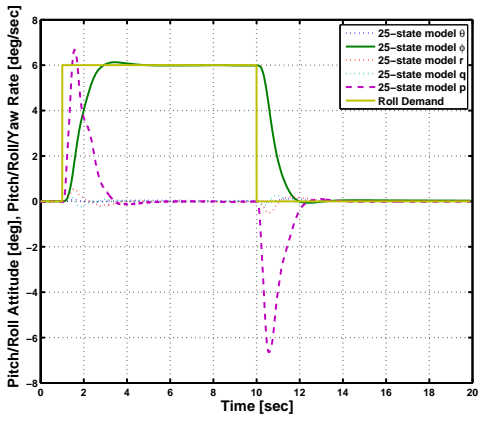


Lateral response (50%)



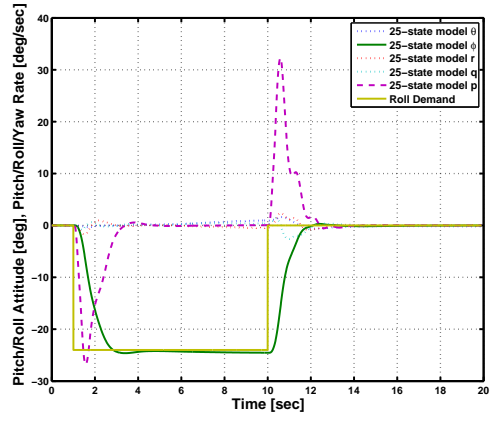
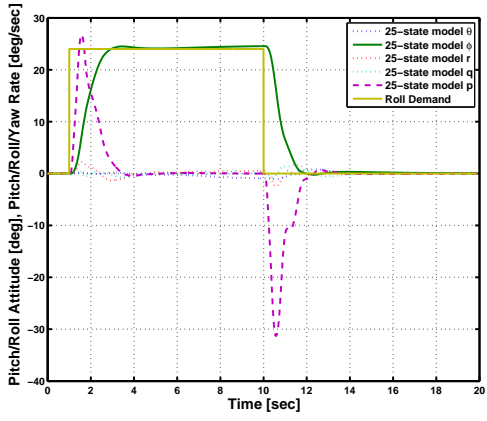
Lateral response (-50%)

Figure 7.14: Nonlinear roll attitude symmetry - 40kts/0ft



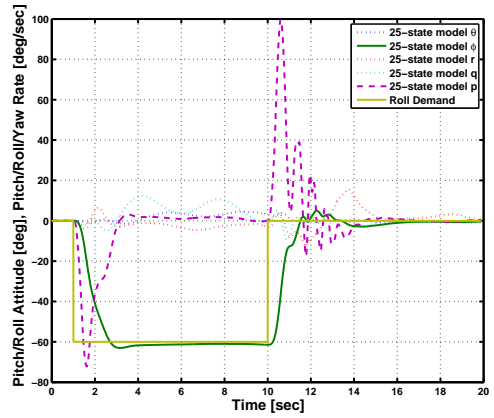
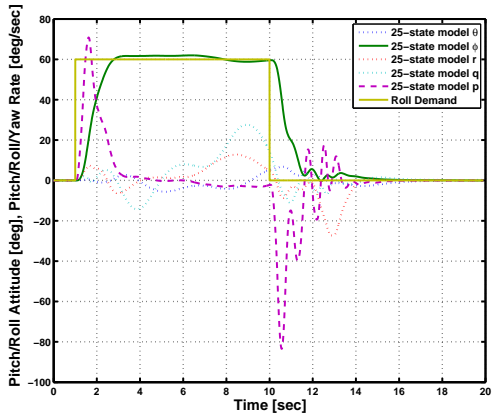
Lateral response (5%)

Lateral response (-5%)



Lateral response (20%)

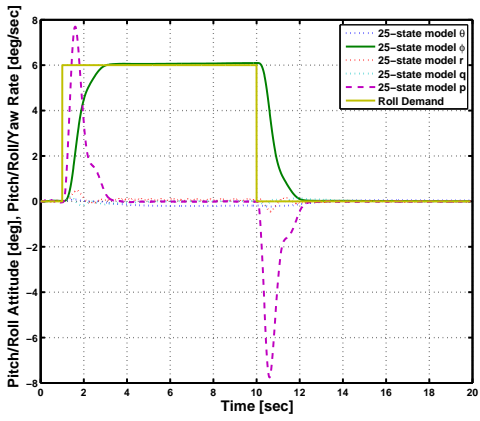
Lateral response (-20%)



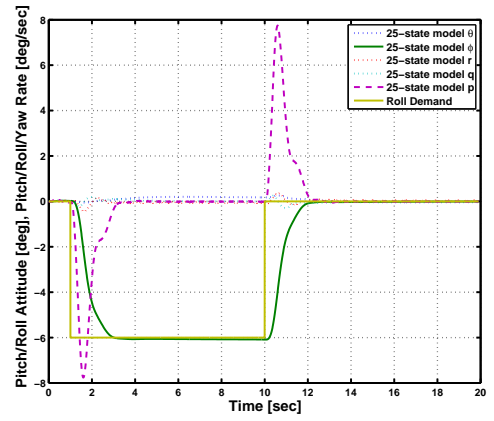
Lateral response (50%)

Lateral response (-50%)

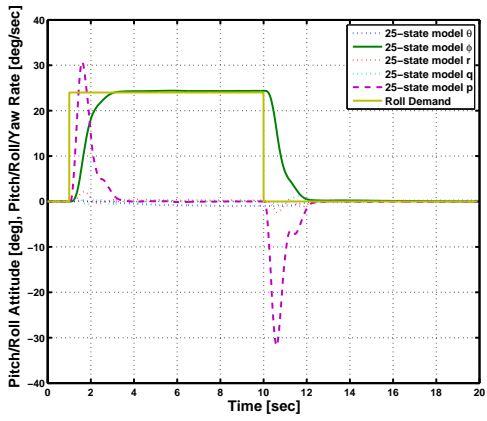
Figure 7.15: Nonlinear roll attitude symmetry - 00kts/0ft



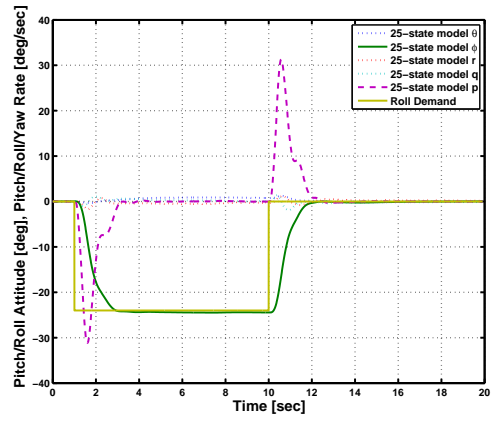
Lateral response (5%)



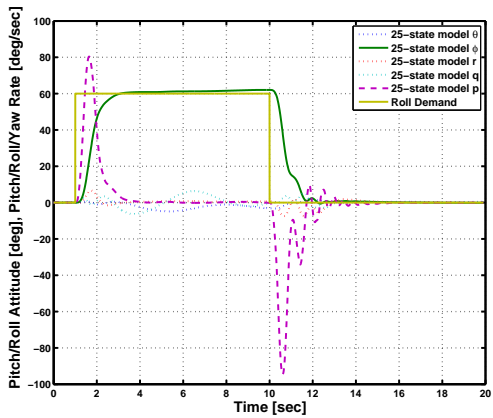
Lateral response (-5%)



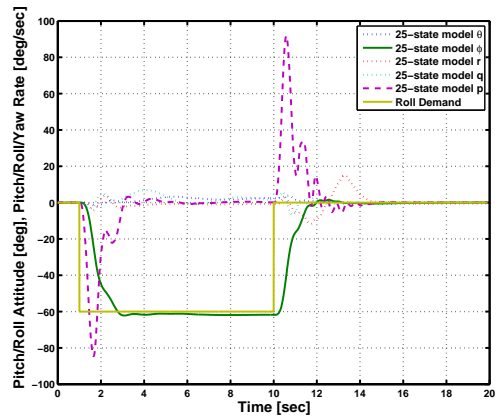
Lateral response (20%)



Lateral response (-20%)

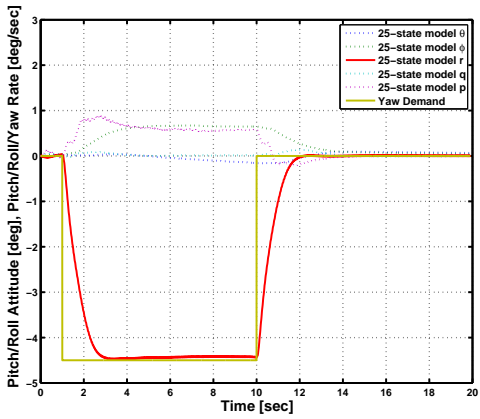


Lateral response (50%)

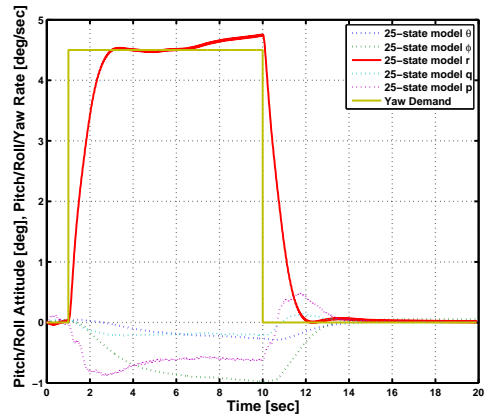


Lateral response (-50%)

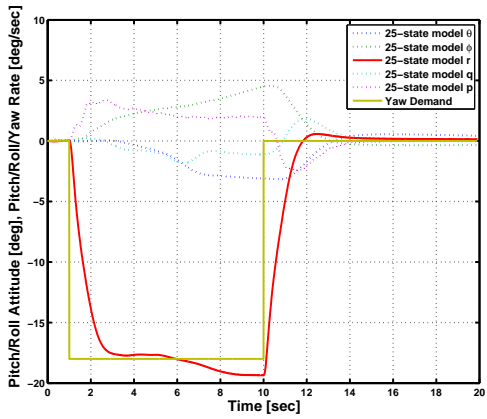
Figure 7.16: Nonlinear roll attitude symmetry - 80kts/2500ft



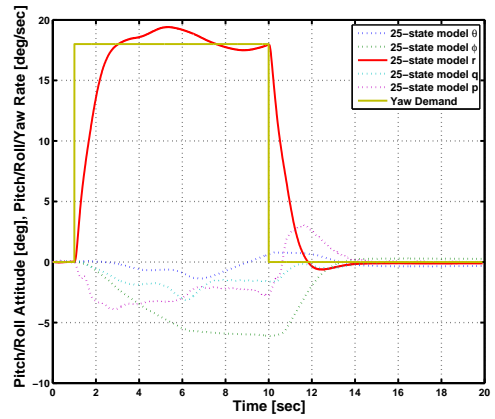
Directional response (5%)



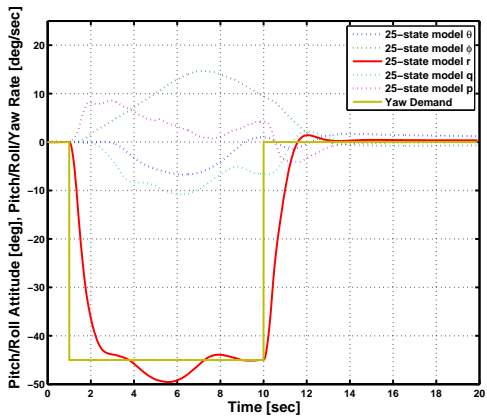
Directional response (-5%)



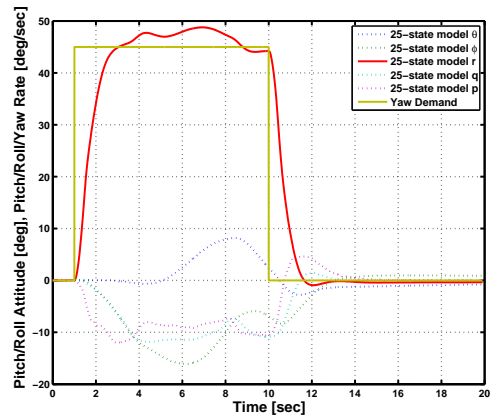
Directional response (20%)



Directional response (-20%)

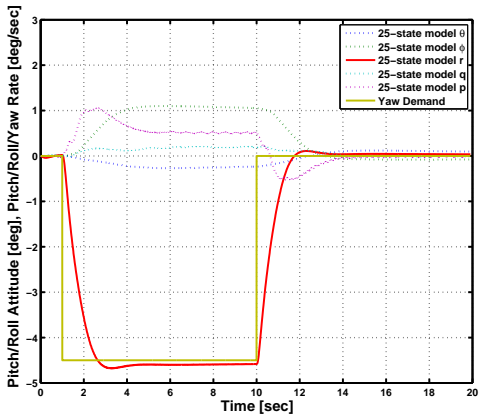


Directional response (50%)

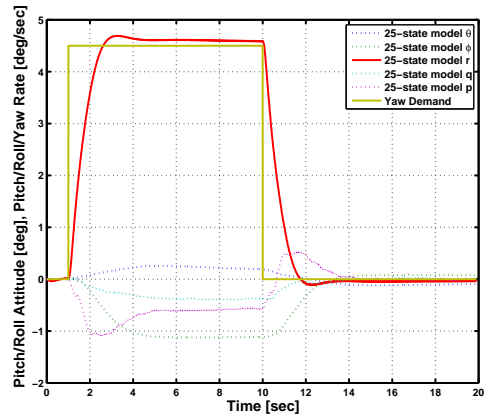


Directional response (-50%)

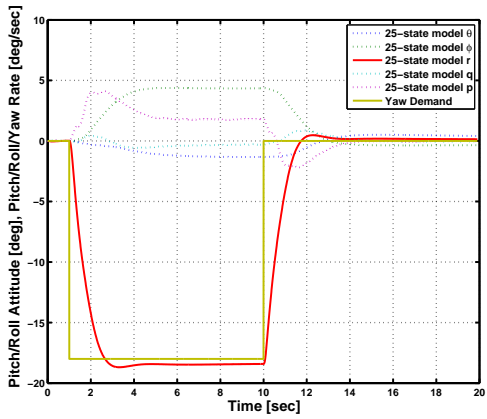
Figure 7.17: Nonlinear yaw rate symmetry - 40kts/0ft



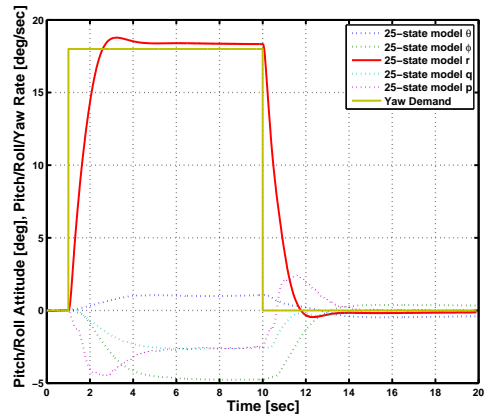
Directional response (5%)



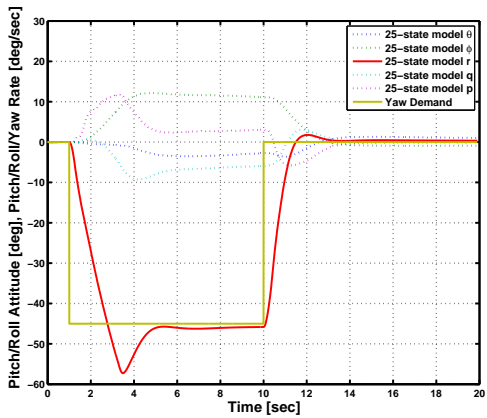
Directional response (-5%)



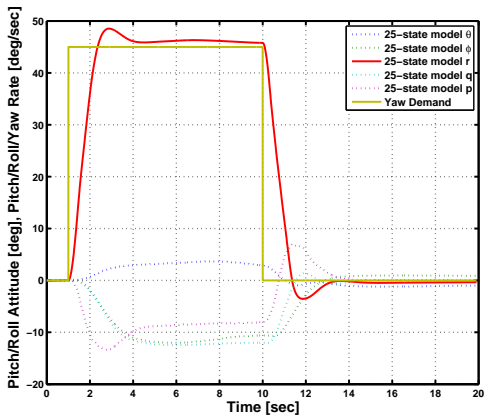
Directional response (20%)



Directional response (-20%)

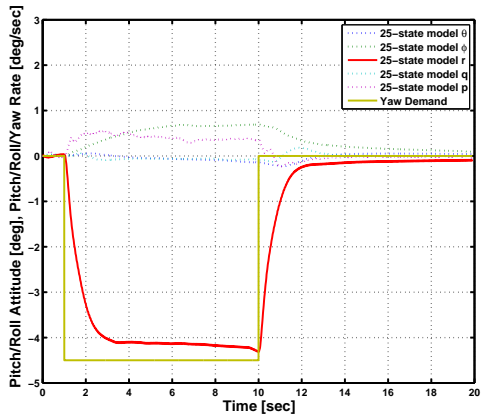


Directional response (50%)

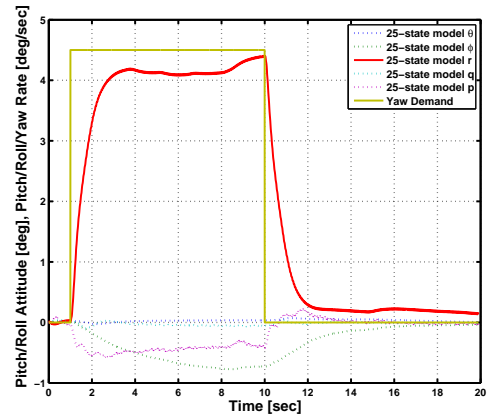


Directional response (-50%)

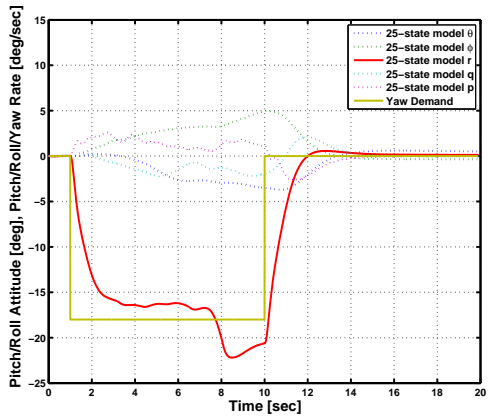
Figure 7.18: Nonlinear yaw rate symmetry - 00kts/0ft



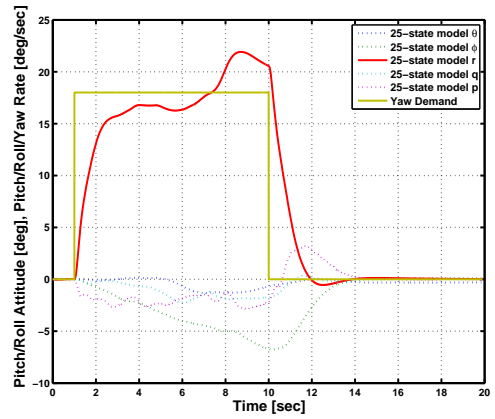
Directional response (5%)



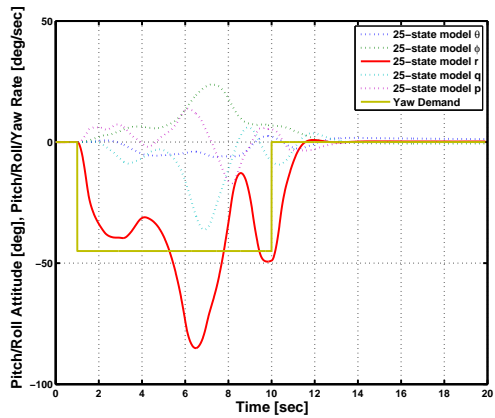
Directional response (-5%)



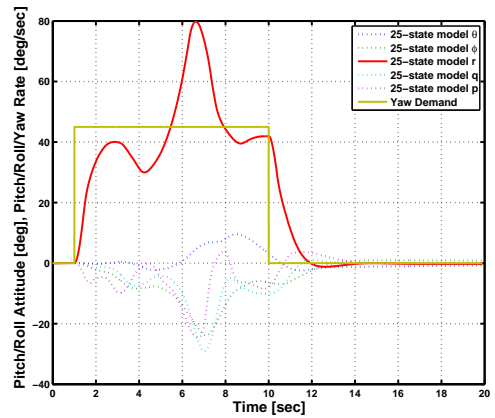
Directional response (20%)



Directional response (-20%)



Directional response (50%)



Directional response (-50%)

Figure 7.19: Nonlinear yaw rate symmetry - 80kts/2500ft

## 7.2 Limited authority simulation results

This section presents the results obtained using the nonlinear EH101 model which should provide a more accurate appraisal of the LA controller's performance. In addition to the standard nonlinear FM, this model incorporates nonlinearities which are present in the mechanical interlinks. This second source of nonlinearities is noteworthy because the mathematical derivation ensuring identical small-signal performance for the FA and LA controllers is based on the assumed linearity of these interlinks. This assumption is not quite satisfied here and small differences are expected, even in the small signal performance. The results presented here are compared to the linear (i.e. based on the linear EH101 model) LA predictions from Chapter 6 that would indicate the success of the linear LA controller within a nonlinear environment. These results were also compared to the FA responses that were seen in the previous section to give an indication of how well it copes with both the internal (series and parallel actuator saturation) and external (nonlinear mechanical interlinks model) nonlinearities in order to match the nonlinear FA responses.

### 7.2.1 Longitudinal response (pitch-down)

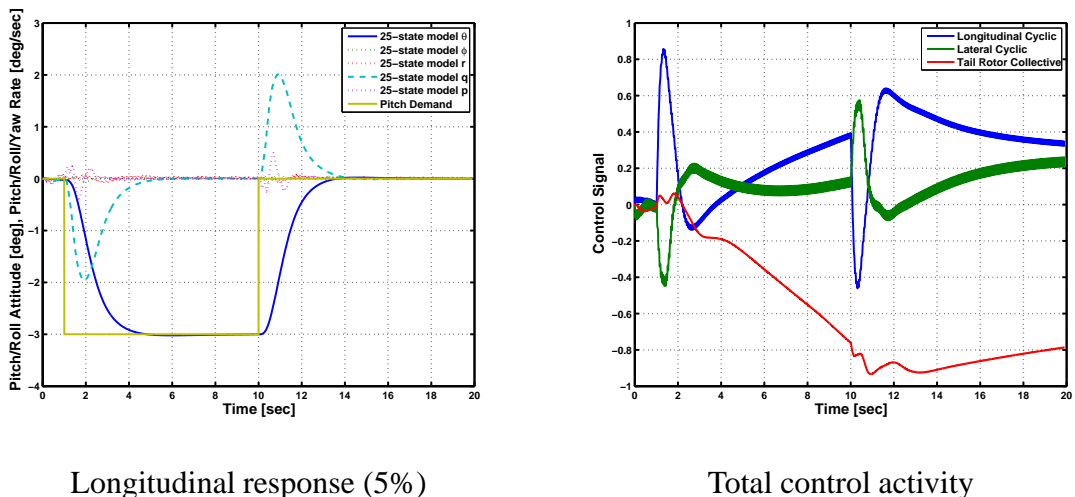
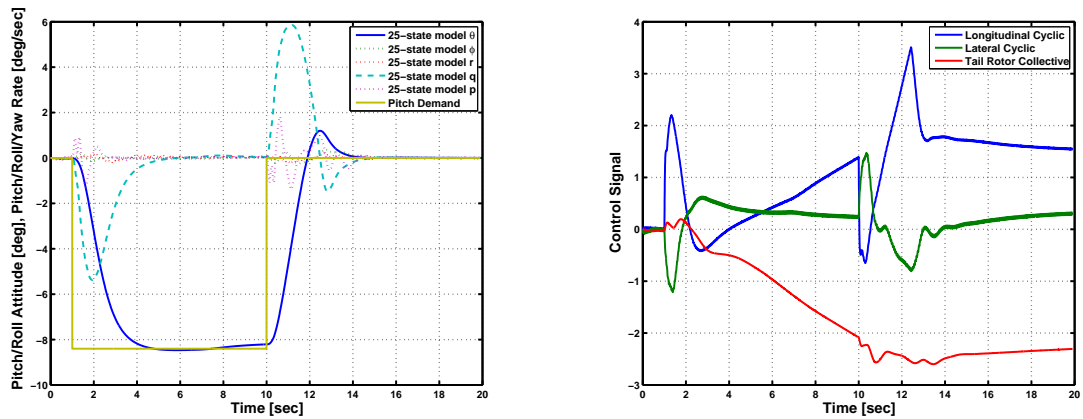


Figure 7.20: Nonlinear LA pitch attitude response - 40kts/0ft

The nonlinear model was initially analysed for low magnitude pitch-down demands - an example response to a pitch-down demand of 5% (3 deg) is shown in Figure 7.20. It was observed that despite the nonlinearity, the small signal pitch attitude response was identical



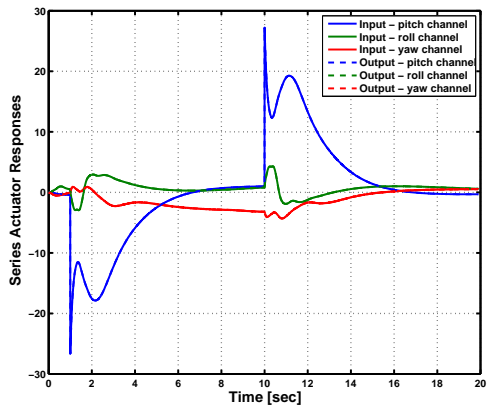
Longitudinal response (14%)

Total control activity

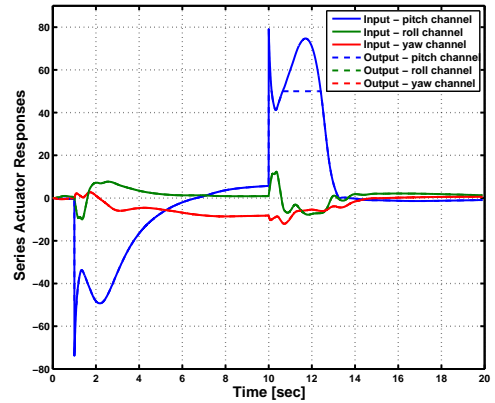
Figure 7.21: Nonlinear LA pitch attitude response - 40kts/0ft

to the linear LA response. The series and parallel actuator responses at the 5% demand are presented in Figures 7.22 and 7.23 respectively, and their performance was also observed to be identical to the linear analysis. The “noise” like feature in the control activity is in fact a simulation artefact due to the nonlinear model of the helicopter that uses an individual blade element of the rotor rather than the normal disc model. They are present throughout the nonlinear responses, however, they are more exaggerated in the above plot due to the low y-axis scale. The nonlinear responses only began to differ from their linear predictions at demands of 8% ( $-4.8$  deg) and greater as the nonlinearity within the model became more dominant at these demands. Also, as the series and parallel actuators did not saturate at this demand magnitude, it ensured that the nonlinear LA responses were identical to the nonlinear FA responses. However, this similarity began to deteriorate at pitch-down demands greater than 12% (7.2 deg) and this was due to the series actuators saturating for short periods. The pitch attitude limit at which the series actuators started saturate was not influenced by the nonlinearities in the system.

Once the pitch channel was subjected to larger pilot demands, degradations became more evident in the responses and the level of agreement with the nonlinear FA responses weakened further. These deteriorations were predominantly due to the magnitude saturation of series actuators. This is illustrated through the plots in Figure 7.21 that show the response to a pitch demand of 14% ( $-8.4$  deg) along with the corresponding series and parallel actuator responses in Figures 7.22 and 7.23 respectively. As the stick demand is increased further

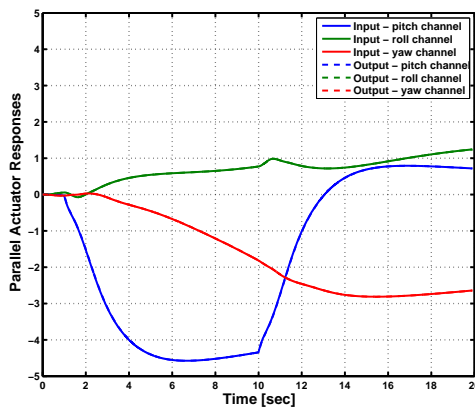


Series actuator response (5%)

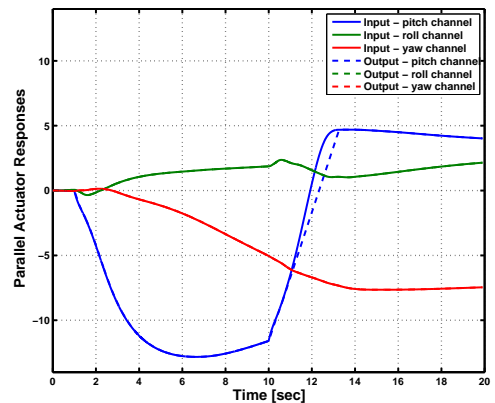


Series actuator response (14%)

Figure 7.22: Series actuator response



Parallel actuator response (5%)



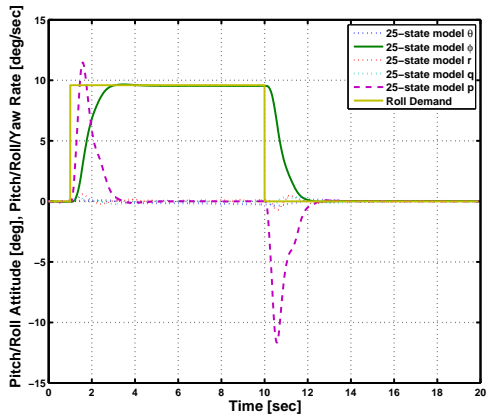
Parallel actuator response (14%)

Figure 7.23: Parallel actuator response

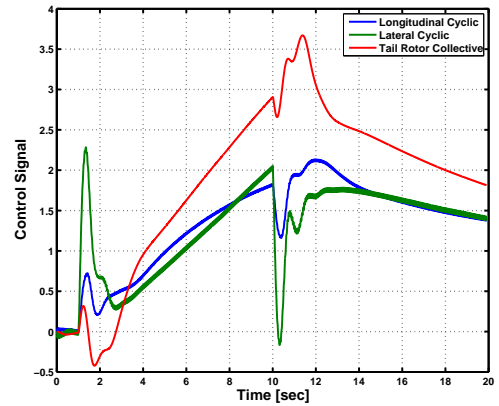
from 14%, the parallel actuators also begin to experience rate limiting which affects their ability to drive the series actuator output to zero, hence prolonging the periods of magnitude saturation and causing the helicopter to revert to more open-loop type behaviour. The maximum pitch demand that produced a tolerable longitudinal response was found to be 18% ( $-10.8$  deg) and, as expected, was lower than the linear prediction of 20% ( $-12$  deg).

## 7.2.2 Lateral responses (roll-right)

Although, the general pattern was similar to the longitudinal channel, the lateral channel was able to accommodate a larger amount of pilot stick deflection. 16.0% (19.2 deg) was

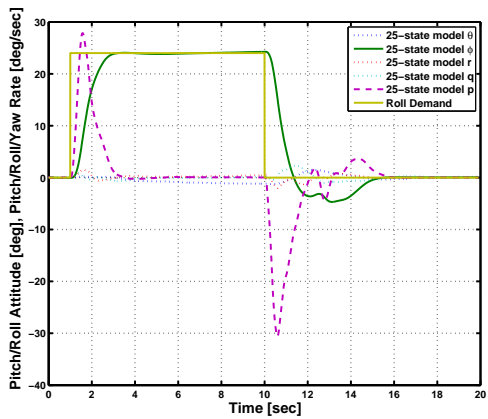


Lateral response (8%)

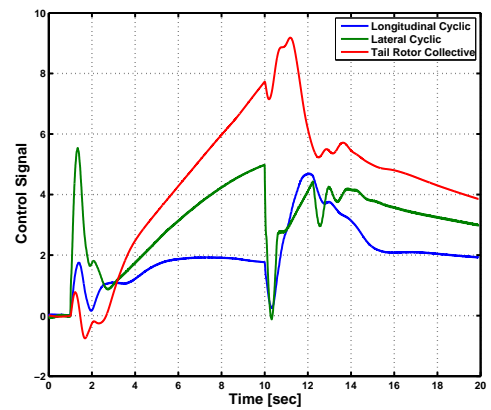


Total control activity

Figure 7.24: Nonlinear LA roll attitude response - 40kts/0ft



Lateral response (20%)

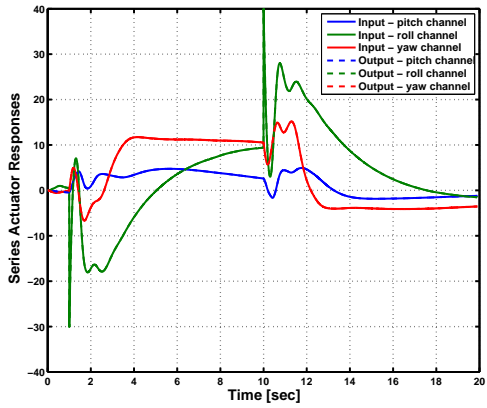


Total control activity

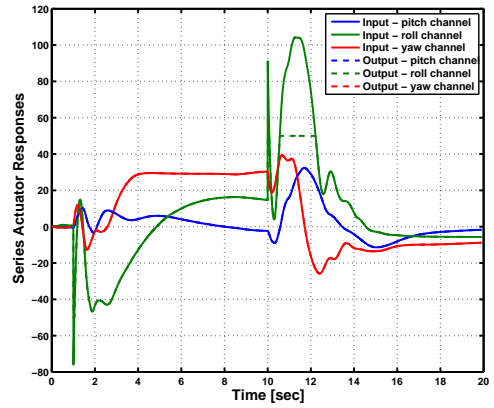
Figure 7.25: Nonlinear LA roll attitude response - 40kts/0ft

the maximum roll attitude demand that produced lateral responses that were true to their linear predictions. This also was the limit where the LA responses began to differ from the nonlinear FA responses and was similar to the demand limit that was observed during the linear LA analysis. Nonlinearities due to unmodelled dynamics did not influence the limit of applicable roll attitude demand for an identical nonlinear FA response. For roll attitude demands greater than 16.0%, minor deteriorations began to appear, however, these were not significant enough to class the response as unstable. Instabilities in the form of open-loop type behaviour were only observed once roll demand magnitude greater than 24.0% (28.8 deg) were applied.

Figures 7.24, 7.26 and 7.27 show the lateral channel response and the series and parallel

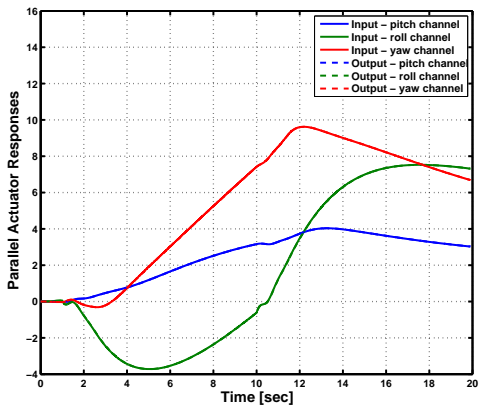


Series actuator response (8%)

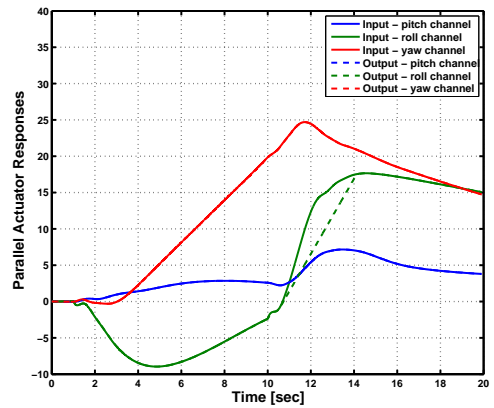


Series actuator response (20%)

Figure 7.26: Series actuator response



Parallel actuator response (8%)



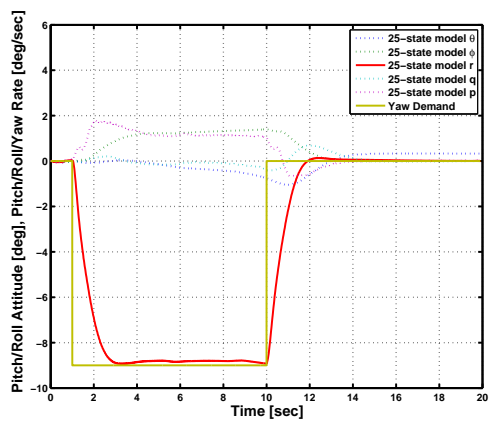
Parallel actuator response (20%)

Figure 7.27: Parallel actuator response

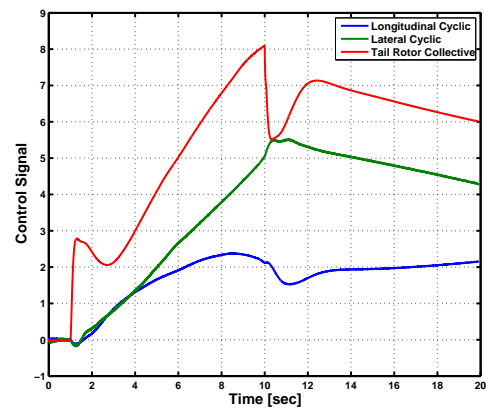
actuator activity corresponding to a roll attitude demand of 8.0% (9.6 deg). The workload was shared between the series and parallel actuators in a similar manner to the longitudinal channel with the series actuators being heavily active during the first few seconds, followed by a slower parallel actuator response to gradually drive the series actuator control signal to zero. Also presented in the above figures is the response and the series and parallel actuator activity to a larger roll attitude demand of 20% (24 deg). The slight degradation observed in the roll attitude response is caused by both series and parallel actuator saturations. Comparing the actuator responses for the above demands, it was noted that as long as the parallel actuators were not rate limited they were able to drive the series actuators to zero and make sure that they were not active for a long periods of time. At larger roll attitude demands, the

lateral channel parallel actuator experiences rate limiting and this restricted their ability to drive the lateral channel series actuator to zero, hence causing longer periods of saturation and the corresponding deterioration in the response. Also, in spite of the differences in the linear and nonlinear models, the parallel and series actuators did not saturate earlier than the linear analysis. This resulted in a maximum applicable roll attitude demand of 24.0% (28.8 deg).

### 7.2.3 Directional response (right pedal forward)

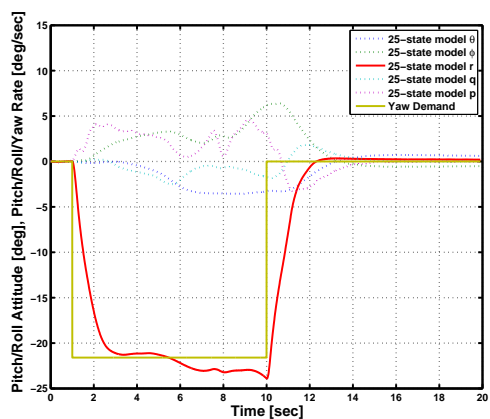


Directional response (10%)

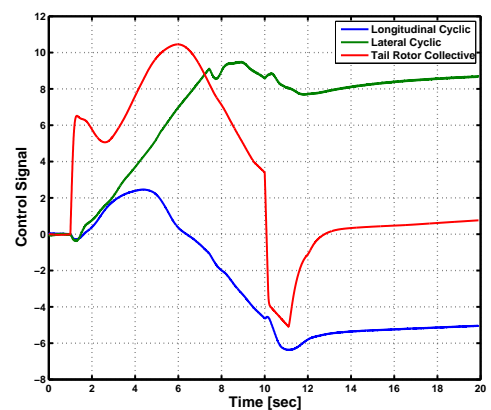


Total control activity

Figure 7.28: Nonlinear LA yaw rate response - 40kts/0ft



Directional response (24%)



Total control activity

Figure 7.29: Nonlinear LA yaw rate response - 40kts/0ft

Unlike the longitudinal and lateral channels, the low magnitude yaw rate responses were not

in total agreement to their respective linear predictions, as an undershoot of 2.0% was noticed in the nonlinear responses. This undershoot was also observed during the nonlinear FA responses, therefore, despite being dissimilar to the linear predictions the directional channel produced identical nonlinear FA responses up to a pedal input of 14% ( $-12.6$  deg/s). Again in spite of the presence of nonlinearities, this limit was observed to be similar to that observed during linear LA analysis. An illustration of this small signal performance is presented in the example plot in Figure 7.28 that shows the response to a pedal input of 10% ( $-9.0$  deg/s). Figures 7.30 and 7.31 show the corresponding series and parallel actuator behaviour and the plots show the workload being shared between the actuators. Here as well, the series actuators show significant activity at the initial stage and then the slower parallel actuators take over to ensure that the series actuator activity is reduced to zero.

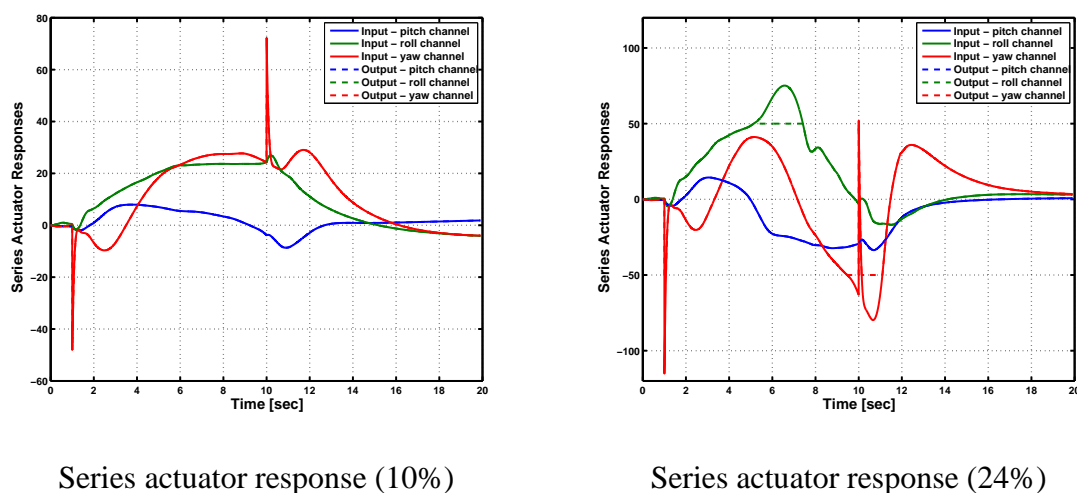
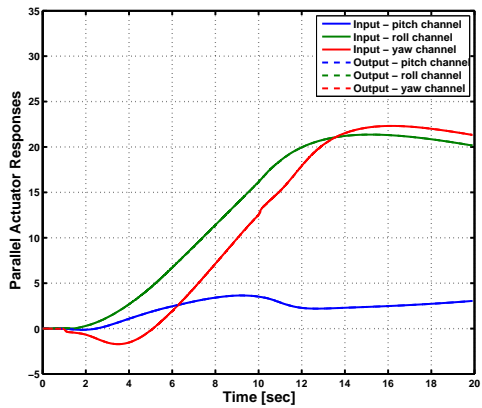
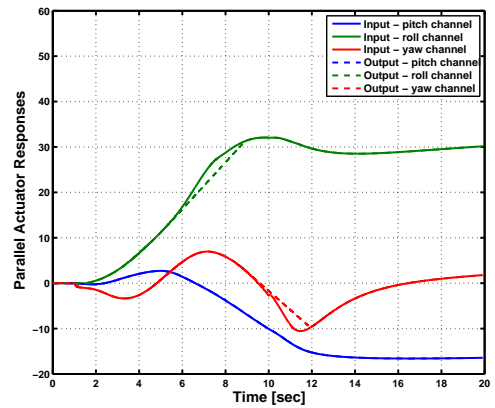


Figure 7.30: Series actuator response

Figures 7.29, 7.30 and 7.31 show the response to a pedal input of 24% ( $-21.6$  deg/s). During larger inputs as well (such as the one shown in the example plot), the series actuators display a fast initial activity, however as the parallel actuators are also saturated, they are further held back in their ability to drive the series actuator's output to zero and the directional channel series actuator remained saturated for longer periods of time. As the demand magnitudes were increased, the series and parallel actuators in the other channels were also saturated, thus deteriorating the responses to open-loop type behaviour. The maximum applicable yaw rate demand for a stable response was noted as 26% ( $-23.4$  deg/s).



Parallel actuator response (10%)



Parallel actuator response (24%)

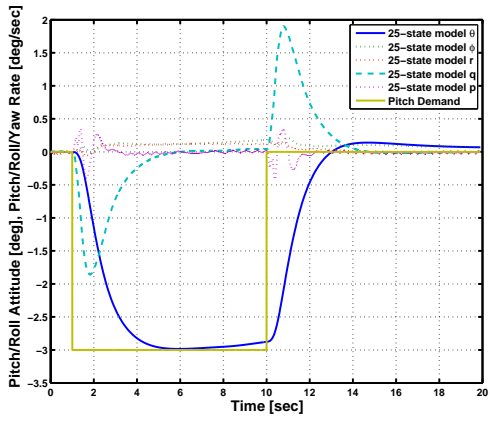
Figure 7.31: Parallel actuator response

	Maximum pilot input		
	Pitch attitude $\%(deg)$	Roll attitude $\%(deg)$	Yaw rate $\%(deg/s)$
<b>For identical response</b>	10 (-6.0)	16 (19.2)	14 (-12.6)
<b>For stable response</b>	18 (-10.8)	24 (28.8)	26 (-23.4)

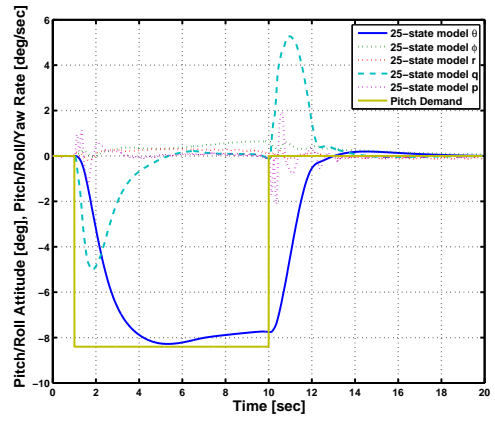
Table 7.2: Summary of nonlinear results

### Design point results summary

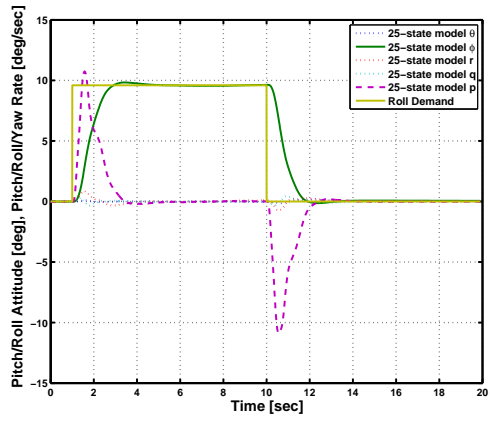
This section has presented the nonlinear LA responses achieved due to the varying magnitudes of stick and pedal inputs. At low magnitude pilot demands, these responses, except the directional channel, were in agreement to their linear predictions and at larger demands, where the nonlinearities were more severe, insignificant to significant discrepancies were observed between the linear and nonlinear responses. Also, the limits on applicable pilot demands for identical nonlinear FA responses were observed to be similar to those predicted during the linear LA analysis. The discrepancies at larger pilot demands were tolerable to a certain demand level and at demands greater than these limits the helicopter reverted to a more open-loop type behaviour. Overall, it was observed that there was a pilot demand range level that matched the FA responses and a larger level of demand range where the responses were different, but, stable and these limits are summarised in Table 7.2.



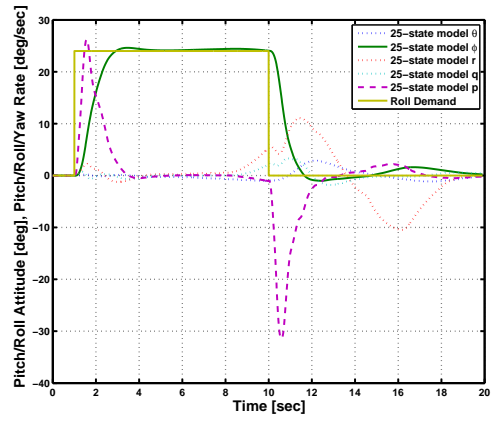
Longitudinal response (5%)



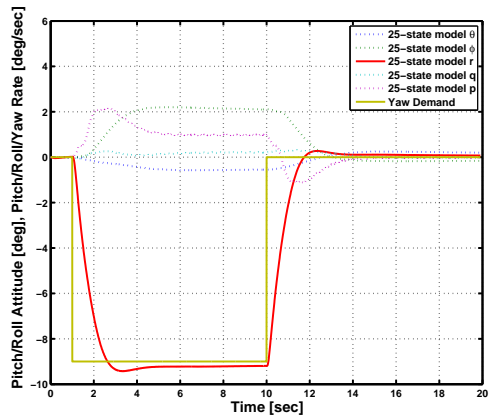
Longitudinal response (14%)



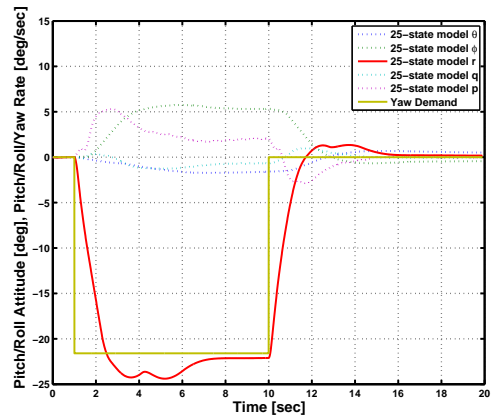
Lateral response (8%)



Lateral response (20%)



Directional response (10%)

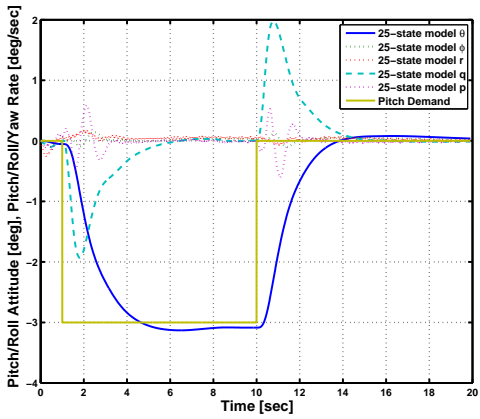


Directional response (24%)

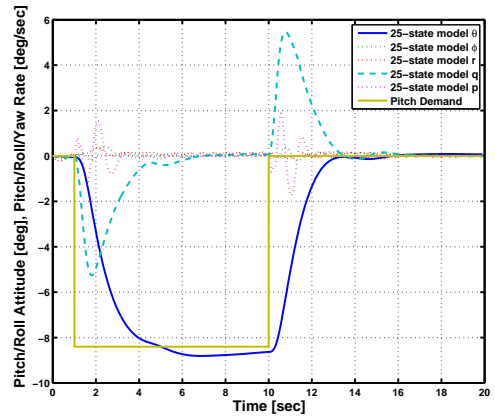
Figure 7.32: Nonlinear LA responses - 0kts/0ft

#### **7.2.4 Robustness**

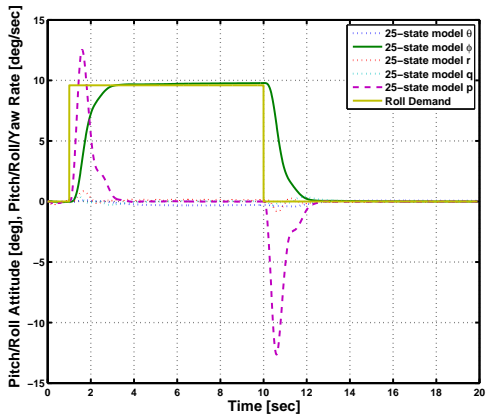
In a similar manner to the linear analysis, other flight conditions were also considered in order to examine the robustness property of the LA controller. Recall, during linear analysis, it was predicted that the longitudinal and lateral responses (at the off-design operating points) matched their respective linear FA responses until saturation. The maximum stick input before the helicopter reverted to open-loop behaviour was noted to be consistent for all the flight conditions. The only discrepancy was in the directional channel where the system reached instability for very low pedal inputs at the particular operating condition of 80kts/2500ft.



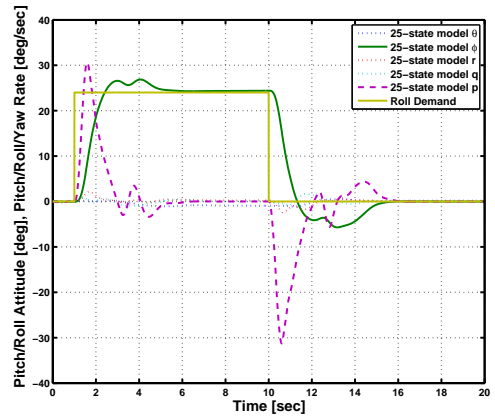
Longitudinal response (5%)



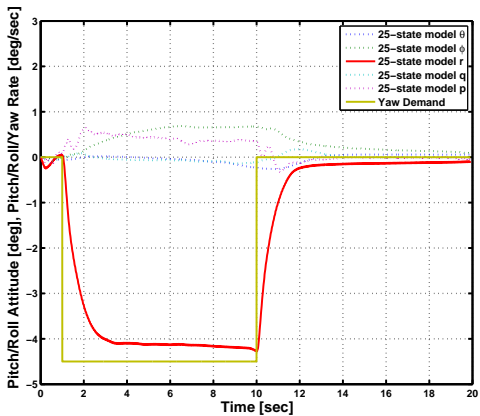
Longitudinal response (14%)



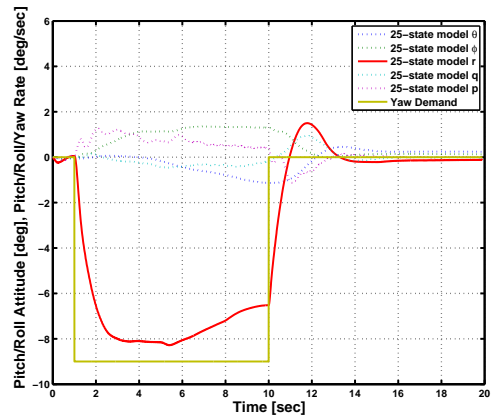
Lateral response (8%)



Lateral response (20%)



Directional response (5%)



Directional response (10%)

Figure 7.33: Nonlinear LA response - 80kts/2500ft

The plots in Figures 7.32 and 7.33 show the nonlinear responses at the off-design operating points of 0kts/0ft and 80kts/2500ft respectively. At the hover flight condition, for low magnitude pilot demands all the channels were true to their respective linear predictions. As

the demand magnitudes were increased, the level of discrepancy between the linear predictions and the nonlinear responses was more significant. In terms of matching the nonlinear FA responses the maximum pilot demand in each channel was around the same value. This was also true for the values of pilot demands that guaranteed stable but non-identical responses. At the high speed/high altitude flight condition similar trends were observed. The only anomaly was observed in the directional channel because at a significantly low pedal input of 10% ( $-9.0$  deg/s) and without any series and parallel actuator saturation the yaw rate response reverted to open-loop behaviour. This anomaly was also predicted during the linear LA analysis. The limits obtained at the other tested flight conditions are listed in Tables 7.3 and 7.4.

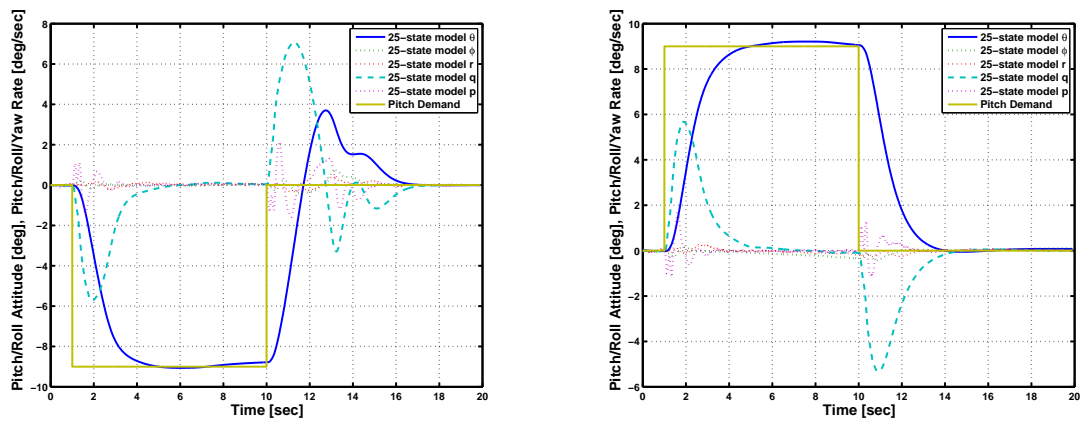
### **7.2.5 Note on symmetry**

There are certain differences expected, as seen in the FA analysis, between the responses obtained for positive pilot demands to the responses obtained for negative pilot demands due to the nonlinear nature of helicopter dynamics. Symmetry of responses for the EH101 helicopter has already been analysed during the FA controller analysis and it thus becomes important to also assess the capability of the LA controller in replicating the FA responses due to negative pilot demands.

#### **Longitudinal response (pitch-up)**

At low magnitude stick inputs, i.e. below 5% (3 deg), both the on- and off-axis features of the pitch-up responses were generally similar to that of the pitch-down responses. As the magnitude was increased, the responses to positive and negative demands started to differ. The maximum stick input for identical nonlinear FA response during pitch-down analysis was noted as 10% (6 deg) and during pitch-up analysis this limit was noted to be 14% (8.4 deg). This pitch-up limit was lower than the limit predicted during linear LA analysis. Also, a stable response, not identical to the nonlinear FA responses, was achievable up to a maximum pitch-up demand of 17% (10.2 deg). These differences between the pitch-up and pitch-down responses is further illustrated in Figure 7.34 which shows the response to pitch inputs of 15% and  $-15\%$ . The response to the 15% pitch-up demand showed less degradation as

compared to the pitch-down response. There was also a greater level of similarity observed with the pitch-up response to the nonlinear FA response. At the hover condition, an identical FA response was achievable up to a pitch-up demand of 13% (7.8 deg) and the maximum limit for a tolerable response, was noted to be 17% (10.2 deg). The limits on the applicable pilot demands at the high speed/high altitude flight condition was also observed to be around the same value as above.



Longitudinal response (15%)

Longitudinal response (-15%)

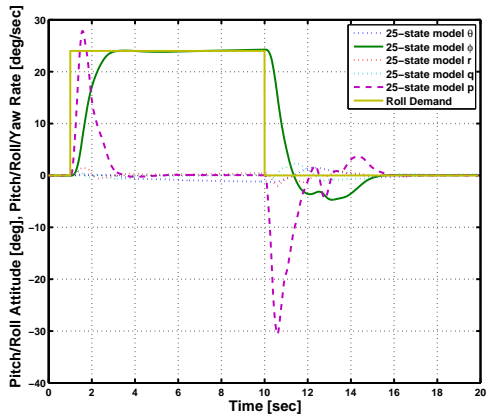
Figure 7.34: Nonlinear LA pitch attitude symmetry - 40kts/0ft

### Lateral response (roll-left)

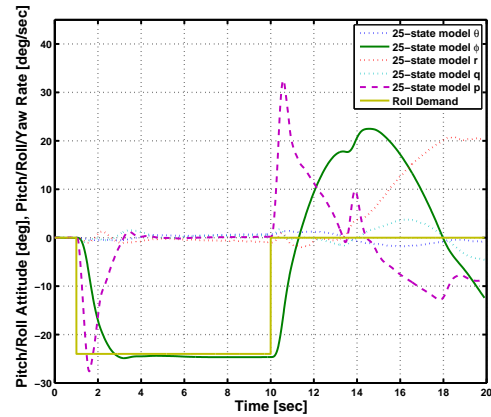
The roll responses were generally symmetrical at all flight conditions. A notable difference was seen at the design point where the maximum roll-left demand for a stable response was observed to be 18% (21.6 deg) which was lower than the roll-right limit of 28.8 deg. This lower limit for negative roll demand is further illustrated in Figure 7.35, where the responses to the roll inputs of 20% and -20% are presented. This comparative plot shows the greater deterioration in roll-left response and this was predominantly due to the early saturation of series actuators. Other flight conditions also experienced premature saturation during roll-left analysis which then resulted in a lower limit on roll-left demands for a stable response.

### Directional response (left pedal forward)

At low magnitude pedal inputs, i.e. below 10%, both positive and negative yaw rate responses showed identical short term features. However, the left pedal input response devel-



Lateral response (20%)



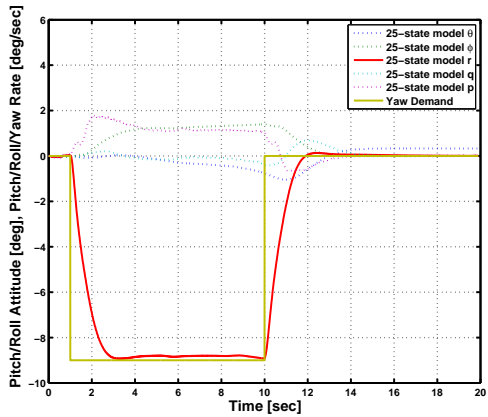
Lateral response (-20%)

Figure 7.35: Nonlinear LA roll attitude symmetry - 40kts/0ft

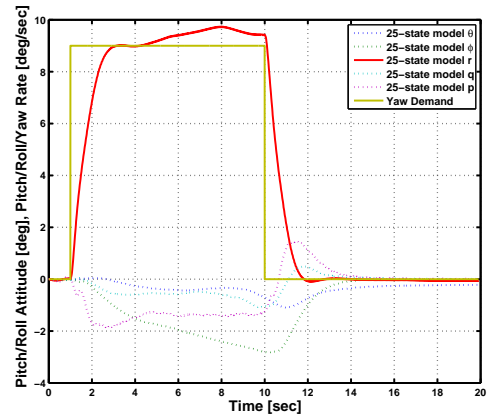
oped a significant transient just after 4 seconds (Figure 7.36) that caused some tracking error in performance. As pedal demand magnitude was increased, the responses to positive inputs showed minor degradations and the responses to negative demands showed an improvement (Figure 7.37), as a quicker recovery of the error in tracking was observed. Once the series actuators have reached magnitude saturation, the level of degradation in the off-axis responses was a lot stronger for negative yaw rate demands. The example plot in Figure 7.37 presents the response to a pedal input of  $-15\%$  ( $13.5 \text{ deg/s}$ ) and comparing this to the response to a demand of  $15\%$  shows this elevated level of off-axis degradations in the former. Generally, the pedal limits that guaranteed identical nonlinear FA response were unchanged for all flight conditions. This was also the case for the limits that guaranteed a stable response. The irregularity was again observed in the high speed/high altitude flight condition where the range of pilot demands was significantly smaller.

## 7.2.6 Summary

The nonlinear LA results presented here have been predominantly true to their linear predictions. At low magnitude pilot demands, the LA architecture is capable of preserving the FA behaviour. However, there was a maximum pilot input limit beyond which minor degradations began to appear in the performance. Furthermore, these degradations were only tolerable up to a certain extent. The limit for both identical and tolerable nonlinear responses was observed to be similar to that predicted during the linear analysis in Chapter

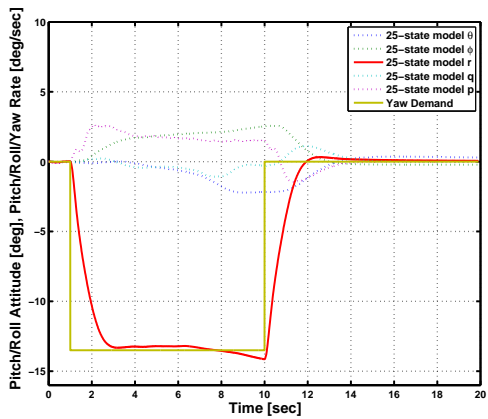


Directional response (10%)

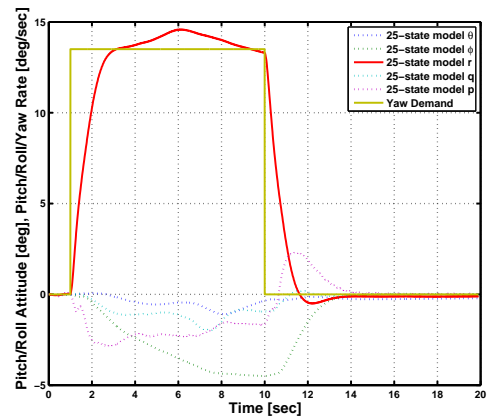


Directional response (-10%)

Figure 7.36: Nonlinear LA yaw rate symmetry - 40kts/0ft



Directional response (15%)



Directional response (-15%)

Figure 7.37: Nonlinear LA yaw rate symmetry - 40kts/0ft

6. It was particularly noteworthy that FA type behaviour was preserved by the LA controller, for small pilot demands, across the flight envelope. The LA controller was also capable of reproducing the FA controller’s counter cross-coupling and symmetry in response properties to a satisfactory level.

Tables 7.3 and 7.4 present the maximum stick/pedal input that could be applied in order to produce an identical FA response and a stable (non-identical) response respectively, with respect to changes in flight conditions. It can be seen from the values that the longitudinal and lateral channel limits are consistent with variation in flight conditions. The directional channel shows a significant drop in limit values for both identical and stable responses.

Thus far the analysis of both the FA and LA controller has been based on time domain

	<b>Max pilot demand</b>					
<b>Flight Condition</b>	Pitch attitude $\%(deg)$		Roll attitude $\%(deg)$		Yaw rate $\%(deg/s)$	
40kts/00ft	10 (-6.0)	-14 (8.4)	16 (19.2)	-16 (-19.2)	14 (-12.6)	-16 (14.4)
00kts/00ft	8 (-4.8)	-13 (7.8)	14 (16.8)	-14 (-16.8)	18 (-16.2)	-18 (16.2)
80kts/2500ft	12 (-7.2)	-11.5 (6.9)	18 (21.6)	-15 (-18.0)	6 (-5.4)	-10 (7.2)

Table 7.3: Summary of max input for identical response

	<b>Max pilot demand</b>					
<b>Flight Condition</b>	Pitch attitude $\%(deg)$		Roll attitude $\%(deg)$		Yaw rate $\%(deg/s)$	
40kts/00ft	18 (-10.8)	-18 (10.8)	24 (28.8)	-18 (-21.6)	26 (-23.4)	-27 (24.3)
00kts/00ft	17 (-10.2)	-17 (10.2)	20 (24.0)	-18 (-21.6)	23 (-20.7)	-23 (20.7)
80kts/2500ft	16 (-9.6)	-15 (9.0)	23 (27.6)	-19 (-22.8)	10 (-9.0)	-12 (10.8)

Table 7.4: Summary of max input for stable response

analysis to standard pulse inputs. A MATLAB Handling Qualities Toolbox [34] was used to supplement the above computer aided controller designs in order to integrate handling qualities provided by the pilot into the complete design and analysis cycle.

## **7.3 Handling qualities rating assessment**

The Aeronautical Design Standard (ADS)-33 document details the guidelines for assessing the performance of helicopter control system. The document provides both quantitative and qualitative criteria for evaluation of such systems; some require pilot comments, however there are those that are based on either simulated responses or flight test results. The results presented here were produced by utilising the following quantitative criteria (discussed in Chapter 3):

1. small amplitude input response - short-term assessment is conducted by deducing the bandwidth and phase delay parameters and mid-term assessment concerns the damping factor at frequencies below the bandwidth found earlier,
2. moderate amplitude input response - handling qualities are assessed from the ratio of peak rate to peak attitude change for different magnitude of change in attitude,
3. large amplitude input response - ratings are provided by the maximum demand that could be applied to control system before the responses become unstable, and
4. inter-axis coupling - ratings are judged based on the level of interactions between the channels.

### **7.3.1 Small amplitude input criteria**

The small amplitude ADS-33 criteria are essentially those which assess the response of the helicopter to small amplitude pilot demands where the helicopter behaves in an essentially linear manner. For such small amplitude pilot commands, the magnitude and rate-limits of the series and parallel actuators respectively, are not excited and thus, according to the formulae presented in Chapter 5, the FA and LA control laws behave identically. Thus, this section presents results from the ADS-33 small amplitude assessment of the FA controller and this alone is necessary since for these small inputs, the LA controller behaves in exactly the same manner.

The small amplitude handling quality assessment involved calculating the bandwidth and phase delay parameters using the 25-state linear model of the EH101. Bandwidth is defined

by the frequency at which the phase has fallen to  $-135$  deg and phase delay is the measurement of the rate of change of phase with frequency beyond this bandwidth frequency. Together these two parameters are used to quantify the controller's tracking performance and generally, designers seek to achieve a high bandwidth along with a low phase delay. Table 7.5 shows the bandwidths, phase delays and handling quality level induced in the rotorcraft at various flight conditions by the FA controller. It shows that both bandwidth and phase delay values remain consistent throughout the flight envelope. Figure 7.38 depict the calculated ADS-33 handling qualities for the pitch and roll channels in the combat/target tracking scenario (the most demanding environment), in fully attended operations (UCE (usable cue environment) = 1) and for other divided attention operations (UCE > 1). UCE defines the type of environment that the helicopter is operating and it allows to quantify the HQR given by the pilot, where UCE > 1 represents degraded environment conditions where the pilots attention may be divided [3]. Also, yaw channel results for combat and fully attended operations scenarios are shown in Figure 7.39. The values show that the controller bestows Level 1 handling qualities in the most demanding of environments and that, as far as these measures are concerned, appreciable degradation does not occur as the flight conditions are altered. It is important to note that the values presented here are only predictions based on linear models and on-axis responses. Although, at the beginning of the project it was envisaged that there would be opportunity for piloted simulation results in which a test pilot would assess the controllers using various ADS-33 criteria on the AgustaWestland simulator. For a number of reasons this did not materialise and with the project coming to a completion there was no real opportunity to do this. However, previous studies such as [65, 66, 67, 85] have indicated good correlation between predicted and achieved bandwidths and phase delay during piloted simulations.

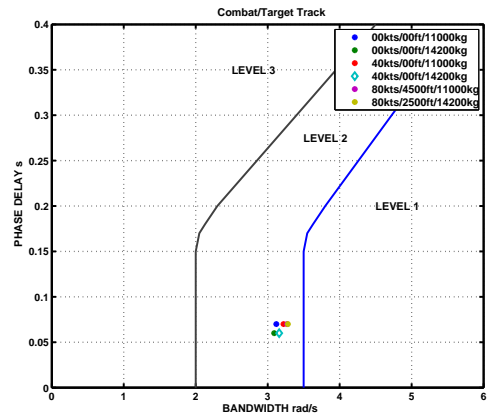
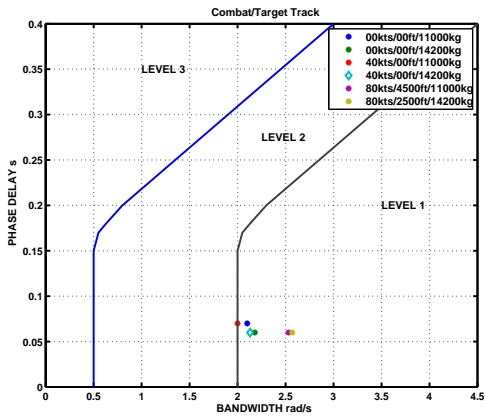
A damping factor of at least 0.35 is required in the pulse responses in order to satisfy mid-term Level 1 handling qualities criterion [50]. The 2 DOF  $\mathcal{H}_\infty$  loop shaping methodology was capable of inducing damping factor of 0.7, 0.8 and 2.0 in the pitch, roll and yaw channels respectively. This ensured a damping factor that was well above the requirement for a Level 1 handling quality. Overall, the small amplitude demand criteria predicted that the FA controller induced a Level 1 handling quality.

Flight condition	Axis	Bandwidth	Phase Delay	Handling Quality		
				Combat	UCE=1	UCE>1
<b>40kts/00ft/14200kg</b>						
	Pitch	2.13	0.06	1	1	1
	Roll	3.16	0.06	2	1	1
	Yaw	2.64	0.07	2	1	n/a
<b>Hover/14200kg</b>						
	Pitch	2.13	0.06	1	1	1
	Roll	3.09	0.06	2	1	1
	Yaw	2.54	0.07	2	1	n/a
<b>80kts/2500ft/14200kg</b>						
	Pitch	2.57	0.06	1	1	1
	Roll	3.28	0.07	2	1	1
	Yaw	3.12	0.06	2	1	n/a
<b>40kts/00ft/11000kg</b>						
	Pitch	2.05	0.07	1	1	1
	Roll	3.22	0.07	2	1	1
	Yaw	2.43	0.07	2	1	n/a
<b>Hover/11000kg</b>						
	Pitch	2.10	0.07	1	1	1
	Roll	3.12	0.07	2	1	1
	Yaw	2.50	0.07	2	1	n/a
<b>80kts/4500ft/11000kg</b>						
	Pitch	2.53	0.06	1	1	1
	Roll	3.27	0.07	2	1	1
	Yaw	3.05	0.06	2	1	n/a

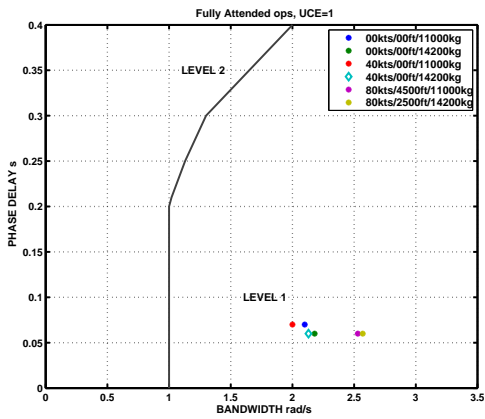
Table 7.5: Small amplitude short term handling quality ratings

### 7.3.2 Moderate amplitude input criteria

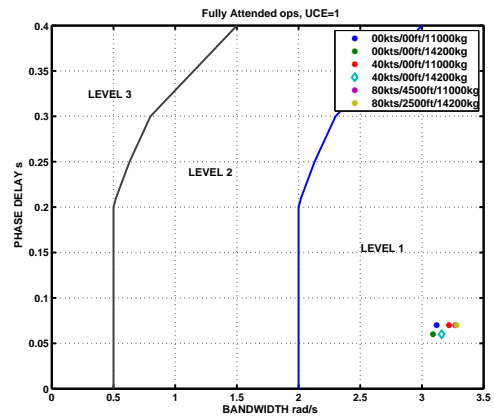
The moderate amplitude requirements are also known as *attitude quickness*. It is a ratio of peak achievable rate to the peak attitude change and the value is associated with different



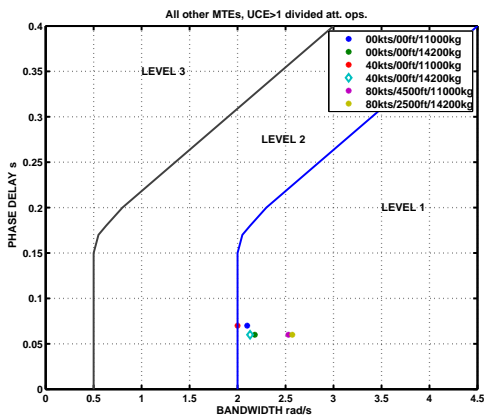
### Combat (pitch)



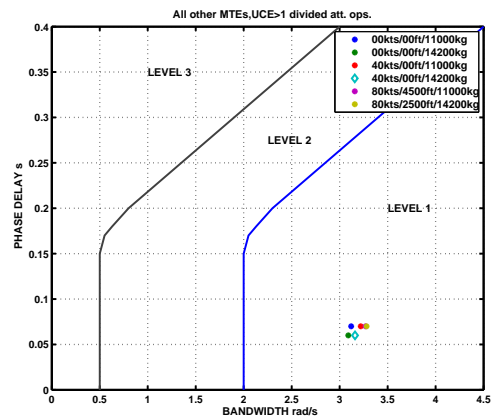
### Combat (roll)



### UCE = 1 (pitch)



### UCE = 1 (roll)



### Other (pitch)



### Other (roll)



Figure 7.38: ADS plot for pitch and roll performance

handling qualities levels. This criteria is structured in such a way that the over and under shoot characteristics of the attitude response will ensure poor handling quality rating. It is also important to appreciate that this measure is particularly relevant for Rate Command

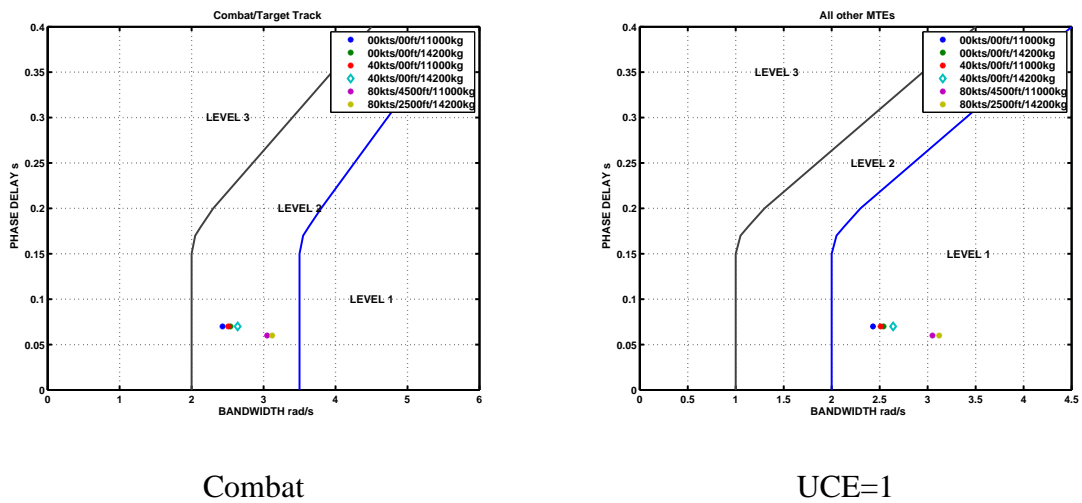
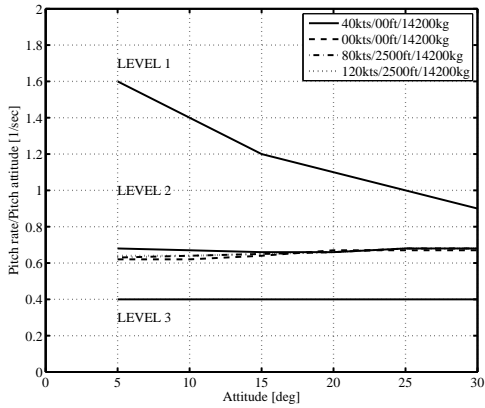


Figure 7.39: ADS plot for yaw performance

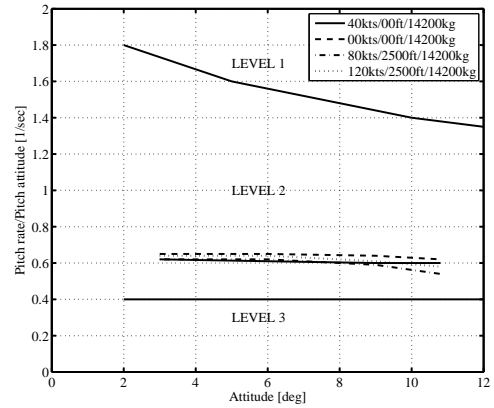
response types, which compared to ACAH response types tend to offer more agility to the response at the expense of stability [54]. Attitude quickness is expected to be degraded here as the response type sought here is attitude control and in such response types stability of responses is given priority over agility.

The moderate amplitude analysis of the longitudinal channel was conducted for pitch attitude demands ranging from 5% to 50%. The predicted longitudinal attitude quickness with both FA and LA controllers along with the ADS-33 requirement levels are shown in Figure 7.40. It can be seen that the Level 2 requirements was satisfied in this channel by the FA controller at all tested flight conditions and this behaviour was also replicated by the LA controller. It should be noted, that LA analysis was limited to a maximum pitch attitude demand of 18% (10.8 deg), as the helicopter reverted to open loop type response at larger demands. The attitude quickness values for the longitudinal channel with both FA and LA controllers are summarised in Tables 7.6 and 7.7 respectively.

The lateral channel analysis was conducted for roll attitude demands from 8% to 50%. At the lower end of this range, attitude quickness criteria for Level 1 handling quality are stricter and relax for larger roll attitude demands. The attainable lateral attitude quickness at various flight conditions along with the ADS-33 requirements are shown in Figure 7.41. It shows that for low attitude demands the FA controller is only capable of inducing Level 3 handling quality and as the demand magnitude is increased (beyond 35 deg) the induced handling quality improves to Level 1. As the helicopter reverts to open loop type behaviour at de-



Pitch attitude quickness - FA



Pitch attitude quickness - LA

Figure 7.40: Pitch attitude quickness

Flight condition		Pitch demand (%)				
		10	20	30	40	50
<b>40kts/00ft/14200kg</b>	Attitude quickness	0.68	0.67	0.66	0.66	0.68
	Handling quality	2	2	2	2	2
<b>0kts/00ft/14200kg</b>	Attitude quickness	0.62	0.62	0.64	0.67	0.67
	Handling quality	2	2	2	2	2
<b>80kts/2500ft/14200kg</b>	Attitude quickness	0.63	0.64	0.65	0.66	0.68
	Handling quality	2	2	2	2	2
<b>120kts/2500ft/14200kg</b>	Attitude quickness	0.64	0.64	0.65	0.66	0.68
	Handling quality	2	2	2	2	2

Table 7.6: FA pitch attitude quickness

mands greater than 25% (30 deg) due to the complexities in the LA controller architecture the moderate amplitude analysis for the LA controller was only conducted to this limit. The LA controller, prior to system instability, was only capable of inducing a Level 3 handling quality at all the flight conditions. Attitude quickness values for the lateral channel are summarised in Tables 7.8 and 7.9.

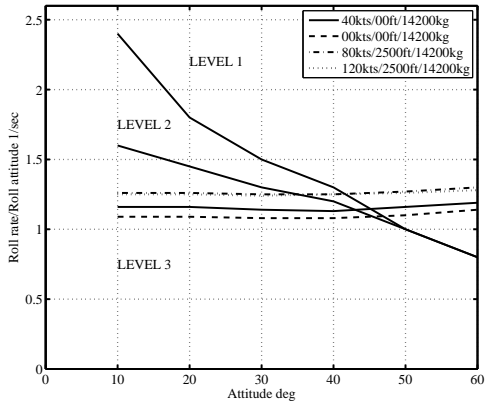
Flight condition		Pitch demand (%)			
		5	10	15	18
<b>40kts/00ft/14200kg</b>					
	Attitude quickness	0.65	0.65	0.64	0.62
	Handling quality	2	2	2	2
<b>0kts/00ft/14200kg</b>					
	Attitude quickness	0.62	0.61	0.60	0.60
	Handling quality	2	2	2	2
<b>80kts/2500ft/14200kg</b>					
	Attitude quickness	0.62	0.62	0.59	0.54
	Handling quality	2	2	2	2
<b>120kts/2500ft/14200kg</b>					
	Attitude quickness	0.64	0.64	0.61	0.58
	Handling quality	2	2	2	2

Table 7.7: LA pitch attitude quickness

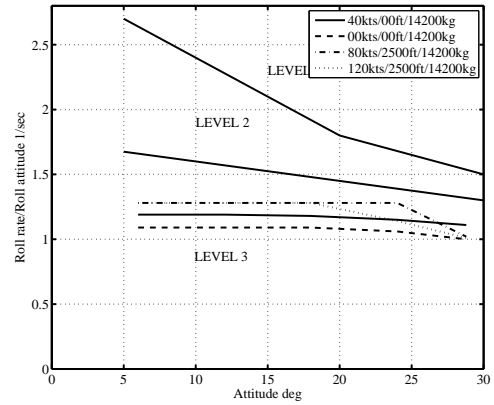
It can be seen from the above analysis that, for both longitudinal and lateral channels, Level 1 handling quality cannot be satisfied over the total range with either FA or LA controller. As the controller in this study was designed to seek an ACAH type response, i.e. focus more on stability than agility, from the helicopter, attitude quickness levels were expected to be degraded and are not as integral as the other categories in judging the ability of such controllers. Degradation in the values was predominantly due to the high damping factor induced by the controllers which effectively slowed the responses. The response speed and in turn attitude quickness could be increased by reducing the damping factor, however, this would then reduce the controller bandwidth and degrade the handling quality levels induced at other criteria.

### 7.3.3 Large amplitude input criteria

The FA and LA controllers were designed using linear approximations and this criterion judges the capability of the two controllers at situations where these approximations are no



Roll attitude quickness - FA



Roll attitude quickness - LA

Figure 7.41: Roll attitude quickness

Flight condition		Roll demand (%)					
		5	10	20	30	40	50
<b>40kts/00ft/14200kg</b>	Attitude quickness	1.16	1.16	1.14	1.13	1.16	1.19
	Handling quality	3	3	3	3	1	1
<b>0kts/00ft/14200kg</b>	Attitude quickness	1.09	1.09	1.08	1.08	1.10	1.14
	Handling quality	3	3	3	3	1	1
<b>80kts/2500ft/14200kg</b>	Attitude quickness	1.26	1.26	1.25	1.25	1.27	1.30
	Handling quality	3	3	3	2	1	1
<b>120kts/2500ft/14200kg</b>	Attitude quickness	1.25	1.25	1.24	1.24	1.26	1.28
	Handling quality	3	3	3	2	1	1

Table 7.8: FA roll attitude quickness

longer valid. The handling qualities level in the large amplitude category is judged by the maximum pilot demand that can be applied before the helicopter becomes unstable. The maximum required pilot demand varies depending upon the task to be performed and these are divided into following categories - limited agility task, such as hover; moderate agility task, such as slalom; aggressive agility task, such as sidestep and; target acquisition and

Flight condition		Roll demand (%)				
		5	10	15	20	25
40kts/00ft/14200kg						
	Attitude quickness	1.19	1.19	1.18	1.15	1.11
	Handling quality	3	3	3	3	3
0kts/00ft/14200kg						
	Attitude quickness	1.09	1.09	1.09	1.06	1.00
	Handling quality	3	3	3	3	3
80kts/2500ft/14200kg						
	Attitude quickness	1.28	1.28	1.28	1.28	1.02
	Handling quality	3	3	3	3	3
120kts/2500ft/14200kg						
	Attitude quickness	1.28	1.28	1.28	1.14	1.01
	Handling quality	3	3	3	3	3

Table 7.9: LA roll attitude quickness

track, such as turn to target. A summary of the required maximum pilot demand in order to satisfy Level 1 and 2 large amplitude criteria is shown in Table 7.10 and further details on this are available in [3].

Ability category	Required max demand					
	Pitch (deg)		Roll (deg)		Yaw (deg/s)	
	Level 1	Level 2	Level 1	Level 2	Level 1	Level 2
Limited	±15	±7	±15	±10	±9.5	±5
Moderate	±20	±13	±60	±30	±22	±9.5
Aggressive	±30	±20	±60	±30	±60	±22
Target acquisition and track	±30	±20	±60	±30	±60	±22

Table 7.10: Large amplitude handling quality rating requirement

With the FA architecture, Level 1 rating was predicted in the pitch channel for all four cat-

egories as a stable helicopter response was achievable up to the required maximum demand of  $\pm 30$  deg. The lateral channel produced a stable response up to a roll attitude demand of  $\pm 60$  deg and this corresponded to a Level 1 rating in all the agility categories. The directional channel produced a stable response for maximum pedal input of  $\pm 45$  deg/s and this corresponded to a Level 2 rating for aggressive agility and Level 1 for limited to moderate agility category. This analysis was further extended to other flight conditions as well and it was noted that the longitudinal and lateral channels predicted the same Level as at the design point. The directional channel, however, showed a discrepancy in only the high speed/high altitude flight condition where the maximum demand was observed as  $\pm 20$  deg/s. This limit corresponded to borderline Level 2 handling quality in aggressive agility category and Level 1 in moderate to limited agility categories. A summary of the FA results at the design point are tabulated in Table 7.11.

Ability category	Achieved max demand			HQR		
	Pitch (deg)	Roll (deg)	Yaw (deg/s)	Pitch	Roll	Yaw
<b>Limited</b>	$\pm 30$	$\pm 60$	$\pm 45$	1	1	1
<b>Moderate</b>	$\pm 30$	$\pm 60$	$\pm 45$	1	1	1
<b>Aggressive</b>	$\pm 30$	$\pm 60$	$\pm 45$	1	1	2
<b>Target acquisition and track</b>	$\pm 30$	$\pm 60$	$\pm 45$	1	1	2

Table 7.11: FA large amplitude handling quality rating

However, with the LA architecture, due to actuator saturation, the maximum pilot demand before instability (at the design point) was observed to  $\pm 10.8$  deg,  $-24/28.8$  deg, and  $-23.4/24.3$  deg/s, in the longitudinal, lateral and the directional channel respectively. As a consequence the handling quality rating for limited agility tasks was Level 1 for directional and lateral channels and Level 2 for longitudinal channel. Whereas, for moderate to aggressive agility large amplitude analysis predicted Level 2-3. The longitudinal and lateral channels predicted the same handling quality levels at other flight conditions as well. However, the directional channel showed a large drop in maximum applicable demand at the high speed/high altitude flight condition which resulted in degradation in the predicted handling quality level. Overall, a low handling quality level was expected for LA architecture as the

limit of applicable pilot demands was restricted by the series and parallel actuator saturation limits. A summary of the LA results at the design point are tabulated in Table 7.12.

Ability category	Achieved max demand			HQR		
	Pitch (deg)	Roll (deg)	Yaw (deg/s)	Pitch	Roll	Yaw
<b>Limited</b>	$\pm 10.8$	$-21.6/28.8$	$-23.4/24.3$	2	1	1
<b>Moderate</b>	$\pm 10.8$	$-21.6/28.8$	$-23.4/24.3$	3	3	1
<b>Aggressive</b>	$\pm 10.8$	$-21.6/28.8$	$-23.4/24.3$	3	3	2
<b>Target acquisition and track</b>	$\pm 10.8$	$-21.6/28.8$	$-23.4/24.3$	3	3	2

Table 7.12: LA large amplitude handling quality rating

### 7.3.4 Inter-axis coupling criteria

ADS-33 also places specification on inter-axis coupling, i.e. the manner in which pitch is affected by roll, and vice-versa. It states that for a Level 1 handling quality the ratio of roll attitude due to pitch attitude commanded change following an input should not exceed 0.25. Table 7.13 presents the pitch to roll and roll to pitch coupling values with both FA and LA controller at selected flight conditions. Although, the FA controller produces comparatively lower values than LA, all values are below the Level 1 requirement of 0.25. The multivariable characteristics of  $\mathcal{H}_\infty$  loop shaping control law were effectively responsible for countering inter-axis coupling and inducing optimum handling qualities to the helicopter.

### 7.3.5 Summary

This section has presented the quantitative ADS-33 predictions of both the FA and LA controller. The small amplitude short-term and mid-term assessments have shown that Level 1 handling qualities can be achieved in pitch, roll and yaw, creating a high bandwidth, stable control platform. The test for the controller's effectiveness against inter-axis coupling also predicted a Level 1 handling quality rating. Moderate amplitude (attitude quickness) analysis showed that the FA controller was capable of inducing a Level 2 handling quality in the longitudinal and a Level 3-to-1 in the lateral channel with increase in pilot attitude demand.

<b>Flight condition</b>		<b>Full authority</b>	<b>Limited authority</b>
<b>40kts/00ft/14200kg</b>			
	pitch to roll	0.07	0.03
	roll to pitch	0.05	0.06
<b>0kts/00ft/14200kg</b>			
	pitch to roll	0.05	0.10
	roll to pitch	0.04	0.06
<b>80kts/2500ft/14200kg</b>			
	pitch to roll	0.03	0.04
	roll to pitch	0.04	0.07
<b>120kts/2500ft/14200kg</b>			
	pitch to roll	0.04	0.05
	roll to pitch	0.04	0.07

Table 7.13: Nonlinear inter-axis coupling

The LA controller also induced the same handling quality level in the longitudinal channel as the FA controller, however, in the lateral channel the induced handling quality level was maintained at Level 3. The degraded level of handling quality was expected because the controller was designed with more emphasis on stability and damping than quickness. Finally, FA controller was capable of inducing predominantly a Level 1 handling quality in all three channels during the large amplitude demand analysis. The maximum applicable demand in LA architecture was only a percentage of the full scale stick deflection which meant that the LA controller could only induce Level 2/3 handling quality depending upon the task to be performed. Overall, the ADS-33 evaluation predicted a reasonably good level of handling quality rating for both the FA and LA controllers, although the controllers were not specifically designed to meet the ADS-33 requirement.

## 7.4 Conclusion

This chapter has presented the nonlinear simulation responses along with a quantitative ADS-33 analysis of both the FA and LA controllers for the EH101 helicopter. The nonlinear FA

responses have positively substantiated the application of 2DOF  $\mathcal{H}_\infty$  loop shaping method. The linear controller, as shown in Chapter 4, was designed using an 8-state approximation of the EH101 helicopter and was highly effective in providing stable responses for the entire flight envelope without the aid of gain scheduling. However, minor deteriorations were noticed at the extremes of pilot demand range. The low inter-axis coupling emphasized the multivariable nature of the chosen methodology.

The nonlinear LA responses acquired by implementing the linear controller that was designed using the transformation formulae described in Chapter 5 agreed with the linear responses seen in Chapter 6 in terms of the maximum applicable pilot demand that produced a stable response. Also the small signal responses obtained using the LA controller were identical to the respective FA responses, thereby giving support to the transformation method. The maximum applicable pilot demands and the responses to demands up to that limit were quite consistent throughout the flight envelope which further highlighted the effectiveness of the transformation formulae in preserving the robustness and counter coupling properties of the linear FA controller.

The ADS-33 analysis yielded interesting results. Not surprisingly, it revealed that in the small amplitude tests both FA and LA controllers performed similarly well, with both controllers bestowing Level 1 handling qualities ratings on the rotorcraft. Furthermore, it was also seen and perhaps this was a little more surprising and encouraging that, provided the pilot demands were not excessively large, both the LA and FA controllers were able to achieve good large signal handling qualities on the aircraft, although the FA system was superior in this respect due to the absence of the various actuator limits. Perhaps the most surprising aspect of the ADS-33 analysis was the poor performance of both controllers in the moderate amplitude attitude quickness tests, where both controllers performed to Level 3, which indicates quite poor performance. As noted earlier this may be due to the ACAH nature of the control laws and, perhaps, also due to the nature of the attitude quickness test which is somewhat crude in nature (one might argue that it “rewards” poorly damped control systems since their quickness can be greater than better damped systems). Thus, due to the emphasis on stability and damping in design, both FA and LA systems did poorly in this test. Thus, despite some varied handling ratings, the LA and FA controllers were both thought to perform reasonably well in the ADS-33 tests, with the FA obviously showing superiority in

some aspects due to the absence of troublesome series/parallel actuator limits. It should also be noted that the controllers were not specifically designed to satisfy ADS-33 requirements and therefore, more fine tuning of the controllers could improve their associated ratings.

Overall, the advantages of  $\mathcal{H}_\infty$  loop shaping methodology are evident from the results. The transformation formula was able to preserve the robustness and counter-coupling properties of the FA controller in the LA architecture. Small signal performance matching verified the effectiveness of the proposed LA design. However, there are avenues that should be explored, such as anti-windup compensation for enhancing the proposed LA architecture further, especially in improving the large signal performance. Also, it is important to note that the designs had not considered the pilot in the loop and this human element is expected to improve upon the range of applicable demands.

# Chapter 8

## Conclusions and recommendations

### 8.1 Conclusion

This thesis has considered the design and evaluation of a systematic method for constructing LA flight control systems. The proposed method has been applied to a realistic case-study: the AgustaWestland EH101 helicopter. Traditional LA architectures have tended to provide helicopters with basic stability augmentation and have tended to be designed in quite “mysterious” ways. In particular, the treatment of the parallel actuators in the design of such systems has not been theoretically satisfactory. The results in this thesis demonstrate how a given FA controller can be implemented in a LA architecture in a completely methodical manner, allowing the LA system to take advantage of the FA system’s “optimum” performance, at least for small pilot demands. It is hoped that the results here provide a useful approach for practitioners wishing to design LA systems and therefore will allow current helicopters to benefit from some sort of FA performance without a complete overhaul of their flight control systems. The main outcomes of the study are described below.

#### 8.1.1 Design of a robust FA controller

This study was essentially divided into two halves with the initial phase involving the design of a robust FA control system for the EH101 helicopter. The FA controller was designed using 2DOF  $\mathcal{H}_\infty$  loop shaping methodology due to its capability to deal with multivariable

systems that are subjected to uncertainties and also because they provide robust stabilisation to coprime factor uncertainty description. Coprime factor uncertainty description is ideal for representing uncertainties in helicopters as they are capable of representing unstable plants and they also allow sensible description of lightly damped resonant poles - both scenarios are highly likely within helicopters. The FA controller was designed using an 8-state linear representation of the EH101 helicopter and this was tested across the entire flight envelope using both linear and nonlinear models.

### **Main outcomes**

Desktop simulation results from the FA architecture, along with quantitative handling quality ratings analysis, have validated the choice of methodology as the controller designed using the 8-state linear model was capable of producing highly satisfactory responses throughout the helicopter flight envelope. Moreover, this was achieved without the aid of gain scheduling. These results have demonstrated the potential desirable flying qualities achievable by a FA FCS. Some of the notable advantages of this system over its LA counterpart, normally used in FCS design, is that the FA system allows good performance to be achieved even at high levels of pilot command and there is no point at which a *sudden* degradation of performance occurs due to series/parallel actuator saturation. Therefore, even in aggressive piloting situations, the pilot can always rely on the FA controller to deliver acceptable decoupling and response types; this is considerably more difficult, or impossible, to achieve with a LA controller with the types of series/parallel actuator limits present in typical helicopters today.

### **8.1.2 Derivation of the transformation formulae**

The second phase of the study included the proposal of a LA architecture along with a systematic formulae that would take the above FA controller, or any arbitrary 2DOF FA controller for that matter, and “transform” it to acquire an equivalent LA controller. It is important to note that the formulae presented here accounts for the presence of the parallel actuators in the architecture and they are somewhat more involved than the more simplified approaches used in [35] and [85]. Parallel actuators are used to drive the steady state series

actuator output to zero and is of critical importance in LA architectures. With this in mind two design schemes were presented. The first scheme uses the stick datum (pilot demand + parallel actuator output) as the reference demand to the electronic controller. Although, this architecture is commonly observed within current helicopter hardware, there are certain disadvantages (i.e. complex internal loop and pilot stick back drive) due to the point at which the parallel actuator output is included. An alternate scheme was also presented, where the pilot stick demands are fed directly to the electronic controller without interference from the parallel actuator output. The advantage of this scheme is that the architecture is simpler with no complex internal loop issues. It would be difficult to implement this scheme within current generation of helicopter hardware, however, it is considered to be feasible for an electronic implementation of LA architectures, and would also prevent the pilot's stick from being back-driven. Therefore, the first scheme was chosen as the proposed architecture for the LA control system analysis.

The transformation formulae were applied to the above FA controller and the resultant LA control system was analysed using both linear and nonlinear models of the EH101 across the entire flight envelope. This provided an opportunity to compare the responses from the two architectures in order to analyse the capability of the proposed LA architecture in replicating the FA behaviour.

### **Main outcomes**

The transformation formulae derived in this study provides a systematic method for the construction of LA architectures that would encompass the small signal behaviour of an arbitrary FA controller. This is of significance because, apart from the studies like [33], [35] and [84], there has been little in the way of methodical and rigorous theory that would assist the design of LA control systems.

Parallel actuators were highly significant in this architecture as they were directly involved in the series actuator compensator design process, whereas in previous studies they were only added in an ad-hoc manner once the compensator was designed.

### **8.1.3 Case study results**

Both FA and LA control systems were extensively tested on a nonlinear flight mechanic model provided by AgustaWestland. For small pilot commands both control systems showed desirable to adequate performance across the tested portion of the flight envelope, despite no gain scheduling being employed. Moreover, for moderately sized pilot inputs, it was seen that the LA controller was still able to furnish the helicopter with adequate response types, although the series/parallel actuator saturation obviously degraded the response when compared with the FA system. Such extensive simulations are believed to be encouraging for the method proposed and support its applicability.

## **8.2 Recommendations for future work**

### **Use of anti-windup compensation**

Within LA architecture, actuator saturation occurs at large pilot demands due to the strict limitations on series actuator authority. As seen with the responses in this study, saturation can degrade performance and also with unstable plants it could compromise closed loop stability. Although parallel actuators are used in the proposed architecture to offload the series actuators by driving their steady state output to zero, they themselves are subject to rate-limiting that introduces more nonlinearity into the system, which further degrades the performance. As mentioned in the introduction, during saturation the helicopter shows unstable behaviour and becomes more difficult to fly. In order to limit this performance degradation anti-windup (AW) compensators form a possible solution. AW compensators are driven by the difference between the saturated and unsaturated series actuator signals and remains inactive until saturation occurs. However, during saturation the compensator becomes active and tries to artificially reduce the controller input to drive the controller output below the saturation level. All AW literature assume that the control system architecture is FA and various AW schemes have been put forward which can guarantee stability of such closed loop systems [18]. The challenge with LA architecture is not as simple because of the complex interactions between the PFCS and the AFCS control inputs. However, with the aim to preserve performance and also to have a large stability domain, it is known that AW compensators go some way

towards this, although it is hard to calculate this explicitly.

### **Piloted simulation**

Due to the role of the pilot in control and stabilisation for large demands, a necessary next stage in the assessment of these results is piloted simulation. This will enable the determination of acceptable levels of parallel actuator activity and it may be the case that the level determined by simulation in this report is too high for a typical pilot to feel comfortable. However, a redesigned parallel actuator controller leads to a simple series actuator controller re-design using the formulae provided here.

### **Parallel actuator study**

Another point worthy of investigation is the situation, which is currently implemented in the EH101, where the parallel actuators are only active when no pilot input is applied. In this case, the parallel actuators do not assist in pilot-in-the-loop tasks and purely act to stabilise the trim position. Preliminary investigation of this architecture suggested that controllers similar to those proposed here appear to perform reasonably well, but as the parallel actuators are only active for zero pilot commands (stick/pedals centred), the tracking performance degrades significantly. In this case, the tracking control effort is governed purely by the series actuator controller and it makes sense to design the series actuator controller independently of the parallel actuator controller.

Also important in the parallel actuator study would be to find alternative strategies to design the highly critical parallel actuator compensator,  $K_P$ . In this study,  $K_P$  was chosen as bank of integrators that was required to drive the series actuator output in each channel to zero in steady state. Although the compensator was successful in accomplishing its main objective, it was believed that its performance could be optimised further. For instance, the current bank-of-integrator structure, while simple, offers little flexibility for tuning the parallel actuator compensator. As with classical control system design it might be beneficial to add lead-lag elements to the controller to allow more refinement in system performances. Similarly, as the parallel actuator controller is, by nature, multivariable, additional improvement could be made by making the controller non-diagonal. Finally, the parallel actuator

controller could also be designed by optimisation techniques, such as  $\mathcal{H}_\infty$ , in order to obtain even better performance - although at the expense of significantly increasing the complexity of the parallel actuator control system

# Bibliography

- [1] Alford A., “HEAT/NAOMI Simulation Model Developers Guide”, 2003, AgustaWestland Propriety.
- [2] Amaral T.G.B. and Crisotomo M.M., “Automatic Helicopter Motion Control Using Fuzzy Logic”, 10<sup>th</sup> *IEEE International Conference*, Vol. 2, pp. 860-863, 2001.
- [3] Anonymous, “ADS-33D Handling Qualities Requirements for Military Rotorcraft”, *US Army Aviation System Command*, St. Louis, MO, USA, 1998.
- [4] Anonymous, “Rotorcraft Flying Handbook”, *Federal Aviation Administration*, Skyhorse publishing, New York, 2007.
- [5] Anonymous, “Manual for General Aircraft Maintenance Volume 5”, March 2009  
*http : //www.tpub.com.*
- [6] Apkarian P., Samblancat C., Le Letty L. and Patton R., “A Two Feedback Loop Robust Helicopter Control Based on Eigenspace Techniques and  $\mathcal{H}_\infty$  Synthesis”, *Proceeding of 29th IEEE Conference on Decision and Control*, vol. 6, pp. 3337-3339, 1990.
- [7] Baillie S., Morgan J.M., Mitchell D. and Hoh R., “The Use of Limited Authority Response Types to Improve Helicopter Handling Qualities During Flight in Degraded Visual Environment”, *AHS 51st Annual Forum*, Washington D.C., pp. 89-95, May 1995.
- [8] Baillie S. W., Morgan J. M. and Goheen K. R., “Practical Experiences in Control System Design using the NRC Bell 205 Airborne Simulator”, *AGARD Flight Mechanics Panel Symposium on Active Control*, Italy, 1994
- [9] Balas G., Doyle J.C., Glover K., Packard A. and Smith R., “ $\mu$  analysis and synthesis toolbox”, MUSYN Inc. and The Mathworks Inc., 1991.

- [10] Bates D.G., Gatley S.L., Postlethwaite I. and Berry A.J., “Integrated Flight and Propulsion Control Design using  $\mathcal{H}_\infty$  loop-shaping Techniques”, *Proceedings of IEEE Conference on Decision and Control*, pp. 1523-1528, 1999.
- [11] Bates D.C. and Postlethwaite I., “Robust Multivariable Control of Aerospace Systems”, Control and Instrumentation Group, Department of Engineering, University of Leicester, June 2002.
- [12] Bernstein D.S., “Matrix Mathematics: Theory, Facts, and Formulas”, Princeton University Press, 2009.
- [13] Cooper G.E., and Harper R.P., “The Use of Pilot Rating in the Evaluation of Aircraft Handling Qualities”, NASA TN D-5153, April 1969.
- [14] Christensen K., Koelzer H., Hollifield P., Wiggins L. and Olmstead M., “A Method to Determine Maximum Flight Control Authority Through Hardover Failure Testing”, *AHS 65th Annual Forum*, Texas, May 2009.
- [15] Damen A. and Weiland S., “Robust Control”, Measurement and Control Group, Department of Electrical Engineering, Eindhoven University of Technology, July 2002.
- [16] Doyle J.C., Glover K., Khargoenkar P.P., Francis B.A., “State-space Solutions to Standard  $\mathcal{H}_2$  and  $\mathcal{H}_\infty$  Control Problems”, *IEEE Transactions on Optimal Control*, Vol. 34, pp. 831-847, August 1989.
- [17] Dudgeon G.J.W., Gribble J.J. and O’Reilly J., “Individual Channel Analysis and Helicopter Flight Control in Moderate- and Large-Amplitude Manoeuvres”, *Control Engineering Practice*, Vol. 5, pp. 33-38, 1997.
- [18] Edwards C. and Postlethwaite I., “Anti-windup and Bumpless-transfer Schemes”, *Automatica*, Vol. 34, pp.199-210, 1998.
- [19] Enns R. and Si J., “Helicopter Trimming and Tracking Control Using Direct Neural Dynamic Programming”, *Proceeding of IEEE Transactions on Neural Network*, Vol. 14, pp. 929-939, 2003.
- [20] Esmeral J.S., “Antiwindup Synthesis using Riccati Equations”, *PhD Thesis*, Department of Engineering, University of Leicester, September 2007.

- [21] Farret D., Duc G. and Harcaut J.P., “Reduced Order  $\mathcal{H}_\infty$  loop-shaping Control of a Missile Pitch Axis over a Wide Flight Envelope”, *Nonlinear Studies*, Vol. 11, pp. 199-214, 2003.
- [22] Ferreres G. and M’Saad M., “Parametric Robustness Analysis of a Missile Autopilot”, *Proceedings of the AIAA Conference of Guidance and Dynamics*, Vol. 19, pp. 621-627, 1996.
- [23] Foster N.P., “Advanced Multivariable Control Law Design for Future ACT Rotorcraft”, *PhD Thesis*, Department of Engineering, University of Leicester, August 1995.
- [24] Gahinet P. and Apkarian P., “A LMI Approach to  $\mathcal{H}_\infty$  Control”, *International Journal of Robust and nonlinear Control*, Vol. 4, pp. 421-448, 1994.
- [25] Glover K. and Doyle J.C., “State-space Formulae for all Stabilising Controllers that Satisfy as  $\mathcal{H}_\infty$  norm Bound and Relations to Risk Sensitivity”, *Systems and Control Letters*, Vol. 11, pp. 167-172, 1988.
- [26] Glover K., Sefton J. and McFarlane D., “A Tutorial on loop-shaping and  $\mathcal{H}_\infty$  Robust Stabilisation”, *Transactions of the Institute of Measurement and Control*, Vol. 14, pp. 157-168, 1992.
- [27] Green M. and Limebeer D.J.N., “Linear Robust Control”, Prentice Hall, New York, 1990.
- [28] Gu D.-W., Petkov P.Hr. and Konstantinov M.M., “Robust Control Design with MATLAB”, Springer-Verlag, 2005.
- [29] Hald, U.B., Hesselbaek M.V., Holmgaard J.T., Jensen C.S., Jakobsen S.L. and Siegmundfeldt M., “Autonomous Helicopter - Modelling and Control”, Department of Control Engineering, Aalborg University, May 2005.
- [30] Hoagg J.B. and Bernstein D.S., “Nonminimum Phase Zeros”, *IEEE Control Systems Magazine*, pp. 45-57, June 2007.
- [31] Hoh, R.H., “Evaluation of Limited Authority Attitude Command Architectures for Rotorcraft”, *AHS 58th Annual Forum*, Phoenix, Arizona, May 2003.

- [32] Holdbridge R.D., Hindson W.S. and Bryson A.E. , “LQG Design and Flight Test of a Velocity Command System for a Helicopter”, *Proceedings of AIAA Guidance, Navigation and Control*, 1985
- [33] Howell S.E., Howitt J. and Gubbels A.W., “Advances in Partial Authority Flight Control Augmentation”, *27th European Rotorcraft Forum*, Russia, September 2001.
- [34] Howitt J., “MATLAB Toolbox for Handling Qualities Assessment of Flight Control Laws”, *Proceedings of IEE Control*, Scotland, 1991.
- [35] Howitt J., Strange M.E., Dudgeon G.J.W. and Whalley M.S., “An investigation of the Impact of Automatic Flight Control System Saturation on Handling Qualities in Hover/Low Speed Manoeuvres”, *AHS 54th Annual Forum*, Washington D.C., May 1998.
- [36] Hurwitz A., “On the conditions under which an equation has only roots with negative real parts”, pp. 7282 in Bellman R.E. and Kalaba R., eds. *Selected papers on mathematical trends in control theory*, New York, (1895) 1964.
- [37] Hyde R.A., “ $\mathcal{H}_\infty$  Aerospace Control Design - a VSTOL Flight Application”, Springer-Verlag, 1995
- [38] Johnson W., “Model for Vortex Ring State Influence on Rotorcraft Flight Dynamics”, Ames Research Centel, Moflett Field, California, December 2005.
- [39] Johnson W., “Helicopter Theory”, Dover Publications Inc., New York, 1994.
- [40] Philips C., Karr C. L. and Walker G. W., “Helicopter Flight Control with Fuzzy Logic and Genetic Algorithms”, *Engineering Applications of Artificial Intelligence*, Vol. 9, pp.175-184, 1996.
- [41] Key D.L. and Heffley R.K., “Piloted Simulator Investigation of Techniques to Achieve Attitude Command Response with Limited Authority Servos”, *Technical Report*, NASA Ames Research Center, 2002.
- [42] Kureemun R., Walker D.J., Manimala B. and Voskuijl M., “Helicopter Flight Control Law Design Using  $\mathcal{H}_\infty$  Techniques”, *44th IEEE Conference on Decision and Control and European Control Conference*, pp. 1307-1312, Spain, 2005.

- [43] Khalil H.K., “Nonlinear Systems”, Prentice Hall, New Jersey, 2002.
- [44] Le Ballois S. and Duc G., “ $\mathcal{H}_\infty$  Control of Earth Observation Satellite”, *Proceedings of the AIAA Conference of Guidance, Navigation and Control*, Vol. 19, pp. 628-635, 1996.
- [45] Leishman J., “Principles of Helicopter Aerodynamics”, Cambridge University Press, 2000.
- [46] Leitner J., Calise A. and Prasad J.V.R., “Analysis of Adaptive Neural Networks for Helicopter Flight Control”, *AIAA Journal of Guidance, Control and Dynamics*, Vol. 20, pp. 972-979, 1997.
- [47] Liceaga-Castro J., Verde C., O’Reilly J. and Leithead W.E., “Helicopter Flight Control using Individual Channel Design”, *Proceedings of IEEE Conference on Control Theory and Applications*, Vol. 142, pp. 58-72, 1995.
- [48] Hoyle, D., Hyde, R., and Limebeer, D., “A  $\mathcal{H}_\infty$  Approach to Two Degrees of Freedom Design”, *Proceedings of the 30th IEEE conference on decision and control*, Brighton, UK, pp. 1581-1585, 1991.
- [49] Magni J., Bennani S. and Terlouw J., “Robust Flight Control: A Design Challenge”, Springer-Verlag, 1997.
- [50] Mannes M. A., Gribble J.J. and Murray-Smith D.J., “Helicopter Flight Control Law Design Methodologies”, September 1991.
- [51] Mansur M.H. and Tischler M.B., “An Empirical Correction for Improving Off-axis Responses in Flight Mechanics Helicopter Models”, *Journal of the American Helicopter Society*, pp. 94-102, 1998.
- [52] McFarlane, D. and Glover, K., “ $\mathcal{H}_\infty$  Design Procedure using Robust Stabilisation of Normalised Coprime Factors”, *Proceedings of the 27th IEEE Conference on Decision and Control*, pp. 1343-1348, Austin, TX, 1988.
- [53] McFarlane D and Glover K., “Robust Control Design Using Normalised Coprime Factor Plant Descriptions”, *Lecture Notes in Control and Information Sciences*.

- [54] McGeoch D.J., McGookin E.W. and Houston S.S., “Sliding Mode Implementation of an Rate Command Flight Control System for a Helicopter in Hover”, *Control 2004*, University of Bath, UK, 2004.
- [55] McGeoch D.J., McGookin E.W. and Houston S.S., “Sliding Mode Implementation of an Attitude Command Flight Control System for a Helicopter in Hover”, *Acta Polytechnica*, Czech Technical University, Prague, vol. 45, 2005.
- [56] McLean D. and Matsuda H., “Helicopter Station-keeping: Comparing LQR, Fuzzy-logic and Neural-net controllers”, *Engineering Applications of Artificial Intelligence*, Vol. 11, pp. 411-418, 1998.
- [57] Moir I. and Seabridge A., “Aircraft Systems: Mechanical, Electrical and Avionics Subsystems Integration”, Wiley, 2008.
- [58] Nair A., Turner M.C., Postlethwaite I. and Howitt J., “Single Loop Limited Authority Control: an Architectural Study”, *European Control Conference*, July 2007.
- [59] Nair A and Turner M.C., “Design of a Full Authority  $\mathcal{H}_\infty$  Controller for the AgustaWestland EH101 Helicopter”, *Technical Report*, February 2008.
- [60] Nair A and Turner M.C., “Design of a Limited Authority Controller for the AgustaWestland EH101 helicopter”, *Technical Report*, February 2009.
- [61] Padfield G. D., “Helicopter Flight Dynamics: The Theory and Application of Flying Qualities and Simulation Modelling”, UK: Blackwell Science Ltd.
- [62] Papageorgiou G., “Robust Control System Design:  $\mathcal{H}_\infty$  loop-shaping and Aerospace Applications”, *PhD Thesis*, Department of Engineering, Darwin College, Cambridge, July 1998.
- [63] Papageorgiou G. and Glover K., “Design of a Robust Gain Scheduled Controller for the High Incidence Research Model”, *Proceedings of the AIAA Conference of Guidance, Navigation and Control*, pp. 1613-1623, 1999.
- [64] Pavel M.D. and Padfield G.D., “Defining Consistent ADS-33 Metrics for Agility Enhancement and Structural Loads Alleviation”, *AHS 58th Annual Forum*, Montreal, Canada, June 2002.

- [65] Postlethwaite I., Turner M.C. and Herrmann G., “Robust Control Applications”. *Annual Reviews in Control*, Vol. 31, pp. 27-39, 2000.
- [66] Postlethwaite I., Prempain E., Turkoglu E. and Turner M.C., “Various  $\mathcal{H}_\infty$  Controllers for the Bell 205 Helicopter: Design and Flight Test”, *Proceedings of International Federation on Automatic Control World Congress*, Barcelona, 2002.
- [67] Postlethwaite I., Prempain E., Turner, M. C., Turkoglu, E., Ellis, K., Gubbels, A. W., “Design and Flight Testing of Various  $\mathcal{H}_\infty$  Controllers for the Bell 205 Helicopter”. *Control Engineering Practice*, Vol. 13, pp. 383-398, 2005.
- [68] Prouty R., “More Helicopter Dynamics”, Potomac, MD Phillips Publishing Company, 1999.
- [69] Prouty R.W., “Helicopter Performance Stability and Control”, Krieger Publishing Company, December 2001.
- [70] Sadler G., “Early History of the Helicopter”, *PhD thesis*, 1995.
- [71] Samar R., “Robust Multi-mode Control of High Performance Aero-Engines”, *PhD Thesis*, Department of Engineering, University of Leicester, UK, 1995
- [72] Skogestad S. and Postlethwaite I., “Multivariable Feedback Control - Analysis and Design”, Wiley, 1996.
- [73] Prempain E. and Postlethwaite I., “Static  $\mathcal{H}_\infty$  Loop Shaping control of a Fly-by-wire Helicopter”, *Automatica*, Vol. 41, pp. 1517-1528, 2005.
- [74] Smerlas A.J., “Robust Multivariable Control of Helicopters: From Mathematical Models to Flight Tests”, *PhD Thesis*, Department of Engineering, University of Leicester, March 1999.
- [75] Smerlas A.J., Postlethwaite I., Walker D.J., Gubbels A.W., Baillie S.W., Strange M.E., Howitt J., and Horton R.I., “Design and Flight Testing of an  $\mathcal{H}_\infty$  Control law for the Bell 205 Fly-by-wire Helicopter”. *Proceedings of AIAA Guidance Navigation and Control conference*, Boston, MA, 1998.

- [76] Smerlas A.J., Postlethwaite I. and Walker D.J., “ $\mathcal{H}_\infty$  Loop-shaping: The Bell 205 Case Study”, *Proceedings of the AIAA Conference of Guidance, Navigation and Control*, pp. 1605-1612, 1999.
- [77] Smerlas A.J., Postlethwaite I., Walker D.J., Gubbels A.W., Strange M.E. and Howitt J., “Evaluating  $\mathcal{H}_\infty$  Controllers on the NRC Bell 205 Fly-by-wire Helicopter”. *Control Engineering Practice*, Vol. 9, pp. 1-10, 2000.
- [78] Strange, M. E. and Howitt, J., “Configuration of the DERA HELISIM Model to Represent the Flight Dynamics of the NRC Bell 205 Fly-by-wire Research Helicopter”. *DERA Technical Report*, 1997.
- [79] Stoichescu D.A., Manolescu A., Vasile D. and Vasile D., “Advanced Flight Control Design Using Quantitative Feedback Theory and Dynamic Crossfeeds”.
- [80] Scotson P.G., Sun X.D. and Balfour G., “Application of Loop Shaping H-infinity Control to Diesel Engine Anti-Oscillation Strategy”, *to appear in SAE 2001 ATT Conference and Exposition*, Barcelona, Spain, 2001.
- [81] Sun X.D, Scotson P. and Balfour G., “A Further Application of Loop Shaping  $\mathcal{H}_\infty$  Control to Diesel Engine Control - Driven Idle Speed Control”, *SAE 2002 World Congress*, Detroit, Michigan, 2002.
- [82] Thomas K., “How to Fly Helicopter”, TAB Books, 1975.
- [83] Trentini M., “Mixed Norm Control of a Helicopter”, *PhD Thesis*, Department of Mechanical and Manufacturing Engineering, University of Calgary, April 1999.
- [84] Turner M., “Robust Control of Systems Subject to Input Nonlinearities with Application to High Performance Helicopters”, *PhD thesis*, Department of Engineering, University of Leicester, January 2000.
- [85] Turner, M. C., Walker D.J. and Alford A., “Design and Ground-based Simulation of an  $\mathcal{H}_\infty$  Limited Authority Flight Control System for the Westland Lynx Helicopter”. *Aerospace Science and Technology*, Vol. 5, pp. 221-234, 2001.
- [86] Vidyasagar, M., “Control System Synthesis: A Factorisation Approach”, MIT Press, 1985.

- [87] Wade R.L. and Walker G.W., “Flight Test Results of the Fuzzy Logic Adaptive Controller - Helicopter (FLAC-H)”, *Proceedings of SPIE - The Society of Optical Engineering*, Vol 2738, pp. 200-208, 1996.
- [88] Walker D. J., “Multivariable Control of the Longitudinal and Lateral Dynamics of a Fly-by-wire Helicopter”. *Control Engineering Practice*, Vol. 11, pp. 781-795, 2003.
- [89] Walker D. J., and Postlethwaite I., “Full Authority Active Control System Design for a High Performance Helicopter”. *Proceedings of the 16th European Rotorcraft Forum*, Glasgow, UK, Vol III.3.2, pp. 1-14, 1990.
- [90] Walker D.J., Turner M.C., Smerlas A., Gubbels A.W. and Strange M.E., “Robust Control of Longitudinal and Lateral Dynamics of the Bell 205 Helicopter”, *American Control Conference*, Vol. 4, pp. 2742-2746, 1999.
- [91] Walker D.J., Turner M.C. and Gubbels A.W., “Practical Aspects of Implementing  $\mathcal{H}_\infty$  Controllers on a FBW Research Helicopter”, *Active Control Technology for Enhanced Performance Operational Capabilities of Military Aircraft, Land Vehicles and Sea Vehicles*, Vol. 31, pp. 1-8, Germany, 2000.
- [92] Wan E.A. and Bogdanov A.A., “Model Predictive Neural Control with Applications to a 6 DOF Helicopter Model”, *Proceedings of the American Control Conference*, Vol. 1, pp. 488-493, 2001.
- [93] Whalley M.S., Howitt J. and Clift S.P., “Optimisation of Partial Authority Automatic Flight Control Systems for Hover/Low Speed Maneuvering in Degraded Visual Environment”, *AHS 55th Annual Forum*, Montreal, Canada, May 1999.
- [94] Yue A. and Postlethwaite I., “Improvement of Helicopter Handling Qualities using  $\mathcal{H}_\infty$  Optimisation”. *IEEE Proceedings Control Theory and Applications*, Vol. 137, pp. 115-129, 1990.
- [95] Yue A., “The Improvement of Helicopter Handling Qualities using  $\mathcal{H}_\infty$  Optimisation”, *PhD thesis*, Department of Engineering, University of Oxford, 1988.

- [96] Zames G., “Feedback and Optimal Sensitivity: Model Reference Transformations, Multiplicative Seminorms and Approximate Inverses”, *IEEE Transactions on Automatic Control*, Vol. 26, pp. 301-320, 1981.
- [97] Zames G. and Francis B.A., “A New Approach to Classical Frequency Methods: Feedback and Minimax Sensitivity”, *IEEE Transactions on Automatic Control*, Vol. 20, pp. 867-874, 1981.
- [98] Zhou K., Doyle J.C. and Glover K., “Robust and Optimal Control”, Prentice Hall, New Jersey, 1996.